

**Preclinical assessment of anti-HIV agent nelfinavir as
drug-repurposing strategy against high-grade serous
ovarian cancer**

by

Mahbuba Rahman Subeha

Faculty of Medicine and Health Sciences
Department of Pathology
McGill University
Montreal, Quebec, Canada

A thesis submitted to McGill University in partial fulfillment of the requirements
of the degree of Doctor of Philosophy

© Mahbuba Subeha, 2022

TABLE OF CONTENTS

ABSTRACT	V
RESUMÉ	VIII
ACKNOWLEDGEMENTS	IX
AUTHOR CONTRIBUTIONS	X
ORIGINAL CONTRIBUTION TO KNOWLEDGE	XI
RESEARCH COMMUNICATIONS	XIII
LIST OF ABBREVIATIONS	XV
LIST OF FIGURES	XIX
LIST OF TABLES	XXI
CHAPTER 1 - LITERATURE REVIEW AND INTRODUCTION	1
1.1 Ovarian cancer: current status and challenges to address	2
1.1.1 Epidemiology	2
1.1.2 Histological subtypes of ovarian cancer	2
1.1.3 Histopathological presentation of high-grade serous ovarian cancer	4
1.1.4 Genetic alterations in high-grade serous ovarian cancer	6
1.1.5 Tissue of origin in high-grade serous ovarian cancer	8
1.1.6 Staging of ovarian cancer	12
1.1.7 Dissemination of ovarian cancer within the body	13
1.1.8 Disease presentation of high-grade serous ovarian cancer	15
1.1.9 Treatment modalities of high-grade serous ovarian cancer	17
1.1.9.1 Surgery	17
1.1.9.2 Evolution of systemic therapy in ovarian cancer	19
1.1.9.1 Modes of administration of systemic therapy and associated toxicity	21
1.1.9.4 Treatment of relapsed and resistant disease	24
1.1.9.5 Targeted therapy	25
1.1.10. Emergence of platinum-resistance in cells	27
1.2 Prospect of drug repurposing in developing novel and adjunct chemotherapy	31
1.3 The anti-cancer properties of the anti-HIV drug nelfinavir	38
1.3.1 Introduction	38
1.3.2 Potential mechanisms whereby nelfinavir exerts its anti-cancer effect	41
1.3.2.1 Cell cycle arrest	41
1.3.2.2 Cell death	43
1.3.2.3 Endoplasmic reticulum (ER) stress and unfolded protein response	49
1.3.2.4 Autophagy	56

1.3.2.5 Inhibition of the proteasome	61
1.3.2.6 Signal transduction pathways	64
1.3.2.7 Oxidative stress and mitochondria	71
1.3.2.8 Tumor microenvironment	72
1.3.2.9 Multidrug-resistant efflux pumps	74
1.3.2.10 Summary of mechanisms of actions of nelfinavir as an anti-cancer agent	77
1.3.3 Antitumor effects of nelfinavir: preclinical evidence in vivo	78
1.3.4 Current status of clinical trials	84
1.3.5 Conclusions	92
1.4 Thesis rationale and objectives	94
CHAPTER 2 - MATERIALS AND METHODS	97
2.1 Cell culture and reagents	98
2.2 Cell proliferation and viability assay	101
2.3 Assessment of the sensitivity of the PEO cell line series to cisplatin	102
2.4 Cell cycle analysis	103
2.5 Clonogenic survival assay	103
2.6 Measure of <i>XBPI</i> mRNA splicing	104
2.7 Western blot analysis	106
2.8 Puromycin incorporation assay	108
2.9 Autophagic flux	108
2.10 Drug interaction analysis	109
2.11 Statistical analysis	109
CHAPTER 3 - RESULTS	110
3.1 Nelfinavir inhibits growth, reduces viability, increases hypo-diploid DNA content, and blocks clonogenic survival of high-grade serous ovarian cancer (HGSOC) cells regardless of platinum sensitivity	111
3.2 Sensitivity toward nelfinavir is enhanced over time when compared with the short-term toxicity	117
3.3 Nelfinavir triggers the unfolded protein response, enhances the expression of cell-cycle inhibitor protein p27 ^{kip1} , and induces cell death in HGSOC cells of differential platinum sensitivities	119
3.4 Nelfinavir triggered the unfolded protein response in association with lysosomal impairment but without affecting the autophagic flux	122

3.5 Nelfinavir-induced unfolded protein response (UPR) is not associated with the inhibition of the proteasome	126
3.6 ER stress response induced by nelfinavir is associated with cleavage of executioner caspase-7 and increased proapoptotic Bcl-2 family member Bax in a time- and concentration-dependent manner	129
3.7 Nelfinavir toxicity is associated with short-term sustained mRNA translation that contributes to the UPR, followed by long-term concentration-dependent inhibition of global protein synthesis	131
3.8 Nelfinavir inhibits AKT and ERK phosphorylation and triggers DNA damage	137
3.9 Nelfinavir induced G1 arrest associated with increased p27 ^{kip1} and concomitant reduction of cyclin-dependent kinase 2	140
3.10 Bortezomib is cytotoxic against HGSOC cells of differential platinum sensitivity	143
3.11 Nelfinavir potentiates the toxicity of the proteasome inhibitor bortezomib without modifying its proteasome inhibitory capacity	146
3.12 Nelfinavir and Bortezomib combinedly exert cytostatic effects on HGSOC cells by enhancing cell cycle inhibitor p27 ^{kip1}	151
3.13 Nelfinavir targets cells that have acquired resistance to cisplatin upon long-term culture in the presence of the DNA damaging agent	154
3.14 Nelfinavir does not re-sensitize cisplatin-resistant cells to short-term cisplatin therapy within pharmacologically relevant concentrations	158
CHAPTER 4 - DISCUSSION AND CONCLUSION	162
APPENDIX	177
REFERENCES	223

ABSTRACT

Platinum-based therapy following tumor-debulking surgery has been the backbone of treatment for high-grade serous ovarian cancer (HGSOC) since the 1970s; however, high recurrence of platinum-resistant disease necessitates the development of improved alternative therapies. Repurposing market-available drugs as cancer therapeutics carries the prospect of reducing the timeframe and cost of drug development, posing potential benefits to drug-resistant as well as financially underprivileged patients. Nelfinavir (NFV), an orally available anti-HIV drug, has shown promising effects against diverse cancers as demonstrated through a myriad of preclinical studies and clinical trials; however, its remedial benefits against HGSOC are unknown.

In this study, we explored the therapeutic efficacy of NFV on HGSOC cells generated from patients when platinum-sensitive or resistant. Acute drug toxicity was assessed by total cell count, percent viability, and the level of hypo-diploid DNA content following 72 hours (h) of treatment with NFV. Living cells that tolerated 72 h of NFV exposure were subjected to further drug-free re-incubation for 14-21 days, to assess the residual anti-clonogenic potential of the drug. NFV triggered a concentration-dependent reduction of total cell number and viability, with a parallel increase in hypo-diploid DNA content in HGSOC cells of differential platinum sensitivity. A concentration-dependent reduction in the number of colonies – originating from cells that evaded acute toxicity – suggested long-term residual toxicity of NFV.

Western blot analysis of underlying molecular mechanisms revealed activation by NFV of the three signaling arms of the unfolded protein response (UPR): PERK, IRE1 α and ATF6 – in a similar manner to classical endoplasmic reticulum (ER) stressor tunicamycin (TN). Modulation of the UPR in response to NFV was accompanied by the inhibition of global protein synthesis as analyzed through a non-radioactive method by labelling the nascent polypeptides with puromycin. A time-course experiment revealed that inhibition of mRNA translation is a late effect during NFV treatment, as suggested from a sustained level of puromycylation during the early stages of NFV treatment. Continuous mRNA translation during the early stages of NFV treatment was associated

with concurrent splicing of *XBPI* mRNA and transient dephosphorylation of eIF2 α , which were abrogated by protein synthesis inhibitor cycloheximide. These observations suggested that protein accumulation in the presence of NFV is causative, at least in part, of the induction of NFV-mediated ER stress. Modulation of the UPR and the protein synthesis machinery was associated with a proapoptotic environment, evidenced by the enhanced expression of ATF4, CHOP, proapoptotic protein Bax and cleavage of executioner caspase-7. Western blot analysis further revealed enhanced phosphorylation of γ H2AX, suggesting NFV-mediated induction of DNA damage, which was associated with decreased proliferation signals driven by the AKT and ERK pathways. NFV increased the level of autophagosome-associated protein LC3II in HGSOC cells of varying platinum sensitivities; however, the autophagic flux was not increased during co-treatment with NFV and lysosomal inhibitor bafilomycin A1, suggesting a likely impairment of the lysosome by NFV, which impeded autophagosome clearance. Drug interaction between NFV and cisplatin was assessed by the Chou-Talalay method utilizing the combination index (CI) measured from the total cell count. On cells of low cisplatin sensitivity, the combination of NFV and cisplatin showed no synergistic interaction. Conversely, the combination of NFV with the proteasome inhibitor bortezomib (BZ) caused a synergistic drug interaction in HGSOC cells with high or low sensitivity to cisplatin; however, NFV did not promote inhibition of the proteasome as a singular agent. Cell cycle analysis indicated an arrest at G1 phase during NFV and BZ combination in HGSOC cells with high or low sensitivity to cisplatin. This phenomenon was associated with enhanced expression of cell cycle inhibitor p27^{kip1} and increased phosphorylation of γ H2AX, contributing to the potentiation of effects between NFV and BZ.

Our study collectively demonstrates that NFV can therapeutically target HGSOC cells of differential platinum sensitivities via multipronged mechanistic approaches, suggesting its prospective repurposing benefit either as a singular agent or in combination with a proteasome inhibitor.

RÉSUMÉ

La chimiothérapie à base de platine est le pilier du traitement du cancer séreux de haut grade de l'ovaire (HGSOC) depuis les années 1970. Cependant, la récurrence fréquente d'une maladie résistante au platine nécessite le développement de thérapies alternatives. La réutilisation de médicaments disponibles sur le marché en tant que thérapies contre le cancer offre la possibilité de réduire le délai et le coût du développement, ce qui présente des avantages potentiels pour les patients. Nelfinavir (NFV), un médicament anti-VIH, a montré des effets prometteurs contre divers cancers, mais ses avantages curatifs contre HGSOC sont inconnus.

Dans cette étude, nous avons exploré l'efficacité thérapeutique du NFV sur des cellules HGSOC générées à partir de patients sensibles ou résistants au platine. La toxicité aiguë du médicament a été évaluée par le nombre total de cellules, le pourcentage de viabilité et le niveau d'ADN hypo-diploïde après 72 heures (h) de traitement avec NFV. Les cellules vivantes qui ont toléré 72 h d'exposition au NFV ont été soumises à une nouvelle incubation sans traitement pendant 14 à 21 jours, afin d'évaluer le potentiel anti-clonogénique du médicament. NFV a déclenché une réduction, dépendante de la concentration, du nombre total de cellules et de leur viabilité, avec une augmentation de l'ADN hypo-diploïde dans les cellules HGSOC. Une réduction, dépendante de la concentration, du nombre de colonies, provenant de cellules qui ont échappé à la toxicité aiguë, a suggéré une toxicité résiduelle à long terme du NFV. L'analyse par Western blot des mécanismes moléculaires de NFV a révélé l'activation des trois bras de signalisation de la réponse de la protéine dépliée (UPR) - PERK, IRE1 α et ATF6 - d'une manière similaire à la tunicamycine (TN), déclencheur de stress du réticulum endoplasmique (RE). La modulation de l'UPR en réponse au NFV était accompagnée de l'inhibition de la synthèse protéine globale telle qu'analysée en marquant les polypeptides naissants avec de la puromycine. La traduction continue de l'ARNm au cours des premiers stades du traitement par NFV était associée à un épissage de l'ARNm de XBP1

et à une déphosphorylation de eIF2 α . Ces observations suggèrent que l'accumulation de protéines est responsable de l'induction du stress RE médié par NFV. La modulation de l'UPR et de la synthèse des protéines a été associée à un environnement pro-apoptotique, mis en évidence par l'expression accrue d'ATF4, CHOP, l'augmentation du rapport Bax: Bcl2 et le clivage de caspase-7. L'analyse par Western blot a révélé une phosphorylation accrue de γ H2AX, suggérant une induction de dommages à l'ADN médiée par NFV, associée à une diminution des signaux de prolifération entraînés par les voies AKT et ERK. NFV a augmenté le niveau de protéine LC3II associée à l'autophagosome dans les cellules HGSOC, cependant, le flux autophagique n'a pas été augmenté pendant le co-traitement avec le NFV et un inhibiteur lysosomal, suggérant une altération probable du lysosome par NFV. L'interaction entre NFV et cisplatine a été évaluée par la méthode de Chou-Talalay en utilisant l'indice de combinaison (IC) mesuré à partir du nombre total de cellules. Sur les cellules de faible sensibilité au cisplatine, la combinaison de NFV et de cisplatine n'a montré aucune interaction synergique. À l'inverse, la combinaison du NFV avec le bortézomib (BZ), un inhibiteur du protéasome, a provoqué une interaction synergique dans les cellules HGSOC, mais le NFV n'a pas favorisé l'inhibition du protéasome en tant qu'agent singulier. L'analyse du cycle cellulaire a indiqué un arrêt à la phase G1 avec la combinaison NFV et BZ dans les cellules HGSOC avec une sensibilité élevée ou faible au cisplatine. Ce phénomène était associé à une expression élevée de l'inhibiteur du cycle cellulaire p27^{kip1} et une phosphorylation accrue de γ H2AX.

Notre étude démontre que NFV peut cibler les cellules HGSOC de sensibilités différents au platine via des approches mécanistes à plusieurs volets, suggérant son avantage potentiel de réaffectation, en tant qu'agent singulier ou en combinaison avec un inhibiteur du protéasome.

ACKNOWLEDGEMENTS

I want to take this opportunity to thank my supervisor, Dr. Carlos Telleria, for giving me the opportunity to pursue this degree and for his continuous support throughout the journey. My heartfelt thanks to Dr. Alicia Goyeneche for teaching me all the technical methods and providing valuable advice regarding the thesis. I have learnt so much from Dr. Telleria and Dr. Goyeneche, not only in terms of science and academia but also about the life beyond that. I would also like to thank Dr. Edith Zorychta and Dr. Hua Ling for their dedication toward the Department of Pathology and all the graduate students. I would especially like to thank them for accommodating me when I needed support as an international student and as a parent.

I would like to thank the members of my advisory committee, Dr. Pierre Fiset, Dr. Siham Sabri and Dr. Koren Mann, for providing valuable advice toward my thesis. Thanks to Dr. Carolyn Baglole, Dr. Ruben Caron and Dr. Miguel Burnier for valuable advice on the thesis. I would also like to thank the Rivkin Center for Ovarian Cancer, the Charles O. Monat Foundation, and the Department of Pathology in McGill University for providing the funds for this project. Thanks to Dr. Julia Burnier and Prisca Bustamante for the collaboration on the project.

Many thanks to Sabrina Ritch for her friendship and support throughout my PhD journey. Thanks to Farah Abdalbari, Robert Dube, Michael Lisio, Sarah Alghamdi, Silvana Ferreira, Federica Ghersha, Ben and Riwati. I am grateful to have had the chance to work with you all and learn so much.

Thanks to my parents Shamun Nahar and Muhammad Habibur Rahman. Without their unwavering support, I would not be here today. Thanks to my husband, Sazzad, for his care and support. Many thanks to my brothers Maruf and Hasan for always being there for me. I am also thankful to my family and friends in Bangladesh and abroad for continuing to encourage me. And last but not least, thanks to my daughters Yashfi and Aziza for their love, laughter and hope.

AUTHOR CONTRIBUTIONS

This doctoral thesis is based on the original research work conducted by me, Mahbuba Subeha, under the guidance of supervisor Dr. Carlos Telleria. The thesis was written in traditional format by me in accordance with the *Guideline for Thesis Preparation* from McGill University. Two manuscripts based on this thesis were written by me. Dr. Carlos Telleria provided guidance, valuable feedback, and edits regarding the thesis and both manuscripts.

All the experiments described in this thesis were organized, performed, and analyzed by me, with important advice received from Dr. Carlos Telleria and Dr. Alicia Goyeneche, except the works mentioned below. Dr. Alicia Goyeneche taught technical methods and helped to optimize the experimental procedures.

The experiments to determine the IC_{50} of cisplatin on PEO1, PEO4, and PEO6 cells were conducted by Michael Lisio, which are mentioned in Table 3.2. Michael Lisio also developed PEO1X cells from PEO1 cells as a part of his master's thesis. In this thesis, the effects of nelfinavir were investigated by me on PEO1X cells, which are mentioned in Figure 3.16.

In the experiment mentioned in Figure 3.9, the cell culture, treatment, and RNA sample collection were conducted by me, and the reverse transcription polymerase chain reactions (RT-PCR) were conducted by Prisca Bustamante. Dr. Julia Burnier provided with her supervision and the reagents for the RT-PCR. The result from this experiment is included in the second manuscript, and both Prisca Bustamante and Dr. Julia Burnier provided valuable feedback regarding the manuscript.

The English abstract was translated into French by Sabrina Ritch.

The entire project was funded by The Rivkin Center for Ovarian Cancers, the Charles O. Monat Foundation and funds from the Department of Pathology.

ORIGINAL CONTRIBUTION TO KNOWLEDGE

1. In this study, we report for the first time a comprehensive account of the anti-cancer effects of nelfinavir against high-grade serous ovarian cancer (HGSOC) cells having differential platinum sensitivity. The cells were derived from and traced back to original HGSOC patients who evolved from platinum-sensitive to platinum-resistant disease. We investigated the effect of nelfinavir on multiple pathways in HGSOC cells, namely, cell cycle, cell death, cell survival and proliferation, DNA damage, endoplasmic reticulum (ER) stress, autophagy, and proteasome inhibition. Prior to this current study; nelfinavir has been tested against 23 types of cancers [1]; however, only one study by Delaney *et al.* investigated the role of nelfinavir against HGSOC using a single cell line (OVCAR3) in the context of a single mechanism— autophagy [2].
2. We provide mechanistic evidence for the first time about the early protein synthesis status of HGSOC cells in response to nelfinavir. By using a non-radioactive method of tagging nascent polypeptides with a drug named puromycin [3,4], we were able to visualize the status of mRNA translation in HGSOC cells in response to nelfinavir. We report that during the early phase of nelfinavir treatment, sustained mRNA translation is associated with the cleavage of *XBPI*, indicating the initiation of ER stress, which can be reversed upon blocking the mRNA translation by cycloheximide. This result indicates that early sustained mRNA translation by nelfinavir is causative of ER stress. With increasing time of treatment, we observed that nelfinavir eventually diminished protein synthesis. Most studies that investigated nelfinavir-mediated ER stress so far have reported the inhibition of protein synthesis, which is the late effect during nelfinavir-treatment on cancer cells [5].

3. We report long-term residual toxic effects of nelfinavir HGSOC cells upon drug withdrawal on HGSOC cells, which is separate from the acute toxicity induced by nelfinavir. We first treated HGSOC cells with different concentrations of nelfinavir for 72 hours (h) and isolated 1000 viable cells that withstood the treatment. We then subjected those 1000 alive cells to colony-forming assay by incubating in drug-free media for 14-21 days. We were able to observe a decrease in the number of colonies even when the drug was absent, indicating sustained residual effects of nelfinavir in HGSOC cells likely due to sustained DNA damage. This method is different from the traditional colony forming assays, in which the long-term effect of a drug is measured by observing the number of colonies directly generated from cells treated continuously for 10-14 days [6], which does not indicate residual toxicity.
4. Guan and colleagues identified site-2 protease (S2P) as a putative target of nelfinavir that inhibited the proteolysis of ATF6 [7]. In HGSOC cancer cells, we observed the cleavage of ATF6 in response to nelfinavir that excluded S2P as a possible upstream target of nelfinavir in these cells.
5. In summary, we report the mechanistic processes associated with nelfinavir-induced toxicity against HGSOC cells of different sensitivities to platinum; we report that the toxicity involves DNA damage, reduced survival and proliferation signals, lysosomal inhibition, and a proapoptotic shift of the unfolded protein response associated to the ER stress pathway.

RESEARCH COMMUNICATIONS

Published manuscript:

- Subeha, M.R.; Telleria, C.M. The Anti-Cancer Properties of the HIV Protease Inhibitor Nelfinavir. *Cancers (Basel)* 2020, 12, doi:10.3390/cancers12113437.
- Subeha, M.R.; Goyeneche, A.A.; Bustamante, P.; Lisio, M.A.; Burnier, J.V.; Telleria, C.M. Nelfinavir Induces Cytotoxicity towards High-Grade Serous Ovarian Cancer Cells, Involving Induction of the Unfolded Protein Response, Modulation of Protein Synthesis, DNA Damage, Lysosomal Impairment, and Potentiation of Toxicity Caused by Proteasome Inhibition. *Cancers* **2022**, 14, 99.

Published abstracts:

1. Subeha, M.R.; Goyeneche, A.A.; Telleria, C.M. Mechanistic role of nelfinavir as drug-repurposing strategy against high-grade serous ovarian cancer. **2021**. AACR Annual Meeting 2021; April 10-15, 2021 and May 17-21, 2021; Philadelphia, PA **DOI:** 10.1158/1538-7445.AM2021-1013 Proceedings: AACR Annual Meeting 2021; April 10-15, 2021 and May 17-21, 2021; **Philadelphia, PA, USA**
2. Subeha, M.R.; Goyeneche, A.A.; Lisio, M.A.; Telleria, C.M. Abstract A74: The HIV protease inhibitor nelfinavir, alone or in combination with the proteasome inhibitor bortezomib, is cytotoxic to high-grade serous ovarian cancer cells regardless of platinum sensitivity. **2020**. **DOI:** 10.1158/1557-3265.OVCA19-A74 Published July 2020 AACR Special Conference on Advances in Ovarian Cancer Research; September 13-16, 2019; **Atlanta, GA, USA**
3. Subeha, M.; Zhang, L.; Goyeneche, A.; Telleria, C. Abstract NT-111: The antiprogesterin/antiglucocorticoid mifepristone and the HIV protease inhibitor nelfinavir cause endoplasmic reticulum stress and potentiate the toxicity of proteasome inhibition in high-grade serous epithelial ovarian cancer cells. **2019**., Published November 2019. **DOI:** 10.1158/1557-3265 OVCASYMP18-NT-111 12th Biennial Ovarian Cancer Research Symposium; September 13-15, 2018; **Seattle, Washington, USA**

Oral presentations:

1. Subeha M, Goyeneche A, Telleria C. **Oral presentation:** The Anti-HIV Drug Nelfinavir is Cytotoxic Towards High-Grade Serous Ovarian Cancer Cells Regardless of Platinum Sensitivity. 9th Biennial Canadian Conference on Ovarian Cancer Research (May 2018) **Edmonton, Alberta, Canada**; Category: Targeting Essential Vulnerabilities in Ovarian Cancer - From DNA Repair to Drug Resistance. (**Travel Award** received from the conference)
2. Subeha M, Goyeneche A, Telleria C. **Rapid fire talk:** Repurposing Anti-HIV Drug Nelfinavir as Adjunct Chemotherapy for High-Grade Serous Ovarian Cancer, Programme de recherche sur le Cancer Research Program, McGill University Health Center Research Institute, **June 2021**

Poster presentations:

Subeha M, Goyeneche A, Telleria C Nelfinavir exerts cytotoxicity in high-grade serous ovarian cancer cells via modulation of protein synthesis, endoplasmic reticulum stress, and DNA damage. Canadian Virtual Conference on Ovarian Cancer Research, Poster Discussion Group — Exploring novel treatments (**May 2021**)

Subeha M, Goyeneche A, Lisio M, Telleria C Nelfinavir targets platinum-sensitive and platinum-resistant high-grade serous ovarian cancer cells as a monotherapy and in combination with a proteasome inhibitor. Finlayson Research Day, Department of Pathology, McGill University, Montreal, QC. (**May 2019**) (**Moy Fong Chen Travel Award**)

Subeha M, Goyeneche A, Lisio M, Zhang L, Telleria C The anti- HIV drug Nelfinavir is cytotoxic towards high-grade serous ovarian cancer cells regardless of platinum sensitivity. Finlayson Research Day, Department of Pathology, McGill University, Montreal, QC, Canada. (**May 2018**)

Subeha M, Goyeneche A, Lisio M, Zhang L, Telleria C The anti- HIV drug Nelfinavir is cytotoxic towards high-grade serous ovarian cancer cells regardless of platinum sensitivity. Finlayson Research Day, Department of Pathology, McGill University, Montreal, QC, Canada. (**May 2017**)

LIST OF ABBREVIATIONS

ABC	ATP-binding cassette
AIDS	Acquired immunodeficiency syndrome
AIF	Apoptosis-inducing factor
AML	Acute myeloid leukemia
AMPK	5'-AMP-activated protein kinase
ANOVA	Analysis of variance
AKT	Protein kinase B
ATF3	Activating transcription factor 3
ATF4	Activating transcription factor 4
ATF6	Activating transcription factor 6
ATP	Adenosine triphosphate
ATR	Ataxia telangiectasia, mutated (ATM) and RAD3-related protein
AUC	Area under the plasma-concentration time curve
BAF	Bafilomycin A1
BER	Base excision repair
Bax	Bcl-2-associated X protein
Bcl-2	B-cell lymphoma 2
BRCA	Breast cancer type 1 susceptibility protein
BZ	Bortezomib
BrdU	Bromodeoxyuridine
CAF	Cancer associated fibroblast
CDK	Cyclin dependent kinase
CHK1	Checkpoint kinase 1
CHOP	CCAAT-enhancer binding protein homologous protein
CHX	Cycloheximide
CI	Combination index
CIC	Cortical inclusion cyst
CYP2C19	Cytochrome P450 2C19
CML	Chronic myeloid leukemia
COX-2	Cyclooxygenase-2
CT	Computer tomography
CTR1	Copper transporter protein 1
DR	Death receptor
DEN	Diethylnitrosamine
DMC	Dimethylcelecoxib
DNA	Deoxyribonucleic acid
DSB	Double strand breaks
eIF2 α	Eukaryotic initiation factor 2 α
eEF2	Eukaryotic elongation factor 2
eEF2K	Eukaryotic elongation factor 2-kinase
EGFR	Epidermal growth factor receptor
ER	Endoplasmic reticulum
ERAD	ER associated degradation
ERK	Extracellular signal regulated kinase

ERp44	Endoplasmic reticulum protein 44
ERO1-L α	Endoplasmic reticulum oxidoreductin-1 like protein α
EOC	Epithelial ovarian cancer
FACS	Fluorescence activating cell sorting
FADD	Fas-associated protein with death domain
FAK	Focal adhesion kinase
FAS	Fatty acid synthase
FDA	Food and drug administration
FFPE	Formalin-fixed paraffin-embedded
FIGO	International Federation of Gynecology and Obstetrics
FMISO-PET	¹⁸ F-fluoromisonidazole positron emission tomography
FTE	Fallopian tube epithelium
FTSEC	Secretory epithelial cells of the distal fallopian tube
GADD34	Growth arrest and DNA damage inducible protein 34
GBM	Glioblastoma multiforme
GFP	Green fluorescent protein
GRP78	Glucose regulated protein if 78 kDa
GSH	Glutathione
h	Hours
HAART	Highly active antiretroviral treatment
HCC	Hepatocarcinoma cells
HDM2	Human homolog of mouse double minute 2
HDAC	Histone deacetylase
HER2	Human epidermal factor receptor 2
HGSOC	High-grade serous ovarian cancer
HIF1 α	Hypoxia inducible factor 1 α
HIPEC	Hyperthermic IP chemotherapy
HIV	Human immunodeficiency virus
HIV-PI	HIV protease inhibitor
HPV	Human papillomavirus
hPSC	Human pancreatic stellate cells
HR	Homologous recombination
HSPA5	Heat shock 70 kDa protein 5
HSP90	Heat shock protein 90
H2AX	H2A histone family member X
H ₂ O ₂	Hydrogen peroxide
IDS	Interval debulking surgery
IGFR	Insulin-like growth factor receptor
IP	Intraperitoneal
IRE1 α	Inositol-requiring enzyme 1 α
ISR	Integrated stress response
IV	Intravenous
JNK	JUN-amino terminal kinase
KS	Kaposi's sarcoma
LAPC	Locally advanced pancreatic cancer
LRRC8	Leucine-rich repeat containing 8

MAPK	Mitogen-activated protein kinase pathway
3MA	3-methyladenosine
mTOR	Mammalian target of rapamycin
3-MA	3-methyladenine
MDR	Multidrug resistance
MDR1	Multidrug resistant 1
MRP-4	Multidrug resistance protein 4
MEF	Mouse embryonic fibroblasts
min	Minutes
MM	Multiple myeloma
mPTP	Mitochondria permeability transition pore
MMP-2	Matrix metalloproteinase- 2
MMP-9	Matrix metalloproteinase- 9
MMR	Mismatch repair
NAC	N-acetylcysteine
NACT	Neoadjuvant chemotherapy
NCATS	The US National Center for Advancing Translational Sciences
NCI	National Cancer Institute
NER	Nucleotide excision repair
NET	Neuroendocrine tumor
NFV	Nelfinavir
NO	Nitric oxide
NSCLC	Non-small cell lung carcinoma
OS	Overall survival
OSE	Ovarian surface epithelium
PAP	Papanicolaou
PARP	Poly ADP-ribose polymerase
PBS	Phosphate buffered saline
PBMC	Peripheral blood mononuclear cells
PCNA	Proliferating cell nuclear antigen
PDI	Protein disulfide isomerase
PE	Phosphatidyl ethanolamine
PERK	Protein kinase RNA-like endoplasmic reticulum kinase
PET	Positron emission tomography
PFS	Progression free survival
P-gp	P-glycoprotein
PFA	Paraformaldehyde
PI	Protease inhibitors
PI	Propidium iodide
PI3KCA	Constitutive active PI3K
PTEN	Phosphate and tensin homologue
P27 ^{kip1}	Cyclin dependent kinase inhibitor p27 (a.k.a.KIP1)
Rag	Ras-related GTPase
RIP	Regulated intramembrane proteolysis
RNA	Ribonucleic acid
ROS	Reactive oxygen species

RT-PCR	Reverse transcription polymerase chain reaction
sATF6	Soluble transcription factor 6
SBRT	Stereotactic body radiotherapy
SIRT3	Sirtuin-3
STAT3	Signal transducer and activator of transcription 3
S1p	Site 1 protease
S2P	Site 2 protease
SEE-FIM	Sectioning and Extensively Examining the Fimbriated End
SET	Solid, pseudo-Endometrioid and/or Transitional cell carcinoma-like
SESN2	Sestrin-2
SEER	Surveillance, Epidemiology and End Results Program
SRC	Tyrosine kinase Src
SREBP1	Sterol regulatory binding protein- 1
siRNA	Small interference RNA
SSB	Single strand break
STR	Autosomal short tandem repeat
STIC	Serous tubular intra-epithelial carcinomas
STIL	Serous tubal intraepithelial lesion
TCGA	The cancer genome atlas
TN	tunicamycin
TNBC	Triple negative breast cancer
TNF	Tumor necrosis factor
TRAIL	Tumor necrosis factor related apoptosis inducing ligand
TRIB3	Tribbles homolog-3
TSC	Tuberous sclerosis complex
TUNEL	Terminal deoxynucleotidyl transferase (TdT) dUTP Nick-END Labelling
UPR	Unfolded protein response
VEGF	Vascular endothelial growth factor
VRAC	Volume regulated anion channels
XBP-1	X-box binding protein -1

LIST OF FIGURES

Figure 1.1 Representation of heterogeneity in the histopathological presentation of high-grade serous ovarian cancer (HGSOC)	5
Figure 1.2 The origin of HGSOC	11
Figure 1.3 Estimated time required for each step of drug development	32
Figure 1.4 Schematic representation of multiple approaches to repurpose drug	35
Figure 1.5. Nelfinavir (NFV) competitively binds with the specific sequence of HIV-aspartyl protease to inhibit the required cleavage of gag/gag-pol polypeptides for the maturation of the virion	38
Figure 1.6 Schematic representation of the unfolded protein response pathway (UPR) in response to the endoplasmic reticulum (ER) stress developed as a result of misfolded or unfolded proteins in the ER	50
Figure 1.7 The process of autophagy	57
Figure: 1.8 Summary of mechanisms of action of nelfinavir as an anti-cancer agent	77
Figure 2.1 Schematic representing the development of HGSOC cell lines utilized in this study	99
Figure 2.2 Experimental design of clonogenic survival assay	104
Figure 3.1 Morphological characteristics of PEO cells	113
Figure 3.2 Nelfinavir inhibits growth, reduces viability, increases hypo-diploid DNA content, and blocks clonogenic survival of HGSOC cells regardless of platinum sensitivity	115
Figure 3.3 Nelfinavir triggers the unfolded protein response, enhances the expression of cell-cycle inhibitor protein p27 ^{kip1} , and induces cell death in HGSOC cells of differential platinum sensitivities	120
Figure 3.4 Nelfinavir triggers unfolded protein response in HGSOC cells	123
Figure 3.5 Nelfinavir causes lysosomal impairment without affecting the autophagic flux in HGSOC cells	125

Figure 3.6 Nelfinavir does not inhibit the proteasomes in HGSOC cells	128
Figure 3.7 ER stress response induced by nelfinavir is associated with cleavage of executioner caspase-7 and increased proapoptotic Bcl-2 family member Bax in a time- and concentration-dependent manner	130
Figure 3.8 Nelfinavir toxicity is associated with short-term sustained mRNA translation followed by long-term concentration-dependent inhibition of global protein synthesis	132
Figure 3.9 The short-term sustained mRNA translation by nelfinavir is required for the subsequent induction of ER stress	134
Figure 3.10 An inhibitor of eIF2 α dephosphorylation, salubrinal, restores nelfinavir-mediated cytotoxicity	136
Figure 3.11 Nelfinavir inhibits AKT and ERK phosphorylation and triggers DNA damage	138
Figure 3.12 Nelfinavir induced G1 arrest associated with increased p27 and concomitant reduction of cyclin-dependent kinase 2	141
Figure 3.13 Bortezomib is cytotoxic against high grade serous ovarian cancer cells of differential platinum sensitivity	144
Figure 3.14 Nelfinavir potentiates the toxicity of the proteasome inhibitor bortezomib in HGSOC cells	149
Figure 3.15 Combination of nelfinavir and bortezomib promotes the accumulation of p27 and phosphorylation of H2AX without further enhancing bortezomib mediated proteasomal inhibition	152
Figure 3.16 <i>In vitro</i> nelfinavir is not cross-resistant toward cisplatin	156
Figure 3.17 Nelfinavir does not re-sensitize low-cisplatin sensitive HGSOC cells back to cisplatin	161
Figure 4 Schematic representation of the proposed mechanism of nelfinavir on HGSOC cells	175

LIST OF TABLES

Table 1.1 FIGO staging classification for cancer of the ovary, fallopian tube, and peritoneum	12
Table 1.2 Examples of successful drug repurposing events	37
Table 1.3 Antitumor effects of nelfinavir in animal models	79
Table 1.4 Updated clinical trial list including nelfinavir (2020)	88
Table 2.1 Source and dilutions of antibodies utilized in this work	107
Table 3.1 Concentration of cisplatin needed to achieve 50% reduction in clonogenic survival (IC_{50}) of the HGSOC cell lines studied	112
Table 3.2 Comparison of concentrations of nelfinavir (NFV) required to achieve 50% reduction in the total number of cells during short-term studies (72 h), and 50% reduction in the clonogenic survival during long-term therapy	118
Table 3.3 Analysis of drug interaction between nelfinavir and bortezomib	147
Table 3.4 Analysis of drug interaction between nelfinavir and cisplatin	160

CHAPTER 1

-

LITERATURE REVIEW AND INTRODUCTION

1.1 Ovarian cancer: current status and challenges to address

1.1.1 Epidemiology

Ovarian cancer is currently the seventh most common form of cancer and the eighth leading cause of cancer-related death among women worldwide [8]. In 2020, the estimated new cases for ovarian cancer were 313,959 worldwide, among which the number of predicted deaths was 207,252 [9]. In the United States, the estimated new cases were 21,750 in 2021, whereas the estimated deaths due to ovarian cancer were 13,940 [10]. According to Canada Cancer Statistics 2019, 1 in 75 women run the risk of developing ovarian cancer in their lifetime and 1 in 90 women has the probability of dying from it [11]. The median age of diagnosing ovarian cancer is at 63 years, and the majority of cases appear at 55 years and older [12]. Despite considerable advancement in cancer diagnostics and therapeutics, the 5-year survival rate of ovarian cancer has remained unimproved since the breakthrough diagnosis of platinum-based drugs for chemotherapy in the 1970s. According to the Surveillance, Epidemiology and End Results Program (SEER) of the United States National Cancer Institute (NCI), the 5-year relative survival adjusted between 2011-2017 is 49.1%. [12]. The lack of improvement in 5-year survival can be attributed to the emergence of treatment resistance disease and inefficient screening and early diagnostic methods leading to late occurrences. Consequently, ovarian cancer remains a global health challenge to women worldwide to this day, which requires improved diagnostic and therapeutic options.

1.1.2 Histological subtypes of ovarian cancer

From the perspective of a pathologist, ovarian cancer has been regarded as a neoplasm of multiple distinct entities rather than a unitary disease [8]. Histologically, 90% of all ovarian cancer are considered to be of epithelial origin, and the rest appear from germ cells or sex-cord-

stromal tissue [13]. Epithelial ovarian cancer (EOC) can be further subdivided into four categories according to the histological appearances: serous, mucinous, clear-cell, and endometrioid [14]. Depending on the cellular aberration, the serous and endometrioid ovarian cancers are stratified into low- and high-grade cancers. Low-grade serous ovarian cancer is characterized by tumors of borderline malignancy with abnormalities in the *RAS* pathway (*KRAS*, *BRAF* and *ErbB2*). High-grade serous ovarian cancer (HGSOC) rarely demonstrates aberration in the *RAS* pathway and carries distinct molecular and histological features. Similarly, low-grade endometrioid cancer demonstrates a frequent activating mutation in the WNT- β -catenin pathway, unlike its high-grade counterpart [15]. Aside from the clinically delineated four histotypes, rarer subtypes are also diagnosed at times, namely, malignant transitional cell (Brenner) tumors, mixed type and undifferentiated carcinoma [16].

Vaughan and colleagues correlated the origins of invasive ovarian carcinoma according to the histological similarity with non-ovarian tissues. Mucinous invasive carcinomas resemble the tissue of the gastrointestinal tract, and are often metastasized from the stomach, colon and appendix. Endometrioid and clear cell carcinomas resemble the morphology of endometriosis and are considered to derive from retrograde menstruation. High-grade serous ovarian cancer cells are derived from the distal fallopian tube or ovarian surface epithelium [14].

Kurman and Shih proposed the dualistic model of ovarian carcinogenesis, which led to a paradigm shift in the understanding of the pathogenesis [16]. According to the model, EOC can be divided into Type I and Type II carcinomas. Type I cancers usually present in an indolent fashion with a unilateral cystic neoplasm. These tumors are genetically stable and p53 wild type; however, they demonstrate frequent mutations in RAS-MAPK and PI3K-AKT pathways. This category includes the low-grade serous, mucinous, and Brenner's subtype and accounts for 10%

of ovarian cancer-related deaths. Conversely, type II ovarian carcinomas are high-grade and aggressive and present in advanced stages in 75% of cases. 90% of all ovarian cancer deaths occur through type II lesions. Widespread genomic instability due to chromosomal copy number alterations, frequent mutations of TP53, and deficient homologous recombination repair pathway are the hallmarks of type II ovarian carcinomas [16].

1.1.3 Histopathological presentation of high-grade serous ovarian cancer

High-grade serous ovarian cancer (HGSOC) is the most aggressive subtype of EOC and accounts for approximately 70% of all ovarian cancer-related deaths [17]. Analysis of stained tissue sections demonstrates heterogeneous histopathological features (**Figure 1.1**), typical of HGSOC [8,18]. The tumor can present as a solid mass—with or without slit-like presentation. Glandular, papillary, and cribriform presentations are also common, resembling the epithelium of the fallopian tube. Necrosis may present among the solid masses [8,16,19]. An HGSOC tissue section loaded with tumor-infiltrating lymphocytes is known as SET (Solid, pseudo-Endometrioid and/or Transitional cell carcinoma-like)—typically associated with mutation of the gene *BRCA1* [20]. Cytology of HGSOC is characterized by large hyperchromatic and pleomorphic nuclei, suggestive of high-grade nuclear atypia. A plethora of visible mitotic figures results in high mitotic index of HGSOC cells. Areas of calcification known as psammoma bodies are also typical of HGSOC [19].

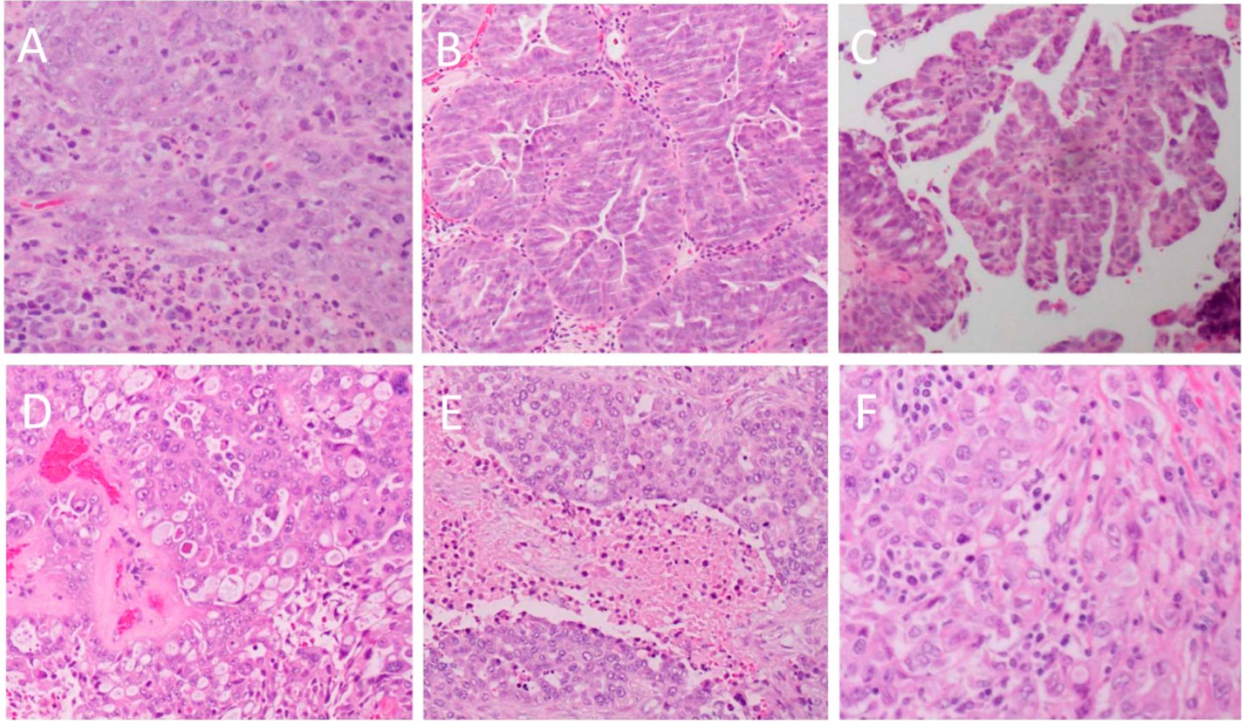


Figure 1.1: Representation of heterogeneity in the histopathological presentation of HGSOC: (A) solid architecture, (B) glandular architecture with slit-like appearances, (C) papillary features, (D) cribriform and pseudoendometrioid appearance, (E) necrosis in a solid structure, (F) infiltration of lymphocytes. Image adopted from [8].

Frequently used immunohistochemical markers for detecting HGSOC tissues include p53, WT-1, and p16. Mutation of p53 is almost invariably present in HGSOC, and immunohistochemistry usually renders strong nuclear positivity in nearly all the cells. However, if cells carry nonsense mutation of p53, instead of the frequent missense mutation generally detected in the case of HGSOC, the resultant truncated protein is usually undetectable, confounding the diagnosis [19]. High Ki-67 staining suggests a high proliferation index, which is a characteristic of HGSOC when compared with low-grade cancers [19]. Positive staining is also

detected in the case of epithelial marker CK7, ARID1A, and marker of Müllerian origin PAX8. 80% of HGSOC tissues carry estrogen receptor (ER), while 30% stain positive for progesterone receptor (PR) [8,19].

1.1.4 Genetic alterations in high-grade serous ovarian cancer

The cancer genome atlas (TCGA) unraveled the genomic landscapes of HGSOC by whole-exome sequencing of samples obtained from 316 patients. The result indicated high chromosomal instability, with frequent DNA gain and losses. Other than frequent TP53 mutations, point mutations in other genes were rare, which was in contrast with type I EOCs having wild-type TP53 and frequent mutations in BRAF, KRAS, PTEN, CTNNB1, and PIK3CA [17]. Mutation in TP53 has been suggested as an early event in the development of HGSOC, and 96% of HGSOC seemed to carry somatic TP53 mutations [21]. One study demonstrated that missense mutation in TP53 happens in 70.4% of cases, whereas the contributions of frameshift, nonsense, and splice mutations were 12%, 8.67%, and 5.1%, respectively [22].

Depending on the nature of the mutation, the functionality of p53 differs. 80% of total mutations are located in the central DNA binding domain leading to a loss of function of the transcriptional activity. Missense mutation may result in dominant-negative protein being unable to participate in tetramerization. Furthermore, mutant p53 may be stabilized within the cells due to the lack of proteasomal degradation because of diminished interaction with HDM2. Increased stability may also paradoxically confer a gain of function oncogenic activity. Nevertheless, mutant TP53 is an important genetic signature of HGSOC, even present in the early precursor lesions [22].

The second common genetic alteration found in HGSOC is the somatic, germline, or epigenetic mutation in *BRCA1* and/or *BRCA2*, and to a lesser extent, other proteins involved in the

homologous recombination pathway [23]. The TCGA study reported that 12.5% of HGSOC patients carry BRCA1 mutation, whereas 11.5% carry BRCA2 mutations, and the percentage of germline mutations is higher than somatic mutations in both cases. By contrast, instead of point mutations, the HGSOC genome carries significant copy number variation due to genomic instability that results in the amplification or loss of many genes. Prominent genes undergoing focal amplification in HGSOC are *CCNE1*, *MYC* and *MECOM*. *PTEN*, *RAD51C*, *RAD15*, *ATM*, and *ATR*—components of the homologous recombination pathway have also been reported to be altered [17]. Aside from the impaired homologous recombination DNA repair pathway, other pathways chronically altered in HGSOC are RB1 (67%), PI3K/Ras (45%), and NOCTH (22%) [17].

Tothill *et al.* analyzed 285 predominantly high-grade serous ovarian tumor samples to identify molecular subtypes within the vast molecular diversity observed in large genomic datasets of ovarian cancer [24]. The authors segregated differential gene expressions in six clusters (C1-C6) and correlated with patient prognosis. Cluster C3 and C6 were described to be unrelated to HGSOC. Cluster 1 was characterized by reactive stromal signature and increased expressions of genes participating in extracellular matrix production, tissue remodeling, cell signaling, angiogenesis and cell adhesion. Histologically, tissues carrying C1 signature showed desmoplastic reaction characterized by myofibroblast infiltration within the stroma. Clinically, patients from whom the tumors representing the C1 cluster were obtained reported to have poor overall prognosis. C2 was described as “immunoreactive” due to enhanced expression of genes associated with immune cell activation and high percentage of tumor-infiltrating CD3+ T-lymphocyte present in tumor samples. C2 was associated with better overall survival. C4 was described to show low stromal response with a similar gene expression pattern to C2; however, these samples showed

enhanced CA-125. C4 was also correlated with a better prognosis. C5 demonstrated a mesenchymal feature with enhanced expression of certain *HOX* genes, high-mobility group members, WNT/catenin and cadherin signaling pathways. C5 was associated with poor overall survival [24]. Based on the finding of Tothill *et al.*, subsequent studies by the TCGA subcategorized HGSOC into four molecular subtypes: immunoreactive, differentiated, proliferative, and mesenchymal [17,25]. Similar to the previous study, the immunoreactive subgroup was associated with good prognosis, the mesenchymal and proliferative subtypes were associated with poor prognosis, and the differentiated subgroup was associated with an intermediary level of prognosis [25].

1.1.5 Tissue of origin in high-grade serous ovarian cancer

For decades, determining the precise source of origin of the most prevalent and fatal ovarian cancer subtype—HGSOC—has been debated. Initially, Fathalla *et al.* suggested the hypothesis of “incessant ovulation” characterized by the female ovulatory cycles undergoing chronic repair and regeneration promoting the ideal proinflammatory and pro-oxidative environment for carcinogenesis [26,27]. Multiple studies supported the idea that suppressing ovulation by pregnancy, breastfeeding, or the use of hormone-containing oral contraceptives, reduced the risk factor of developing HGSOC, which bolsters the hypothesis of the ovarian surface epithelium (OSE) as the primary source of HGSOC [26,28,29]. It has also been demonstrated that the OSE has the tendency to invaginate the surface of the ovary and create cortical inclusion cysts (CIC), which are exposed to hormonal changes sufficient for metaplastic transitioning [28].

Two findings contended the idea establishing metaplastic OSE as the root cause of HGSOC, which are: 1) Absence of any identifiable precursor lesion or *in situ* carcinoma in the

ovaries in a number of HGSOC patients [29,30]; 2) The histological resemblance of HGSOC tissue with the extra-ovarian tissues originating from the Müllerian duct, especially the fallopian tube [31]. Positive outcomes in risk-reducing prophylactic salpingo-oophorectomy in BRCA mutated patients suggest the possible involvement of the fallopian tube in the pathogenesis of HGSOC [16].

Piek *et al.* identified small dysplastic changes in the fallopian tube of BRCA mutation carriers [32]. These lesions were later described as serous tubular intra-epithelial carcinomas (STICs). STICs were described to be devoid of ciliated cells and located at the fimbriated region of the fallopian tube, close to the ovaries [28]. Studies showed 38% of BRCA mutant women carried STICs [33], and the frequent presence of p53 mutation and DNA damage marker γ H2AX within the STICs correlated with HGSOC incidence [30,34]. Kindelberger *et al.* demonstrated that 52% of patients in advanced stage HGSOC carry STICs, strengthening the claim of the fallopian tube as a source of HGSOC [34]. Karnezis *et al.* suggested the stem-like properties of the cells at the fimbriated end of the fallopian tube acts as a transitional zone, like that of the cervix, prone to carcinogenesis [35].

In order to better characterize the early precursor lesion in the risk-reducing salpingo-oophorectomy specimen of *BRCA* mutated patients, a new pathological protocol has been developed known as Sectioning and Extensively Examining the Fimbriated End (SEE-FIM), in which the tube is extensively sectioned and entirely submitted for histologic assessment. Routine SEE-FIM has helped to detect lesions preceding STIC, p53-signature, and serous tubal intraepithelial lesion (STIL) [36]. p53 signature bearing cells are normal-looking tubal epithelia that overexpress p53, whereas STIL shows cytological atypia that falls short of STIC [18,37,38]. While p53 signature, STIL, and STIC show similar strong and diffuse p53 immunorepression in

at least 12 consecutive secretory cells in the standard tissue section, the proliferation index measure by Ki-67 is much lower in p53 signature in STIL (<3%) than STIC (>10%) [36].

A new unifying theory connects both OSE and the fallopian tube as the primary source of HGSOC via a process called “endosalpingiosis”, where early implantation of secretory epithelial cells of the distal fallopian tube (FTSEC) within the OSE may lead to the incorporation of fallopian tube tissue in the cortical inclusion cysts (CIC) of the ovaries, promoting metaplasia [35,39]. Recently two studies indicated the dualistic origin of HGSOC (**Figure 1.2**). Zhang *et al.* reported the formation of HGSOC phenotype in genetically engineered mouse models carrying organoids generated from *RB* inactivated and *TP53* mutated fallopian tube epithelium (FTE) as well as OSE; however, the tumors derived from FTE and OSE carried distinct transcriptome and differential chemosensitivity patterns. Tumors originating from OSE showed longer latency on metastasis and lower penetrance to metastatic tissue [40]. Lo Riso and colleagues utilized a DNA methylation tracer to identify the variance between FTE and OSE, and correlated the identified criteria with formalin-fixed paraffin-embedded (FFPE) HGSOC tumor samples. The authors observed that the HGSOC cells from the FFPE samples retained DNA methylation trace of two different cells of origin: FTE and OSE [41], suggesting dual sites of origins for HGSOC.

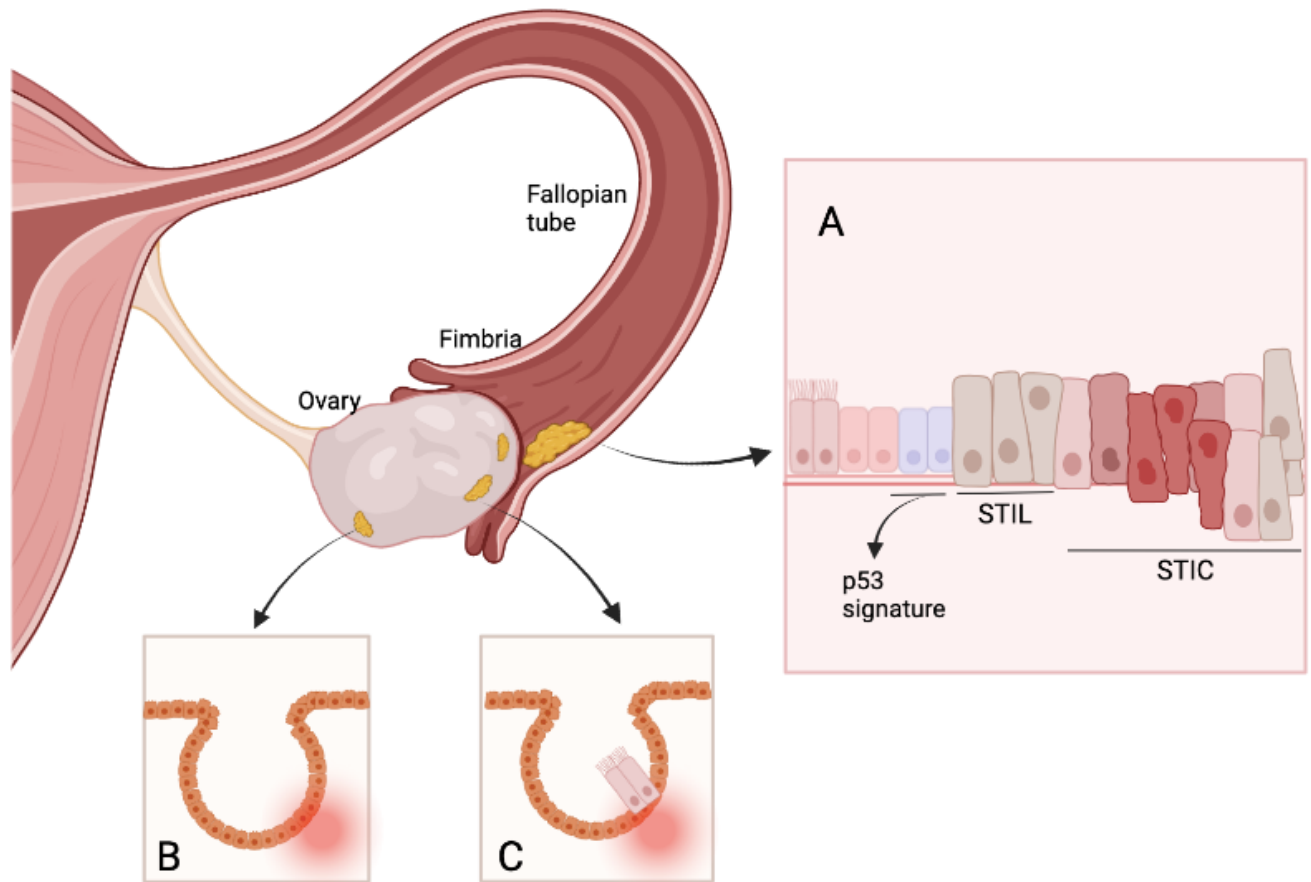


Figure 1.2: Origin of HGSOc: A. At the fimbriated end of the fallopian tube, precancerous lesion is formed. (From left to right) Normal tubal ciliated epithelium transitions by losing cilia, acquiring p53 signature (blue cells), forms serous tubal intraepithelial lesion (STIL) and serous tubal intraepithelial carcinoma (STIC). STICs can become invasive within the fallopian tube and can detach and invade surrounding tissues like the ovaries and the peritoneum. (B) Cortical inclusion cysts at the surface of the ovaries may undergo hormonal and inflammatory changes leading to metaplasia. (C) Early implantation of secretory fallopian tube epithelium in the cortical inclusion cyst, known as endosalpingiosis, may undergo metaplasia. (Diagram created on <https://biorender.com/>)

1.1.6 Staging of ovarian cancer

The Gynecologic Oncology Committee of FIGO revised the staging of ovarian cancer, which incorporated the ovarian, fallopian tube, and peritoneal cancers [42]. Previously, the staging protocol considered the ovary as the sole primary site for ovarian cancer, which confounded accurate diagnosis as many ovarian cancers may present without any primary lesion in the ovaries. Furthermore, incorporating the fallopian tube in the staging of ovarian cancer has been essential due to the emerging perspective establishing the fallopian tube as important primary sites of origin for more than 80% of cases of HGSOE [43].

Table 1.1 enlists the different stages of 2014 International Federation of Gynecology and Obstetrics staging classification of ovarian, fallopian tube, and peritoneal cancer [42].

Table 1.1: FIGO staging classification for cancer of the ovary, fallopian tube, and peritoneum

Stage	Staging criteria
Stage I	Tumor confined to ovaries or fallopian tube
IA	Tumor limited to one ovary with the capsule intact or fallopian tube; no tumor on the surface of the ovary or fallopian tube, no malignant cells in the ascites or peritoneal washing
IB	Tumor limited to both ovaries with the capsule intact or fallopian tubes; no tumor on the surface of the ovary or fallopian tubes, no malignant cells in the ascites or peritoneal washing
IC	Tumor limited to one or both ovaries or fallopian tubes with any of the following:
<i>IC1</i>	-Surgical spill
<i>IC2</i>	-Capsule ruptured before surgery or tumor on ovarian or fallopian tube surface
<i>IC3</i>	-Malignant cells in the ascites or peritoneal washings
Stage II	Tumor involves one or both ovaries or fallopian tubes with pelvic extension (below pelvic brim) or peritoneal cancer
IIA	Extension and/or implants on the uterus and/or fallopian tubes and/or the ovaries
IIB	Extension to other pelvic intraperitoneal tissues
Stage III	Tumor involves one or both ovaries or fallopian tubes, or peritoneal cancer, with cytologically or histologically confirmed spread to the peritoneum outside of the pelvis and/or metastasis to the retroperitoneal lymph nodes
IIIA1	Positive retroperitoneal lymph nodes only (cytologically/ histologically)

<i>IIIA1(i)</i>	-Metastasis up to 10 mm in the greatest dimension
<i>IIIA1(ii)</i>	-Metastasis more than 10 mm in the greatest dimension
IIIA2	Microscopic extra-pelvic (above the pelvic brim) peritoneal involvement with or without positive retroperitoneal lymph nodes
IIIB	Microscopic peritoneal metastasis beyond the pelvis up to 2 cm in greatest dimension, with or without metastasis to the retroperitoneal lymph nodes
IIIC	Macroscopic peritoneal metastasis beyond the pelvis more than 2 cm in greatest dimension, with or without metastasis to the retroperitoneal lymph nodes (includes extension of the tumor to the capsule of the liver and spleen without the parenchymal involvement of either organ)
Stage IV	Distant metastasis excluding peritoneal metastasis
IVA	Pleural effusion with positive cytology
IVB	Parenchymal metastases and metastases to extra-abdominal organs (including inguinal lymph nodes and lymph nodes outside of the abdominal cavity)

The 5-year survival rates of patients according to the stages, regardless of the histology, are as follows: 89% for stage I EOC, 71% for stage II EOC, 41% of stage III EOC, and 20% for stage IV EOC [44]. Unfortunately, symptoms are generally detected at the advanced stages in 75-80% of cases of EOC [19]. Only 13% of the serous ovarian cancers are diagnosed at the early stages: stage I or II. In the case of HGSOE, early detection of the disease results in 55% of patients with 10-year survival, whereas late-stage diagnosis leads to 15% of patients with 10-year survival [45].

1.1.7 Dissemination of ovarian cancer within the body

A unique feature of epithelial ovarian cancer (EOC) metastasis is the lack of spread through hematogenous or lymphatic routes like other cancers of epithelial origin. In particular, the spreading of HGSOE is orchestrated toward the adjacent organs within the peritoneal cavity by either direct extension or detachment of cells from the primary tumor [30]. Notably, there is no anatomical barrier between the fluid-filled peritoneal cavity and the tumors located in the ovaries or fallopian tubes, which could aid in restricting the spread of the disease through the transcoelomic

route [46,47]. Exfoliated cells from the primary tumor site become suspended in the peritoneal fluid and are spread through the passive force of gravity and diaphragmatic movement during respiration to reach the secondary deposit sites [30]. The fatty omentum has been documented to be the most invaded, approximately in 80% of HGSOC cases. The reliance of HGSOC cells toward β -oxidation of fatty acids has been demonstrated during co-culturing of adipocytes with ovarian cancer cells, which could explain the predilection for the omentum, wherein proinflammatory cytokines and IL-8 released from the adipocytes promoted homing and invasion of cancer cells [48].

The development of malignant ascites is a key presenting feature in advanced stage HGSOC, which has been correlated with secondary blockage of the lymphatic system and release of angiogenic factors promoting vascular permeability [30]. Release of vascular endothelial growth factor (VEGF) has been associated with the development of ascites during transcoelomic metastasis of EOC, and the use of VEGF antagonists reduced the volume of accumulated ascitic fluid and the frequency of required drainage of ascites [47,49,50].

One lingering question in the pathobiology of HGSOC has been understanding the role of the multicellular clusters found in the ascitic fluid of patients. Recently, it has been demonstrated that the three-dimensional floating clusters obtained from HGSOC patients during different stages of the disease are able to replicate the disease in animal models with histological features resembling HGSOC; this study indicates the necessity of considering the role of multicellular deposits and the interactions within the tumor microenvironment as a potential therapeutic target for HGSOC [51].

Understandably, hematogenous metastasis has been grossly disregarded in the metastasis of EOC due to the absence of disease in advanced-stage patients who received

peritoneovenous shunts spilling a considerable amount of tumor cells in the circulation [52]. However, the presence of cancer cells in the circulation of EOC challenges the existing paradigm of intraperitoneal dissemination only [53]. Furthermore, the recent emergence of *in vivo* studies has demonstrated that tail-vein introduction of ovarian cancer cells may preferentially deposit into the ovaries and replicate the clinical presentation of EOC, which underpins the need for further understanding of possible hematological dissemination in ovarian cancer [54].

1.1.8 Disease presentation of high-grade serous ovarian cancer

Early-stage EOCs are either asymptomatic or non-specific, which contributes to the delayed diagnosis. Aggressive EOC subtype HGSOE is rarely detected during early stages; the median age of diagnosis is 63 years in the US [12]. Patients typically present with abdominal pain, bloating, diarrhea or constipation, nausea, weight loss, and acid reflux. Depending on the spread of the disease, more symptoms may arise, like, fatigue, back pain, tenesmus, elevated urinary frequency, vaginal bleeding, and respiratory symptoms of cough and dyspnea. Specific signs in advanced stages include ascites, increased abdominal girth, palpable abdominal masses, and pleural effusion due to distant metastasis [13,19].

To date, no singular screening method has proven to be sufficiently effective in the early detection of EOC and contributing to reducing mortality [8]. Elevation of blood CA125—a transmembrane glycoprotein of the membrane-associated mucin class—in the blood plasma, along with positive transvaginal ultrasonography, has provided benefit in early detection, but failed to improve patient outcome [55,56]. Furthermore, early detection of heritable BRCA mutation and associated prophylactic salpingo-oophorectomy has been reported to be positive in preventing the onset of ovarian cancer [57]. An international collaborative endeavour has been in place for

developing an early detection methodology of endometrial and ovarian cancer. In this study, the authors analyzed DNA extracted from the fluid obtained during the routine Papanicolaou (PAP) test. Out of 245 ovarian cancer patients, 34% demonstrated early-stage disease. The group further reported that intrauterine sampling with a TAO brush—a small flexible brush utilized to span the entire inside of the uterus for a complete sampling of the endometrium [58] – showed higher detection than endocervical sampling with a PAP brush, which was 45% percent out of 51 ovarian cancer patients. Furthermore, circulating tumor DNA was assessed from the blood plasma of 83 ovarian cancer patients and 43% of them were reported to carry circulating tumor DNA. The authors suggested that the combination of PAP brush samples and plasma samples increases the sensitivity of detecting ovarian cancer [59].

Initial diagnosis is made via radio imaging by CT, MRI, or PET following pelvic and rectovaginal examination and transvaginal sonography [8]. Radio-imaging typically presents hyper-vascular peritoneal masses with omental or peritoneal nodules. Serum CA125 is usually significantly high in advanced-stage disease ranging 500-1000 U/mL; however, serial detection of CA125 has more prognostic value than its role in diagnosis. Following the initial favourable response to platinum-based drugs, CA125 is decreased; however, a relapse of disease is usually associated with re-elevation of CA125 in the serum. As long as the patient remains sensitive to platinating agents, CA125 is decreased following each chemo-cycle; however, elevated CA125 despite re-challenging with platinum indicates initiation of clinical resistance to platinum-based treatment [8,23].

1.1.9 Treatment modalities of high-grade serous ovarian cancer

1.1.9.1 Surgery

Surgery followed by cytotoxic chemotherapy is the mainstay treatment protocol for HGSOC. Upon initial diagnosis of the disease, debulking surgery is performed that involves laparotomy through a midline incision, with a full exploration of the abdominal cavity in an attempt to remove all the visible tumor growth with concomitant hysterectomy, salpingo-oophorectomy and omentectomy [60]. The aim of the surgery is to achieve complete resection, which is defined by the absence of any macroscopic residual disease. The aggressive surgical technique also involves systematic dissection of the pelvic and para-aortic lymph nodes; however, the recent LION (Lymphadenectomy In Ovarian Cancer) study suggested the omission of the resection of clinically negative lymph nodes to reduce postoperative morbidity and mortality in patients with advanced EOC [61]. The debulking surgery in HGSOC is performed preferably by a gynecologic oncologist, not by a general surgeon, if feasible, as the level of macroscopic residual disease has been established as the most relevant prognostic factor of progression-free survival (PFS) and overall survival (OS) [8]. In practice, due to the prevalence of patients presenting initially with advanced metastatic disease, achieving complete resection is difficult, and the objective of the surgeon is to establish the optimal degree of cytoreduction—defined by the presence of residual cancer with a diameter no more than 1 cm. The presence of any macroscopic disease with a diameter greater than 1 cm is termed as suboptimal cytoreduction [8,60]. In 2009, Du Bois *et al.* conducted a meta-analysis of three clinical trials on patients receiving debulking surgery (AGO-OVAR 3, 5, and 7), and observed a 63.5% and 70.1% reduction in the survival of patients receiving optimal and suboptimal cytoreduction, respectively, in comparison with the patients receiving complete resection [62]. The superiority of complete resection over optimal and suboptimal

cytoreduction resulting in improved patient survival was further proven in subsequent analyses of newer clinical trials [63-65].

Due to extensive disease or logistical inaccessibility, the primary debulking surgery may be withheld, and the patients are generally treated with three cycles of chemotherapy prior to the surgery. The practice of chemotherapy before surgical reduction of tumor is known as neoadjuvant chemotherapy (NACT), and the debulking surgery after NACT is termed as interval debulking surgery (IDS) [60]. Two randomized trials indicated no survival benefits between primary debulking surgery and IDS [66,67]; however, criticism has been arisen due to potential recruitment bias of advanced-stage patients and low frequency of complete resection [60]. As such, an additional clinical trial is ongoing to assess the efficacy between NACT followed by IDS and primary debulking surgery with complete resection (NCT02828618), in order to fine-tune the current surgical protocol.

The prospect of secondary debulking surgery in patients having a recurrence of the disease has been debated. In randomized trial DESKTOP III/ ENGOT OV20, patients with a relapsed disease but still sensitive to traditional chemotherapy, showed improved survival by 5 months when complete resection was achieved than the patients without undergoing surgery [60,68]. However, in the Gynecology Oncology Group (GOG) 0213 study on patients with platinum-sensitive recurrence treated with targeted therapy bevacizumab, patients with secondary surgery showed no survival benefit over the patients without surgery [69]. Since the inclusion criteria and study protocol varied between these two trials, the benefit of secondary surgery in recurrent EOC needs to be further evaluated in newer studies. In an alternate approach, studies are ongoing to test the feasibility of imaging and laparoscopy to achieve resection and surgical staging during the management of EOC patients [70-72].

1.1.9.2 Evolution of systemic therapy in ovarian cancer

Patient management of EOC with surgery is associated with systemic therapy, which has been evolved extensively over the years. The chronology of adapting systemic therapies started when ovarian cancer was successfully treated with cytotoxic chemotherapy [8]. In the 1950s, the first class of chemotherapeutic drugs introduced in the treatment regimen were alkylating agents. The alkylating agents added bulky alkyl groups to guanine nucleotide bases, physically inhibiting the DNA synthesis and causing DNA damage response. Some important alkylating agents used in ovarian cancer are melphalan, thiotepa, and cyclophosphamide [73]. Later, other types of cytotoxic agents were introduced in the treatment regimen of ovarian cancer, namely, methotrexate, 5-fluorouracil, doxorubicin, and hexamethylmelamine [74]. Initially, the mentioned cytotoxic agents were used as a single agent; however, it was soon realized that combining different therapies having diverse mechanistic approaches may provide with synergistic benefits and may reduce the risk of chemoresistance. The common combination regimen used to treat ovarian cancer prior to the 1970s consisted of cyclophosphamide and doxorubicin, with the addition of methotrexate and 5-fluorouracil [74].

The discovery of the biological functions of cisplatin drove a paradigm shift in the systemic therapeutics of many cancers, including that of the ovaries. Cisplatin—*cis*-diamminedichloroplatinum—is a platinum compound originally synthesized by Michele Peyrone in 1845, hence known as Peyrone’s salt [75]. In 1965, Dr. Barnett Rosenberg discovered the growth inhibitory properties of cisplatin on *Escherichia coli* [76] and, by 1968, he demonstrated marked regression of murine sarcoma-180 in response to non-lethal dosing of cisplatin at 8 mg per kg [77]. Following Dr. Rosenberg’s experiment, interest around cisplatin gained traction, and the first

cancer patient was treated by 1971—ultimately leading to the first approval against testicular and bladder cancers by the US Food and Drug Administration (FDA) in 1978 [75].

In 1976, cisplatin demonstrated considerable efficacy in a phase II study in patients with advanced adenocarcinoma of the ovary refractory to the then conventional chemotherapy. 9 out of 34 patients showed therapeutic responses ranging from 3 to 15 months [78]. From 1984 to 1986, multiple randomized clinical trials were conducted in patients with ovarian cancer, which tried combining cisplatin with the conventional chemotherapeutic regimen available at the time [79-82]. In 1986, a phase III trial conducted by the Gynecologic Oncology Group (GOG) tested the efficacy of cyclophosphamide and doxorubicin with or without cisplatin in EOC patients, where the cisplatin receiving group showed nearly doubled complete response rate and progression-free survival (PFS), and better overall survival (OS) compared to the group not receiving cisplatin [81]. Later, the same group demonstrated that the combination of cisplatin and cyclophosphamide was equally effective with or without doxorubicin against EOC, displacing doxorubicin from the existing treatment protocol [82]

In the late 1980s, the group of drugs called taxanes, isolated from the bark of the pacific yew tree (*Taxus brevifolia*), were emerging as cancer therapeutic—of which paclitaxel was the prototypical drug [83]. The taxanes inhibit the depolymerization of the β tubulin, leading to the stabilization of the microtubular cytoskeleton and halting the formation of the mitotic spindle [83,84]. As a result, the treated cells undergo mitotic failure, accumulating in the metaphase [85]. It is believed that the microtubule-stabilizing effect is associated with taxane-mediated cell death [86]. Paclitaxel showed promising efficacy against ovarian adenocarcinoma by 1992 [87]. In a landmark study in 1996, ovarian cancer patients were treated with either cisplatin or cyclophosphamide with or without paclitaxel. The cisplatin-paclitaxel group demonstrated better

PFS, OS and higher response rate, prompting the displacement of cyclophosphamide in the ovarian cancer treatment regimen [88]. In the meantime, due to the increasing toxicity of cisplatin, a new platinum derivative, carboplatin, has been developed as a better alternative resulting in improved renal function [89]. Finally, in subsequent clinical trials, patients were tested with carboplatin or cisplatin with or without paclitaxel [90-93], and the combination of carboplatin or cisplatin with paclitaxel has been established as the standard of care since then [74].

1.1.9.3 Modes of administration of systemic therapy and associated toxicity

Ovarian Cancer Practice Guideline by the National Comprehensive Cancer Network (NCCN) provided the latest recommendations for treating HGSOc patients following upfront primary debulking surgery [94]. For stage I disease, paclitaxel and carboplatin combination is preferred. The standard dosing is paclitaxel 175 mg/m² intravenously over 3 hours followed by carboplatin area under the plasma concentration-time curve (AUC) 5-6 intravenously over 30 minutes. The cycle is repeated every 3 weeks for 6 cycles [94]. For stage II to stage IV diseases, intraperitoneal (IP) or intravenous (IV) drug administration can be performed. The IP protocol is paclitaxel 135 mg/m² IV over 3 hours or continuous infusion over 24 hours on day 1, followed by cisplatin 75-100 mg/m² IP infused as rapidly as possible via IP port on day 2. On day 8, paclitaxel 60 mg/m² IP infusion is given via IP port as rapidly as possible. This cycle is repeated every 3 weeks for 6 cycles. The IV protocol for stage II to IV HGSOc recommends paclitaxel 175 mg/m² IV over 3 hours followed by carboplatin AUC 5-6 IV over 30-60 minutes, every 3 weeks for 6 cycles. Variations of these protocols are: 1) paclitaxel 80 mg/m² over 1 hour on days 1, 8, and 15. Carboplatin is given on day 1 following paclitaxel, AUC 5-6 over 30-60 minutes. The cycle is repeated every 3 weeks for 6 cycles; 2) paclitaxel 60 mg/m² over 1 hour followed by carboplatin

AUC 2 IV over 30 minutes, weekly for 18 weeks [94]. Variations of the existing protocol are provided in the NCCN guideline for adjustment with patients' needs and to be administered under physicians' discretion, which include different dosage and scheduling as well as other drug combinations; however, platinum derivatives are considered the base drugs for all protocols of systemic therapy for HGSOC [94].

Although the current NCCN guideline suggests the use of carboplatin for HGSOC patients because of its low toxicity profile, cisplatin is still administered routinely throughout the world, and the target concentration is 75 mg/m² [60]. The current therapeutic protocol has been established from the inferences of multiple clinical trials aimed at optimizing the combination of multiple drugs. Bookman *et al.* suggested from a 5-arm phase III randomized controlled trial combining paclitaxel and cisplatin regimen with either gemcitabine, pegylated liposomal doxorubicin, or topotecan, that doublet chemotherapy is optimal [95]. Weekly dose-dense chemotherapy with paclitaxel with carboplatin once every three weeks showed promising improvement in PFS and OS in Japanese women [96,97]. However, two similar studies, the Multicenter Italian Trials in Ovarian Cancer (MITO-7), and the ICON8 (NCT01654146), did not recapitulate the improvement of PFS, indicating possible inter-racial variation of sensitivity toward platinum-paclitaxel therapy [98,99]. In the GOG-0262 study, (NCT01167712) weekly dose-dense paclitaxel and carboplatin once every three weeks was given with or without antiangiogenic agent bevacizumab. The arm not receiving bevacizumab resulted in a small improvement of PFS of 3.9 months [100].

A classic presentation of advanced stage HGSOC is intraperitoneal dissemination; as such, it is conceivable that direct exposure of the intraperitoneal metastatic deposits toward chemotherapy might be beneficial. Studies have shown a 20-fold increase in the local

concentration of cisplatin and a 1000-fold increase in the local concentration of paclitaxel through the IP route [101,102]. Several randomized trials showed significant improvement in PFS and OS through IP administration [103,104]; however, trials giving cisplatin at a dose of 100 mg/m² showed significant toxicity in patients [105]. As such, the cisplatin IP dose has been targeted at 75 mg/m² up till now [60], since the first recommendation of IP cisplatin by the US National Cancer Institute in 2006 [106]. Replacing cisplatin for carboplatin for IP infusion improved the tolerability; however, it is yet to be cleared whether the regimen is as efficacious as IP cisplatin infusion [104]. A randomized, multicenter phase III trial on 245 patients demonstrated the efficacy of adding a cycle of hyperthermic IP chemotherapy (HIPEC) to the abdominal cavity at the time of surgery. The median recurrence-free survival of the group receiving cytoreductive surgery without HIPEC was 10.7 months, whereas it was 14.2 months in the group undergoing surgery with HIPEC. The median OS in the non-HIPEC group with surgery was 33.9 months, whereas the median OS in the HIPEC group with surgery was 45.7 months [107]. Nevertheless, IP administration of cisplatin induces considerable toxicity, although the benefits outweigh the risks in advanced patients, and routine hydration with supplemental electrolytes pre- and post-administration of cisplatin is recommended [94]

Administration of cisplatin is associated with several toxic reactions to the patients and requires additional management pre- and post-chemotherapy. Standard-dose (50-100 mg/m²) IV cisplatin undergoes a rate of elimination of 25% within 24 hours and 50% within 5 days, among which 90% of elimination is achieved through renal excretion [108]. Single dose of 50 mg/m² results in renal toxicity in 28-36% patients [109]. Hydration with at least 3 liters of isotonic saline solution per day and post-hydration mannitol reduces the risk of renal failure due to cisplatin-induced renal injury [108]. Antioxidants selenium and vitamin E have been suggested to reduce

cisplatin-induced reactive oxygen species (ROS) associated ototoxicity [110], hepatotoxicity [111] and neurotoxicity [112]. Marked nausea and vomiting is expected in most of the patients, with diarrhoea, loss of appetite, metallic taste, and mucositis [109]. Supportive medications for gastrointestinal side effects are famotidine, ondansetron, olanzapine, and aprepitant. To reduce allergic reactions, dexamethasone and diphenhydramine are added. Routine administration of magnesium sulphate is preferred to avoid hypomagnesemia [113].

1.1.9.4 Treatment of relapsed and resistant disease

Approximately 80% of HGSOc patients develop relapsed disease after the first administration of platinum-based chemotherapy, among which almost 50% remain responsive to platinum [13]. However, the sensitivity to platinum eventually diminishes over time, leading to platinum-resistant disease [8,13]. By definition, a platinum-free interval for more than 6 months is known as platinum-sensitive disease, whereas a platinum-free interval of less than 6 months is considered platinum-resistance [60]. During remission, 2 to 4 monthly follow-ups of CA-125 is performed to monitor for disease relapse [13]. The disease can be asymptomatic at the beginning, despite an increment of the level of CA-125, which is considered as an early sign of disease relapse [13]. The doubling of CA-125 level above the upper limit of normal is confirmatory for disease relapse [114]. Rustin and colleagues have shown no improvement in patient outcome if standard therapy is re-commenced early during the asymptomatic phase, compared to delayed treatment [115]. Unless the disease has recurred with a discrete, localized mass diagnosed through radioimaging, a second cytoreductive surgery is not common [8]. Palliative surgery is required in some patients to relieve intestinal obstruction [114]. In platinum-sensitive patients, standard platinum-based therapy can be re-initiated; however, it may lead to a potential life-threatening

platinum hypersensitivity reaction [13]. In platinum-resistant patients, disease recurrence is managed by salvage therapy with a 10-15% average response rate and PFS of 3-4 months. Salvage therapy is provided with the use of the following drugs: pegylated liposomal doxorubicin, topotecan, gemcitabine, etoposide, and vinorelbine [13].

1.1.9.5 Targeted therapy

The principle of targeted therapy is based upon targeting altered signaling pathways leading to cancerous changes in normal cells. Two small-molecule inhibitors have been approved as targeted therapies against HGSOc: poly (ADP-ribose) polymerase (PARP) inhibitors and bevacizumab [60]. Bevacizumab, a humanized monoclonal antibody against vascular endothelial growth factor (VEGF), was approved for ovarian cancer on June 13, 2018 by the FDA [116]. Bevacizumab, acting as an antiangiogenic agent, has proven to be effective in reducing ascites due to VEGF induced capillary leakiness [60]. Two landmark trials prompted the approval of bevacizumab for ovarian cancer: GOG0218 [117] and ICON7 [118], showing significant improvement in PFS to concurrent and maintenance administration of bevacizumab. In the ICON7 trial, the high-risk group with inoperable stage III and stage IV disease showed maximum benefit with a median overall survival of 9 months with bevacizumab therapy [119]. A recent randomized phase III trial MITO16B-MaNGO OV2B-ENGOT OV17 suggested that bevacizumab increases PFS at recurrence, following initial first-line therapy including bevacizumab [120]. Pujade-Laurine and colleagues reported significant improvement in PFS during platinum-resistant recurrence when bevacizumab was given with weekly paclitaxel, doxorubicin, or topotecan [121]. Despite beneficial effects, bevacizumab induces considerable toxicities resulting in delayed wound healing, bowel perforation and fistula formation, and hypertension [60].

Other antiangiogenic agents currently on trials are pazopanib, sorafenib, sunitinib, cediranib, aflibercept, and AMG386 [60]. Among these, cediranib has shown single-agent activity in both platinum-sensitive and -resistant disease and has shown improved PFS when combined with the standard cytotoxic therapy or as maintenance therapy [122,123].

PARP inhibitors utilize the phenomenon of “synthetic lethality”, where the loss of function of a single gene is withstood by the cells; however, additional loss of function of another gene results in lethality [124]. PARP enzymes are required for base excision repair (BER) of DNA single-strand breaks (SSB). Inhibition of PARP results in the accumulation of a multitude of SSBs, which leads to the collapse of the replication forks and ultimately leads to the DNA double-strand breaks (DSB) that need to be repaired by homologous recombination [125]. A majority of HGSOc patients are deficient in the homologous recombination DNA damage repair pathway, especially the group harbouring mutations to the genes *BRCA1/2*—important mediators of the homologous recombination pathway [126]. Several PARP inhibitors are available for the treatment of HGSOc: olaparib, niraparib, and rucaparib [60]. Early phase I trial showed a 28% radiologic response in patients receiving 200 mg olaparib twice daily [127]. Subsequent phase II trial suggested better efficacy of olaparib than pegylated liposomal doxorubicin in *BRCA1* mutated patients [128]. A second phase II study reported a 50% objective response rate in *BRCA*-wild type cohort of recurrent HGSOc and a 60% objective response rate in *BRCA*-mutated cohort of platinum-sensitive recurrent HGSOc [129]. In 2014, olaparib was approved by the European Medicines Agency (EMA) for use as a maintenance therapy in platinum-sensitive recurrent disease in *BRCA* mutated patients [13]. A phase III study SOLO2 also confirmed the efficacy of olaparib as maintenance therapy in *BRCA* mutant patients with platinum-sensitive recurrent disease [130]. Based on two clinical trials, rucaparib and niraparib have been approved to treat relapsed HGSOc

irrespective of *BRCA* mutations. In these phase III trials, rucaparib and niraparib were administered as maintenance therapy, which prolonged the PFS of both *BRCA* wild type and *BRCA* mutant patients of platinum-sensitive recurrent HGSOc disease [131,132].

1.1.10 Emergence of platinum-resistance in cells

Cisplatin resistance phenotype may develop at different levels of the mechanism of action of cisplatin. The anti-cancer mechanism of cisplatin can be divided into two modules: cytoplasmic and nuclear [133]. Plasma-resident cisplatin enters the cells via passive diffusion or active transport by copper transporter protein (CTR1) [134]. Within the cells, the chloride concentration is lower (4-20 mM) than that of the extracellular milieu (100 mM), which causes displacement of the chlorides within the cisplatin molecule by water—a process known as aquation [135]. Mono- and di-aquated cisplatin are active compounds and potent electrophiles, which can bind with endogenous nucleophiles like reduced glutathione (GSH), metallothioneins, cysteine residues of intracellular proteins, methionine, etc.; exhausting the cytoplasmic reduced equivalents and inducing oxidative stress [133]. Parallely, the intracellular antioxidant system inactivates the aquated cisplatin [133].

Inside the nucleus, aquated cisplatin can bind with the DNA with a predilection for the N7 site of the imidazole ring of guanine, leading to the formation of platinum-DNA mono-adducts, intra- and interstrand adducts [75,136]. Previously, most of the cisplatin-induced cytotoxicity had been attributed to platinum-DNA adducts, especially 1,2-intrastrand ApG and CpG crosslinks [137]; however, it has been proven afterwards that only 1% of cisplatin can bind with genomic DNA [138], and cisplatin is also cytotoxic within the cells without the nucleus—containing only the cytoplasm, likely by targeting the mitochondria [139]. The formation of platinum adducts

creates distortion of the DNA recognizable by multiple DNA damage repair systems, especially the nucleotide excision repair (NER) and the mismatch repair (MMR) systems [133]. Initially, and when the damage is not extensive, cells are arrested at the S and G2 phase of the cell cycle to maintain DNA integrity and halt mitosis [140]. However, cisplatin-induced irreparable DNA damage leads to apoptotic death, which involves the activation of the ataxia telangiectasia, mutated (ATM) and RAD3-related protein (ATR) and their downstream effector checkpoint kinase 1 (CHK1). CHK1 phosphorylates the tumor suppressor protein p53 at serine 20, which stabilizes the protein [141]. Activated p53 leads to activation of cell death through a variety of mechanistic pathways, which may involve mitochondrial outer membrane permeabilization or death receptor mediated signaling [142,143]. Cisplatin adducts have also been shown to modulate p73, JUN-amino terminal kinase (JNK), and p38 mitogen-activated protein kinase [133].

Pre-target resistance to cisplatin may arise due to decreased intracellular accumulation of cisplatin or enhanced intracellular sequestration of cisplatin [133]. Knockdown of CTR1 in mouse embryonic fibroblasts led to decreased accumulation of cisplatin [134]. Holzer and Howell demonstrated that clinically relevant concentrations of cisplatin mediate the downregulation of CTR1 via proteasome-mediated degradation, which may contribute to acquired cisplatin resistance [144]. Over the past decade, multiple transporters for intracellular cisplatin influx have been proposed, like, OCT2, OCTN1, OCTN2, volume regulated anion channels (VRAC), and their roles in cisplatin resistance are emerging [145]. For instance, VRACs are composed of leucine-rich repeat containing 8 (LRRC8) motifs [146]. A CRISPR-Cas9 mediated genome-wide knockout screen for cisplatin resistance in *BRCA1*-mutated ovarian cancer cells showed a significant hit on LRRC8D [147]. Among the multidrug-resistant proteins (MRP), MRP2 has shown significant efflux of cisplatin from the cisplatin-resistant cells [148]. Sequestration of cisplatin by intracellular

antioxidant reserves limits the level of reactive cisplatin. As such, elevated GSH, glutathione *S*-transferase and γ -glutamylcysteine synthetase have been associated with cisplatin resistance [133].

On target resistance to cisplatin is mediated by the repair of intra- and inter-strand DNA adducts of cisplatin, which can be achieved by increased recognition of adducts, increased rate of reparation, or increased tolerability to cisplatin-induced DNA lesions [133]. The majority of cisplatin-mediated intra-strand DNA lesions are removed by NER to maintain DNA integrity [133]. Among at least 20 protein participants in NER, the role of ERCC1 has been extensively studied, which forms a heterodimer with ERCC4 and incises DNA at the 5' end of the bulky cisplatin-induced DNA lesion [149]. ERCC1 has been negatively correlated with cisplatin sensitivity in multiple neoplasms [133]. The MMR system can also participate in cisplatin-induced DNA damage repair [133]. Mutations in genes involved in MMR pathways, especially *MSH2* and *MLH1*, have been implicated in acquired cisplatin resistance in multiple studies [133]. Translesion synthesis, a replicative bypass process, has been implicated in the continuation of DNA replication in spite of the cisplatin-induced DNA lesion [145]. Wojtaszek *et al.* demonstrated that a small molecule that inhibits translesion synthesis may increase cisplatin sensitivity [150].

Inter-strand DNA adducts by cisplatin can lead to double-strand breaks and induce the homologous recombination (HR) DNA damage repair pathway [133]. HR deficiency, especially via mutation of *BRCA1* and *BRCA2*, has been reported to confer cisplatin sensitivity to cancer cells [151]. Sakai *et al.* demonstrated that restoration of HR proficiency via secondary mutation in the *BRCA2* gene was responsible for 50% of cisplatin-resistant clones of pancreatic cancer cells *in vitro* [152]. Furthermore, in mouse models of *BRCA1*-deficient mammary tumor, the maximum tolerated dose of cisplatin was not able to elicit secondary drug resistance, implicating a major role of HR deficiency in cisplatin sensitivity [153,154]. Pajic *et al.* suggested that drug-tolerant cells

remained in a quiescent state in the *BRCAl*-mutated tumor, which was not completely eradicated by the maximum tolerated dose of cisplatin. Tumor regrowth eventually happened from the drug-tolerant cells; however, the cisplatin sensitivity persisted due to HR deficiency [154]. On the other hand, Cooke *et al.* reported that drug-resistant clones preexist in the heterogenous ovarian tumor mass without giving rise to newer mutations for acquired resistance [155].

Post-target resistance may be elicited due to alteration of signal transduction pathways required for apoptosis in response to DNA-damage response [133]. Elevated levels of antiapoptotic proteins Bcl-2, Bcl-xL, and Mcl-1 have been correlated with cisplatin resistance in squamous cell carcinoma of the oropharynx [156] and non-small cell lung carcinoma [157]. Increased level of caspase inhibitory protein survivin has been negatively correlated with cisplatin response and patient outcome [133]. Furthermore, survival pathways, such as – autophagy and activated PI3K/AKT, can also confer non-specific resistance to cisplatin [133].

Recent reports indicate novel resistance mechanisms toward cisplatin elicited by tumor microenvironment and the immune system [145]. Wang *et al.* demonstrated that cancer-associated fibroblasts (CAF) protected the cancer cells from cisplatin-induced apoptosis in tumors harboring both cancer cells and CAFs; the mechanism involved the release of glutathione and cysteine from the CAFs [158]. Cells from innate and adaptive immune system can also modulate the sensitivity to cisplatin [145]. For instance, in a co-culture of tumor cells with monocytes, cisplatin and carboplatin activated IL-10 secreting M2 macrophages, which activated the tolerogenic STAT3 pathway [159]. Furthermore, CpG oligonucleotides, which are agonists of toll-like receptor 9, increased the anti-tumor effects of cisplatin by downregulating DNA repair genes, *XPC*, *XRCC6*, *XRCC2* [160].

1.2 Prospect of drug repurposing in developing novel and adjunct chemotherapy

The drug discovery and development pipeline underwent massive improvement over past decades by structure-based drug discovery, launching of newer biotechnology companies, increased R&D investment and expenditure in pharmaceutical companies [161]. However, the current scenario of cancer drug development is not adequate to the real-life need of the patients. Out of 5000-10000 prospective anti-cancer drug candidates, only one receives approval from the United States Food and Drug Administration (FDA), and 5% of the cancer-related drug compounds may be ready for entering a Phase 1 trial [162]. Most of the currently available cancer drugs are still highly expensive with minimal improvement to the overall patient survival and are associated with multiple side effects and possible drug resistance, which necessitates alternative efforts for drug development [163,164].

Drug development comprises of design and production of compounds, examining the efficacy, toxicity, pharmacokinetic, and pharmacodynamic profiling on *in vitro* and *in vivo* studies, prior to testing the efficacy in humans in four Phases (I-IV). Most drugs fall short on efficacy in the Phase II trials, despite proving efficacy in the Phase I trial, which likely means that the drug did not hit the target effectively during Phase II [161]. However, diverse diseases demonstrate common molecular origins, which suggests that almost 90% of the approved drugs and the compounds that nearly missed approvals could provide secondary off-target efficacy to newer indications [161]. The strategy to provide newer indications to already approved and market-available drugs is called drug repositioning, drug repurposing, therapeutic switching, indication switching, drug reprofiling, etc. This strategy has garnered considerable attention over the past decades. The advantage of drug repurposing is that the pharmacokinetics, pharmacodynamics, and toxicity profiles of the drugs are already approved via preclinical and Phase I studies, allowing

rapid translation into Phases II and III clinical studies [161,165]. Currently, basic drug development requires an average of 13 years of research (**Figure 1.3**), and an investment of US\$1.8 billion for transitioning a single chemical compound from the bench to the patient's bedside [166]. The prospect of drug repurposing significantly reduces the time and associated cost, providing chances to the pharmaceutical companies to maximize their return on investments. It has been estimated that the rate of molecular entities that enter the market through a regular drug development route is 10% and 50% from Phase II and Phase III clinical trials, respectively, whereas the rates are 25% and 65% for repurposed compounds [161].

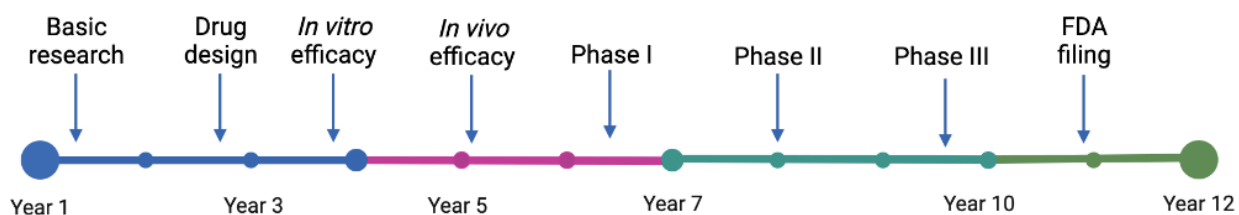


Figure 1.3: Estimated time required for each step of drug development. Major steps of drug development are basic research, drug design, preclinical toxicity and efficacy testing *in vitro* and *in vivo*, and human trials up to FDA filing. Modified from [161].

The idea of drug-repurposing is not new, and historically a handful of drugs have been repurposed to the market for newer indications. A derivative of glutamic acid, thalidomide, was initially approved in the 1950s to be used as sedative-hypnotic to tackle morning sickness during pregnancy [167]. However, in 1961, the drug was withdrawn from the market due to reports of widespread teratogenic effects [168]. Further investigations associated antiangiogenic [169] and DNA-damaging properties [170] of thalidomide with the lethal teratogenic effect; however, paradoxical implication of the anti-angiogenic effect of thalidomide was described in case of

refractory myeloma by Singhal and colleagues [171]. As such, a large number of multicenter clinical trials were launched to test the anti-cancer efficacy of thalidomide, leading to its approval by the FDA for multiple myeloma [167]. Similarly, a synthetic steroid mifepristone was developed in the early 1980s as an inhibitor of the glucocorticoid receptor to treat Cushing's syndrome [172]. However, during preclinical assessment, mifepristone—then termed RU-38486—was found to terminate pregnancy [173], rapidly acquiring a different identity as an abortifacient drug. It was discovered that mifepristone exerted its abortifacient activity by inhibiting the uterine progesterone receptors [174], which led to its fast FDA approval for medical termination of pregnancies in 2000 in combination with prostaglandin analogues [175]. After 12 more years, mifepristone was finally approved for its initially intended use—Cushing's syndrome, on February 12, 2012 [175]. In another example, systematic review and meta-analyses indicated that chronic usage of metformin had been associated with lower risk and incidences of diverse cancers in diabetic patients [176]. Metformin has been in use to manage type II diabetes for over four decades and has been shown to activate a key regulator of cellular metabolism, the AMP-activated protein kinase (AMPK), which is a negative regulator of mammalian target of rapamycin (mTOR)—a master gene for cancer cell survival [161]. Metformin has been shown to downregulate mTOR via activating AMPK [177] as well as Ras-related GTPase (Rag) [178], which may contribute to its secondary anti-cancer effects. With a daily dosage of 500 mg/day, which is within the range of anti-diabetic dosing (250-500 mg/day), a reduction in the incidence of gastroenterological cancers in diabetic patients has been reported [179]. Moreover, the discovery and approval of bortezomib (BZ) for cancer is another success story of rapid translational research of chemical compounds—originally developed for a different indication. Bortezomib is a boronic acid compound with the propensity to bind with the 26S proteasomal subunit, which can specifically diminish the chymotrypsin-like activity of the

proteasome [180]. The development of bortezomib, the first in class proteasome inhibitor, was part of a project led in the company Myogenics in 1993, which focused on targeting the ubiquitin-proteasome pathway to inhibit cancer-related muscle wasting (cachexia) due to fast protein degradation [181]. Prior to that, drugs containing the boronate group were generally disregarded within the medicinal chemists, due to failed phase II trials as anti-inflammatory agents against emphysema. However, in the meantime, bortezomib was proven efficacious against tumor models of lung cancer by reducing the tumor size and metastasis. Thus, the focus of bortezomib was shifted towards its anti-cancer properties, especially via inhibiting the NF- κ B pathway [180]. Bortezomib was one of the compounds which were fast-tracked within a record time for the approval against relapsed or refractory multiple myeloma in 2003 [181]. To date, usage of bortezomib has been further approved for previously untreated multiple myeloma, light chain amyloidosis, lymphoplasmacytic lymphoma, mantle cell lymphoma, and peripheral T-cell lymphoma. Bortezomib is also potentially effective against other hematologic malignancies like acute myeloid leukemia, acute lymphoblastic leukemia, diffuse large B-cell lymphoma, and plasmablastic lymphoma [180].

Parvathaneni and colleagues have aptly divided the repurposing approaches into two broad categories: 1) Serendipitous, and 2) Hypothesis driven (**Figure 1.4**) [165]. Repurposing of sildenafil—an anti-hypertensive drug of the group phosphodiesterase type 5 inhibitor group—has been a classic example of a coincidental finding of novel usage, which was later FDA approved for erectile dysfunction disorder and pulmonary hypertension [182]. Hypothesis-driven repurposing approaches are considered more structured and can be divided into two more subcategories: 1) Experimental approach, and 2) Computational approach. Experimental approaches include binding assays and phenotypic approaches. Targets enabled through proteomics and mass

spectrometry can be further validated by utilizing binding assays to determine newer therapeutic indications. For instance, quinone reductase 2—a new target determined for tyrosine kinase inhibitor crizotinib—is considered a binding partner of acetaminophen in cell culture [165]. The phenotypic approach utilizes traditional *in vitro* and *in vivo* disease modeling to determine newer indications and mechanisms of action for approved drugs. One recent example of the phenotypic approach for screening a compound library is identifying the filopodia inhibiting properties of L-type calcium channel blocker anti-hypertensive drugs within cancer cells to prevent cancer cell invasion [183]. Computational approaches involve data mining and bioinformatic analyses to determine newer usage for available chemical compounds. The approach can be more focused as being drug-centric and target-centric, or can start from a larger data set in knowledge-based, pathway- or network-based and genetic-signature based approaches (**Figure 1.4**) [165]. In our current study, we employed a hypothesis-driven experimental phenotypic approach to repurposing the anti-infective agent nelfinavir against HGSOc, based on the available information on the anti-cancer properties of nelfinavir [1].

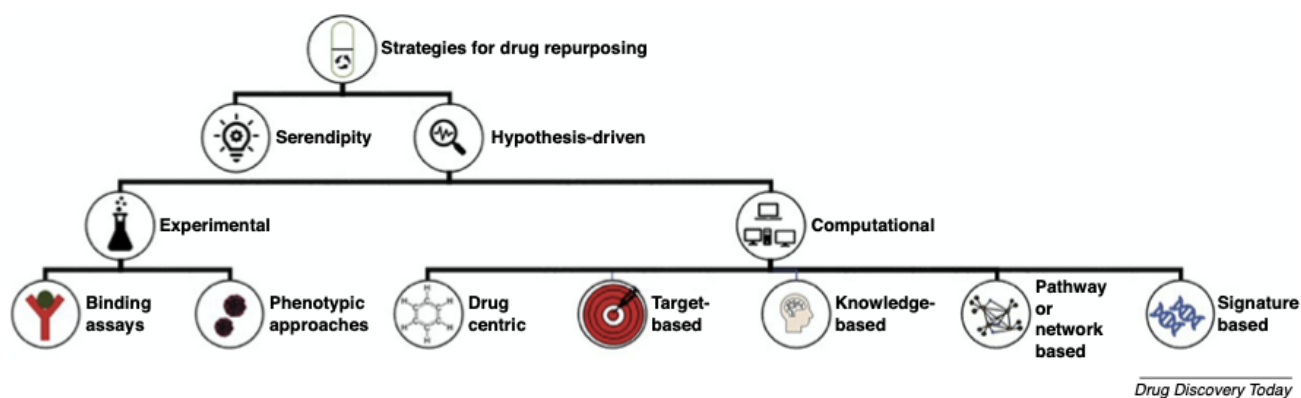


Figure 1.4: Schematic representation of multiple approaches to repurpose drugs. Adopted from [165]

The prospects of repurposing drugs come with its own set of positive significances as well as challenges. On one hand, approval for newer indications broadens the scope of better managing patients who are suffering from orphan diseases as well as treatment-refractory stages of cancer. Orphan diseases, according to the US criteria, are diseases that have low prevalence affecting less than 200,000 people (Orphan drug act, 1983) [184]; as such, less R&D is dedicated toward these diseases from traditional pharmaceutical companies. A number of cancers and rare genetic disorders fall within the category of orphan diseases contributing to high mortality rate due to lack of sufficient treatment options, for which drug-repurposing may be a viable solution [175]. Nevertheless, successful drug-repurposing can provide a higher global revenue stream for the pharmaceutical companies as well as out-licensing probability for a new indication while retaining the patent for the original indications, ultimately stimulating market growth [165]. Additionally, in a resource-limited setting, drug repurposing may create low-cost alternatives for financially underprivileged patients. On the contrary, repurposing for newer indications is not free from the challenges of financial liabilities within the industry, stringent regulatory requirements, rigorous market analysis, and preservation of intellectual properties [161,165]. The US National Center for Advancing Translational Sciences (NCATS) has been advocating for discovering new therapeutic uses of existing molecules for nearly a decade, by allocating financial incentives for small pharmaceutical companies or academic research as well as promoting public-private sector interactions. Overall, at present, it seems upon overcoming the bureaucratic and financial challenges from the pharmaceutical companies, drug-repurposing may ultimately benefit patients with diverse backgrounds of clinical history and socioeconomic patterns by providing viable therapeutic options fast and with less cost.

Table 1.2: Examples of successful drug repurposing events (modified from [185])

Drug name	Original indication	New indication	Year of approval
Zidovudine	Cancer	HIV/AIDS	1987
Minoxidil	Hypertension	Hair loss	1988
Thalidomide	Morning sickness	Multiple myeloma	2006
Mifepristone	Cushing's syndrome	Termination of pregnancy	2000
Sildenafil	Angina	Erectile dysfunction	1998
Celecoxib	Pain and inflammation	Familial adenomatous polyposis coli	2000
Rituximab	Cancers	Rheumatoid arthritis	2006
Ketoconazole	Fungal infection	Cushing syndrome	2014
Aspirin	Analgesia	Colorectal cancer	2015
Raloxifene	Osteoporosis	Breast cancer	2007
Atomoxetine	Parkinson disease	Attention deficit hyperactivity disorder	2002
Duloxetine	Depression	Stress urinary incontinence	2004
Dapoxetine	Analgesia and depression	Premature ejaculation	2012
Topiramate	Epilepsy	Obesity	2012
Fingolimod	Transplant rejection	Multiple sclerosis	2010

1.3 The anti-cancer properties of the anti-HIV drug nelfinavir

1.3.1 Introduction

Aspartyl protease inhibitors (PIs) are a group of drugs designed to target the aspartyl protease enzyme of the human immunodeficiency virus (HIV). The ribonucleic acid (RNA) in HIV encodes for two polyproteins—gag and gag-pol—which are cleaved at specific regions by an aspartyl protease for the maturation of the nascent virions through morphologic changes and condensation of the nucleoprotein core [186]. To date, ten HIV-PIs have been approved by the FDA; they contain a synthetic analogue of the gag-pol polyprotein, having a sequence of phenylalanine-proline at 167 and 168 regions (Figure 1.5) [187,188]. The HIV-PIs currently available in the market are nelfinavir, saquinavir, ritonavir, indinavir, amprenavir, fosamprenavir, lopinavir, atazanavir, darunavir, and tipranavir [188,189]. The HIV-PIs exert their therapeutic benefit by inhibiting subsequent HIV infection in a patient; however, they do not exert any action on cells already carrying integrated proviral DNA [186]. Thus, HIV-PIs have been in use in combination with reverse transcriptase inhibitors to treat HIV-infected patients, constituting the standard protocol of highly active antiretroviral treatment (HAART) [190].

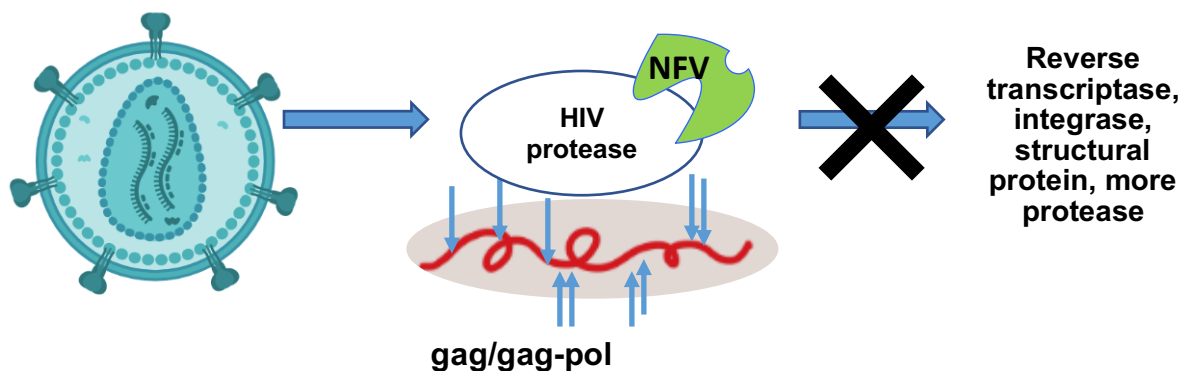


Figure 1.5: Nelfinavir (NFV) competitively binds with the specific sequence of HIV-aspartyl protease to inhibit the required cleavage of gag/gag-pol polypeptides for the maturation of the virion.

Rational drug designing of the HIV-PIs as peptidomimetics—based on the amino acid sequence recognized by the HIV aspartyl protease—was intended to drive competitive binding of the drug at the active site of the enzyme and disrupt the enzyme-substrate reaction [191]. Mammalian aspartyl proteases are weaker in cleaving and inhibiting the maturation of HIV polyproteins than the HIV-residing enzyme; thus, it was expected that the HIV-PIs would spare the human proteases and induce minimal toxicity. However, soon after the introduction of the HIV-PIs in the HAART protocol, pleiotropic off-target effects of the HIV-PIs were reported. The emergence of reports of remission from AIDS-associated cancers suggested anti-neoplastic properties of HIV-PIs to be a potentially important off-target effect. For instance, Niehuse *et al.* reported a case of complete regression of AIDS associated Kaposi's Sarcoma (KS) in a 5-year old child undergoing HAART regimen consisting of HIV-PI nelfinavir and reverse transcriptase inhibitors zidovudine and lamivudine [192]. Lebbé [193] and Krischer [194] also reported regression of KS in HIV-infected adults undergoing combination therapies of HIV-PIs and reverse transcriptase inhibitors. Initially, the reduction in AIDS-associated cancers was attributed to the immune-reconstitution of the body because of improved CD4+ T cell count and the reduction of overall viral load; however, later reports suggested that direct off-target anti-cancer action by HIV-PIs could be possible. Sgadari *et al.* suggested that the antiangiogenic properties of indinavir and saquinavir contributed to the regression of KS in mice models [195,196], whereas Schmidtke *et al.* demonstrated that ritonavir could affect the cellular proteasome activity in addition to its immunomodulatory and virus-reducing actions [197]. Thus, multiple preclinical reports suggesting the pleiotropic effects of HIV-PIs initiated the research for their possible anti-neoplastic properties.

Nelfinavir is a first-generation HIV-PI, which was approved by the FDA in March 1997 [198,199] for treating HIV infection. Due to the emergence of second and third generation HIV-PIs, nelfinavir has been progressively displaced from the HAART protocol [200]; however, nelfinavir exhibited maximum anti-neoplastic efficiency among the HIV-PIs. Wu *et al.* suggested that a unique *cis*-decahydroisoquinoline-2 carboxamide moiety may be responsible for the higher anti-neoplastic efficiency of nelfinavir. Analysis through a bioinformatical virtual docking system suggested that nelfinavir can potentially bind at the ATP binding site of the EGFR (ERBB1) protein, which was structurally compared with the same-site binding of the EGFR inhibitor lapatinib [201]. Further molecular docking approaches predicted the probability of binding of nelfinavir with cellular kinases [202] and Hsp90 β protein [203], which may also contribute to its anti-cancer properties. In 2007, in a landmark paper by Gills *et al.*, the preclinical anti-neoplastic efficiency of nelfinavir was demonstrated in the NCI60 cancer cell panel [204].

Long-term treatment with nelfinavir in HIV-infected patients led to adverse events such as hyperglycemia, insulin-resistance, and lipodystrophy, denoting mechanisms of action of nelfinavir disparate from its anti-viral activity [186]. One of the mechanisms by which insulin resistance is triggered in the body is by the inhibition of the IGF/Akt pathway, which is upregulated in many cancers. Thus, from the observation of insulin resistance, it was postulated that nelfinavir could act as an inhibitor of the Akt pathway in cancer, which was later demonstrated in preclinical studies [204]. To date, multiple research groups have used multi-pronged approaches to understand and implement the anti-cancer properties of nelfinavir in preclinical settings and clinical trials, with the aim of repurposing the drug as a potential chemotherapeutic agent against a multitude of cancers.

Data available from preclinical studies and toxicity profiling may contribute to the rapid repurposing of nelfinavir in the clinical setting. Furthermore, the recent emergence of nelfinavir in generic form [205] following patent expiration may reduce the cost of treatment because of drug repurposing. Minimal toxicity in clinical trials and ease of introduction through oral route may also be an important consideration for repurposing nelfinavir.

1.3.2 Potential mechanisms whereby Nelfinavir exerts its anti-cancer effect

1.3.2.1 Cell cycle arrest

Nelfinavir has been shown to inhibit cellular proliferation in multiple cancers, and a number of studies focused on the ability of nelfinavir to regulate the cell cycle. Bruning et al. reported that nelfinavir reduced the level of cell cycle proteins cyclin A, cyclin B, cyclin D3, cyclin dependent kinase (CDK) 1, CDK2, and proliferating cell nuclear antigen (PCNA) in ovarian cancer cell lines in a time-dependent manner [206]. The authors further reported nelfinavir-mediated reduction of cyclin B and CDK1 in leukemia cells, which was associated with a reduction of cells in the G2/M phase of the cell cycle and a striking increase of cells with sub-G1 DNA content, suggesting an effect of nelfinavir on both the apoptotic pathway and the cell cycle [207]. A similar result was observed in cervical cancer cells, where nelfinavir-treated cells showed a decrease in S phase with a marked increase in sub-G1 DNA content. The changes were accompanied by decreased expression of cyclins D3 and B in nelfinavir-treated cells. The authors further observed an increase of the cell-cycle regulatory and proapoptotic protein p53 in nelfinavir-treated cervical cancer cells carrying the wild-type p53 gene [208]. Chow et al. demonstrated that nelfinavir caused accumulation of liposarcoma and fibrosarcoma cells in the G1 phase of the cell cycle, which was associated with increased expression of cell cycle inhibitor p21^{cip1}, and decreased level of PCNA

[209]. Jiang and colleagues [210] reported a significant accumulation of nelfinavir-treated melanoma cells also in the G1 phase; a dose of 15 μ M nelfinavir caused a time-dependent decrease in the kinase activity of CDK2 in the melanoma cells, which was attributed to the reduced activity of CDK2-specific phosphatase Cdc25A, because removal of the inhibitory phosphate groups at the Thr¹⁴ and Thr¹⁵ positions by Cdc25A renders CDK2 fully active. These authors suggested that proteasome-mediated degradation of Cdc25A was responsible for the reduced activity of CDK2, resulting in the G1-arrest of the melanoma cells. A reduced CDK2 activity resulted in reduced phosphorylation of the Rb protein at the Ser⁶⁰⁸ position. Reduced phosphorylation of Rb inhibits its dissociation from the transcription factor E2F—making it impossible for the cells to cross the restriction point and enter the S phase [210]. Jensen et al. reported G1-arrest of thyroid cancer cells in response to nelfinavir in a dose-dependent manner with a concomitant reduction in the level of CDK4, cyclin D1, and phospho-Rb [211]. Sato and colleagues reported dose-dependent reduction of cyclin D1 and CDK4 in bladder cancer cells in response to nelfinavir monotherapy. A robust increase in sub-G1 DNA content was observed during combination therapy with nelfinavir and ritonavir in such cells [212]. In similar experiments, Okubo et al. described nelfinavir-mediated dose-dependent accumulation of sub-G1 DNA content in renal cancer cells with concomitant reduction of cyclin D1 and CDK4—a phenomenon further aggravated by the addition of panobinostat, an inhibitor of histone deacetylases (HDAC) [213,214]. Soprano et al. reported slight accumulation of breast cancer cells in the G1 phase following treatment with nelfinavir for 24 hours, associated with a clear reduction of cell cycle regulatory proteins cyclin D, E, A, B and phospho-Rb, and with an increase of the cell cycle inhibitory protein p21^{cip1}; strikingly, the cell cycle regulatory effects of nelfinavir observed in breast cancer cell lines were not evident in healthy breast epithelial cells [215]. In hepatocellular carcinoma cells (HCC), a 24-hour treatment

with varying doses of nelfinavir resulted in G1 arrest; however, the changes in underlying regulatory proteins were not explored [216]. Veschi et al. observed nelfinavir-mediated G1-arrest of pancreatic cancer cells in a cell-type-specific manner; protein levels of cyclin D3 and B1 were downregulated in response to nelfinavir monotherapy in pancreatic cancer cells, and were further decreased when nitroxoline and erlotinib were added to the treatment [217]. Xiang and colleagues observed a dose-dependent G1-arrest of cervical cancer cells in response to nelfinavir with a concomitant dose-dependent reduction in cell proliferation observed through a BrdU incorporation assay. The authors suggested a role of oxidative stress in cell cycle regulation following nelfinavir treatment, as they observed a reversal of the inhibition of nelfinavir-mediated cell proliferation during co-treatment with the reactive oxygen species (ROS) scavenger N-acetylcysteine (NAC) [218]. It was also reported that cervical cancer cells accumulate in the G2/M phase following co-treatment with nelfinavir and metformin, which was associated with increased expression of p53 and p21^{cip1} [219]. Taken together, the reports indicate that the effects of nelfinavir on the cell cycle may be specific to the cancer cell type, and, in most instances, is an early event during treatment, which precedes the induction of cell death pathways.

1.3.2.2 Cell death

Nelfinavir-induced cell death in cancer cells is evident in many studies; however, the death modalities seem to be different depending on the cancer cell types and the experimental conditions used. Flow cytometric analysis of nelfinavir-treated lung cancer cells H157 and A549 revealed that nelfinavir increased the percentage of sub-G1 DNA contents more potently than in cells treated with ritonavir and saquinavir, indicating a superior anti-cancer potency of nelfinavir compared to other HIV-PIs. Increased sub-G1 DNA contents and pyknotic nuclei in the nelfinavir-treated lung cancer cells were associated with the cleavage of caspase-8 and caspase-9, suggesting the

activation of both extrinsic and intrinsic apoptotic pathways. At the downstream level, the activation of caspase 9 and 8 converged into the cleavage of executioner caspases—caspase-3 or caspase-7 or both, which further cleaved the apoptotic target poly ADP-ribose polymerase (PARP) [204,220]. To determine if caspase activation is imperative to cell death induced by nelfinavir treatment on cancer cells, a pan-caspase inhibitor, zVAD, was applied during treatment with nelfinavir on lung cancer cells; zVAD reduced nelfinavir-induced sub-G1 DNA content, at least in part confirming a nelfinavir-induced caspase-dependent cell death mechanism.

Cell death induced by nelfinavir in lung cancer cells was also associated with the induction of endoplasmic reticulum (ER) stress and autophagy, while the inhibition of autophagy by 3-methyladenine (3MA) further increased the number of dead cells, suggesting a compensatory protective role of autophagy [204,220]. It is possible that a shift in the balance of the pro-death and pro-survival mechanisms during nelfinavir treatment commands the ultimate fate of the cancer cells, which could explain the parallel activation of autophagy during nelfinavir-induced cell death [204]. Collateral activation of cell-protective mechanisms during impending death has also been reported in nelfinavir-treated ovarian and leukemia cells. The authors demonstrated the upregulation and increased phosphorylation of mitochondrial protective antiapoptotic protein Mcl-1 in cancer cells in response to nelfinavir, which was decreased during co-treatment with sorafenib—a known downregulator of Mcl-1, contributing to further reduction of cell survival [207,220]. Mitochondrial membrane potential was unaltered in both ovarian cancer and leukemia cells during nelfinavir treatment; however, activation of caspases 8, 9, 7, and 3, and the cleavage of downstream PARP were evident in leukemia cells [207,220]. Contrary to the reports of Bruning et al. [207,220], Xiang and colleagues observed a reduction of the mitochondrial membrane potential during nelfinavir inflicted death on cervical cancer cells [218]. The increased number of

apoptotic cervical cancer cells treated with nelfinavir was associated with an increased production of ROS, which predominantly originated from the membrane-compromised mitochondria. The addition of a mitochondria-targeted antioxidant reduced the number of apoptotic cervical cancer cells treated with nelfinavir, indicating an important role of mitochondrial ROS in nelfinavir-induced cell death.

Immunoblots revealed the localization of apoptosis-inducing factor (AIF)—a proapoptotic mitochondrial flavoprotein—in the nucleus and the reduction of its level in the mitochondrial extracts of cervical cancer cells treated with nelfinavir [218]. Translocation of AIF from the mitochondria to the nucleus has been implicated in caspase-independent cell death [221]. Xiang et al. concluded that nelfinavir was able to induce apoptosis in a caspase-independent manner through ROS production and AIF translocation. Additionally, the nelfinavir-mediated apoptosis, in this case, was not abolished when the pan-caspase inhibitor zVAD was added, which further proved the concept of caspase-independent cell death [218]. Soprano and colleagues also observed a concomitant rise in ROS production during nelfinavir-induced death in breast cancer cells. In response to nelfinavir, the cells had an increased level of proapoptotic Bak protein and a reduction of the level of procaspase-9, which was associated with an increased level of mitochondrial cytochrome c in cytosolic lysates, indicating the activation of the intrinsic apoptotic pathway [215].

Activation of classical apoptotic pathways following nelfinavir treatment has been reported in a number of studies. Cleavage of caspase-3 has been reported after nelfinavir monotherapy in multiple myeloma (MM), and thyroid cancer cells [211,222,223]. Bruning et al. described apoptosis in both estrogen receptor positive and negative breast cancer cells associated with PARP cleavage during nelfinavir therapy [224], which was also evident in chemotherapy sensitive and resistant breast cancer cells [225]. The combination of nelfinavir and dimethylcelecoxib (DMC)—

a close structural analog of celecoxib that lacks cyclooxygenase-2 (COX2) inhibitory function—resulted in enhanced cleavage of caspase-7 and PARP in breast cancer cells [225]. During triple therapy with nelfinavir, DMC, and chloroquine, Thomas et al. observed a reduction in colony formation in triple-negative breast cancer (TNBC) cells, which was associated with the cleavage of caspases 3 and 7. The authors further observed an increase of apoptotic cells in tumors derived from TNBC xenografts identified by the positive terminal deoxynucleotidyl transferase (TdT) dUTP Nick-End Labelling (TUNEL) assay [226]. Davis and colleagues reported cleavage of caspase-7 in nelfinavir-treated cisplatin-sensitive and resistant cervical cancer cells, which corroborated similar findings in breast cancer cells [227,228]. In pediatric leukemia cells treated with nelfinavir, PARP cleavage was associated with the cleavage of upstream apoptosis initiator caspase-9 [229]. Liu et al. observed a re-sensitization of doxorubicin-resistant chronic myeloid leukemia (CML) cells during co-treatment of suboptimal doses of nelfinavir with doxorubicin, which resulted in increased apoptosis associated with caspase-3 cleavage, increased proapoptotic protein Bax, and decreased antiapoptotic protein Bcl-2 [230]. In castration-resistant prostate cancer cells, nelfinavir did not activate caspase-3 at low doses; however, in combination with docetaxel and curcumin, caspase-3 was activated, which resulted in DNA fragmentation and cleavage of PARP [231]. Positive TUNEL cells were enhanced in tumors derived from castration-resistant prostate cancer xenografted mice treated with nelfinavir, curcumin, and docetaxel, compared to untreated controls [231]. Yang et al. also observed potentiation of toxicity among nelfinavir and docetaxel in non-small cell lung carcinoma (NSCLC) cells, which was associated with increased TUNEL positive cells and a reduction of the antiapoptotic protein Bcl-2 [232]. Increased TUNEL positive cells were also observed during nelfinavir treatment in prostate cancer cells in vitro and in vivo [233]. In HCC, dual treatment of nelfinavir and proteasome inhibitor oprozomib resulted

in enhanced activation of caspase 3/7 compared to individual therapy with oprozomib. Increased TUNEL positive cells were present in diethylnitrosamine (DEN) induced hepatotoxic model of HCC xenografted mice having received nelfinavir and oprozomib treatment, compared to the control group [234]. Nelfinavir, alone and in conjunction with nitroxoline (antibiotic with anticancer properties) and erlotinib (EGFR inhibitor), resulted in reduced cell viability, PARP cleavage, and colony formation in pancreatic cancer cells [217]. Gupta and colleagues demonstrated that nelfinavir reduced the level of pro-survival protein survivin and increased proapoptotic protein Bax in meningioma cells, and that the effects were synergistically aggravated in combination with tyrosine kinase inhibitor imatinib. In vivo, tumors from meningioma xenografts showed increased TUNEL positive cells in groups receiving dual treatment of nelfinavir and imatinib [235]. In renal cancer cells, Okubo et al. observed that nelfinavir induced cell death associated with PARP cleavage, enhanced protein level of proapoptotic NOXA, and a gradual decrease of pro-survival protein survivin [213]. A high dose of nelfinavir further potentiated renal cancer cell death by the HDAC inhibitor panobinostat [214].

Activation of death receptor-mediated extrinsic apoptotic pathways has been implicated during nelfinavir therapy on multiple cancer types. The transmembrane death receptors belong to the tumor necrosis factor gene (TNF) superfamily. Among different ligands, tumor necrosis factor related-apoptosis inducing ligand (TRAIL) has been characterized to induce death upon binding with corresponding death receptors (DR)—DR4/TRAIL-R1 and DR5/TRAIL-R2 [236]. Receptor-ligand interaction leads to downstream recruitment of adaptor protein—Fas-associated protein with death domain (FADD), and promotes subsequent recruitment and activation of initiator caspase-8. Aggregation and activation of caspase-8 culminate with the activation of executioner caspases to drive apoptosis. TRAIL has been considered an important addition to the anti-cancer

drug inventory, and recombinant human TRAIL and monoclonal antibodies targeting TRAIL receptors have been promoted as chemotherapeutics [236,237]. Nelfinavir has been shown to enhance the expression of DR5 receptors in p53 mutant glioblastoma cells; however, it was not sufficient to induce death as a monotherapy. Nonetheless, the combination of nelfinavir and TRAIL promoted potent transactivation of DR5, which induced cell death in glioblastoma cells evidenced by increased sub-G1 DNA content, activation of caspases 8,9,3, and cleavage of PARP. The authors further demonstrated that nelfinavir-mediated potentiation of TRAIL involved ER-stress related transcription factors ATF4 and CHOP [237]. DR5 is a downstream target of the p53 protein; thereby, p53 mutation may render resistance to TRAIL in cancer cells. However, the ability of nelfinavir to increase DR5 in a p53 independent manner can be used as a tool to increase TRAIL sensitivity in p53 mutated cancer cells [237]. Okubo et al. also demonstrated nelfinavir-mediated potentiation of TRAIL in renal cancer cells, where the decrease in viability during the combination of TRAIL and nelfinavir was reversed by the addition of DR4 and DR5 blocking antibodies. The authors also demonstrated dose-dependent upregulation of both DR4 and DR5 receptors in response to nelfinavir in renal cancer cells [213]. Bruning et al. demonstrated that nelfinavir increased the mRNA level of DR5 in ovarian cancer cells within 48 hours while the level of membrane resident DR5 increased after 48 to 72 hours. Nelfinavir was also shown to potentiate the cytotoxic effects of TRAIL in ovarian cancer cells [238]. Similarly, nelfinavir-mediated upregulation of DR5 and sensitization to TRAIL was observed in cervical cancer cells [208]. Chow et al. observed an increased level of Fas—another death receptor that initiates extrinsic apoptosis upon binding with Fas ligand—and proapoptotic protein Bax in liposarcoma cells treated with nelfinavir [209].

1.3.2.3 Endoplasmic reticulum (ER) stress and unfolded protein response (UPR)

ER stress is a cellular condition induced by an imbalance in cellular protein homeostasis. Internal and external noxious stimuli can lead to the accumulation of misfolded proteins in the ER lumen, which instigates an adaptive unfolded protein response (UPR) aiming at reducing the protein load, and restoring cellular homeostasis by correct refolding of proteins (**Figure 1.6**) [239,240]. ER-resident chaperone of 78 kDa, glucose-regulated protein (GRP78) is responsible for detecting intraluminal misfolded proteins, leading to the activation of ER-stress sensors inositol-requiring enzyme 1- α (IRE1 α), protein kinase RNA-like endoplasmic reticulum kinase (PERK), and activating transcription factor 6 (ATF6), which are the upstream components of the UPR. At the downstream level, three outcomes can be expected initially: global inhibition of protein synthesis to reduce overall protein load, enhanced and selective synthesis of chaperone proteins to facilitate protein re-folding, and degradation of proteins mediated by the proteasome. Late-stage or exhaustive ER stress shifts from a pro-survival to a lethal mode initiating cell death [240]. ER stress has been frequently associated with cancer cells because glucose shortage and cellular hypoxia—two factors stimulating ER stress—are also known as important facilitators of tumor growth. Elevated ER stress in surviving cancer cells provides a therapeutic window for ER stress-stimulating chemotherapeutic drugs, as the drug-amplified ER stress can lethally target the cancer cells sparing the healthy cells, having no or minimal ER stress [240].

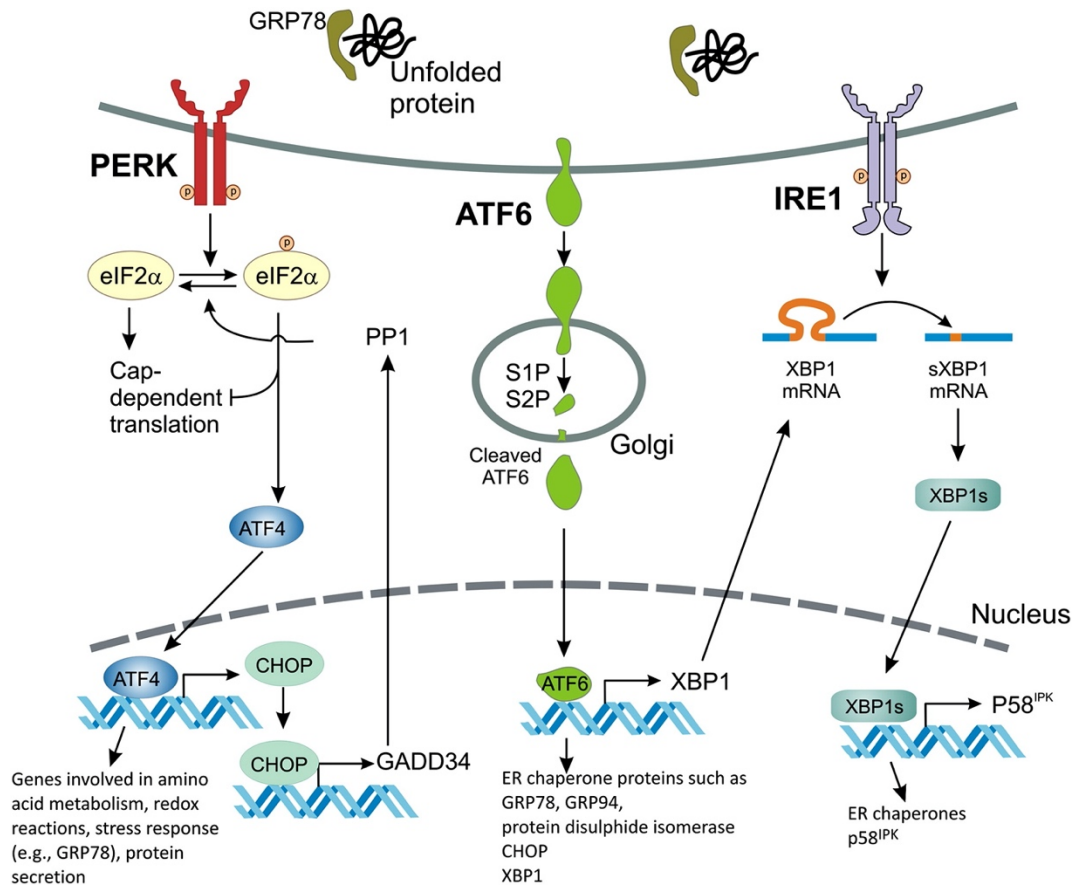


Figure 1.6: Schematic representation of the unfolded protein response pathway (UPR) in response to the endoplasmic reticulum (ER) stress developed as a result of misfolded or unfolded proteins in the ER. Adopted from [241].

Nelfinavir has demonstrated to have potent ER stress modulating effects against cancer cells in multiple studies. In time-dependent experiments, Gills et al. demonstrated phosphorylation of eukaryotic initiation factor 2α (eIF2α), a downstream effector of PERK, and enhanced expression of ER stress-related proteins such as transcription factor 3 (ATF3) and CCAAT-enhancer-binding protein homologous protein (CHOP) in nelfinavir-treated lung, breast, and

prostate cancer cells [204]. The authors also reported synergistic aggravation of ER stress markers in NSCLC and multiple myeloma (MM) cells during combined treatment of nelfinavir and the proteasome inhibitor bortezomib. It was implicated that ER stress played a crucial role in inducing cytotoxicity, since the silencing of ER stress-related proteins ATF3, CHOP, and PERK resulted in the reduction of cell death [242]. Bono et al. reported that nelfinavir, as a monotherapy, also increased the expression of CHOP and ATF4 in MM cells [222]. Further, in a NSCLC xenograft model, combined treatment of nelfinavir and bortezomib showed increased protein levels of ER stress markers GRP78, CHOP, p-eIF2 α , and X-box binding protein-1 (XBP-1) [243]. In malignant glioblastoma cells, Pyrko et al. discovered nelfinavir-mediated increase in the expression of GRP78, CHOP, and ER stress-related death mediator caspase-4; the importance of ER stress in nelfinavir derived cytotoxicity was further underscored when siRNA-mediated silencing of GRP78 reduced clonogenic survival [244]. Cho et al. also observed dose-dependent increase in the ER stress-related proteins GRP78 and CHOP in breast cancer cells (MCF7, BT-474) and in their chemotherapy-resistant counterparts. The authors also observed that siRNA-mediated reduction of GRP78 contributed to reduced colony formation in nelfinavir-treated chemo-sensitive and resistant breast cancer cells underpinning the ER stress-driven cytotoxicity of nelfinavir [225]. Furthermore, Bruning et al. reported that nelfinavir treatment increased ER stress markers in breast and ovarian cancer cells [206,224]. More recently, Mahamheed et al. reported that nelfinavir was highly effective to inhibit the growth of HCC cells in vitro and in vivo when combined with the PERK inhibitor ISRIB, which is an experimental drug that inhibits the integrated stress response (ISR); the ISR is a term that encompasses the phosphorylation of eIF2 α not only by PERK, but also by other kinases including PKR, GCN2 and HRI [245].

At the downstream level of nelfinavir-mediated ER stress, ATF4 inhibited the activity of the mammalian target of rapamycin (mTOR) by activating sestrin-2 (SESN2) protein, which contributed to the inhibition of protein translation [228]. In TNBC cells, dual treatment by ER stress-aggravating compounds, nelfinavir and celecoxib, resulted in increased levels of GRP78, ATF3, and CHOP, which were further enhanced when the autophagy inhibitor chloroquine was added to the combination [226]. Chakravarty et al. suggested that nelfinavir sensitizes doxorubicin-resistant breast cancer cells back to doxorubicin via upregulation of ER stress proteins ATF4 and CHOP. ATF4 and CHOP further upregulated a death sensor, tribbles homolog-3 (TRIB-3), which inhibited Akt phosphorylation and activated the apoptotic pathway facilitating chemosensitization [246]. Mathur et al. further demonstrated ER stress and TRIB-3 mediated chemosensitization of castration-resistant prostate cancer cells to docetaxel during the combination of nelfinavir and curcumin [231]. In liposarcoma and prostate cancer cells, nelfinavir led to the accumulation of sterol regulatory binding protein-1 (SREBP-1) and ER stress protein ATF6 [7,247]. SREBP1 is a key regulator of adipocyte differentiation and lipid synthesis in cells [248]. Both SREBP-1 and ATF6 are ER-resident transcription factors that are translocated and cleaved in the Golgi apparatus by site-1 protease (S1P) and site-2 protease (S2P) in a process named regulated intramembrane proteolysis (RIP) to release the active transcription factors [249]. Guan et al. mechanistically demonstrated that the nelfinavir-mediated accumulations of full-length SREBP-1 and ATF6 in prostate cancer cells were the outcome of inhibition of the enzyme S2P by the drug [250]. Additionally, nelfinavir and nelfinavir analogues increased the level of GRP78 in prostate cancer cells and decreased the level of the SREBP-1 target enzyme fatty acid synthase (FAS). At the mRNA level, a time-dependent increase of the mRNAs coding for ER stress-related

genes ATF6, GRP78, and XBP-1 was observed during treatment by nelfinavir in castration-resistant prostate cancer cells [250].

Protein synthesis machinery is exploited by tumor cells to generate oncogenic signals; as such, targeting the components of mRNA translation can be beneficial to halt tumor growth [251]. De Gassart et al. mechanistically demonstrated that nelfinavir could inhibit protein synthesis in two possible ways—by inhibiting translation initiation and elongation [251]. Nelfinavir was shown to activate the eukaryotic elongation factor 2 kinase (eEF2K) and interfere with protein synthesis by phosphorylating and inhibiting the eukaryotic elongation factor 2 (eEF2) [252]. The authors further observed that nelfinavir promoted phosphorylation of eIF2 α and activated downstream ATF4, CHOP, and growth arrest and DNA damage inducible protein 34 (GADD34) in cervical cancer cells and mouse embryonic fibroblasts (MEFs) [5]. Initial phosphorylation of eIF2 α inhibits global synthesis of proteins; however, in case of prolonged and irreversible proteotoxic damage, activated GADD34 recruits protein phosphatase 1 and dephosphorylates eIF2 α to restart mRNA translation and facilitate the synthesis of proteins necessary for cell death.

Hyperactivated mTOR complex has been implicated in many cancers, mostly as a consequence of the inhibition of the upstream regulator protein tuberous sclerosis complex (TSC). Loss of function mutations in Tsc1 or Tsc2 withdraw the inhibitory action over mTOR and leads to excessive and aberrant protein synthesis [253]. Johnson et al. demonstrated that basal ER stress was elevated in Tsc2^{-/-} MEFs, which was further aggravated by nelfinavir, evidenced from increased mRNA level of CHOP and spliced XBP-1 and increased protein levels of GRP78 and IRE1 α [253]. The authors also observed that nelfinavir-mediated increase in mRNA and protein levels of ER stress markers were further increased by the addition of bortezomib in Tsc2^{-/-} mTOR-hyperactive cells. Dual therapy by nelfinavir and bortezomib resulted in increased expression of

CHOP and ATF4 in the tumors derived from xenograft models of mTOR hyperactive cells [254]. Moreover, combined therapy of nelfinavir and mefloquine (an analogue of chloroquine) or salinomycin (an anti-cancer antibiotic) resulted in activation of the ATF4-CHOP-GADD34 arm of the ER stress pathway in *Tsc2^{-/-}* mTOR-hyperactive cells [255,256]. Tian et al. also reported phosphorylation of eIF2 α and increased protein levels of ATF4 and CHOP in response to nelfinavir in glioblastoma cells [237]. Phosphorylation of eIF2 α was also reported in nelfinavir-treated pediatric refractory leukemia cells [229]. In renal cancer cells, ER stress was shown to be induced by nelfinavir, as evidenced by the increase of GRP78, ER resident protein 44 (ERp44), and endoplasmic oxidoreductin-1 like protein α (ERO1-L α) [213]. Dual treatment by nelfinavir and HDAC inhibitor panobinostat also activated ER stress in renal cancer cells [214]. Sato et al. demonstrated aggravation of ER stress during combined treatment of nelfinavir and ritonavir in bladder cancer cells evidenced from increased GRP78, ERp44, and ERO-1L α [212].

Kawabata et al. reported that dual therapy of nelfinavir and bortezomib involves ER stress induction and aggravation of proteotoxic stress in NSCLC and leukemia cells. The authors observed that a dose of 10 μ M nelfinavir was not sufficient to activate caspases; however, combined treatment of nelfinavir and bortezomib induced strong cleavage of caspases-8, 9, 3, and 7, with subsequent cleavage of the downstream effector PARP. Inhibition of protein synthesis by cycloheximide reduced the percentage of dead cells during combination therapy of nelfinavir and bortezomib, suggesting the necessity of proteotoxic pressure for apoptosis [242]. This concept was further demonstrated in malignant glioma cells during nelfinavir monotherapy and in renal cancer cells during combination therapy of nelfinavir and panobinostat. In both instances, inhibition of protein synthesis by cycloheximide rescued the cells from nelfinavir-induced cell death [214,244]. Pyrko et al. also observed ER stress-related death in nelfinavir-treated malignant glioblastoma

cells, which was associated with activation of ER stress-related caspase-4 [244]. Kraus et al. observed ER stress-related death and caspase-4 activation in MM cells during the combination of nelfinavir and bortezomib. Furthermore, nelfinavir showed higher synergistic lethal potency with bortezomib and carfilzomib than other HIV-PIs in MM cells and facilitated overcoming bortezomib and carfilzomib resistance [257]. Likewise, in leukemia cells, nelfinavir reduced viability alone and in a synergistic manner when combined with bortezomib [258]. Bruning et al. observed a similar synergistic cell death by dual treatment of nelfinavir and bortezomib in cervical cancer cells with activation of ER stress proteins GRP78 and ATF3 [208].

Activation of ER stress following chemotherapy with nelfinavir as a single agent or in combination with other chemotherapy, such as bortezomib, has been reported in patient samples. Blumenthal et al. reported phosphorylation of eIF2 α at serine 51 and enhanced levels of CHOP and ATF3 in the peripheral blood mononuclear cells (PBMC) of patients receiving nelfinavir to treat solid cancer at the maximum tolerated dose of 3125 mg twice daily [243]. Driessen et al. reported increased GRP78, CHOP, and ER stress-related protein disulfide isomerase (PDI) in PBMC of MM patients receiving both nelfinavir and bortezomib [259]. Hitz and colleagues observed enhanced levels of CHOP and IRE1 α in PBMC of lenalidomide-refractory multiple myeloma patients receiving combination therapy of nelfinavir, lenalidomide, and dexamethasone [260].

Morphologically, vacuolization and expansion of the ER have been demonstrated in ER stress-activated cells treated with nelfinavir. Bruning et al. reported increased vacuolization of the cytoplasm in ovarian cancer cells following treatment with nelfinavir, which colocalized with ER-resident proteins and GRP78 observed through immunofluorescence microscopy [206]. Gills et al. also observed nelfinavir mediated vacuolization in lung cancer cells, which colocalized with

immunofluorescent aggregates containing ER-targeted sequence of calreticulin [204]. Mahoney and colleagues reported ER swelling following the treatment of nelfinavir in chronic lymphocytic leukemia cells with increased accumulation of fluorescent calnexin protein, suggesting accumulation of misfolded ER proteins [261]. In glioblastoma cells, Pyrko et al. observed, through transmission electron microscopy, swelled ER cisternae during nelfinavir treatment [244]. Kawabata et al. observed that nelfinavir-mediated vacuolization was reduced during treatment with protein synthesis inhibitor cycloheximide [242]. Notably, cycloheximide treatment inhibited the cytotoxicity towards renal cancer cells receiving the combination of panobinostat and nelfinavir, underscoring the role of protein overload in nelfinavir-associated toxicity [214].

1.3.2.4 Autophagy

Autophagy is an evolutionarily conserved catabolic process involved in digesting misfolded proteins or cellular organelles, and recycling cellular compounds or macromolecules to overcome energy and nutrient deprivation [262] (**Figure 1.7**). Different assays are utilized to assess the autophagic status of cells, among which tracking the expression of the microtubule-associated ubiquitin-like light chain protein 3 (LC3) is performed frequently [263]. In immunoblots, endogenous LC3 is visualized as two protein bands: a cytosolic component LC3I and a membrane-bound phosphatidylethanolamine (PE) conjugated component LC3II. The membrane-bound LC3II is a component of autophagosomes, and its enhanced expression indicates an increase in their numbers. Increased autophagosomes, however, maybe the outcome of either acceleration of the autophagic process or impairment of lysosomal activity. Thus, enhanced LC3II at a given time point may not readily indicate an increased rate of autophagy. Instead, the increased rate of autophagy is assessed by measuring autophagic flux. To determine the autophagic flux, the expression level of LC3II is studied in the presence of a lysosome inhibitor; an additive increase

of LC3II expression in the presence of a lysosome inhibitor such as bafilomycin A1, will indicate increased flux in contrast to a lack of change in LC3II expression—which will indicate lysosome impairment. Alternatively, time-sensitive tracking of degradation of p62—a ubiquitinated substrate of autophagy—can confirm autophagic flux [263]. Visualization of autophagosomes under the electron microscope, measurement of LC3 labelled puncta through immunofluorescence, and measurement degradation of green fluorescent protein (GFP) labelled LC3 by FACS are also ways to determine the autophagic status of cells [262].

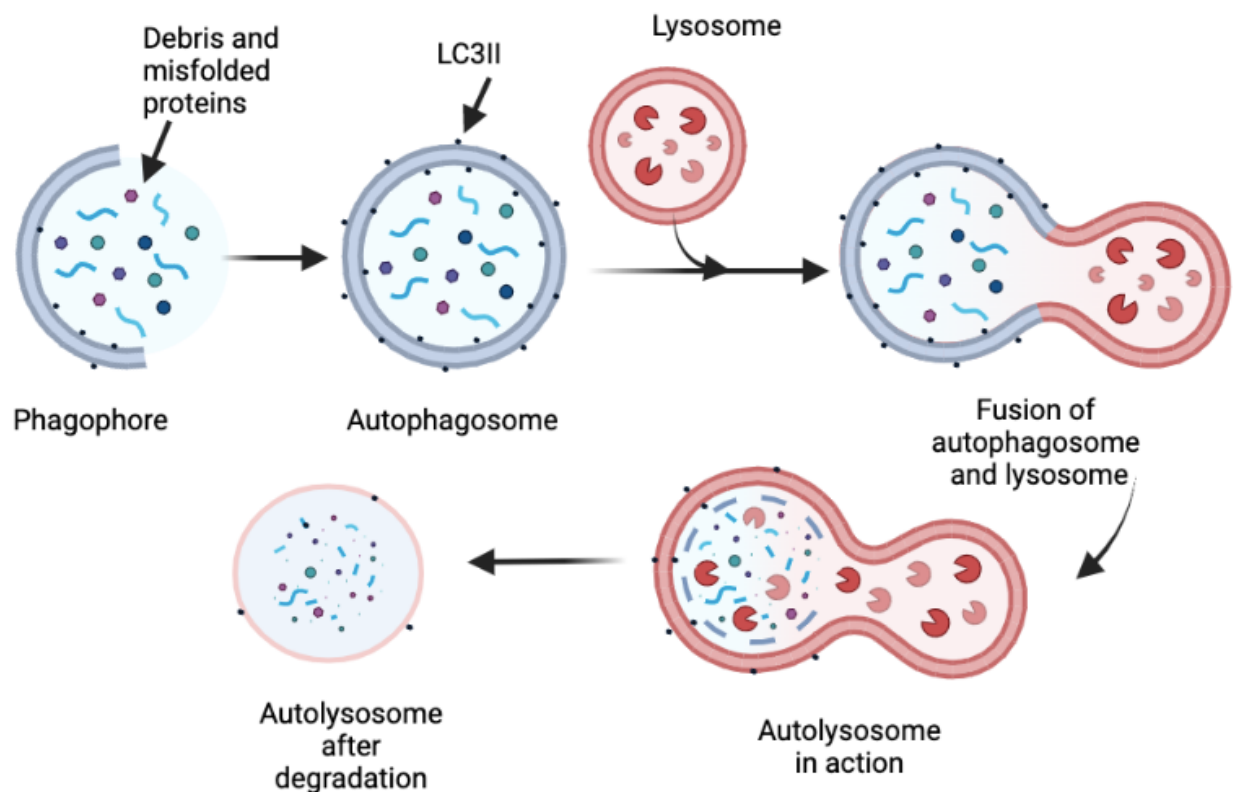


Figure 1.7: The process of autophagy starts with the engulfment of the cytosolic debris and misfolded proteins to form autophagosomes. The autophagosome binds with the lysosome to create an autolysosome. Lysosomal enzymes aid in degrading the internal content. LC3II is the

membrane-associated protein in the autophagosome that can be used to assess the autophagic process within the cell. (Diagram created on <https://biorender.com/>).

Gills et al. described the autophagy-inducing properties of nelfinavir in NSCLC cells. The authors observed an increase in the membranous form of LC3, known as LC3II, suggesting increased formation of autophagosomes [204]. Nelfinavir also increased the GFP labelled fluorescent LC3 aggregates, which was abrogated by the addition of autophagy inhibitor 3-MA. Transmission electron microscopy of nelfinavir treated human oral squamous cell carcinoma H157 cells revealed evidence of organelle containing degradative autophagosomes. The authors linked ER stress as an upstream activating factor of autophagy and concluded that the induced autophagy could be a compensatory survival mechanism, as the inhibition of autophagy by 3-MA resulted in enhanced cytotoxicity [204]. Enhanced apoptosis due to combined treatment of nelfinavir and 3-MA was also observed in refractory pediatric leukemia cells [229]. Gill et al. later highlighted four possible mechanisms by which nelfinavir could exert its autophagy-inducing properties. Firstly, nelfinavir-mediated mTOR inhibition could be linked with autophagy as a consequence of transient Akt inhibition. Secondly, ER stress induced by nelfinavir likely induces pro-survival autophagy through phosphorylation of eIF2 α and increased expression of ATF4. Thirdly, enhanced eukaryotic elongation factor 2 kinase (eEF2K) mediated phosphorylation of elongation factor 2 (EF2) by nelfinavir possibly activates autophagy. Finally, nutrient starvation resulted from the blockade of growth factor receptor signaling by nelfinavir can promote autophagy [264]. Bruning et al. reported that nelfinavir increased the expression of the autophagosome marker LC3B in estrogen receptor-negative breast cancer cells [224]. They also demonstrated that nelfinavir promoted ATF4 driven SESN2 expression in different cells. SESN2 inhibits the mTOR complex—a master down-regulator of cellular autophagy. Thus, by upregulating SESN2,

nelfinavir enhanced the formation of autophagosomes, which were visualized by fluorescent microscopy using an autophagic vesicle detection marker [228]. Guan et al. suggested enhanced autophagy by quantifying the turnover of GFP labelled LC3, utilizing FACS in nelfinavir treated androgen-dependent and castration-resistant prostate cancer cells [7]. Escalante et al. reported reduced co-localization of LC3II and LAMP2 (a lysosomal marker) during nelfinavir monotherapy and in combination with bortezomib in MM cells, suggesting impaired autophagy—likely due to impaired fusion of autophagosomes and lysosomes. The authors further observed a decrease in the level of calpain activity following nelfinavir treatment in MM cells [265]. Calpains are Ca^{2+} dependent cysteine proteases involved in the cleavage of cytoskeletal proteins, signal transducers, and membrane receptors [266]. Calpain deficiency has been shown to be involved in impaired autophagy and activation of the apoptotic switch [266], which was suggested to be a reason for the synergistic lethal interaction between bortezomib and nelfinavir in MM cells [265]. Kushchayeva et al. observed enhanced expression of LC3II in nelfinavir treated medullary thyroid cancer cells with a concomitant degradation of lysosomal substrate p62, indicating an increase in the autophagic process [223]. A similar outcome of enhanced LC3II and decreased p62 was observed in mTOR hyperactive tumorigenic mouse embryonic fibroblast cells—lacking tuberous sclerosis gene ($\text{Tsc2}^{-/-}$)—during nelfinavir monotherapy [253]. In a multidrug-resistant (MDR) breast cancer model (MCF-7/Dox), it was observed an increase of LC3II during combined treatment with nelfinavir and doxorubicin [246]. In nelfinavir treated cisplatin-sensitive ME-180 and cisplatin-resistant (CPR) ME-180 cervical cancer cells, LC3II was also increased [227]. Increased LC3II expression was also seen in PBMC of nelfinavir/lenalidomide/dexamethasone-treated lenalidomide-refractory MM patients [260].

Beclin-1 is a critical regulator of autophagy at the early stage, and changes in beclin-1 expression are monitored to assess the autophagic status in cells [264]. However, change in beclin-1 was not observed during nelfinavir monotherapy [223,229] or combined therapy with other autophagy inhibitors [226]. Gills et al. opined that nelfinavir mediated autophagy may be beclin-1 independent [264].

Autophagy is generally known as a pro-survival mechanism; thus, it has been hypothesized that inhibiting the pathway may provide benefits by aggravating cytotoxicity during cancer therapy. To explore this hypothesis, nelfinavir has been tested in combination with autophagy inhibiting drugs to induce heightened cytotoxicity in the cancer cells. Enhanced cytotoxicity due to the combination of nelfinavir and a class III PI3K and autophagy inhibitor 3-MA in NSCLC and pediatric leukemia cells has been described before, where 3-MA resulted in reduced LC3II [204,229]. A widely used anti-malarial drug chloroquine is an inhibitor of late-stage autophagy and has been used in combination with nelfinavir to demonstrate enhanced cytotoxicity in chronic lymphocytic leukemic cells [261], tuberous sclerosis negative (*Tsc2*^{-/-}) MEF cells, and human lung cancer cells (NCI-H460) [253]. Thomas et al. reported that chloroquine further increased the cytotoxicity of dual treatment of nelfinavir and DMC selectively in TNBC cells [226].

As stated earlier, bafilomycin A1 is an inhibitor of autophagy; it works via inhibition of v-ATPase transporter—preventing entry of protons in lysosomes; thereby, it decreases acidification and functionality of lysosomes. According to Jonhson et al. the combination of nelfinavir and bafilomycin-A1 did not induce cytotoxicity to the same extent as the combination of nelfinavir and chloroquine derivatives in *Tsc2*^{-/-} MEFs. Furthermore, autophagy was not suppressed during the combination of nelfinavir and chloroquine-derivative mefloquine in *Tsc2*^{-/-} cells, which implies that mechanisms other than autophagy may be involved while inducing cytotoxicity by combining

putative autophagy-inhibitors of different chemical natures with nelfinavir [253]. Autophagy-inhibitor mefloquine was shown to enhance nelfinavir mediated cytotoxicity in breast cancer (MCF7), colon cancer (HCT116), lung cancer (NCI-H460), and *Tsc2*^{-/-} cells. The cytotoxicity induced by the combined treatment of mefloquine and nelfinavir was rescued by the addition of methyl pyruvate, indicating energy deprivation as a possible mechanism of the heightened cytotoxicity [254]. Collectively, the reports suggest that nelfinavir can modulate the autophagic process in cancer cells in a cell type-specific manner.

1.3.2.5 Inhibition of the proteasome

The proteasome is a cytoplasmic and nucleoplasmic high molecular weight structure geared towards degrading proteins—tagged with ubiquitin or other ubiquitin-like molecules—to maintain cellular proteostasis [267]. The 26S proteasome contains a cylindrical catalytic 20S core, which is capped on each end by 19S regulatory components. The 20S catalytic core is comprised of α and β subunits, among which β subunits are responsible for specific proteolytic activities: $\beta1/\beta1i$ for caspase-like, $\beta2/\beta2i$ for trypsin-like, and $\beta5/\beta5i$ for chymotrypsin-like activities. The first-generation proteasome inhibitor bortezomib constitutes the mainstay treatment for MM. Second-generation proteasome inhibitors, like carfilzomib, are also available with demonstrated lesser neurotoxicity [268].

Nelfinavir was shown to affect the proteasome in selective cancer cell lines. Bono et al. reported that nelfinavir inhibited the chymotrypsin-like activity of the proteasome of MM cells (U266) and showed enhanced ubiquitination in immunoblots—a surrogate marker of proteasome inhibition—of U266 cells treated for 24 hours with 5 μ M nelfinavir [222]. Driessen et al. demonstrated a moderate decrease in the $\beta2$ and $\beta1/\beta5$ activities of the proteasome after nelfinavir

treatment in PBMC of patients having refractory-MM and other hematologic cancers [259]. Bortezomib targets the $\beta 5$ subunit of the proteasome and inhibits protein degradation [269]. In contrast, enhanced $\beta 2$ activity of the proteasome is associated with bortezomib-resistance in MM patients, whereas a concomitant decrease in $\beta 2$ activity during bortezomib treatment can confer re-sensitization to bortezomib [259,270]. Indeed, a combination of nelfinavir and bortezomib showed a positive response in bortezomib-refractory cancer [205,259]. Kraus et al. also demonstrated proteasomal inhibitory effects of nelfinavir on bortezomib-resistant MM cell lines in vitro, where nelfinavir showed expected bortezomib sensitizing effects [257]. The same group also demonstrated that the proteasomal inhibitory properties of nelfinavir on acute myeloid leukemia (AML) cells especially contributed to the cytotoxic effects of the drug [258]. Kawabata et al. observed proteasome inhibitory effects of nelfinavir on MM (RPMI8226) and NSCLC (H157) cells indicated by enhanced ubiquitination via immunoblot. Although the ubiquitination was moderate during nelfinavir monotherapy, it was considerably enhanced when combined with bortezomib, suggesting a synergistic interaction [242].

Combined treatment of nelfinavir and second-generation proteasome inhibitor carfilzomib was shown to re-sensitize carfilzomib-resistant MM cells to carfilzomib-mediated cytotoxicity and facilitated re-inhibition of proteasomal subunits. The reason for nelfinavir mediated carfilzomib re-sensitization was attributed to the ability of nelfinavir to inhibit the expression of ABCB1—a multidrug-resistant efflux pump—resulting in the reduced efflux of intracellular carfilzomib [271]. Pyrko et al. showed nelfinavir-driven enhanced ubiquitination in glioblastoma cells (U251), indicating proteasome inhibition, which was reversed by the use of protein synthesis inhibitor cycloheximide [244]. Similarly, proteasome inhibition through the dual treatment of nelfinavir and bortezomib was decreased by the addition of cycloheximide [242].

Conversely, some studies reported non-inhibitory effect of nelfinavir on the proteasome. Escalante et al. did not observe a decrease in the chymotrypsin-like activity of the proteasome in response to a pharmacologically relevant concentration of nelfinavir (10 μ M) in MM cells; however, it did not hinder the synergistic cytotoxic effect of bortezomib and nelfinavir [265]. Bruning et al. did not observe, in response to nelfinavir, any change in the chymotrypsin, trypsin, or caspase-like activities of the proteasome in cervical cancer cells and human B-lymphoblastoid cells [208], or any decrease in the chymotrypsin-like activity of the proteasome in breast cancer cells [224]. Moreover, Sato et al. observed an unexpected reduction in the accumulation of ubiquitinated protein during dual therapy of nelfinavir and ritonavir in bladder cancer cells [212]. Jiang et al. reported that nelfinavir promoted the degradation of CdC25A phosphatase—a substrate of the proteasome—in melanoma cells and addition of the proteasomal inhibitor MG-132 halted the degradation. This phenomenon, in fact, suggests an enhancement of proteasomal activity in response to nelfinavir [210].

One possible explanation of the discrepancy in study findings reporting the proteasome inhibitory function of nelfinavir is that the mechanism of action could be diverse and cell-type specific. It is important to address whether nelfinavir targets the mature 26S proteasome or the free 20S subunit, which may not be fully efficient to impair overall proteasomal activity. According to Bono et al., nelfinavir decreased the 26S proteasomal activity in MM cells [222], while other studies reported that nelfinavir targeted the 20S proteasome in breast cancer [272], and head and neck cancer cells [273].

Importantly, it has been reported that the mammalian 20S proteasome can cleave the same site targeted by the HIV-proteases in HIV [186]. Pajonk et al. reported inhibition of the 20S proteasome by the HIV-PI saquinavir in non-HIV associated cancer cells, which was accompanied

by apoptosis and radio-sensitization [274]. Piccinini reported that nelfinavir and saquinavir decreased both the 26S and 20S proteasomal activity in human red blood cells [275]. Recently, Fassmannová et al. proposed that nelfinavir can inhibit proteasome synthesis by inhibiting the transcription factor TCF/Nrf1. Reactivation of TCF/Nrf1 during treatment with proteasome inhibitors results in increased proteasome synthesis—known as the bounce-back response—eliciting resistance to proteasome inhibitors in MM [276]. Nelfinavir possibly inhibits the translation and maturation of TCF/Nrf1, leading to the repression of re-synthesis of the proteasome, which can explain the better outcome in clinical trials administering nelfinavir in bortezomib refractory MM [205,260]. The study by Fassmannová et al. [276] further elicits the possibility that the proteasomal inhibitory property of nelfinavir may not be due to the direct repression of the proteasomal subunits, but rather via an indirect phenomenon.

1.3.2.6 Signal Transduction Pathways

Aberrant signaling pathways are common in cancers and dampening atypical signaling feedback—developed through mutations in the components of the signaling cascades—is a well-established pharmacological strategy against cancer. Multiple studies have demonstrated that nelfinavir can target different cellular signaling pathways. The primary intracellular target of nelfinavir—responsible for its anti-cancer properties—has not yet been identified definitively; however, some groups suggested heat shock protein 90 (HSP90) as a putative primary target through *in silico* and *in vitro* methods. Arodola *et al.* suggested nelfinavir as a more potent binding molecule for HSP90 than other HIV-PIs, through homology modeling, molecular docking simulation, and analysis of binding affinity [203]. Shim *et al.* demonstrated selective anti-tumor activity of nelfinavir in human epidermal growth factor receptor 2 (HER2) positive breast cancer cells [272]. To identify the molecular target, the authors conducted a genome-wide screening of

nelfinavir using haploinsufficiency yeast strains, which revealed HSP82—the yeast orthologue of mammalian HSP90—to be a possible binding partner. Co-immunoprecipitation and trypsin digestion profiling in mammalian cells indicated that nelfinavir might affect HSP90 in a different manner than known HSP90 inhibitors—e.g., geldanamycin and novobiocin. Nelfinavir also decreased the protein level of HSP70 and HSP90 in HER2 positive breast cancer cells, which may have contributed to interrupted protein folding leading to ER stress—suggested from the enhanced phosphorylation of eIF2 α [272]. Kuschayeva *et al.* reported an increase in the level of HSP90 protein in patient samples of hereditary thyroid medullary carcinoma, which was associated with significant metastasis and *RET* mutation [223]. Although the authors did not observe a change in the protein level of HSP90 in response to nelfinavir in *RET* mutated thyroid cancer cells *in vitro*, the signaling of HSP90 client proteins—E-cadherin, tyrosine kinase *Src* (SRC) and connexin-34—was downregulated, suggesting nelfinavir mediated post-translational modification of HSP90 [223]. Mutation of the proto-oncogene *RET* is common in medullary thyroid cancer, and RET protein is a substrate to HSP90 mediated protein folding and processing. Mutant RET can exploit HSP90 for stability, and inhibition of HSP90 can be used as a potential strategy to induce 26S proteasome-mediated degradation of wild type and mutant RET [277,278]. In medullary thyroid cancer cells, nelfinavir decreased the expression of RET and its downstream signaling effectors Akt, ERK1/2 and p70S6K [223].

Akt is an important client protein of HSP90, and Soprano *et al.* demonstrated that nelfinavir promotes dissociation of HSP90-Akt complex without affecting the total Akt at the mRNA and protein level in breast cancer cells [215]. Nelfinavir was shown to decrease both phosphorylated and total levels of Akt in breast cancer cells, along with decreased expressions of downstream proteins of the Akt signaling cascade [215]. Decreased phosphorylation of Akt client proteins

PRAS40, FOXO3a and Bad was also seen in mTOR hyperactivated (*Tsc2^{-/-}*) cells in response to nelfinavir monotherapy and in combination with salinomycin [255]. Shim *et al.* reported decreased phosphorylation of Akt and ERK1/2 in response to nelfinavir in HER2 positive and negative breast cancer cells. In HER2 positive breast cancer cells, nelfinavir dissociated the interaction between HSP90 and HER2, and downregulated total protein levels of Akt and HER2 [272]. Decreased Akt phosphorylation in response to nelfinavir was also evident in MM [222,257], AML [258], pediatric refractory leukemia [229], diffuse B-cell lymphoma [279], doxorubicin-resistant breast cancer [246], prostate cancer [231,233], and NSCLC [204,232].

Downregulation of Akt signaling has been a widely mentioned effect of nelfinavir in cancer cells and has been proposed as a radiosensitizing strategy [6,280,281]. Chronic usage of nelfinavir in HIV infected patients, results in impaired glucose metabolism, insulin resistance, and lipodystrophy, which suggests a probable role of nelfinavir via inhibition of the PI3K-Akt-mTOR pathway. Gupta *et al.* demonstrated Akt dephosphorylation and radiosensitization by nelfinavir in bladder cancer and head and neck carcinoma cells and animal models [6]. The authors further suggested that nelfinavir works mechanistically via proteasome inhibition leading to the activation of the UPR, which forms and activates the phosphatase complex PP1/GADD34 responsible for dephosphorylating eIF2 α and Akt [273]. Infection by human papillomavirus (HPV) has been associated with better response to radiation in head and neck cancer; Gupta and colleagues showed that nelfinavir sensitized both HPV infected and non-infected head and neck carcinoma cells to radiation with a concomitant decrease in phosphorylated Akt [282]. Jiang *et al.* demonstrated that glioblastoma cells lacking wild-type phosphatase and tensin homologue (PTEN) are resistant to radiation and temozolomide, which can be overcome by nelfinavir. Nelfinavir-mediated radiosensitization in PTEN deficient glioblastoma cells was associated with decreased

phosphorylation of Akt [283]. Kimple and colleagues showed that *KRAS* mutation confers resistance to radiation in pancreatic cancer cells, likely due to failure to downregulate Akt phosphorylation. Both nelfinavir and the PI3K-inhibitor LY294002, decreased phosphorylation of Akt in pancreatic cancer cells—expressing either wild-type or mutant *KRAS*, and sensitized them to radiation [284]. Cuneo and colleagues observed decreased angiogenesis in response to nelfinavir, which was associated with decreased Akt phosphorylation in endothelial cells. Additionally, the combination of nelfinavir and radiation showed an additive effect in decreasing angiogenesis in a mouse xenograft tumor model of Lewis lung carcinoma [285]. Nelfinavir mediated reduction of vascular endothelial growth factor (VEGF) and hypoxia-inducible factor 1 α (HIF1 α) through inhibition of PI3K/Akt pathway has been observed by Pore *et al.* in head and neck carcinoma, lung cancer, and glioblastoma cells which contributed in reduced angiogenesis and potentiation of radiotherapy [286,287]. Potentiation of radiotherapy via nelfinavir was also demonstrated in pituitary adenoma cells, which was associated with reduced phosphorylation of ribosomal S6 protein—a downstream effector of the PI3K/Akt/mTOR cascade [288].

Plastaras *et al.* observed a decreased level of Akt phosphorylation in PBMC of HIV-infected patients treated with nelfinavir and saquinavir. The authors suggested that the level of phospho-Akt in PBMCs could be used as a surrogate biomarker to assess pharmacological efficacy in targeting Akt signaling by HIV-PIs [289]. Blumenthal and colleagues reported anti-tumor activity of nelfinavir in patients with solid tumors, which was associated with decreased phospho-Akt in PBMCs [243]. Similarly, Brunner *et al.* reported the radiosensitizing effects of nelfinavir in patients having locally advanced pancreatic cancer, with associated decreased level of phosphorylated Akt in PBMCs of the treated patients [290].

Nelfinavir-mediated decrease of Akt phosphorylation with concomitant anti-tumor activities—observed through cell culture experiments—has not always been translated *in vivo* and in clinical trials. In one study nelfinavir was effective in eliciting anti-cancer effects in the adenoid cystic carcinoma cells, which was associated with Akt dephosphorylation, justifying the usage of nelfinavir in clinical trials [291]. However, Hoover *et al.* did not observe a meaningful positive outcome in a Phase II clinical trial testing the beneficial effects of nelfinavir in patients having adenoid cystic carcinoma [292]. Moreover, Leibscher *et al.* reported nelfinavir-mediated downregulation of phosphorylation of Akt at the Ser473 position in PC-3 prostate cancer cells; however, nelfinavir failed to improve the efficacy of radiation therapy in prostate cancer *in vivo* [293]. Gills and colleagues reported decreased phosphorylation of basal and growth factor activated Akt in response to nelfinavir in lung cancer cells; however, nelfinavir-mediated reduction in Akt phosphorylation was not evident in tumor samples from xenograft models of lung cancer cells. Of notice, despite the discrepancy in Akt phosphorylation status, the anti-tumor efficacy of nelfinavir against lung cancer cells was similar both *in vitro* and *in vivo* [204]. Tumor growth impairment by nelfinavir in xenograft models of HER2 positive breast cancer cells was not associated with reduced phosphorylation of Akt, although decreased Akt phosphorylation by nelfinavir in HER2 positive breast cancer cells was evident *in vitro* [272]. In contrast, activation of Akt has been reported in estrogen receptor-negative breast cancer cells and melanoma cells during the short-term treatment of nelfinavir, which did not hamper the antiproliferative effects of the drug [210,224]. To date, no evidence pointed at a direct interaction of nelfinavir with Akt; however, modulation of Akt in response to nelfinavir indicates upstream signaling activity. Xie *et al.* based on computational prediction and kinase assays proposed binding of nelfinavir to 51 off-target protein kinases, the majority of which belong to the tyrosine kinase, cAMP-dependent, cGMP-dependent

and protein kinase C families—suggesting broad spectrum poly-pharmacological role of nelfinavir, i.e. the possibility of binding of nelfinavir with multiple targets with varying affinity [294,295]. Gills and colleagues demonstrated reduced activation of epidermal growth factor receptor (EGFR) and insulin-like growth factor receptor (IGFR) in response to nelfinavir, leading to downstream inactivation of Akt in NSCLC cells [204].

Nelfinavir has also been demonstrated to target other proliferative signaling cascades. Downregulation of mitogen-activated protein kinase pathway (MAPK)—by decreased phosphorylation of ERK—in response to nelfinavir has been reported in medullary thyroid cancer [223], adenoid cystic carcinoma [291], MM [222,296], and breast cancer cells [272]. However, decreased phosphorylation of ERK in cancer cells is not a universal response to nelfinavir treatment, as nelfinavir did not downregulate ERK phosphorylation in NSCLC [232], pancreatic cancer [284], and pituitary adenoma [288]. Downregulation of phospho-ERK in response to nelfinavir was further observed during combination with doxorubicin in doxorubicin-resistant chronic myeloid leukemia cells [230], and with bortezomib against MM cells [257]. Nelfinavir sensitized BRAF mutated melanoma cells to MEK inhibitors and BRAF inhibitors via SMAD-mediated downregulation of PAX and MITF, and decreased phosphorylation of ERK during combination with inhibitors of MEK or BRAF [297]. Conversely, Bruning *et al.* reported enhanced phosphorylation of ERK in ovarian cancer and cervical cancer cells carrying wild-type p53, which possibly led to the activation of antiapoptotic Mcl-1 protein [208,220]. Enhanced ERK phosphorylation was also reported during the combination of nelfinavir and tamoxifen in estrogen receptor-negative breast cancer cells [224].

Decreased phosphorylation of signal transducer and activator of transcription 3 (STAT3) in response to nelfinavir was observed in MM [222,296] and prostate cancer [233]. Nelfinavir has

also shown to inhibit HDAC [212] and has been shown to synergize with the HDAC inhibitors panobinostat [214] and valproic acid [222]. Of note, inhibition of HDAC6 by nelfinavir leads to enhanced ER stress following inhibition of HSP90 through acetylation leading to protein misfolding, which suggests HDAC inhibitors as potential ER stress aggravating chemotherapeutic agents [298].

Nelfinavir has also been suggested to be involved in altering metabolic signaling. Depletion of ATP has been reported in nelfinavir-treated doxorubicin-resistant chronic myeloid leukemia cells, which can be restored by the addition of exogenous glucose, resulting in the withdrawal of nelfinavir-mediated sensitization to doxorubicin. Metabolic stress incurred by nelfinavir results in the activation of 5'-AMP-activated protein kinase (AMPK) [212,223,253]. AMPK leads to inhibition of mTOR and activates autophagy at the downstream level, facilitating synergism between nelfinavir and autophagy inhibitors, such as chloroquine [253]. Activation of AMPK and downregulation of mTOR also occurred following dual treatment of nelfinavir and salinomycin or mefloquine [255,256]. The addition of the energy substrate methyl pyruvate inhibited nelfinavir and mefloquine-mediated AMPK activation and rescued the cells from cell death [256]. Nelfinavir promotes inhibitory phosphorylation of eEF2 through eEF2K, which leads to the arrest of protein synthesis [251,252]. Nelfinavir-driven activation of eEF2K may or may not be dependent on AMPK [252,264]. Nelfinavir can also inhibit mTOR via activation of ATF4-mediated SESN2, which can also lead to metabolic stress and autophagy [228].

1.3.2.7 Oxidative stress and mitochondria

Regulated production of ROS is crucial for critical cellular functions such as cell growth, differentiation and apoptosis, by promoting oxidative modification of proteins involved in these pathways. However, high production of ROS is detrimental to the cells as it induces damage to the DNA, proteins, and lipids. It has been demonstrated that cancer cells tend to produce excess ROS and have a higher level of basal oxidative stress than normal cells, which suggests a therapeutic benefit of aggravation of oxidative stress through pharmacological intervention, leading to selective cytotoxicity in cancer cells [299]. Anti-cancer properties exerted by nelfinavir has been linked to enhanced oxidative stress. Bruning *et al.* demonstrated that nelfinavir reduced the level of the intracellular antioxidant glutathione (GSH) in TNBC cells in a dose-dependent manner. Nelfinavir-mediated enhanced oxidative stress contributed to reduced cell viability, which was rescued by the addition of exogenous antioxidants—GSH or NAC [224]. Kushchayeva *et al.* showed that nelfinavir reduced the mitochondrial membrane potential in medullary thyroid cancer cells in a dose-dependent manner, with a concomitant increase of γ H2AX—a marker of DNA damage. Enhancement of γ H2AX was mitigated by the addition of exogenous antioxidant NAC, indicating a direct cytotoxic role of nelfinavir-induced oxidative stress in these cells. In a comparative gene expression study, both nelfinavir and hydrogen peroxide (H_2O_2) induced the expression of genes regulating the production of superoxide [300]. Liu and colleagues corroborated nelfinavir-mediated depolarization of the mitochondrial membrane in doxorubicin-resistant CML cells, which resulted in a loss of adenosine triphosphate (ATP)—suggesting induction of metabolic stress. The authors further observed an increase in ROS levels upon the combination of suboptimal doses of doxorubicin and nelfinavir in doxorubicin-resistant CML cells [230]. Xiang *et al.* showed enhanced intracellular and mitochondrial ROS production in cervical cancer cells; nelfinavir-

mediated cellular apoptosis was rescued by the addition of antioxidant NAC and a mitochondria-targeting superoxide and alkyl-radical scavenger Mito-TEMPO, which indicates the role of oxidative stress in nelfinavir induced cytotoxicity [218]. Xia *et al.* demonstrated that nelfinavir, combined with metformin, induced ROS production in cervical cancer cells, with a concomitant increase of NAD-dependent deacetylase sirtuin-3 (SIRT3), which is a primary mitochondrial acetyl-lysine deacetylase required to maintain energy homeostasis in the electron transport chain [219,301,302]. Besse *et al.* showed nelfinavir and lopinavir mediated ROS production in carfilzomib resistant MM cells, which was rescued by the addition of mitochondrial permeability transition pore antagonist decylubiquinone [271].

1.3.2.8 Tumor microenvironment

Nelfinavir plays a role in modulating the tumor microenvironment by inhibiting abnormal angiogenesis, improving oxygenation of the tumor tissue, inhibiting the growth of tumor stem cells, reducing the release of matrix metalloproteinases, and inhibiting cellular invasion. Pore *et al.* demonstrated decreased expression of VEGF in head and neck squamous cell carcinoma, lung cancer and glioblastoma cells in response to nelfinavir, which was associated with reduced angiogenesis *in vivo* [286,287]. Nelfinavir-mediated reduction of VEGF was attributed to decreased phosphorylation of Akt and the transcription factor SP1, and further reduction of HIF1 α . Of note, both SP1 and HIF1 α can bind to the promoter region of VEGF and transactivate the gene [286]. Functionally, decreased VEGF and HIF1 α was associated with increased radiosensitivity during treatment with nelfinavir *in vivo*. The authors further observed a decrease in the hypoxia marker EF5 in nelfinavir-treated tumors, which suggested increased tissue oxygenation despite reduced angiogenesis. As previous studies associated improved tissue oxygenation with radiosensitization

[303], Pore *et al.* speculated that the reduction in VEGF might have led to the normalization of the vascular bed and a reduction in abnormal vessels formation, which promoted better tissue oxygenation and enhanced radiosensitivity [286]. Cuneo *et al.* demonstrated *in vitro* that nelfinavir—alone or in combination with radiotherapy—inhibited the growth of human umbilical vein endothelial cells (HUVEC), and reduced cell migration and invasion. Potent reduction of angiogenesis was also evident in a xenograft model of lung carcinoma in response to the combination of nelfinavir and radiotherapy [285]. Qayum *et al.* demonstrated that nelfinavir altered the abnormal phenotype of the tumor vasculature by decreasing vessel tortuosity and showed physical similarity with the normal vascular system in xenografts of EGFR mutated cells having constitutively active PI3K/Akt signaling. The authors further observed that nelfinavir promoted increased tissue oxygenation and demonstrated anti-proliferative properties [304]. Since hypoxia has been linked with reduced radiation-sensitivity in tumor cells, and increased tumor perfusion is deemed as a way to overcome radiation-resistance [303], the role of nelfinavir in enhancing tissue oxygenation has garnered significant interest.

Yang *et al.* showed nelfinavir-driven downregulation of matrix metalloproteinase-2 (MMP-2) in NSCLC cells [232]. It was shown that protease inhibitors have the potential of downregulating matrix metalloproteinase-9 (MMP-9) and MMP-2 during adipocyte differentiation and in glioblastoma cells [305,306]. Matrix metalloproteinases are important modulators of tumor cell invasion and metastasis; thus, nelfinavir could potentially be used to inhibit tumor progression and metastasis. In functional assays, Xia *et al.* showed that nelfinavir inhibited cell migration and invasion of cervical cancer cells *in vitro*, which was enhanced in combination with metformin [219]. In medullary thyroid carcinoma cells, nelfinavir reduced the level of HSP90 client proteins E-cadherin, SRC, and connexin-43, which was associated with an inhibited adhesive property of

the cancer cells, leading to the reduced spheroid formation and induction of anchorage-dependent cell death (anoikis) [223]. Nelfinavir was also shown to inhibit the invasive property of papillary, follicular, and anaplastic thyroid cancer cells with concomitant reduction of the expression of gap-junction protein connexin-43 and reduced mitochondrial membrane potential [211].

Pancreatic stellate cells are important drivers of desmoplastic reaction—a fibrotic and inflammatory patho-histological change—in pancreatic ductal adenocarcinoma, which is believed to raise radiation resistance in pancreatic cancer [307]. Nelfinavir was reported to sensitize pancreatic cancer cells to radiation with or without the presence of human pancreatic stellate cells (hPSC). Nelfinavir reduced the phosphorylation of focal adhesion kinase (FAK) and Akt in hPSCs. Following administration of nelfinavir *in vivo*, pancreatic tumors, despite being mixed with hPSC, showed improved response to radiotherapy and delayed their growth kinetics [307]. Cancer stem cells possess self-sustaining capacity and are responsible for relapse and dissemination of disease. Darini et al. demonstrated that nelfinavir, along with ritonavir, saquinavir, and lopinavir, was able to kill Oct-4 expressing cancer stem cells [308]. Nelfinavir was also able to decrease the expression of CD209 in monocyte cells, a target required for HIV virions to invade T cells, which could be added to the immunomodulatory anti-cancer properties of the drug [309].

1.3.2.9 Multidrug-resistant efflux pumps

ATP-binding cassette (ABC) transporters are transmembrane proteins responsible for expelling endogenous substrates (amino acids, inorganic anions, hydrophobic metabolites), and exogenous drugs and their toxic metabolites from the cell. Among the 48 members of the ABC-transporter family, p-glycoprotein (P-gp/MDR1/ABCB1) has been extensively studied and shown to be associated with the emergence of resistance to chemotherapy in multiple cancers by

decreasing intracellular concentration of drugs [310]. Nelfinavir has been proposed to be a chemosensitizing agent based on its P-gp modulatory function. Besse *et al.* reported overexpression of P-gp in carfilzomib-resistant MM cell lines and primary cells, which was associated with the limited proteasome-inhibitory activity of carfilzomib. Nelfinavir and lopinavir reduced P-gp mediated efflux of carfilzomib in MM cells indirectly via inhibiting the mitochondria permeability transition pore (mPTP) [271]. Previous attempts to develop and combine P-gp inhibitory drugs in the chemotherapy regimen of MM resulted in undesirable pharmacokinetic events. However, nelfinavir demonstrated positive results in combination with proteasome inhibitors (bortezomib, carfilzomib) against MM patients in clinical trials [205,259,260]. Besse *et al.* suggested that the P-gp inhibitory property of nelfinavir could play a role during the chemosensitization of MM patients to proteasome inhibitors. Furthermore, the level of P-gp in patients could be used as a prognostic marker to stratify MM patients, likely to be benefitted from nelfinavir-proteasome inhibitor combination [271].

The upregulation of P-gp has been associated with the activation of the PI3K/Akt/mTOR survival pathway [311]. Nelfinavir increased the intracellular level of doxorubicin in doxorubicin-resistant breast cancer cells via inhibiting the function and membrane localization of P-gp, which was associated with the downregulation of the PI3K/Akt pathway and activation of ER stress [246]. Kim *et al.* observed nelfinavir-mediated chemo-sensitization of vincristine-resistant oral squamous cell carcinoma cells back to the antimetabolic agent vincristine, which was associated with the induction of late apoptosis and inhibition of P-gp [312].

Increased expression of P-gp confers chemo-resistance in CML. Liu *et al.* demonstrated nelfinavir-mediated sensitization of doxorubicin-resistant CML cells back to doxorubicin and other drugs transported by inhibiting P-gp (colchicine, paclitaxel, imatinib) [230]. Nelfinavir also

increased the intracellular concentration of doxorubicin in doxorubicin-resistance CML cells, which was associated with inhibition of P-gp. Although the mRNA and protein levels of P-gp were unaltered in response to nelfinavir, the reduction in intracellular ATP level and mitochondrial potential was deemed to be associated with the functional inhibition of ATP-dependent P-gp transporters. Co-administration of glucose during nelfinavir and doxorubicin treatment in doxorubicin-resistant CML cells reduced nelfinavir-mediated sensitization to doxorubicin, further confirming the possible role of ATP-depletion in inhibition of P-gp and efflux of doxorubicin. Additionally, molecular docking simulation indicated the possibility of competitive binding of nelfinavir at the ATP binding site of P-gp, inhibiting its function [230]. Paradoxically, nelfinavir has also shown to act as a substrate of P-gp efflux pump, which can increase the activity of P-gp as a compensatory mechanism [313,314] warranting caution while considering the role of nelfinavir as a P-gp inhibitor for drug sensitization. Among other members of ABC transporter proteins, nelfinavir was shown to interact with breast cancer resistant protein (BCRP/ABCG2) [315] and multidrug-resistant protein 4 (MRP4/ABCC4) [316].

1.3.2.10 Summary of mechanisms of action of nelfinavir as an anti-cancer agent

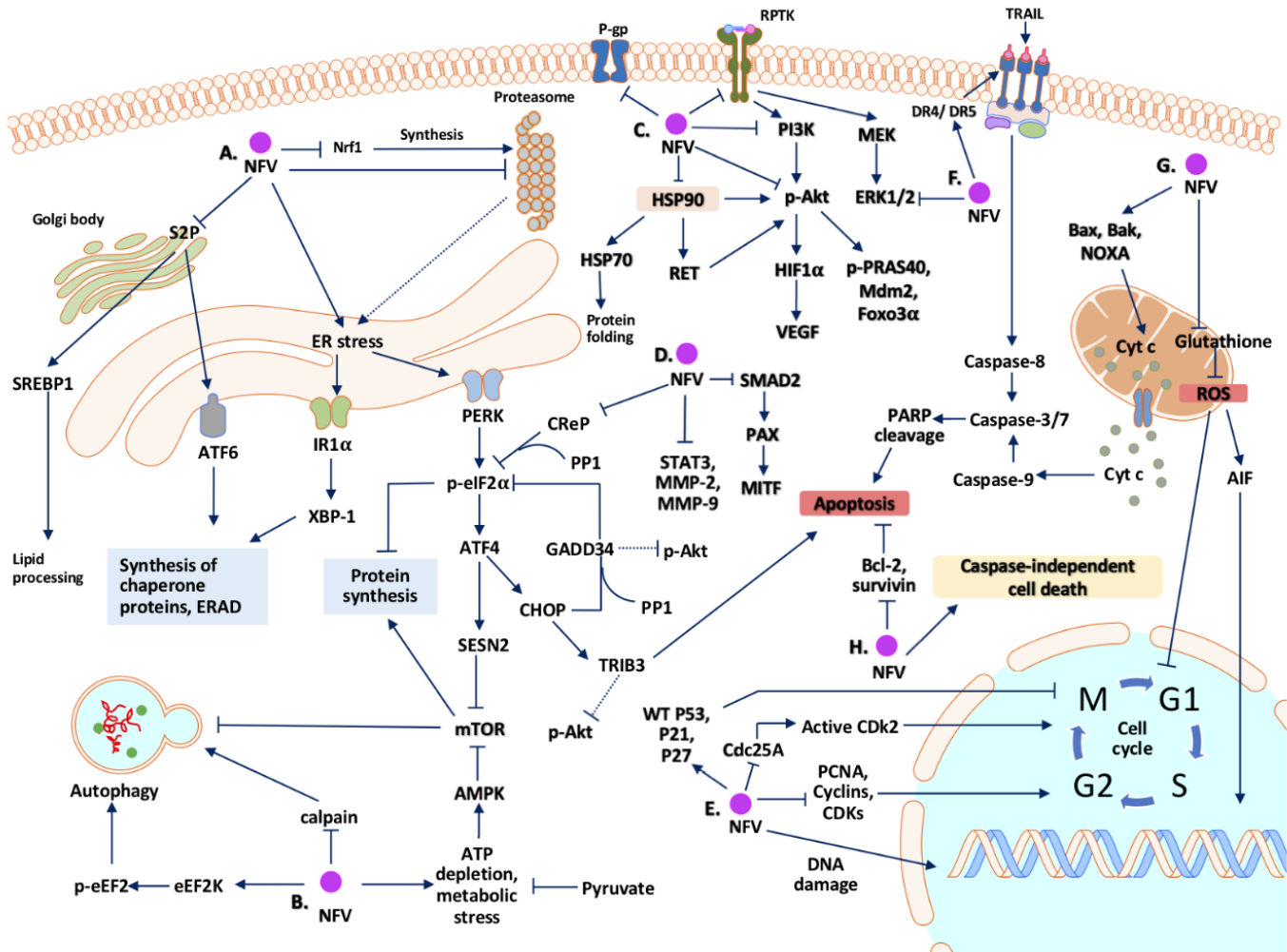


Figure 1.8. (A) Nelfinavir inhibits the Nrf1 dependent synthesis of proteasome subunits and inhibits the proteasome, leading to the accumulation of misfolded proteins that activate IRE1 α and PERK arms of the UPR. PERK activation leads to modulation of protein synthesis and cell death. Nelfinavir also inhibits S2P in the Golgi apparatus causing accumulation of un-cleaved ATF6 and SREBP; (B) Nelfinavir activates autophagy by inhibiting mTOR and by activating eEF2K; however, nelfinavir mediated inhibition of calpain may impair autophagy as well; (C) Nelfinavir can inhibit HSP90 and its interaction with client proteins Akt, RET and HSP70. Nelfinavir can

also cause inhibition of P-gp efflux pump and receptor protein tyrosine kinases (RPTK). Inhibition of PI3K-Akt pathway leads to inhibition of VEGF hindering angiogenesis; (D) Nelfinavir inhibits phosphatase CREP, STAT3, MMP-2/9, and SMAD2 pathway; (E) Nelfinavir promotes DNA damage and can lead to cell cycle arrest by modulating components of cell cycle; (F) Nelfinavir increases the expression of DR4/5 to enhance TRAIL sensitivity and activates the extrinsic apoptotic pathway. Nelfinavir also inhibits the MAPK pathway; (G) Nelfinavir decreases the mitochondrial membrane potential and activates the intrinsic apoptotic cascade. Nelfinavir also inhibits glutathione to increase the production of ROS, leading to cell cycle arrest. Nelfinavir mediated translocation of the apoptosis-inducing factor (AIF) from the mitochondria to the nucleus contributes to cell death; (H) Nelfinavir inhibits the expression of antiapoptotic proteins facilitating apoptosis and contributing to caspase-independent cell death.

1.3.3 Antitumor effects of Nelfinavir: preclinical evidence in vivo

The antitumor effects of nelfinavir have been tested on different mouse xenograft models in order to assess the translatability of the evidence obtained through cell-based experiments. The data regarding nelfinavir treatment, with or without a co-treatment, on in vivo cancer models, are compiled in **Table 2**.

Table 1.3. Antitumor effects of nelfinavir in animal models

Publications (<i>et al.</i>)	Cancer type	Animal Background	Cells and method of xenograft	Dosing of Nelfinavir ± Co- treatment	Time	Main result(s)
Al Assar, 2016 [307]	Pancreatic cancer	Female nude mice	PSN-1, SC ¹ , Flank	20 mg/kg, IP ² ± RT ³ 3.5 Gy	20d	Overcoming radioprotective effect of pancreatic stellate cells
Bono, 2011 [222]	Multiple myeloma	NOD/SCID ⁴ mice	U266-Luc ⁵ , SC, Flank	75 mg/kg, IP	21d	Reduced tumor burden
Chakravarty, 2016 [246]	Breast cancer	Female athymic nude BALB/c mice	MCF-Dox ⁶ , 4 th inguinal mammary gland (orthotopic)	20 mg/kg, IP ± Dox 2mg/kg	6w	Reduced tumor growth and p- AKT
Cuneo, 2007 [285]	Lung cancer	C7/BL6 mice	Lewis lung carcinoma, SC, hind limb	30 mg/kg, oral ± RT 2Gy	3-5d	Reduced vascular density and angiogenesis
Davis, 2016 [227]	Cervical cancer	Female athymic nude mice	ME-180, ME- 180 CPR ⁷ , SC, alternate flanks	250 mg/kg/d, gastric gavage	21d	Reduced tumor growth of both cisplatin sensitive and resistant cells
De Gassart, 2016 [252]	Spontaneous	Immunocomprom ised AGR 129 mice	eEF2K ⁸ WT ⁹ HRasV12, eEF2k ^{-/-} HRasV12, SC. Alternate flanks	100 mg/kg, IP		Tumor growth inhibition in response to nelfinavir in eEF2K WT mice but not in eEF2K deficient mice
Escalante, 2013 [265]	Multiple myeloma	SCID mice	MM.1S, SC	50 mg/kg, oral gavage ± BZ ¹⁰ 1 mg/kg, IV tail vein	Until 10% wt ¹¹ loss	Complete tumor regression in combination group
Gills, 2007 [204]	Lung cancer	Bulb/cAnCrnu/nu mice, athymic nude mice	H157, A548; SC, shoulder and rear flanks	50-100 mg/kg, IP;	10-20 d	Tumor growth delay, ER stress, autophagy

Guan, 2011 [247]	Liposarcoma	SCID mice	Lisa-2, SC, heterotopic model	500 mg/kg/d, diet or 100 mg/kg gastric gavage	41d	Reduced tumor growth
Gupta, 2007 [235]	Meningioma	Male athymic <i>nu/nu</i> mice	IOMM-Lee, SC, right flank	150 mg/kg/d, oral ± Imatinib 100 mg/kg/d	23d	Combined treatment caused tumor growth reduction, ER stress, apoptosis and reduced level of survivin
Gupta, 2005 [6]	Head-neck cancer, bladder cancer	NCr- <i>nu/nu</i> mice	SQ20B (EGFR mutated), T24 (HRas mutated), SC, hind flank	0.6 mg/day, continuous release pellets ± RT 6-8 Gy	Time to reach 1000 mm ³	Combined treatment caused tumor regrowth delay
Jiang, 2007 [283]	Glioblastoma	Female NCr- <i>nu/nu</i> mice	U87MG (PTEN deficient), SC, flank	79 mg/kg/day, Diet ± RT 6Gy	Time to reach 1000 mm ³	Combined treatment caused tumor growth delay; nelfinavir reduced p-Akt
Johnson, 2018 [254]	Tuberous Sclerosis Complex	NOD/SCID female mice	ELT3-V3 (<i>Tsc2</i> ^{-/-}), SC, right flank	30-50 mg/kg, IP ± BZ 0.3-0.5 mg/kg	17d	Combined treatment caused tumor growth reduction, ER stress, apoptosis
Kawabata, 2012 [242]	NSCLC ¹² , multiple myeloma	Athymic NCr <i>nu/nu</i> mice	H157, RPMI8226, SC, both rear flanks	50mg/kg, IP ± BZ 0.5 mg/kg	11-17 d	Combined treatment caused tumor growth reduction, ER stress, apoptosis
Kimple, 2010 [284]	Pancreatic cancer	Athymic BALB/c nude mice	Capan-2, SC, flanks	150 mg/kg, Oral gavage ± RT 200 cGy/day	10d	Combined treatment caused tumor growth

						reduction; nelfinavir reduced p-Akt
Mathur, 2014 [231]	Castration resistant prostate cancer	Athymic nude mice	C4-2B, SC	DTX ¹³ (10mg/kg), ± [nelfinavir (20 mg/kg) and curcumin (100 mg/kg)]	4w	Triple combination caused tumor growth delay and apoptosis
Okubo, 2018 [214]	Renal cancer	BALB/c male nude mice	Caki-2, SC	25mg/kg, IP ± PAN ¹⁴ (2mg/kg)	11d	Combined treatment caused tumor growth reduction, ER stress, apoptosis and histone acetylation
Pore, 2006 [286]	Lung cancer, head neck squamous cell cancer	BALB/c NCr <i>nu/nu</i> mice	A549, SQ20B, SC, flank	79mg/kg/d, diet; ± RT 8 Gy	Time to reach 1000 mm ³	Combined treatment reduced tumor growth; nelfinavir reduced angiogenesis and VEGF ¹⁵
Pore, 2006 [287]	Glioblastoma	BALB/c NCr <i>nu/nu</i> mice	U87, SC	40 mg/ kg/d; diet	5d	Reduced angiogenesis
Pyrko, 2007 [244]	Glioblastoma	Male athymic <i>nu/nu</i> mice	U87, SC	40 mg/kg/d (short- term), 120 mg/kg/d (long- term); gastric gavage	96h (short- term), 6w (long- term)	Tumor growth reduction, ER stress, apoptosis
Qayum, 2009 [304]	Fibrosarcoma, Laryngeal cancer	SCID mice	HT1080, SQ20B, SC, hind leg	20 mg/kg, IP	2w	Reduced tumor hypoxia, increased tumor blood flow, normalized tumor vascular morphology

Shim, 2012 [272]	Breast cancer	BABL/c NCr <i>nu/nu</i> mice	HER2 ¹⁶ positive: HCC1954, BT474; HER2 negative: HCC1937, MDA-MB-231, SC	25 mg/kg, IP; 40 mg/kg, oral	30d	Nelfinavir selectively inhibited the growth of HER2 positive tumors and decreased expression of HER2
Smith, 2016 [297]	Melanoma	Nude mice	A375, M249-R4, SC	25 mg/kg/qd, oral gavage ± MEKi ¹⁷ (25 mg/mg/qd) or BRAFi ¹⁸ (25 mg/kg/qd)	21-33d	Combined treatment caused reduction of tumor growth and expression of PAX and MITF ¹⁹
Thomas, 2012 [226]	Breast cancer	Athymic mice	MDA-MB-468 (TNBC ²⁰), MCF-7, SC, flank	5 mg/kg/d, gavage ± Celecoxib (2mg/kg/d) ± CQ ²¹ (10 mg/kg/d)	3-5d	Triple combination caused tumor growth reduction, ER stress and apoptosis
Vandewynckel, 2016 [234]	Hepatocellular carcinoma	WT 129s2/SvPasCrl mice injected with DEN ¹⁹ (orthotopic model); Athymic nude mice: Foxn1nu/foxn1nu (Xenograft model)	HepG2, SC, right flank	OZ ²² (30 mg/kg/d), intragastric ± nelfinavir (250 mg/kg/d), IP or salubrinal (1mg/kg/d), IP	4w	Decreased tumor growth and increased apoptosis in both orthotopic and xenograft models
Xia, 2017 [219]	Cervical cancer	Female BALB/c nude mice	SiHa, SC, left flank	0.4 mg/kg/d, IP ± metformin 100 mg/kg/d	24d	Reduced tumor growth and PI3K ²³ expression and increased expression of p53 and p21 in response to

						either monotherapy or combined therapy
Xia, 2019 [301]	Cervical cancer	Female BABL/c nude mice	SiHa, SC, left flank	0.4 mg/kg/d, IP ± metformin 100 mg/kg/d	25d	Combined treatment caused tumor growth reduction and enhanced level of sirtuin-3 and MICA ²⁴ , suggesting NK ²⁵ cell mediated lysis
Xiang, 2015 [218]	Cervical cancer	BALB/c nude mice	HeLa, SC, back	1 mg/mouse, IP	20d	Tumor growth reduction, increased apoptosis, nuclear localization of AIF ²⁶
Yang, 2006 [232]	NSCLC	BALB/c triple deficient male nude mice	NCI-H460, SC, bilateral	60 mg/kg, oral gavage	3w	Tumor growth reduction, apoptosis
Yang, 2005 [233]	Prostate cancer	Immunodeficient BALB/c nude mice	LNCaP, SC, bilateral	60 mg/kg, oral gavage	3w	Tumor growth reduction, reduced serum level of PSA ²⁷ , increased fibrosis and inflammatory cells
Zeng, 2011 [288]	Pituitary adenoma	Female nude mice	GH3, SC, right flank	5 µM, oral gavage ± RT 6Gy	Until tumor size 4x	Tumor growth reduction, reduced phospho-S6

¹Subcutaneous, ²Intraperitoneal, ³Radiotherapy, ⁴Non-obese diabetic/severe combined immunodeficiency, ⁵Luciferase, ⁶Doxorubicin, ⁷Cisplatin resistant, ⁸Eukaryotic elongation factor 2 kinase, ⁹Wild type, ¹⁰Bortezomib, ¹¹weight, ¹²Non-small cell lung carcinoma, ¹³Docetaxel, ¹⁴Panobinostat, ¹⁵Vascular endothelial growth factor, ¹⁶Human epidermal growth factor receptor 2, ¹⁷Mitogen-activated protein kinase inhibitor, ¹⁸BRAF inhibitor, ¹⁹Microphthalmia-associated transcription factor; melanoma transcription factor, ²⁰Triple negative breast cancer, ²¹Chloroquine,

²²Oprozomib, ²³Phosphoinositide-3 kinase, ²⁴Major histocompatibility complex class I chain-related gene A, ²⁵Natural Killer, ²⁶Apoptosis-inducing factor, ²⁷Prostate-specific antigen

1.3.4 Current status of clinical trials

Promising preclinical data regarding nelfinavir, as a single agent or in combination with other cancer therapies, on multiple cancers, prompted a series of clinical trials. For instance, Rengan and colleagues reported the outcome of a Phase I/II trial of nelfinavir with concurrent chemoradiotherapy on locally advanced unresectable stage IIIa/ IIIb NSCLC [317,318]. In the Phase I study, the maximum tolerated dose of nelfinavir was determined to be 1250 mg per oral route twice daily. Nelfinavir was administered 7 to 14 days prior to and concurrently with cisplatin, etoposide and radiotherapy at a 66.6 Gy dose. No significant predetermined dose-limiting toxicity was observed. Five of the nine evaluable patients showed complete response, whereas the remaining four patients showed partial response in post-treatment positron emission tomography (PET) derived metabolic evaluation [317]. The Phase I study progressed into a Phase II study where 35 patients with locally advanced unresectable stage IIIa/ IIIb NSCLC were treated with nelfinavir with concurrent chemoradiotherapy. Observed median survival was 41.1 months, and a median progression-free survival was 11.7 months without any unexpected grade 3 or 4 toxicities beyond those of standard chemoradiotherapy [318].

Radiotherapy is a front-line management option for inoperable locally advanced pancreatic cancer (LAPC); however, resistance to radiation is frequent and local disease progression leads to the demise of patients. In the preclinical setting, nelfinavir was shown to increase the sensitivity to radiation via the downregulation of Akt [6], reducing hypoxia [286], and improving tumor microvasculature [304]. Brunner *et al.* first reported a Phase I trial with the use of nelfinavir in conjunction with chemoradiotherapy in inoperable LAPC patients [290]. In this study, 12 patients

started nelfinavir three days before the initiation of radiation therapy and chemotherapy with cisplatin and gemcitabine. Of the 10 evaluable patients, 5 showed complete metabolic response in PET and 6 underwent secondary resection. The median overall survival was 18 months, and most patients showed downregulation of p-Akt in PBMCs; nelfinavir did not contribute to additional or unexpected toxicity to the regimen [290]. The study escalated into Phase II, where 23 patients with an estimated life expectancy ≥ 12 weeks received nelfinavir 1250 mg twice daily prior to and concurrently with radiotherapy and chemotherapy (cisplatin and gemcitabine) [319]. In this study, the median overall survival time-length was 17.4 months, (90% CI: 12.8-18.8%) and one-year overall survival rate was 73.4% (90% CI: 54.5-85.5%). Four of the 6 recruited patients for a sub-study showed reduced hypoxia in ^{18}F -fluoromisonidazole positron emission tomography (FMISO-PET) with a concurrent increase in computed tomography (CT) perfusion denoting increased blood flow. Additionally, 8 of 13 evaluable patients demonstrated the downregulation of p-Akt following initial nelfinavir treatment. However, a high incidence of grade 3 or above gastrointestinal toxicity raised concern, which was attributed to the gemcitabine-cisplatin combination with concurrent large field radiotherapy [319,320]. To address the need to optimize the chemoradiation regime for LAPC, a large-scale multicenter randomized study SCALOP-2 began in March 2016. The study aims at investigating the benefit of induction-chemotherapy by gemcitabine and nab-paclitaxel followed by escalating doses of radiation with or without the radiosensitizer nelfinavir [320]. Recently, Lin *et al.* reported two trials testing the simultaneous use of nelfinavir with stereotactic body radiotherapy (SBRT) on patients having locally advanced or unresectable pancreatic adenocarcinoma [321,322]. In the Phase I study, patients received 3-week cycles of gemcitabine/leucovorin/fluorouracil followed by combinations of nelfinavir and escalating doses of radiation therapy. In this study, a median overall survival was estimated to be

14.4 months, and the maximum tolerated dose combination was deemed SBRT (40Gy)/ nelfinavir (1250 BID) [321]. Additionally, in a prematurely terminated trial, Lin *et al.* tested a chemoimmunotherapy combination gemcitabine/leucovorin/fluorouracil/ oregovomab followed by SBRT (40Gy)/nelfinavir (1250 BID) in LAPC patients [322].

In few studies, nelfinavir was tried as a monotherapy, unlike the mostly tested regimen of nelfinavir in combination with chemotherapy and with or without radiation therapy. Hoover et al. reported a phase II clinical trial in patients with recurrent adenoid cystic carcinoma who no longer responded to the available standard therapeutic options. Patients received doses of 1250 mg of nelfinavir twice daily; however, the progression-free survival did not improve significantly [292]. Conversely, in a Phase I study conducted by Pan *et al.*, 6 patients out of 20 (30%), having recurrent, metastatic or unresectable liposarcoma, showed clinical benefits at different dose levels of nelfinavir [323]. Nelfinavir was reasonably tolerated without any dose-limiting toxicity, and dose escalation was effective up to 3000 mg due to auto-induction of increased plasma clearance at higher doses [323]. Blumenthal *et al.* investigated the effects of nelfinavir monotherapy on adults having advanced solid refractory tumors of different origins [243]. Patients showed well tolerability to nelfinavir with manageable toxicities and the maximum tolerated dose was determined at 3125 mg. Dose-limiting toxicity was reported as grade 4 neutropenia at a high dose level (3750 mg), which was reversible quickly upon temporary discontinuation of the treatment. Out of 28 patients, 1 showed partial response, 3 showed minor response, and 6 showed stable disease on tumor evaluation. Importantly, this study reported the beneficial effect of nelfinavir on a neuroendocrine tumor (NET). Patients showed decreased p-Akt, enhanced p-eIF2 α , and enhanced expression of ATF3 and CHOP analyzed from PBMCs following nelfinavir treatment [243].

Decreased UPR, especially silencing of IRE1 α /XBP1 in MM cells, has been shown to confer resistance to proteasome inhibitor bortezomib [324]. In a phase I study, Driessen *et al.* observed the upregulation of UPR proteins in response to nelfinavir—with or without bortezomib—in PBMCs of advanced MM patients [259]. Among 6 bortezomib and lenalidomide refractory MM patients, 3 showed partial response, and 2 demonstrated minor response to the combination of nelfinavir (2x2500 mg) and bortezomib. Nelfinavir also showed mild inhibition of proteasome activity, which was further enhanced by bortezomib [205,259]. In a phase II trial, 34 patients of bortezomib-refractory MM, a twice-daily dose of 2500 mg of nelfinavir led to an objective response rate of 65% (90% CI, 49%-76%), and was observed with 12 weeks of progression-free survival and a median overall survival of 12 months [205]. Recently, Hitz *et al.* reported a regime of nelfinavir/lenalidomide/dexamethasone, a triad of orally given drugs, tried on 29 patients with lenalidomide refractory MM [260]. Ten of the 29 patients had lenalidomide-bortezomib double-refractory MM; 16 patients showed minor response or better (55%, 95% CI 6-74%), and 9 patients showed partial response (31%, 95% CI 15-51%), with median overall survival of 21.6 months. Lenalidomide and nelfinavir both act as substrates for multidrug resistant 1 (MDR-1) pump, which may have caused competing interactions and inhibited drug efflux, thereby increasing intracellular concentration and clinical effects [260].

Hill *et al.* conducted a clinical trial combining nelfinavir and radiotherapy on 10 patients having advanced metastatic rectal cancer. Unlike previous studies, nelfinavir (1250 mg twice daily) was combined with hypo-fractionated radiotherapy without the addition of chemotherapy. Five patients demonstrated tumor regression as per MRI imaging, and dynamic imaging (p-CT, DCI-MRI) hinted increased perfusion in the tumor area [325]. In another small cohort of 11 patients, Buijsen *et al.* investigated the tolerability of nelfinavir with standard radiotherapy and

capecitabine (825 mg/m² twice daily) in locally advanced rectal cancer patients. Three patients showed pathological complete response and 4 other patients showed major response. Diarrhea appeared to be the most frequent adverse event, which was speculated to be related with high plasma level of nelfinavir due to inhibition of CYP2C9—a metabolizer enzyme of nelfinavir—by capecitabine. The maximum tolerated dose of nelfinavir was deemed 750 mg twice daily [326]. In patients diagnosed with glioblastoma multiforme (GBM), in order to determine the dose-limiting toxicity and maximum tolerated dose of nelfinavir, in conjunction with temozolomide and radiotherapy, Alonso-Basnata and colleagues conducted a phase I trial on 21 patients. Nelfinavir was deemed to be safe when administered with temozolomide (75 mg/m²) and radiotherapy (6000 cGy to the gross tumor volume), and the maximum tolerated dose was 1250 mg, similar to the standard dose given to HIV infected patients [327]. The bulk of clinical trial data are compiled in Table 1.4.

Table 1.4. Updated clinical trial list including nelfinavir (2020)

NCT number	Phase	Cancer type	Concurrent therapy	Timeline	Status	Total patients	Objective	Ref
NCT01485731	I	Cervical cancer	Cisplatin, RT ¹	Jan 2012-Feb 2015	C ²	8	Estimate of adverse event, MTD ³	
NCT00589056	I/II	Stage III NSCLC ⁴	Cisplatin, etoposide, RT	Jun 2007-Mar 2012	C	55	DLT ⁵ , MTD	[318]
NCT01079286	I	Renal cancer	Temsirolimus	Jun 2008-May 2011	C	18	PK ⁶ , PD ⁷ , Dose escalation	
NCT02363829	I	LA ⁸ Cervical Cancer (Stage II-VA)	Cisplatin, Pelvic RT	Feb 2015-Feb 2020	C	6	Number of AE ⁹	

NCT01086332	I/II	Locally advanced pancreatic cancer (LAPC)	Gemcitabine, RT	May 2009- Jul 2015	T ¹⁰	7	DLT	
NCT00704600		Colorectal cancer	Capecitabine, Preoperative RT	Sep 2008 – Jul 2013	C	15	DLT, MTD	[326]
NCT01447589	I/II	NSCLC	Radical radiotherapy	Feb 2012- Oct 2012	W ¹¹	-	MTD, AE	
NCT01445106	I	Solid tumors	-	Dec 2006 - May 2011	C	28	MTD, DLT, PK, PD, antitumor response, blood markers	[243]
NCT01065844	II	Adenoid cystic head and neck carcinoma	-	Oct 2009- Nov 2017	C	15	Tumor progression	[292]
NCT01068327	I	Pancreatic cancer (adenocarcinoma/ Stage III)	Gemcitabine hydrochloride, leucovorin calcium, fluorouracil, RT	Nov 2007- Feb 2015	C	46	DLT, MTD, evaluate surgical resection rate, pathological and radiological response	[321]
NCT04169763	I	Vulvar cancer (Stage II-IVA)	Cisplatin, external beam radiation	Mar 2020- Dec 2023	NR ¹²	18 est. ¹³	DLT, safety, Dose for Phase II	
NCT01108666	II	Inoperable NSCLC (Stage III)	Cisplatin, paclitaxel, etoposide, proton beam radiation	Mar 2010- Dec 2018	T	8	MTD, toxicity, feasibility of proton beam, clinical efficacy	
NCT02024009	I/II	Non-metastatic LAPC	RT, nab-paclitaxel, gemcitabine, capecitabine,	Mar 2016 – Aug 2020	R ¹⁴	289 est.	OS ¹⁵ , PFS ¹⁶ , toxicity, QL ¹⁷	[320]

NCT03422874	I	Lymphoma	Ixazomib (MLN9708)	Aug 2016-Aug 2017	W	-	MTD, Toxicity, PK, PD	
NCT01959672	II	LAPC	Gemcitabine hydrochloride, leucovorin calcium, fluorouracil, oregovomab, RT	Sep 2013-Dec 2018	C	11	Evaluate efficacy and safety of neoadjuvant chemotherapy followed by RT+ nelfinavir	[322]
NCT01164709	I	Advanced hematologic malignancies	Bortezomib	Jul 2010-Nov 2013	C	18	DLT, objective response, AE	[259]
NCT03050060	II	Advanced melanoma, lung and kidney cancer	Atezolizumab, nivolumab, pembrolizumab, RT	Jun 2017-Dec 2021	S ¹⁸	120 est	RR ¹⁹ , OS, PFS, AE, immune correlative studies	
NCT02080416	I	Gamma-herpes related tumor	-	Jul 2014 - Feb 2016	T	1	Lytic activation of viral gene expression by nelfinavir	
NCT01925378	II	Cervical dysplasia	-	Jul 2012-Dec 2022	R	10 est.	Efficacy of nelfinavir	
NCT00791336	II	NSCLC	RT, cisplatin, etoposide	Aug 2008 - Mar 2011	T	1	Pathologic complete response	
NCT00915694	I	GBM ²⁰	Temozolomide, RT	Apr 2009 - Dec 2015	T	15	MTD, DLT, PFS, OS	[328]
NCT03256916	III	Carcinoma cervix (Stage III)	Cisplatin, pelvic RT	Jan 2018 - Sep 2025	R	300	Improvement in 3-yr disease free survival	
NCT03829020	I		Bortezomib, metformin	Apr 2019 -	R	36 est.	MTD, AE, hematological response	

		Relapsed or refractory multiple myeloma		Aug 2021				
NCT02188537	II	Proteasome inhibitor-refractory myeloma	Bortezomib, dexamethasone	Dec 2014 – Apr 2018	C	34	RR, AE, QL	[205]
NCT01555281	I/II	Multiple myeloma	Lenalidomide, dexamethasone	Feb 2012 – Dec 2021	AnR ²¹	33	DLT, ORR ²² , OS, PFS	[260]
NCT00233948	I/II	Liposarcoma	–	Mar 2006 – Jul 2013	T	29	DLT, MTD, ORR	
NCT00002185	II	Kaposi sarcoma	–	–	C	20	Safety and efficacy	
NCT02207439	II	Head and neck carcinoma	RT, platinum-based chemotherapy	Jul 2014 – Dec 2020	AnR	28	Determine locoregional control	
NCT03077451	II	Kaposi sarcoma	–	Mar 2017 – Oct 2020	AnR	36	Efficacy of dose escalation	
NCT00694837	I	GBM	Temozolomide, RT	Mar 2009- Jan 2013	C	6	MTD, toxicity	
NCT01020292	I	Glioma	Temozolomide, RT	Apr 2009- Dec 2017	C	31	MTD, DLT, PFS, OS	
NCT00003008	II	Sarcoma	Indinavir, saquinavir, ritonavir, paclitaxel	Jun 1997- Jun 2006	C	33	Role of HIV-PIs in plasma clearance of paclitaxel	

¹ Radiotherapy, ² Completed, ³ Maximum tolerated dose, ⁴ Non-small cell lung carcinoma, ⁵ Dose limiting toxicity, ⁶ Pharmacokinetics, ⁷ Pharmacodynamics, ⁸ Locally advanced, ⁹ Adverse events, ¹⁰ Terminated, ¹¹ Withdrawn, ¹² Not recruiting, ¹³ Estimated, ¹⁴ Recruiting, ¹⁵ Overall survival, ¹⁶ Progression free survival, ¹⁷ Quality of life, ¹⁸ Suspended, ¹⁹ Response rate, ²⁰ Glioblastoma multiforme, ²¹ Active, not recruiting, ²² Overall response rate

1.3.5 Conclusions

Nelfinavir can target a number of mechanisms in mammalian cancer cells; however, definitive identification of the primary cellular target responsible for anti-tumor efficacy is still needed. Analysis of reports indicating probable intracellular pathways suggests that the mechanisms to impart anti-cancer properties by nelfinavir may be cell type and cancer-specific. A number of phase I and II clinical trials have proven the safety, tolerability, and positive outcome of nelfinavir in cancer patients, with or without co-treatments, especially against pancreatic cancer, NSCLC, and MM [259,290,318]. So far, the completed clinical trials have been single arm and open-labelled involving small cohorts and the available data warrants randomized controlled trials on larger population groups. Accordingly, two large-scale randomized trials are currently ongoing to test the efficacy of nelfinavir with radiotherapy against locally advanced pancreatic cancer (NCT02024009) and cervical cancer (NCT03256916).

Anti-infective dosing of nelfinavir in HIV-infected patients results in maximum plasma concentration of 7-9 $\mu\text{mol/L}$, and reports have shown that anti-cancer effects can be achieved within this range [201,204,206]. However, higher plasma concentration may be needed to elicit anti-cancer properties by nelfinavir against some cancers [226]. As nelfinavir is an inducer and substrate of metabolic enzyme CYP3A4, autoinduction of plasma clearance in high doses is initiated, which prevents increment of plasma concentration during dose escalation, leading to non-linear pharmacokinetics [323]. Enhanced plasma concentration and tissue availability of nelfinavir

can be achieved through molecular modification, drug combination, or nano-particle based administration. Molecular modification through nitric oxide (NO) hybridization of HIV-PIs has emerged as an alternative strategy to increase the anti-cancer efficacy of lower doses, especially in the case of saquinavir [189]. Metabolism of nelfinavir by the enzyme CYP2C19 yields the pharmacologically active metabolite M8 responsible for suppressing the viral replication. M8 has also shown comparable anti-tumor activity to nelfinavir [247]. Kattel *et al.* reported enhanced systemic exposure of nelfinavir due to genetic polymorphism of CYP2C19 in locally advanced pancreatic cancer patients, suggesting that stratification of patients according to the genotype could identify the population likely to benefit from nelfinavir treatment [329].

Overall, the anti-tumor effects of nelfinavir have been tested on an array of cancers with positive results rationalizing its suitability as a potential candidate for drug-repurposing in cancer.

1.4 THESIS RATIONALE AND OBJECTIVES

Ovarian cancer remains a significant source of morbidity and mortality, being the seventh most common cancer among women and the eighth leading cause of gynecologic-cancer-related death in the world [8]. Despite increasing advancement in diagnostics and therapeutic avenues, platinum-based treatment following tumor-debulking surgery persists as the backbone of ovarian cancer treatment for over fifty years. Although 70% of patients respond favourably to the initial platinum-based therapy, flaring of microscopic residual disease and emergence of platinum-resistance are inevitable within 18-24 months, which has contributed to an unimproved 5-year survival rate (47%) since the 1980s [46,330-332]. A maintenance therapy during the window of time between the primary standard of care and the relapse of the disease may lead to improved patient survival.

Repurposing of market-available drugs is a viable alternative to accelerate the availability of newer therapeutic options to patients in urgent need, instead of relying on the prolonged traditional drug development pipeline. We selected a market-available anti-HIV drug, nelfinavir, which has been safely in use as an anti-infective agent for more than two decades. Nelfinavir has demonstrated off-target anti-cancer effects against a variety of cancers, via a multitude of molecular mechanistic avenues. To date, the possible therapeutic efficacy of nelfinavir has not been investigated against HGSOc.

Among nine mechanistic pathways whereby nelfinavir exerts cytotoxic effects in different cancer, the endoplasmic reticulum (ER) stress and the associated unfolded protein response (UPR) have been the most cited ones. The UPR is the cellular adaptive process aimed at relieving the cells from the ongoing proteotoxic stress in the ER due to the accumulation of misfolded or correctly folded proteins. Moderate levels UPR is life-saving and promotes proteostasis [333]. Elevated ER stress can be manifested as a survival mechanism within the cancer cells due to the

suboptimal environment, e.g. hypoxia, low nutrient supply, providing a vulnerable target for exploitation, from which the normal cells thriving in optimal conditions may be spared [334]. For instance, Samanta *et al.* observed elevated ER stress related markers in the tissue samples of serous ovarian cancer [335]. On the other hand, prolonged or aggravated ER stress exhausts all reparation machinery to re-establish proteostasis and shifts the cell fate to death. Aggravation of existing elevated basal ER stress within the cancer cells can be a potent pharmacological strategy to induce cell death. Therefore, we asked the question as to whether nelfinavir can aggravate ER stress in HGSOc cells and lead to cell death.

An important component of the prosurvival UPR is the endoplasmic reticulum-associated degradation (ERAD), where misfolded ubiquitinated protein may be retrotranslocated to the proteasome for degradation, in an attempt to reduce the overall protein load [334]. In theory, blocking of the proteasome might cause retrograde enhancement of protein load, which will further aggravate an already activated ER stress pathway, tipping the cell fate towards cell death. In agreement with this idea, our laboratory had demonstrated previously that induced ER stress in response to mifepristone in ovarian cancer cells was unbalanced toward its proapoptotic fate by combining it with a proteasome inhibitor bortezomib [336]. As such, we raised our second question, similar to the ER stressor mifepristone, whether nelfinavir can potentiate the cytotoxic effect of the proteasome inhibitor bortezomib.

Based on the above rationale, we developed our **overall hypothesis**, “Anti-HIV agent nelfinavir, acting as an ER stressor, is cytotoxic toward high grade serous ovarian cancer cells and potentiates the toxicity of the proteasome inhibitor bortezomib.”

The hypothesis was tested in our study by investigating the following objectives:

Objective 1: To determine if nelfinavir acts as an ER stress aggravator and induces cytotoxicity in high-grade serous ovarian cancer cells;

Objective 2: To investigate the molecular mechanism underlying nelfinavir mediated cytotoxicity against high-grade serous ovarian cancer;

Objective 3: To explore if nelfinavir, acting as an ER stress aggravator, can potentiate the cytotoxicity of the proteasome inhibitor bortezomib.

CHAPTER 2

-

MATERIALS AND METHODS

2.1 Cell culture and reagents

PEO1/PEO4/PEO6 and PEO14/PEO23, two sequentially obtained and spontaneously immortalized polyclonal series of cell lines, were utilized to explore the effects of nelfinavir [337] (**Figure 2.1**). The original patients demonstrated different levels of disease progression and platinum sensitivity during the establishment of each cell line. The first patient was sensitive to cisplatin when the PEO1 cell line was developed from the ascitic fluid following 22 months of the last cisplatin-based therapy. Later, the patient was deemed clinically resistant to cisplatin while PEO4 and PEO6 cells were obtained respectively 10 months and 3 months after the last cisplatin-based therapies. PEO14 cells were established from the ascitic fluid of a second patient during the chemo-naïve stage, and PEO23 cells were developed during the cisplatin-resistant stage of that patient 7 months after the last cisplatin-based therapy [155]. With the written consent from Dr. Langdon (Edinburgh Cancer Research Center, Edinburgh, UK), PEO1, PEO4 and PEO6 cell lines were obtained from Dr. Taniguchi (Fred Hutchinson Cancer Center, University of Washington, Seattle, WA, USA). PEO14 and its longitudinally patient-matched pair PEO23, were obtained from Culture Collections, Public Health England (Porton Down, Salisbury, UK).

To study the effect of nelfinavir on artificially acquired cisplatin-resistance *in vitro* the cancer cell line OV2008 and its cisplatin-resistant pair OV2008 C13 [338] were utilized. OV2008 cells have more recently been disputed of their ovarian origin, suggesting to have a cervical cancer origin instead[339]. However, since the pair OV2008 and OV2008 C13 has been used extensively in previous publications from our laboratory [336,340,341], especially in the context of cisplatin resistance, we utilized them for providing proof of concept and optimizing experimental designs and protocols. OV2008 and its sibling OV2008 C13 were obtained from Dr. Stephen Howell (University of California, San Diego). Finally, the cell line we termed PEO1X was generated from

PEO1 cells following an *in vitro* challenge with cisplatin for 1 h. Following the cisplatin challenge, the damaged cells were washed away, and the remaining clones were allowed to repopulate to generate the PEO1X cell culture (**Figure 2.1**).

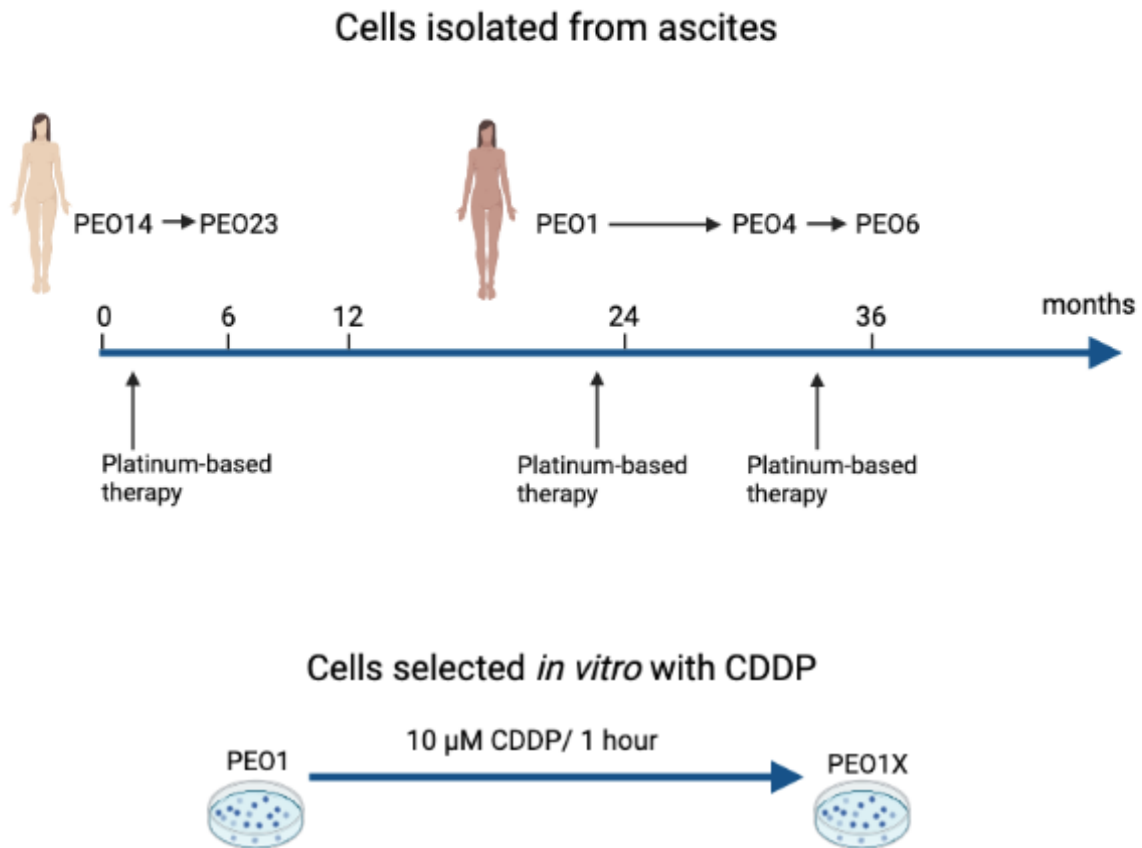


Figure 2.1: The schematics represent at the top paired cell lines derived from the ascites of two different patients [155,337]. We proceeded to utilize one cell line (PEO1) and challenge it with cisplatin (cis-diamminedichloroplatinum / CDDP) for 1 h. Thereafter, the toxic agent was removed, the dead cells were eliminated, and the repopulated cells with slightly different morphology were termed PEO1X. (Diagram created on <https://biorender.com/>).

All cells were cultured in RPMI-1640 (Mediatech, Manassas, VA, USA) supplemented with 5% fetal bovine serum (Atlanta Biologicals, Lawrenceville, GA, USA), 5% bovine serum (Life Technologies, NZ), 1 mM sodium pyruvate (Mediatech), 4mM L-glutamine (Mediatech), 10 mM HEPES (Mediatech), 0.01 mg/mL human insulin (Roche, Indianapolis, IN, USA), 100 IU penicillin (Mediatech), and 100 µg/mL streptomycin (Mediatech). Cell culture was carried out at 37°C in a humidified incubator of 95% air/5% CO₂ in standard adherent plastic plates. Autosomal short tandem repeat (STR) profiling markers were utilized for authentication, which demonstrated ≥80% match between the cell lines used in our study and the genotype of the original patients. The STR was carried out in the authentication core facility of the University of Arizona (Tucson, AZ, USA) [51]. Cells were stored via cryopreservation in liquid nitrogen. Cryopreservation was carried out by immersing the cells (usually 1 million/vial) in commercially available Cryostor® media or in a mixture of fetal bovine serum (Atlanta Biologicals, Lawrenceville, GA, USA) and dimethyl sulfoxide (DMSO) in a ratio of 9:1. Prior to transferring the vials of cells to liquid nitrogen, the cells were gradually pre-frozen at -80°C in a freezing container with isopropanol (Mister Frosty™). The maximum passage number for the cell lines used in the experiments was limited to 10.

The drugs used in this study were as follows: nelfinavir mesylate hydrate (NFV) (Sigma Chemical Co., St. Louis, MO, USA), cis-diamminedichloroplatinum II (cisplatin, Sigma), bortezomib (BZ) (Velcade®, Millennium Pharmaceuticals, Cambridge, MA, USA), tunicamycin (Sigma), puromycin dihydrochloride (Sigma), bafilomycin A1 (Cell Signaling Technology, Danvers, MA, USA), salubrinal (EMD 100hemilumi) and cycloheximide (Sigma). Nelfinavir and tunicamycin were vehiculized in dimethyl sulfoxide (DMSO) to yield 50 mM and 5 mg/ml stock solutions, respectively, and were stored at -20°C. Puromycin dihydrochloride was dissolved in

cell-culture grade water to make an 18.37 mM stock solution, aliquoted, and stored at -20°C until use. Bafilomycin, cycloheximide, and salubrinal were commercially delivered in ready-made stock solutions and were stored at -20°C, 4°C and -80°C, respectively. Bortezomib was dissolved in 0.9% sodium chloride solution to generate a 2.6 mM stock solution which was stored at -20°C. Cisplatin powder was dissolved in isotonic saline solution to generate a stock of 3.33 mM right before starting an experiment. During an experiment, the stock solutions were serially diluted in respective vehicles or culture media to reach the desired treatment doses. The maximum concentration of DMSO in the cell culture was maintained at $\leq 0.1\%$ (v/v).

2.2 Cell proliferation and viability assay

Cell proliferation and viability were assessed via microcapillary cytometry. We described this methodology previously in detail [341]. Briefly, HGSOC cells were subjected to different treatments in triplicates or quadruplicates for different times. After each treatment, cells were trypsinized and centrifuged to yield cellular pellets, which were washed and resuspended in phosphate-buffered saline (PBS), and mixed with the Muse™ Count & Viability Reagents (Luminex Corporation, Austin, TX, USA). The stained samples were analyzed with a microcapillary fluorescence cytometer (Guava® Muse® Cell Analyzer, Luminex), and the data were calculated by the Guava® Muse® Software (Luminex).

The proprietary solution of the Muse® Count & Viability Reagent consists of two dyes: 1) a nuclear DNA binding dye that tags all the nucleated cells, and 2) a viability dye that penetrates the cells with compromised cell membrane, thus tagging all the damaged/dying cells. Upon laser excitation, the Guava® Muse® Cell Analyzer distinguishes between the viable and dying cells

while excluding debris, providing a quantitative estimate of the total number of cells and percent viability.

2.3 Assessment of the sensitivity of the PEO cell line series to cisplatin

The sensitivity of the PEO cell lines to cisplatin was determined using a combination of short-term exposure of the cells to the drug followed by a long-term incubation of remaining live cells in cisplatin-free media. This assay allows determining the long-lasting toxic effects of cisplatin. The drug was introduced into the media to reach final concentrations in the range of 1 to 50 μM . Saline was provided to vehicle-treated cells. Cells received cisplatin-infused media for 1 hour (h), after which time media was removed, cells were washed with PBS, and media without cisplatin was provided for 72 h. The 1 h treatment time with cisplatin was selected to mimic the amount of time cisplatin is typically provided to a patient in a clinical setting. Thereafter, floating and adherent cells were collected and assayed for number and percent viability using fluorescence cytometry as explained above. Subsequently, 1000 viable cells for each treatment group were seeded in 6-well plates and cultured for 10-15 days until the number of cells/colonies in the vehicle-treated plates was ≥ 50 . At the end of the incubation period in cisplatin-free medium, the medium was aspirated, the cells were washed with PBS, and then fixed with 4% paraformaldehyde (PFA) for 30-45 minutes and stained with 0.5% (w/v) crystal violet (Sigma) for 20 minutes before being rinsed with tap water and dried at room temperature. Colonies having ≥ 50 cells were scored manually in an AmScope inverted light microscope with AmScope Software 3.7 (XD Series, United Scope LLC, Irvine, CA, USA) using 10x and 20x objectives. These values were imputed into the CalcuSyn software (Biosoft, Cambridge, UK), which calculated the half-maximal inhibitory concentration or IC_{50} (in μM) for each cell line. The average of two independent

experiments performed in triplicate was used in the determination of the final IC₅₀ value for each cell line.

2.4 Cell cycle analysis

Following treatment, single-cell suspensions were fixed with 4% PFA at room temperature for 1 h. Suspensions were centrifuged at 300 g for 5 min, and pelleted cells were washed twice with PBS. A suspension containing 2×10^5 cells was re-pelleted and resuspended in 0.2 ml of propidium iodide (PI) solution containing 7 U/ml Rnase A, 0.05 mg/ml PI, 0.1 % v/v Triton X-100, and 3.8 mM sodium citrate (Sigma) for 20 min at room temperature or overnight at 4°C protected from light. Cells were analyzed with the Guava® Muse® Cell Analyzer (Luminex), which takes advantage of the capacity of PI to stain DNA, allowing detecting different DNA contents along the cell cycle. The cell cycle application of the Guava® Muse® software was used to analyze the results and to determine relative stages within the cell cycle. The PI-stained particles found containing hypo-diploid DNA content were considered to be in a Sub-G1 state, likely representing apoptotic bodies.

2.5 Clonogenic survival assay

HGSOC cells were treated with increasing concentrations of nelfinavir in triplicates or quadruplicates for 72 h; thereafter, the cells were trypsinized and counted using the method described in the cell proliferation and viability assay. For each treatment group, 1000 live cells were re-plated sparingly in 6-well plates in drug-free media and were incubated for 14-21 days to observe the colony-forming capacity of the cells withstanding the treatment. When the number of cells reached ≥ 50 per colony in the vehicle group, the experiment was terminated by discarding

the media and fixing the cells with 4% PFA. The fixed cells were further stained using 0.5 % crystal violet, and the colonies were counted manually using an inverted light microscope (**Figure 2.2.**)

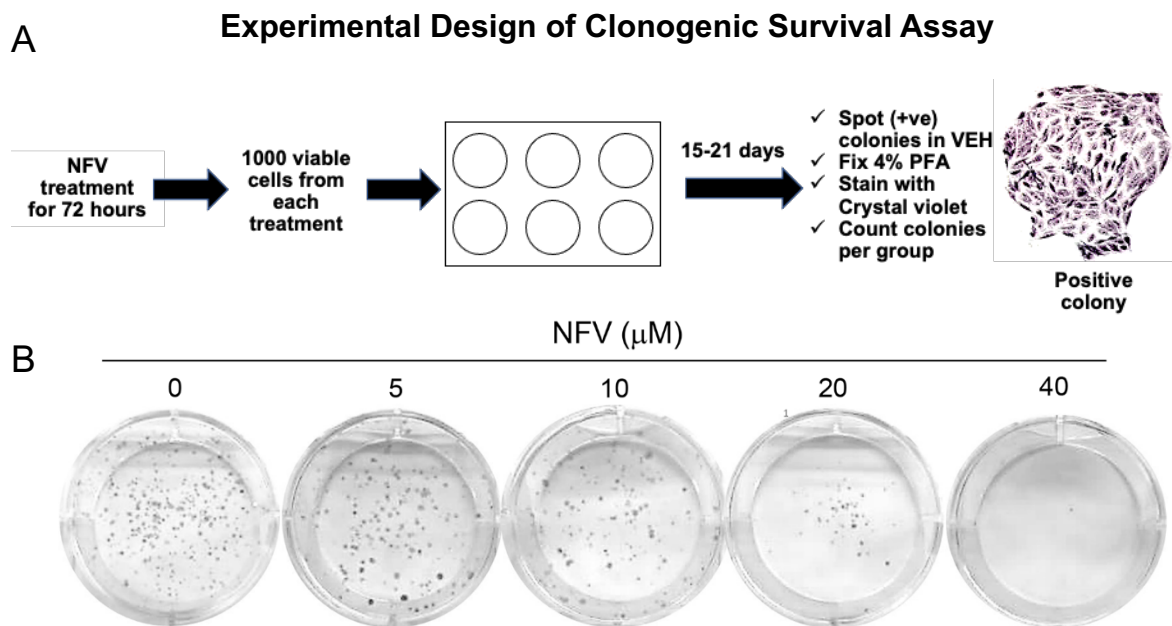


Figure 2.2: (A) Experimental approach to observe residual cytotoxicity following acute exposure to nelfinavir (NFV). (B) Visual representation of a dose-response clonogenic survival assay performed on the PEO1 cell line.

2.6 Measure of *XBPI* mRNA splicing

RNA was isolated using RNAqueous™ - 4PCR DNA-free™ RNA Isolation for RT-PCR kit (Invitrogen by Thermo Fischer Scientific) following the manufacturer's instructions. Briefly, drug-treated cells were mixed with lysis solution and 64% ethanol, scraped, and collected at 4°C. The collection was filtered 3 times via high-speed centrifugation at 15,000 g for 1 min. The filtered

material trapped within the filtration cartridge was mixed with wash solutions and was subjected to high-speed filtration for 3 times. Finally, the RNA was extracted by serially adding 50 μ l of elution solution at 28°C. The collected RNA was flash frozen in liquid nitrogen and then stored at -80°C. Throughout the process of isolation, the level of ribonuclease was kept low by spraying the Rnase Zap[®] RNAase Surface Decontamination solution.

cDNA was synthesized using iScript (BioRad Laboratories, Inc, Hercules, USA) and quantified in a NanoDrop 2000 (ThermoFisher, Waltham, MA, USA). The forward primer for PCR amplification of spliced and total human Xbp1 mRNA was 5'-CCTGGTTGCTGAAGAGGAGG-3' and the reverse primer was 5'CCATGGGGAGTTCTGGAG-3'. For ACTB (β -actin), the primers were 5'ACAGAGCCTCGCCTTTG-3' (forward) and 5'-CCTTGCACATGCCGGAG-3' (reverse). The size of amplified unspliced Xbp1 mRNA is 145 base pairs (bp), the size of amplified spliced Xbp1 mRNA is 119 bp, and the size of amplified ACTB (β -Actin) is 110 bp. All primers were purchased from ID Technologies (Coralville, IA, USA). PCR reactions were performed in a 20 μ l total volume reaction using SsoAdvanced Universal SYBR Green supermix (BioRad), 900 nM primer, 20 ng sample, and RT-PCR Grade Water (Invitrogen, Carlsbad, CA, USA). Using a C100 thermal cycler (BioRad), the following cycling profile was applied: 95°C for 3 min, followed by 35 cycles at 94°C for 30 s, 58°C (60°C for β -Actin) for 30 s, and 72°C for 30 s, with a final extension at 72°C for 5 min. No template control and no reverse transcriptase control were also included in each assay. The PCR products were visualized in 2% agarose gels, which were run at 100V and then imaged in a ChemiDoc MP (BioRad). The gels were stained with SYBR Safe DNA gel stain (Invitrogen). A Low DNA Mass Ladder (Invitrogen) was used to determine the size of the PCR products.

2.7 Western blot analysis

Following treatment, HGSOC cells were washed with ice-cold PBS, scraped, collected, and centrifuged to yield pellets, which were stored in -80°C . Protein lysates were extracted from the pellets using NP40 lysis buffer, and 20 μg of proteins per sample were resolved in 10 or 12% gels (TGX™ FastCast™ Acrylamide kit, Bio-Rad) via electrophoresis. The resolved proteins were transferred to Immuno-Blot® PVDF membranes using a Trans-Blot® Turbo™ Transfer System (BioRad). Membranes were incubated at 4°C overnight in primary antibodies against GRP78, CHOP, IRE1 α , PERK, p-eIF2 α , eIF2 α , ATF4, ATF6, p-CDK2, total CDK2, LC3II, Bcl-2, Bax, Caspase-3, Caspase-7, PARP, p-AKT (Ser-473), p-ERK, p27^{kip1}, γH2AX , ubiquitin, puromycin, and β -actin (see Table 2.1 for details about the origin and dilutions of the used antibodies). Thereafter, membranes were washed and re-incubated with secondary antibodies, and protein detection was performed via a ChemiDoc Imaging System (BioRad) using chemiluminescence (Clarity Western ECL Imaging System, BioRad). Ultraviolet activation of the TGX stain-free gels on a ChemiDoc MP Imaging System (BioRad) was used to control for proper loading; in short, the pre-cast gels include unique trihalo compounds that allow rapid fluorescence detection of proteins without staining. The trihalo compounds react with tryptophan residues in a UV-induced reaction to produce fluorescence that is detected on the PVDF membranes [342]). The original membranes containing detailed information from where the immunoblots images in key results were obtained, are shown in Appendix 1.

Table 2.1: Source and dilutions of antibodies utilized in this work

Antibody	Clone or catalogue	Company	Concentration
PERK	3192S	Cell Signaling Technology	1:1000
GRP78	3177S	Cell Signaling Technology	1:1000
IRE1 α	3294S	Cell Signaling Technology	1:1000
p-eIF1 α	3398S	Cell Signaling Technology	1:1000
eIF2 α	9722S	Cell Signaling Technology	1:1000
ATF4	11815S	Cell Signaling Technology	1:1000
CHOP	5554S	Cell Signaling Technology	1:1000
ATF6	NBP1-40256	Novus TM Biologicals	1:1000
Anti-puromycin	MABE343	EMD Millipore Corp.	1:20000
p-Akt	4058L	Cell Signaling Technology	1:1000
Akt	2920S	Cell Signaling Technology	1:1000
p-ERK	9106L	Cell Signaling Technology	1:1000
ERK	9102L	Cell signaling Technology	1:1000
p-CDK2	2561S	Cell Signaling Technology	1:1000
CDK2	SC-6248	Santa Cruz Biotechnology	1:500
p27	610242	BD Biosciences	1:1000
γ H2AX	05-636	EMD Millipore Corp.	1:1000
LC3B	3868S	Cell Signaling Technology	1:1000
Ubiquitin	3933S	Cell Signaling Technology	1:1000
β -Actin	A5441	Sigma Lifescience	1:10000
PARP	9542L	Cell Signaling Technology	1:1000
Caspase-3	9662S	Cell Signaling Technology	1:1000
Caspase-7	12827S	Cell Signaling Technology	1:1000
Bax	5023S	Cell Signaling Technology	1:1000
Bcl-2	15071S	Cell Signaling Technology	1:1000
Anti-mouse	170-6516	BioRad Laboratories Inc.	1:8000
Anti-rabbit	170-6515	BioRad Laboratories Inc.	1:10000

2.8 Puromycin incorporation assay

The puromycin incorporation assay is a non-radioactive method of quantifying mRNA translation rate. Puromycin is an aminoacyl-tRNA mimetic that can occupy the site A of the ribosome during mRNA translation and thereby terminates the process prematurely. However, short-term exposure enables conjugation of puromycin with the nascent polypeptide chains generating short-lived puromycylated peptides that are released from the ribosome and can be detected by an anti-puromycin antibody on immunoblots. As one molecule of puromycin is incorporated into each released nascent polypeptide, puromycin incorporation is deemed as a sensitive indicator of ongoing mRNA translation rate [3,4]. In our experiments, puromycin was added to the culture media at a final concentration of 1 μ M at 37°C, 30 min prior to the termination of the experiments. Thereafter, the cells were collected and processed for the detection of puromycylated proteins by immunoblot.

2.9 Autophagic flux

We studied autophagic flux as previously described in our laboratory [336]. Briefly, autophagic flux assay is performed by tracking the expression of the autophagosomal membrane-associated protein LC3II in response to a drug treatment, with or without the presence of an inhibitor of the lysosomal function. An increase in the levels of LC3II in response to a drug treatment may indicate either increased autophagy induction or impaired autophagosome removal by the lysosomes. Hence, autophagic flux is a better measure of the autophagic process, as it determines LC3II turnover in the presence or absence of the lysosome inhibitor bafilomycin A1. If LC3II level rise further in the presence of the studied drug plus bafilomycin A1 when compared

to cells treated only with the experimental drug, this means that the rate of autophagy or autophagic flux is increased. In contrast, no change in the expression of LC3II during co-treatment with the lysosome inhibitor indicates accumulation of autophagosomes because of lysosome impairment caused by the drug under study. In our experiments, nelfinavir-treated HGSOC cells were further exposed or not to 100 nM bafilomycin A1 for 1 h before the termination of the experiment. Thereafter, the cells were collected and processed for the detection of LC3II by immunoblot.

2.10 Drug interaction analysis

To determine whether there is pharmacological interaction between nelfinavir and bortezomib, a drug-interaction assay was performed on platinum-sensitive PEO1 cells, and on the less-sensitive to platinum, PEO4. Using total number of cells as a variable, data were analyzed through algorithms in the CalcuSyn software (Biosoft), which uses the combination index (CI) method for predicting drug interaction [343]. We previously described in detail the calculation of the CI [344]. In brief, for a specific drug association, a $CI > 1$ is considered antagonistic, $CI = 0$ means no drug interaction, $CI = 1$ indicates additivism, whereas $CI < 1$ denotes synergism.

2.11 Statistical analysis

For tests involving western blot analysis, the experiments were repeated at least twice with similar outcomes. Numerical data are expressed as the mean \pm SEM. Differences were considered significant if $P < 0.05$. GraphPad Prism 9 (Graphpad Software, La Jolla, CA, USA) allowed for statistical analysis of data using one-way ANOVA followed by Tukey's multiple comparison test, or two-way ANOVA followed by Bonferroni's multiple comparison test.

CHAPTER 3

-

RESULTS

3.1 Nelfinavir inhibits growth, reduces viability, increases hypo-diploid DNA content, and blocks clonogenic survival of high-grade serous ovarian cancer (HGSOC) cells regardless of platinum sensitivity

The overall cytotoxicity of nelfinavir was assessed on HGSOC cells of varying cisplatin sensitivities, which are depicted in **Table 3.1**. Of the five tested cell lines, PEO1, PEO4 and PEO6 were derived from one patient, whereas PEO14 and PEO23 were derived from a second patient. PEO1 demonstrated to be the most sensitive to cisplatin, whereas PEO6 showed to be the least sensitive. Our results also indicate that the cell lines, established at different stages of disease progression, recapitulated *in vitro* the cisplatin sensitivity of the original patients during the time of procuring the cells from ascites, with PEO1>PEO4>PEO6 for patient one, and PEO14>PEO23 for patient two.

Bright-field microscopy was utilized to assess the morphological features of the HGSOC cell lines belonging to two patient-matched series (PEO1/4/6 and PEO14/23) (Figure 3.1). While incubated within standard cell culture conditions, PEO1 demonstrated sheets of spindle-shaped cells grown in monolayers with islands of compact cells. PEO4 cell-line primarily demonstrated two-dimensional islands of polygonal cells and spindle-shaped cells. PEO6 showed clusters of epithelial cells with a tendency to grow in three-dimensional layers and form spheroids. Both PEO14 and PEO23 demonstrated layers of polygonal cells, with PEO23 showing a tendency to grow three-dimensional floating structures in culture. Despite originating from the same patient, these *in vitro* morphological differences are indicative of disease progression and phenotypical heterogeneity—a classical feature of HGSOC. These observations are commensurate with the findings of Langdon and colleagues, who developed and characterized the cell line series back in 1988 [337].

Table 3.1 Concentration of cisplatin needed to achieve 50% reduction in clonogenic survival (IC_{50}) of the HGSOC cell lines studied

Cell Line	IC_{50} (μ M)
PEO1	0.56 ± 0.08
PEO14	0.65 ± 0.06
PEO23	3.36 ± 0.14
PEO4	6.79 ± 0.51
PEO6	8.66 ± 0.25

PEO1, PEO4, and PEO6 are siblings cell lines developed from one patient, whereas PEO14 and PEO23 are sibling cell lines developed from a different patient. All cell lines were generated along disease progression before and after the patients became clinically resistant to cisplatin-based therapy. IC_{50} s are arranged from the more sensitive to the less sensitive to cisplatin *in vitro* regardless of the patient's origin. The sensitivity to cisplatin the cells displays *in vitro* correlates with the clinical response of the patient of origin, with PEO1>PEO4>PEO6 and PEO14>PEO23 [155,337].

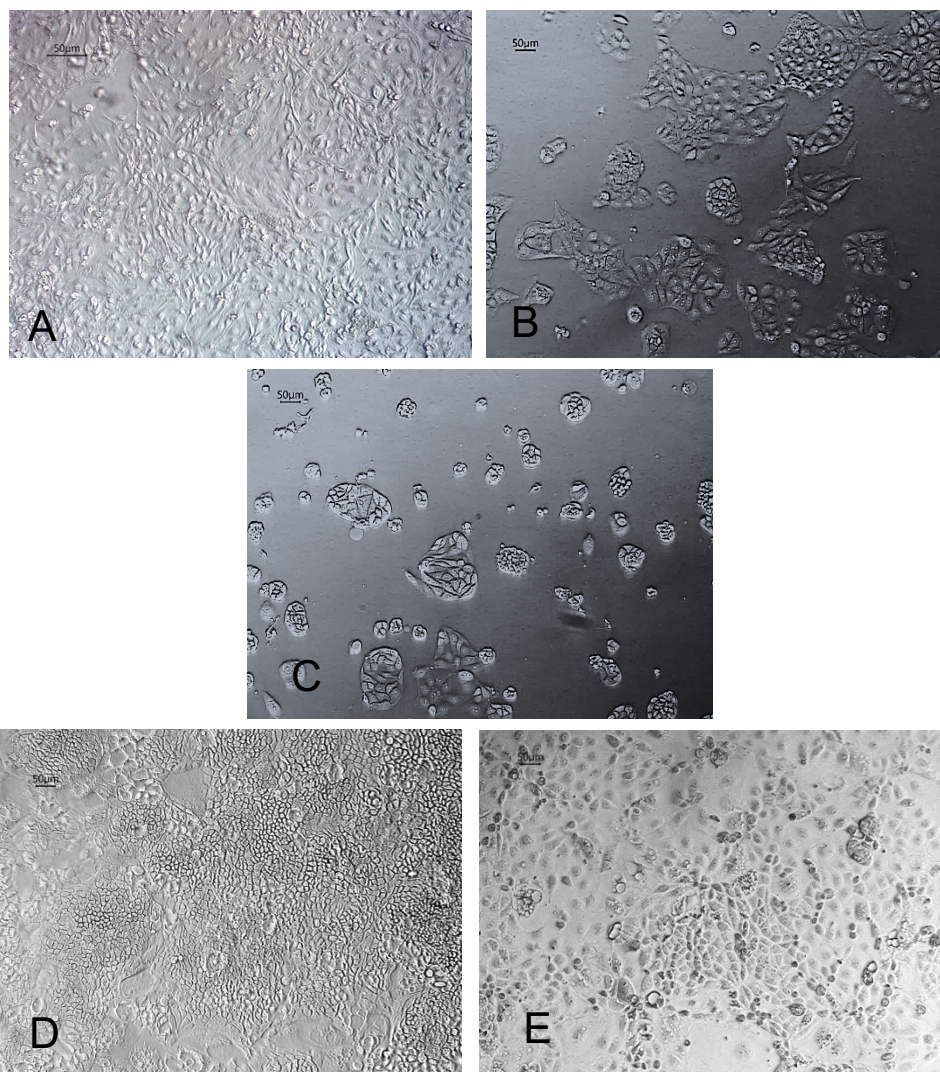
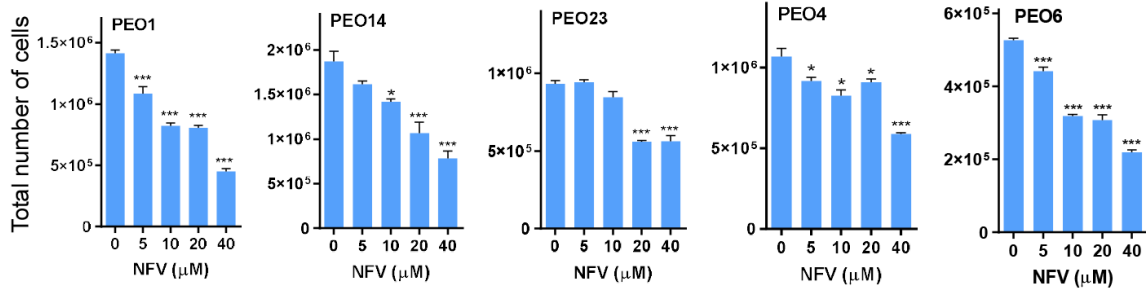


Figure 3.1: Representative images demonstrating in-culture morphological features of PEO1 (A), PEO4 (B), PEO6 (C), PEO14 (D), and PEO23 (E) cells. PEO1 cells demonstrate a monolayer of elongated cells, PEO4 shows islands of polygonal cells, and PEO6 shows three-dimensional cellular clusters. PEO14 and PEO23 demonstrate compact layers of polygonal cells, with PEO23 releasing floating three-dimensional structures in the media. Scale bar=50 μm

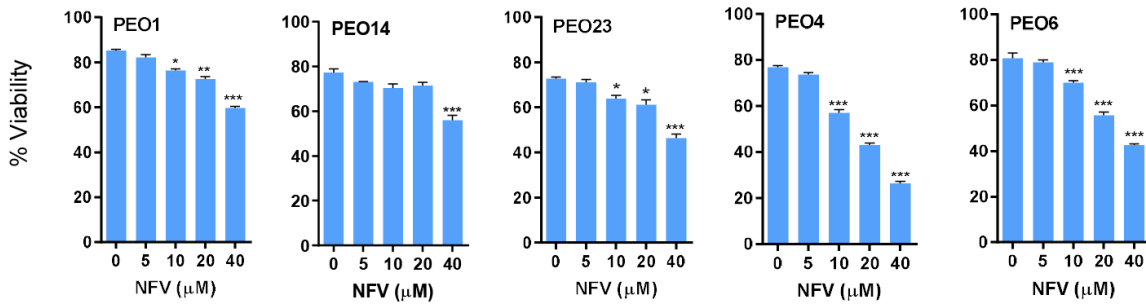
In this study, we assessed cell toxicity in a broad manner, including abrogation of their reproductive capacity (cytostasis), and the actual dying of the cells (lethality), which can be acute and visualized upon short-term incubation (within 72 h), or long-lasting irreversible reproductive impairment visualized in long-term incubations (as observed in clonogenic survival assays). Acute cytotoxicity of nelfinavir towards HGSOC cells was investigated via cell-proliferation and viability assays following 72 h of treatment. We observed that nelfinavir decreased the total number of cells and the percent viability of all the cell lines in a concentration-dependent manner regardless of their platinum sensitivity (**Figure 3.2 A and B**). We further determined that higher concentrations of nelfinavir reduce cellular viability in association with the accumulation of hypodiploid DNA content (a.k.a. Sub-G1 DNA content), denoting that the cells are likely dying by apoptosis (**Figure 3.2 C**). Finally, the long-lasting reproductive impairment caused by nelfinavir in HGSOC cells was reflected by the fact that cells that remained alive after 72 h exposure to nelfinavir had reduced clonogenic capacity when incubated in nelfinavir-free media for 15-21 days depending on the cell lines (**Figure 3.2 D**). In summary, nelfinavir is toxic towards HGSOC cells regardless of their sensitivities to cisplatin, involving short-term reduction in viability and leading to a long-lasting impairment of their reproductive capacities.

Platinum sensitivity

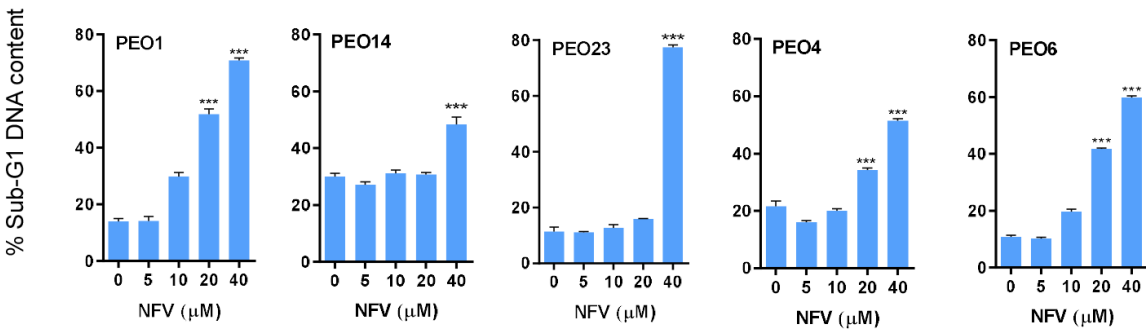
A



B



C



D

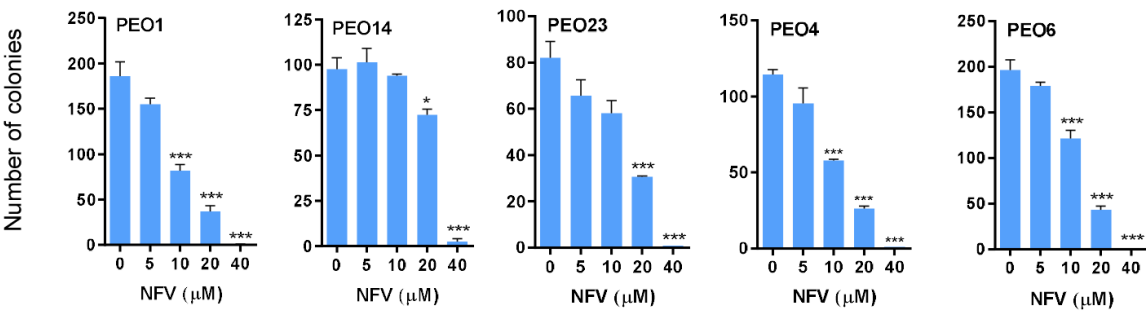


Figure 3.2

HGSOC cells of differential platinum sensitivities were plated in six-well plates in triplicate and, when exponentially growing, were subjected to treatment with the depicted concentrations of nelfinavir (NFV) for 72 h. At the end of the experiment, the cells were trypsinized and subjected to microcytometry analysis to attain the total number of viable cells (A), and percent viability (B). A fraction of the cellular content collected at the end of the incubation with NFV was stained with propidium iodide (PI) and subjected to cell cycle analysis to determine hypodiploid DNA content (C). Finally, 1000 viable cells obtained at the end of the experiment were subjected to a clonogenic survival assay in the absence of treatment to determine delayed toxicity of NFV (D). * $p < 0.05$; *** $p < 0.001$ vs. control (One-way ANOVA followed by Tukey's Multiple Comparison Test). The gray area that goes from higher to lower signifies that the cells are depicted in the order of their decreasing sensitivity to the toxic effects of cisplatin as depicted in **Table 3.1**.

3.2 Sensitivity toward nelfinavir is enhanced over time when compared with the short-term toxicity

Although nelfinavir was able to elicit cytotoxicity in all the tested HGSOC cell lines despite their differential sensitivity toward cisplatin, the range of nelfinavir-mediated effects varied. As such, it was essential to estimate the sensitivity of the tested cell lines toward nelfinavir. We assessed the nelfinavir sensitivity of the cell lines by two approaches; firstly, by utilizing the inhibition of cell growth following 72 h treatment to estimate the IC_{50} , which illustrates nelfinavir sensitivity during short-term therapy. Afterwards, we measured the IC_{50} by utilizing the reduced number of colonies at the end of 14-21 days of drug-free incubation of the cells surviving acute treatment (72 h), which demonstrates the sensitivity of HGSOC cells toward nelfinavir during long-term therapy. We observed that during short-term therapy the PEO14/PEO23 series showed less sensitivity toward nelfinavir ($IC_{50} \sim 20 \mu M$) when compared to the PEO1/PEO4/PEO6 series ($IC_{50} \sim 10 \mu M$) (**Table 3.2**); however, during long-term therapy PEO14/PEO23 demonstrated enhanced sensitivity to nelfinavir ($IC_{50} \sim 15 \mu M$). The sensitivity of the cells from the series PEO1/PEO4/PEO6 did not change between short-term and long-term toxicities. The status of cisplatin sensitivity of the cell lines did not seem similar to their sensitivity toward nelfinavir; for instance, PEO14 showed high sensitivity to cisplatin (**Table 3.1**); however, it was less sensitive to nelfinavir when compared with the other tested HGSOC cells (**Table 3.2**).

Table 3.2 Comparison of concentrations of nelfinavir (NFV) required to achieve 50% reduction in the total number of cells during short-term studies (72 h), and 50% reduction in the clonogenic survival during long-term therapy

Cell Line	IC ₅₀ (□M) Short-term	IC ₅₀ (□M) Long-term
PEO1	10.13 ± 1.68	10.05 ± 0.75
PEO4	12.88 ± 1.91	12.4 ± 2.6
PEO6	10.80 ± 3.3	11.4 ± 0.4
PEO14	22.9 ± 5.18	16.07 ± 4.9
PEO23	21.5 ± 0.02	11.14 ± 0.71

Comparison of sensitivities of PEO1/PEO4/PEO6 and PEO14/PEO23 by determining the IC_{50s} toward nelfinavir following short-term therapy (72 h) and long-term clonogenic assay in nelfinavir-free media. IC₅₀ during short-term therapy was calculated via the CalcuSyn software by utilizing the total cell count of 4 treatment groups (5, 10, 20, and 40 μM) as the variable. Following 72 h of treatment, 1000 alive cells were incubated in drug-free media for 14-21 days, and the resultant numbers of positive colonies (>50 cells) of 4 treatment groups (5, 10, 20, and 40 μM) were utilized to determine the long-term IC_{50s}. Sensitivity of the PEO1/PEO4/PEO6 series towards nelfinavir remained unaltered in short-term and long-term therapies; however, the sensitivity of the PEO14/PEO23 series toward nelfinavir increased during long-term incubation compared to short-term therapy.

3.3 Nelfinavir triggers the unfolded protein response, enhances the expression of cell-cycle inhibitor protein p27^{kip1}, and induces cell death in high-grade serous ovarian cancer cells of differential platinum sensitivities

To determine whether the impaired cell proliferation induced by nelfinavir is in the short-term associated with cell cycle arrest, we incubated HGSOC cells of different platinum sensitivities with increasing concentrations of nelfinavir for 72 h. We measured the expression of the cell cycle inhibitor p27^{kip1} and found it increased in a concentration-dependent manner in all cell lines studied (**Figure 3.3 A**). Moreover, we decided to explore whether nelfinavir-associated cell growth inhibition involves the induction of the ER stress response because this pathway has been reported to be ubiquitously activated by nelfinavir in multiple cancers [1]. We observed that, in all cell lines, nelfinavir upregulates GRP78 (glucose-regulated protein, 78 kDa), which is a member of the family of heat shock proteins of 70 kDa, also termed heat shock 70 kDa protein 5 (HSPA5), and considered a master chaperone [345]; concomitantly, we detected nelfinavir-induced upregulation of CCAAT-enhancer-binding protein homolog protein (CHOP) [346] (**Figure 3.3 A**). Both GRP78 and CHOP are postulated to balance the stress of the ER in opposite manners, with CHOP being a pro-cell death factor and GRP78 a pro-survival factor [334]. This is consistent with the concept that ER stress is primarily a pro-survival mechanism, yet in excess, facilitates cell death [333]. In the previous result, a dose-dependent reduction in the percent viability and colony-forming capacity, and an increase in the hypodiploid DNA contents in response to nelfinavir were suggestive of induction of cell death, which correlates with the induction of proapoptotic ER stress related protein CHOP. Hence, we explored the cleavage of cell-death executioner caspase-3 and its downstream substrate poly (ADP) ribose polymerase (PARP) (**Figure 3.3 B**) in HGSOC cells subjected to increasing concentrations of nelfinavir.

Platinum Sensitivity

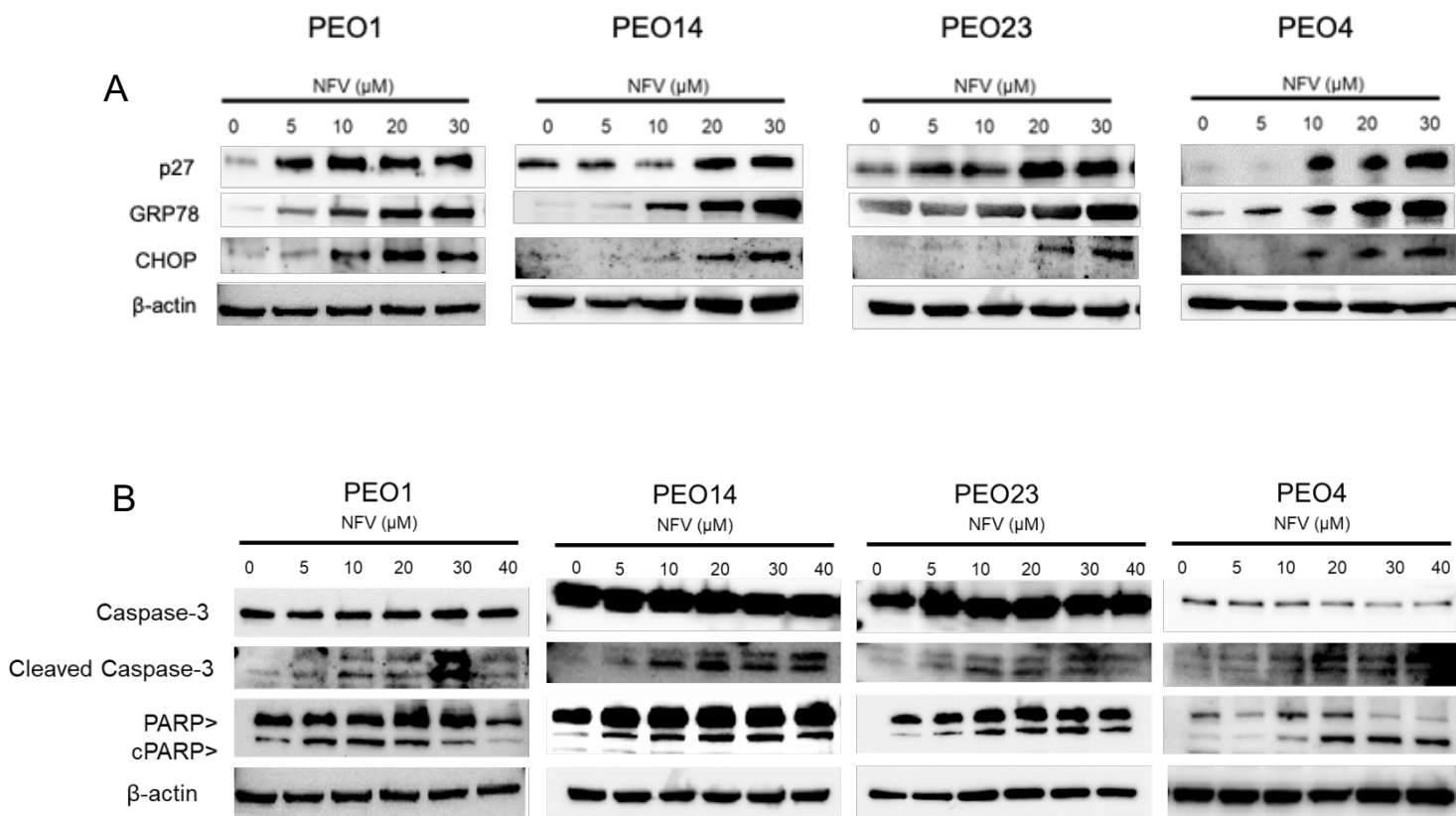


Figure 3.3

PEO cells with different sensitivities to cisplatin were exposed to 5, 10, 20, 30, or 40 μ M nelfinavir (NFV) for 72 h. In all cell lines, NFV (A) increased the expression of cell cycle inhibitor p27^{kip1}, and ER stress related proteins GRP78 and CHOP, and (B) mediated the cleavage of cell-death executioner caspase-3 and its downstream substrate poly (ADP) ribose polymerase (PARP). The gray area that goes from higher to lower signifies that the cells are depicted in the order of their decreasing sensitivity to the toxic effects of cisplatin, as shown in **Table 3.1**. All results presented are representative of at least two independent experiments that had similar outcomes.

3.4 Nelfinavir triggered the unfolded protein response in association with lysosomal impairment but without affecting the autophagic flux

To maintain homeostasis, when the load of unfolded proteins exceeds the folding capacity of the ER, GRP78 detaches from the ER membrane sensors PERK, IRE1 α , and ATF6, and activates the UPR [240,347-350]. These pathways are an adaptive response aimed at restoring homeostasis by inhibiting global protein synthesis, promoting enhanced expression of chaperone proteins, and favoring the degradation of misfolded proteins in the proteasome. We show that the PERK/eIF2 α /ATF4/CHOP pathway of the UPR is stimulated by nelfinavir in a concentration-dependent manner in parallel to the up-regulation of GRP78 (**Figure 3.4 A**). We also compared members of the UPR in response to nelfinavir against that caused by a recognised activator of the UPR, tunicamycin (TN), which is a glycosidase inhibitor causing accumulation of non-glycosylated proteins in the ER [351,352]. We found that similarly to TN, nelfinavir increased GRP78, CHOP, and the other two pathways of the UPR, one involving the endonuclease IRE1 α , and another mediated by activation of ATF6 formed upon its trafficking from the ER to the Golgi apparatus where it is cleaved to release the soluble transcription factor (sATF6) (**Figure 3.4 B**).

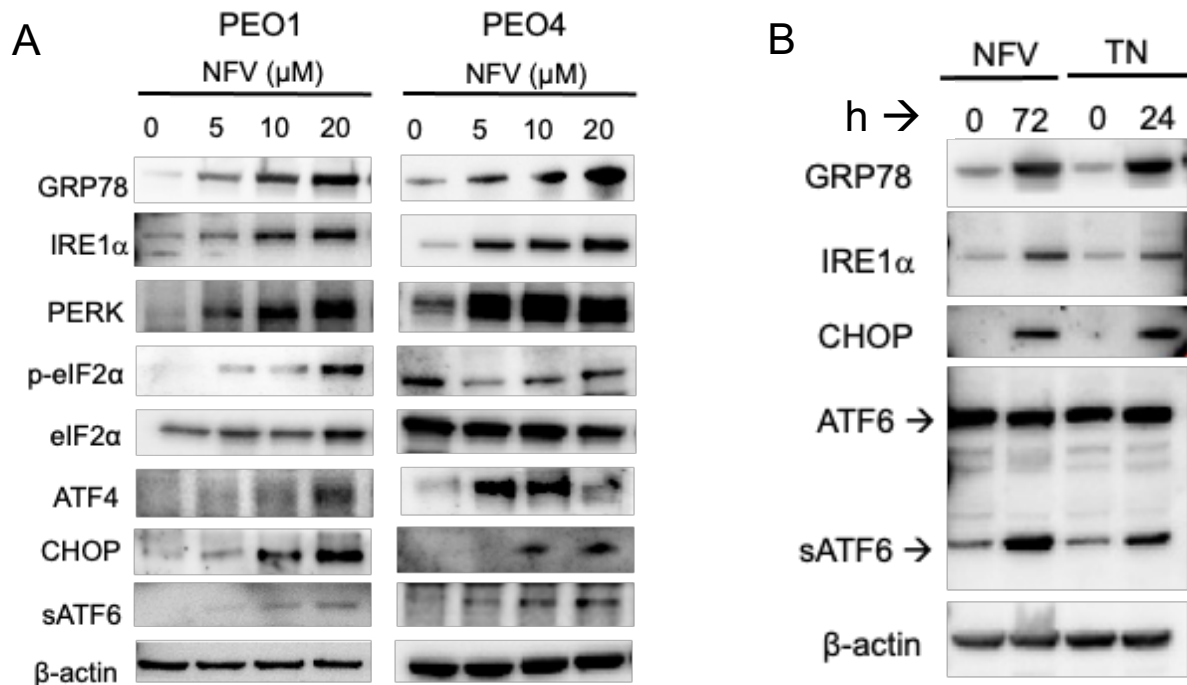


Figure 3.4

(A) PEO1 and its less platinum-sensitive sibling PEO4 were exposed to 5, 10, or 20 μM nelfinavir (NFV) for 72 h. In both cell lines, NFV increased the expression of GRP78, ER stress related proteins of the PERK/eIF2α/ATF4/CHOP pathway and mediated the cleavage of ATF6. (B) PEO1 cells were exposed to 20 μM NFV for 72 h or to 2 μg/ml tunicamycin (TN) for 24 h. NFV elicited UPR in PEO1 cells in a similar manner to canonical ER-stressor TN by increasing GRP78, CHOP, and IRE1α, and mediating cleavage of ATF6. All results presented are representative of at least two independent experiments that had a similar outcome.

Multiple studies have reported activation of autophagy in cancer cells in response to nelfinavir treatment [204,211]. Autophagy is an evolutionarily conserved biological mechanism aimed at disintegrating cellular organelles and bulky misfolded proteins, and recycling macromolecules to compensate for energy and nutrient deprivation [353,354]. Furthermore, the PERK-eIF2 α arm of ER stress has been associated with the modulation of autophagy [333]. To investigate if the ER stressor nelfinavir affects autophagy in HGSOC cells, we treated platinum-sensitive PEO1 cells and its less sensitive patient-matched pair PEO4 with increasing concentrations of nelfinavir for 72 h. We observed a concentration-dependent increase in the level of LC3II protein in both cell lines in response to nelfinavir, suggesting accumulation of autophagosomes (**Figure 3.5 A**). Increased level of LC3II, however, can indicate either a true increase in the dynamic process of autophagy (a.k.a. autophagic flux), or instead, an impairment of the lysosomal activity [355]. To differentiate between these two outcomes, we performed an autophagic flux assay by co-treating the cells with nelfinavir in the presence or absence of the lysosome inhibitor bafilomycin A1. Nelfinavir did not further enhance the level of LC3II when bafilomycin A1 was added to the treatment (**Figure 3.5 B**), suggesting that nelfinavir likely impairs lysosomal function instead of enhancing autophagic flux.

Platinum Sensitivity

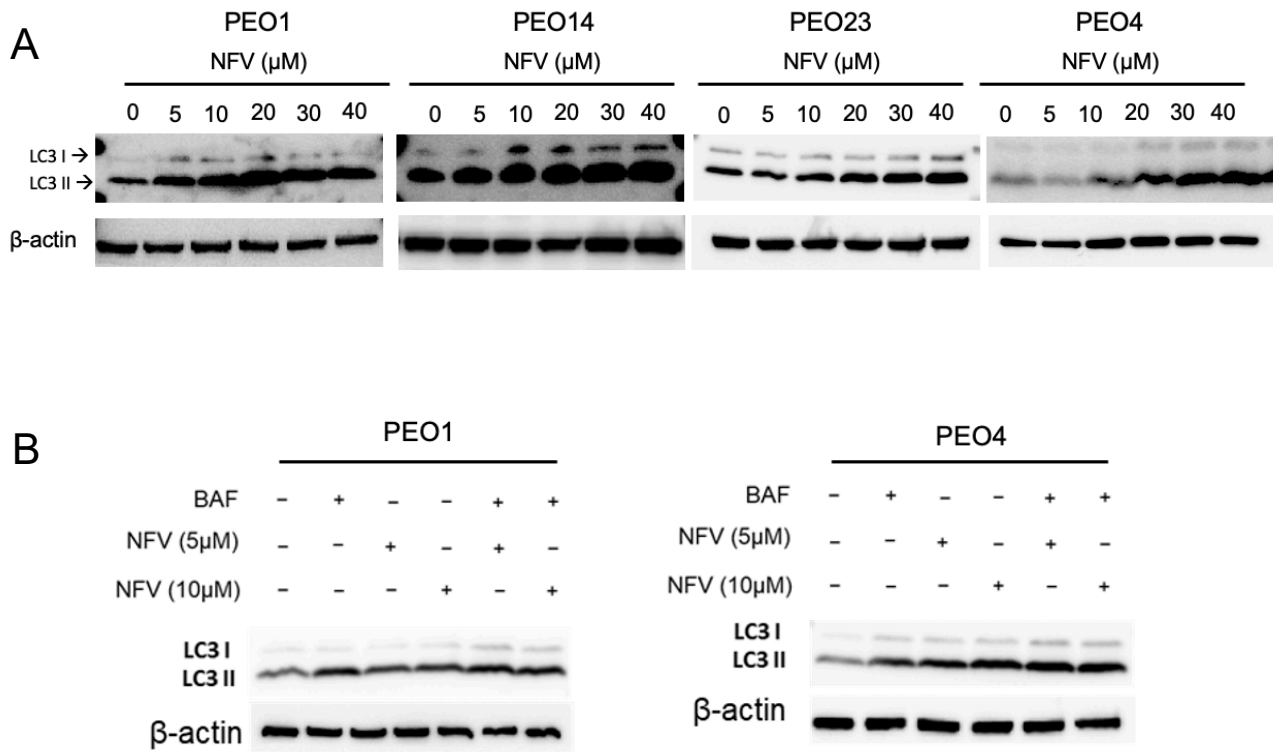


Figure 3.5

(A) In PEO1, PEO14, PEO23, and PEO4 cells treated with various concentrations of nelfinavir (NFV) for 72 h, the autophagosome-related protein LC3II increases in response to NFV in a dose-dependent manner. (B) PEO1 and PEO4 cells were treated with 5 or 10 μM NFV for 72 h, in the absence or presence of 100 nM of the lysosome inhibitor bafilomycin A1 (BAF), which was added 1 h before the termination of the experiment. In both PEO1 and PEO4 cells, the induction of LC3II triggered by NFV was not augmented further by the presence of BAF. All results presented are representative of at least two independent experiments that had a similar outcome.

3.5 Nelfinavir induced unfolded protein response (UPR) is not associated with the inhibition of the proteasome

The proteasome is a vital part of the process of endoplasmic reticulum-associated protein degradation (ERAD)—a critical step of the UPR—whereby the misfolded proteins are retrotranslocated to the cytosol, polyubiquitinated, and ultimately degraded by the proteasome in order to reduce the overall protein load in the ER [356,357]. On the other hand, pharmacological inhibition of the proteasome has been associated with counter accumulation of protein load, leading toward enhanced proapoptotic ER stress—a strategy that has been utilized against highly secretory MM cells [358]. Although nelfinavir has been identified as a potent ER stressor against several cancers, its role in modulating the proteasome has been variable and is likely dependent on the type of cancer [1]. For instance, multiple studies demonstrated that nelfinavir could inhibit the $\beta 2$ and $\beta 5/\beta 5i$ subunits-associated proteolytic activities of the proteasomes in hematological cancers, especially MM [222,259]. Conversely, several studies reported unaltered or even enhanced proteasomal effects in response to nelfinavir on various cancer cell types [208,210,212,265]. Notably, the mammalian 20S proteasome can cleave the same site targeted by the HIV-protease enzymes within the HIV polypeptides, insinuating a possible cross-talk between the proteasome and HIV-protease inhibitor drugs [186].

Since the proteasome is an integral part of the UPR and cellular proteostasis, and accumulating evidence indicates that NFV can likely modulate proteasomal functions, we deemed it essential to explore whether NFV represses the proteasomal functions in HGSOc cells. We treated HGSOc cells having various levels of platinum sensitivities with increasing concentrations of nelfinavir for 72 h to determine if the proteasome was inhibited. Blockage of the proteasome leads to the accumulation of non-degraded poly-ubiquitinated proteins, the level of which can be

visualized and estimated from the appearance of ubiquitin-carrying polypeptides in an immunoblot using anti-ubiquitin antibodies. Thereby, the accumulation of poly-ubiquitinated polypeptides can be used as a surrogate marker of proteasome inhibition.

In nelfinavir treated HGSOC cells, we did not observe an increase of protein poly-ubiquitination in response to increasing concentrations of nelfinavir when compared to the vehicle-treated samples, and a known positive control (OV2008 cells treated with 20 nM BZ for 72 h [336] **(Figure 3.6)**). A lack of the appearance of increased polyubiquitination when compared with untreated cells suggests that nelfinavir did not have an inhibitory effect on the proteasome in the HGSOC cells.

Platinum Sensitivity

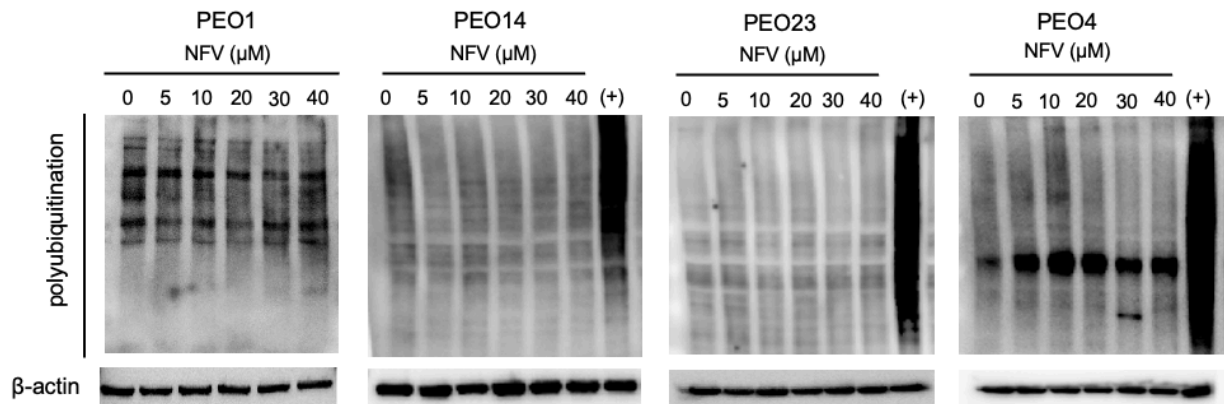


Figure 3.6

Platinum-sensitive PEO1 and PEO14 cells, and their less sensitive-to cisplatin patient-matched siblings PEO4 and PEO23, were exposed to the depicted concentrations of NFV for 72 h. At the end of the experiment, whole cell extracts were obtained, electrophoresed, and western blotted using an anti-ubiquitin antibody. The immunoblots demonstrate an absence of increased polyubiquitination in the treated cells compared to the positive control (+). Positive control was a protein extract obtained from OV2008 cells treated with 20 nM of proteasome inhibitor bortezomib (BZ) for 72 h [336]. All results presented are representative of at least two independent experiments that had a similar outcome.

3.6 ER stress response induced by nelfinavir is associated with cleavage of executioner caspase-7 and increased proapoptotic Bcl-2 family member Bax in a time- and concentration-dependent manner

To characterize further the nelfinavir-induced ER stress and associated UPR in HGSOC cells, we conducted a time-course experiment utilizing a single concentration (20 μ M) of nelfinavir. As predicted, the anti-HIV drug caused a time-dependent increase of ER stress-related proteins GRP78, IRE1 α , ATF4 and CHOP, which was concomitant to the cleavage of executioner caspase-7 and the increase in the proapoptotic protein Bax, while the level of antiapoptotic protein bcl-2 was unaltered (**Figure 3.7 A**); this result is in agreement with the attributed proapoptotic function of ATF4 and CHOP during ER stress [240]. We also found that the activation of caspase-7 and the increase in the level of proapoptotic Bax by nelfinavir is concentration-dependent and occur in both PEO1 and PEO4 sibling cells, which, however, display highly different sensitivities to platinum (**Table 3.2**) (**Figure 3.7 B**). Of note, although the level of proapoptotic protein Bax was increased in both PEO1 and its less platinum-sensitive sibling PEO4, the level of antiapoptotic protein bcl-2 was unaltered in NFV-treated PEO1 cells in response to increasing concentrations, while the level of bcl-2 decreased in PEO4 cells treated with high concentrations of nelfinavir.

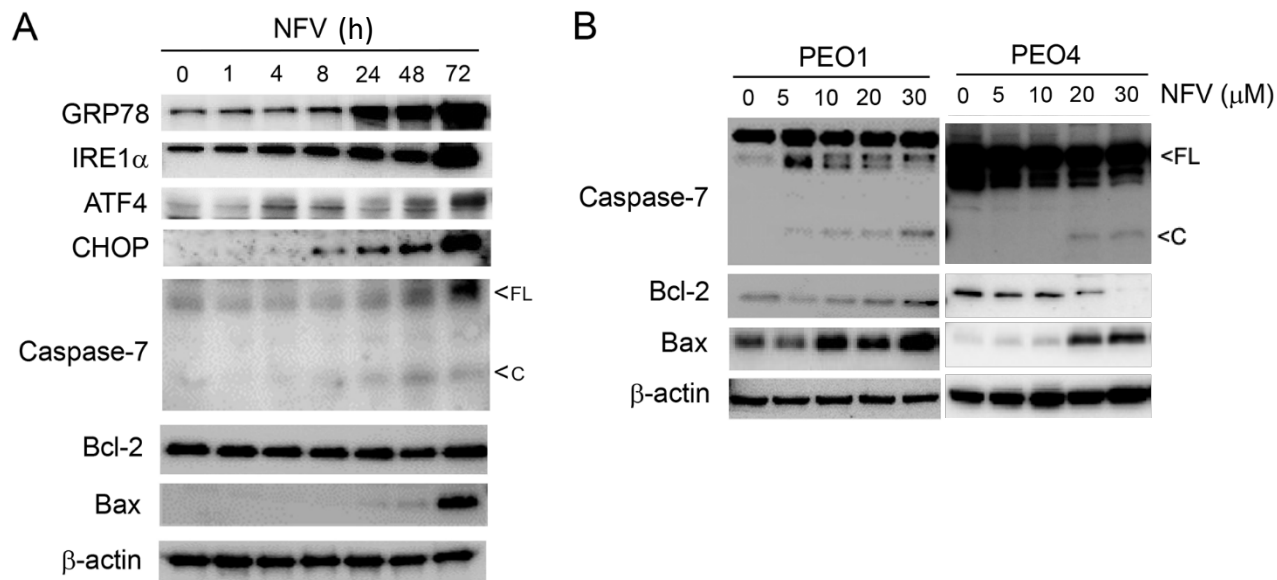


Figure 3.7

(A) PEO1 cells treated with 20 μ M nelfinavir (NFV) for 72 h depict a time-dependent increase in ER stress related proteins GRP78, IRE1 α , ATF4 and CHOP, while inducing the cleavage of executor caspase-7, and an increase in the level of proapoptotic Bax. (B) NFV treatment of both PEO1 and PEO4 cells for 72 h cause a dose-dependent increase in cleaved capsase-7 while increasing the level of proapoptotic protein Bax in both cell lines and decreasing the antiapoptotic protein bcl-2 in PEO4 cells. All results presented are representative of at least two independent experiments that had a similar outcome.

3.7 Nelfinavir toxicity is associated with short-term sustained mRNA translation that contributes to the UPR, followed by long-term concentration-dependent inhibition of global protein synthesis

One of the primary aims of the UPR is to reduce further protein load in the ER by shutting down global protein synthesis yet resume selective cap-independent translation to facilitate cellular recovery from the ongoing proteotoxic stress [240,333]. To understand the effect of nelfinavir on the dynamics of protein synthesis, nelfinavir-treated PEO1 cells were subjected to a puromycin incorporation assay to assess mRNA translation. Nelfinavir inhibited mRNA translation in a concentration- (**Figure 3.8 A**) and time-(**Figure 3.8 B**) dependent manner. However, protein synthesis declined only after 4 h of exposure to nelfinavir because puromycin incorporation was abrogated by the presence of the protein synthesis inhibitor cycloheximide (CHX) (**Figure 3.8 C**).

Reduction of global protein synthesis upon ER stress induction occurs because of the phosphorylation of eIF2 α . This is a polypeptide chain translation initiator factor that limits protein synthesis under conditions of cellular stress based on its capacity to become phosphorylated on serine 51 [359], thus limiting the availability of eIF2 α needed for translation initiation [360]. The basal levels of eIF2 α phosphorylation on serine 51 (p-eIF2 α) are elevated, but are rapidly yet temporarily diminished by nelfinavir for about 4 h without affecting total eIF2 α levels (**Figure 3.8 D**), and concurrently with sustained incorporation of puromycin (**Figure 3.8 C**). This sustained protein synthesis at the beginning of the treatment with nelfinavir is confirmed by the sharp increase in p-eIF2 α and downstream transcription factor ATF4, and reduced puromycin incorporation after 4 h of treatment with nelfinavir in the presence of cycloheximide (**Figure 3.8 C and E**).

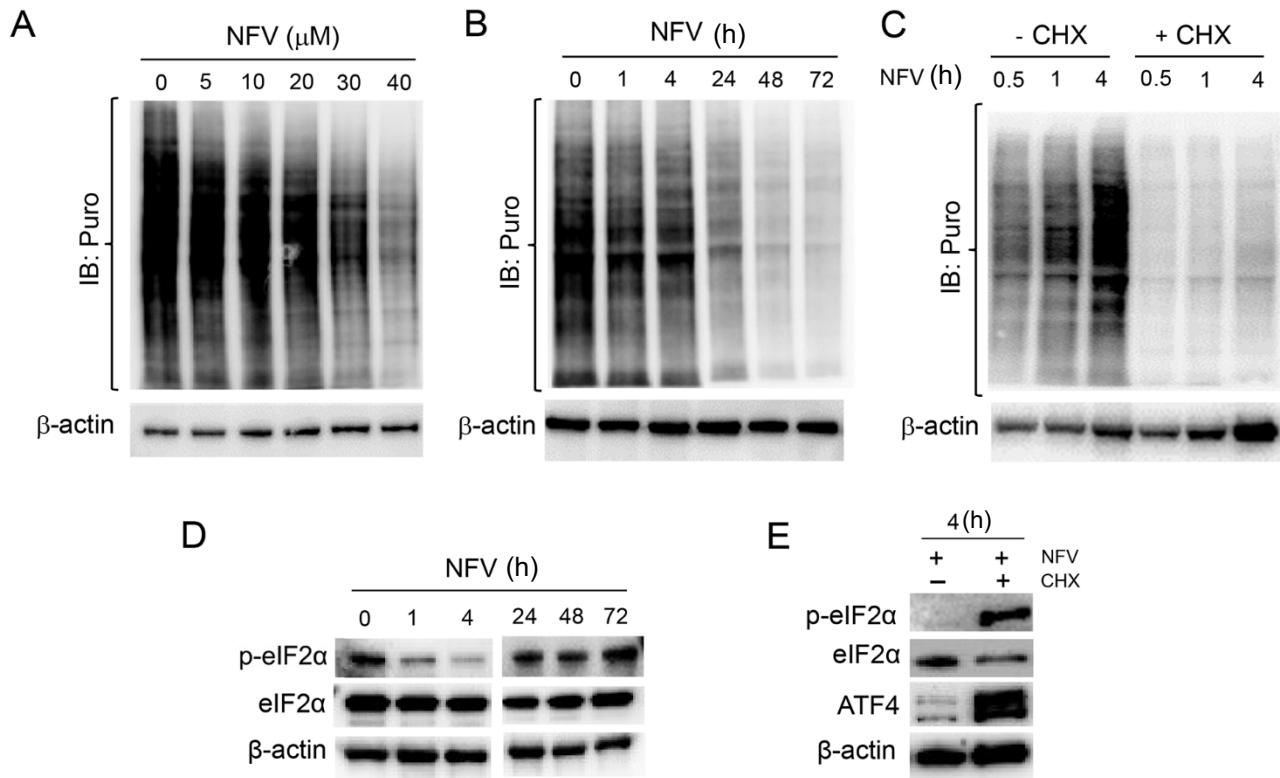


Figure 3.8

Nelfinavir (NFV), in a dose- (A) and time-dependent manner (B), triggers a decrease in the incorporation of puromycin (Puro) into newly synthesized peptides. (C) The incorporation of Puro is sustained in the presence of 20 μ M NFV during the first 4 h of treatment, but it is abrogated by the simultaneous presence of 10 μ g/ml of the protein synthesis inhibitor cycloheximide (CHX). (D) Effect of 20 μ M NFV on the phosphorylation of eIF2 α on Serine 51 (p-eIF2 α) along a 72h incubation period. (E) A short-term (4 h) treatment with 20 μ M NFV associates with low expression of p-eIF2 α and downstream transcription factor ATF4, yet both p-eIF2 α and ATF4 dramatically increase with the simultaneous presence of CHX (10 μ g/ml). All results presented were performed in PEO1 cells and are representative of two experiments that had a similar outcome.

Despite in the long-term nelfinavir-induced ER stress leads to a decline in global protein synthesis (**Figure 3.8 B**), we asked the question as to whether the sustained levels of protein synthesis during the first 4 h following NFV treatment corroborated by reduced p-eIF2 α and sustained puromycin incorporation, further induces ER stress. We answered this question by exposing PEO1 cells to nelfinavir for 4 h, and measuring a non-translatable readout of ER stress, the total, and spliced mRNA coding for XBP1 in the presence or absence of cycloheximide. RT-PCR revealed nelfinavir-mediated early splicing of *XBPI* mRNA, the downstream target of IRE1 α , which was similar to early *XBPI* mRNA splicing induced by the known ER stressor tunicamycin (TN) (**Figure 3.9 A**). This cleavage, however, was prevented by the presence of cycloheximide (**Figure 3.9 B**), suggesting that proteins accumulated during the first 4 h of nelfinavir treatment participate, at least in part, in the causation of ER stress and the unleashing of the UPR. Taken together, these results provide evidence for a cross-talk between ER stress and the modulation of protein synthesis dynamics in HGSOc cells in response to nelfinavir.

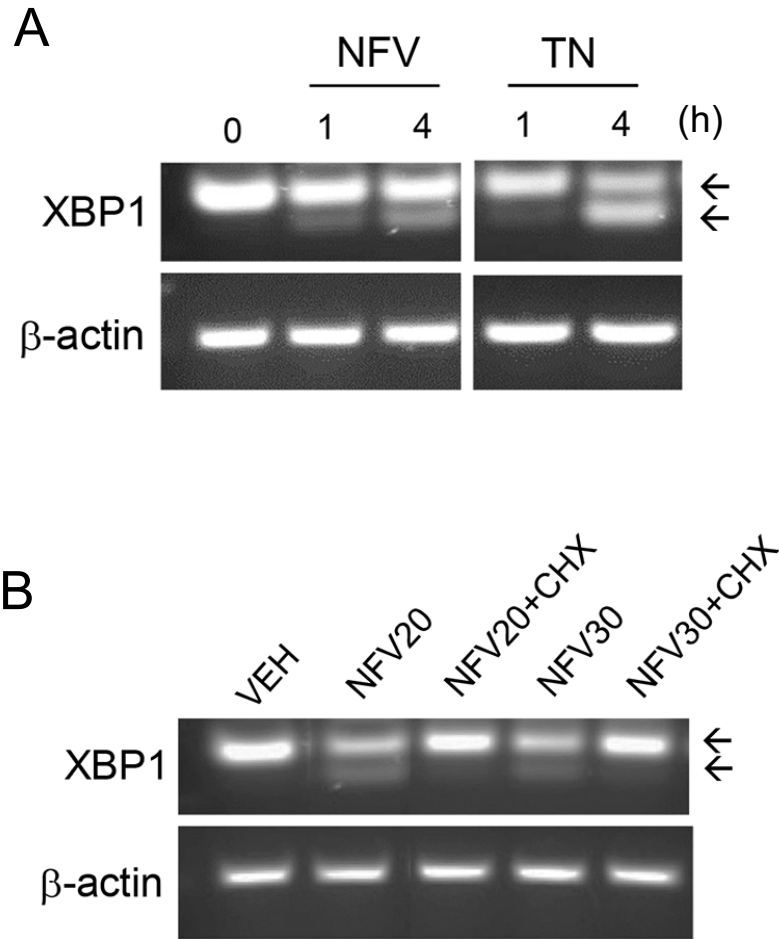


Figure 3.9

(A) Effect of 20 μ M nelfinavir (NFV) on the splicing of *XPB1* mRNA assessed by RT-PCR; TN, tunicamycin (2 μ g/ml). Arrows indicate total and spliced *XPB1* mRNA variants. (B) Splicing of *XPB1* mRNA in cells co-incubated for 4 h with NFV and cycloheximide (CHX, 10 μ g/ml); NFV20, 20 μ M; NFV30, 30 μ M. All results presented were performed in PEO1 cells and are representative of two experiments that had a similar outcome.

In order to answer if restoring the phosphorylation of eIF2 α in the early phase of nelfinavir treatment reverses the initial sustained of mRNA translation, we treated HGSOC cells with nelfinavir and a small molecule inhibitor of eIF2 α dephosphorylation termed salubrinal—a selective phosphatase inhibitor, which has been described as a cytoprotector against ER stressors [361-363]. We observed a reduction in the nelfinavir-induced early elevation of protein synthesis by salubrinal, with the concomitant restoration of phosphorylation of eIF2 α (**Figure 3.10 A**). Expression of ATF4 was reduced in response to co-treatment with nelfinavir and salubrinal. Previously our laboratory had demonstrated similar restoration of p-eIF2 α with the associated reduction in protein synthesis and ATF4 in OV2008 cells by the ER stressor mifepristone [336]. To determine the functional implication of nelfinavir and salubrinal co-treatment, HGSOC cells were subjected to a cell viability assay, which revealed that salubrinal partially abrogated nelfinavir-induced cytotoxicity by improving the deterioration of viability triggered by nelfinavir (**Figure 3.10 B**).

Taken together, our data indicate that nelfinavir modulates the mRNA translation in HGSOC cells by targeting the eIF2 α /ATF4 pathway of the UPR.

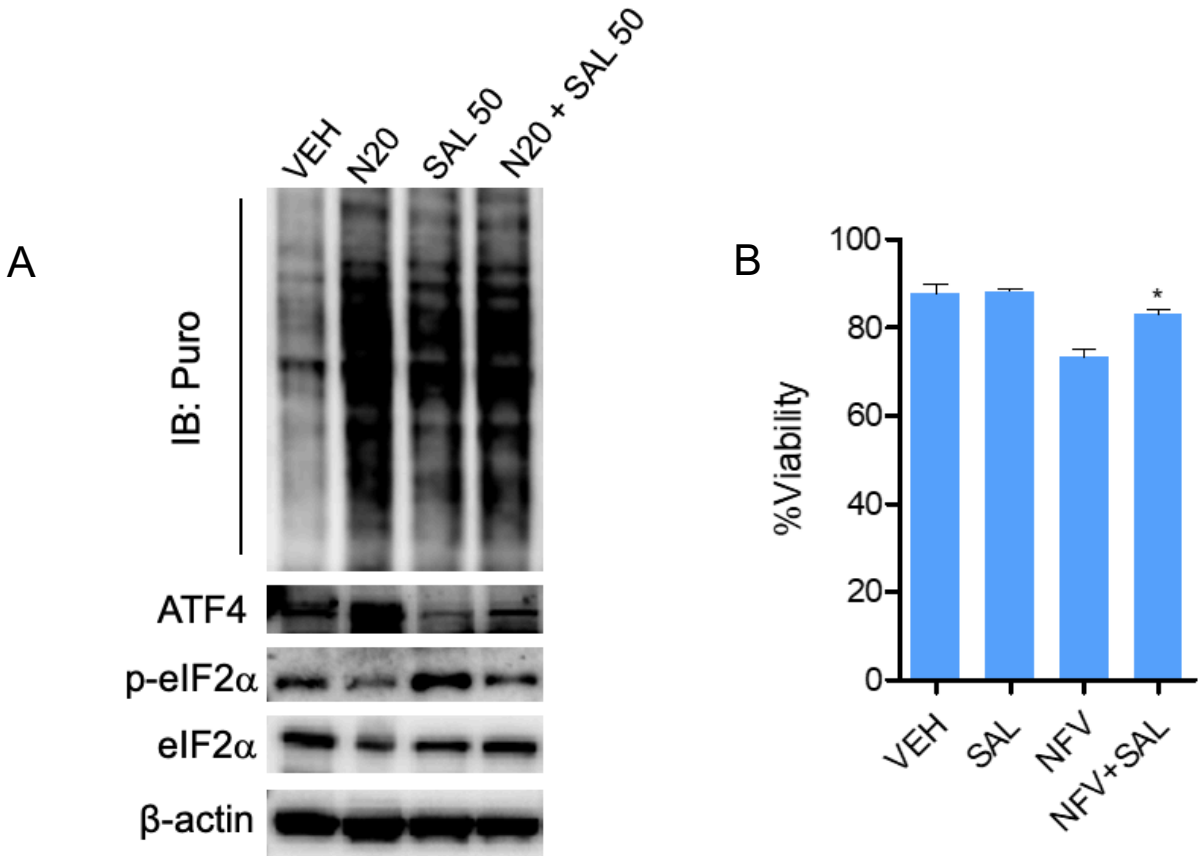


Figure 3.10

PEO1 cells were subjected to (A) NFV 20 μ M, and salubrinal 50 μ M (SAL50) were added individually or concurrently for 4 h in a culture of PEO1 cells. The culture was pulsed with 1 μ M puromycin for 30 minutes at 37°C before stopping the experiment; puromycylated proteins were detected with the mouse antibody clone 12D10. IB: immunoblot. Puro: puromycin. (B) PEO1 cells were treated with 20 μ M NFV, with or without concurrent 50 μ M salubrinal (SAL) for 72 h. At the end of the experiment, the cells were trypsinized and subjected to microcytometry analysis to attain their viability. SAL partially improved the viability of the NFV-treated cells. * $p < 0.05$ vs. NFV (One-way ANOVA followed by Tukey's Multiple Comparison Test).

3.8 Nelfinavir inhibits AKT and ERK phosphorylation and triggers DNA damage

Elevation of cell survival and proliferation are typically favoured by an upregulation of AKT and ERK signaling pathways. Nelfinavir has been shown to reduce the phosphorylation of AKT and ERK in various cancers [272,286]. In this study, we observed a concentration-dependent reduction of phosphorylation of both AKT and ERK in the siblings PEO1 and PEO4 cell lines carrying different sensitivities to cisplatin (**Figure 3.11 A**). In a time-course experiment, it was revealed that nelfinavir mediated an early dephosphorylation of ERK (1-4 h), while downregulation of AKT was visible at a later stage of the treatment (4-48 h) (**Figure 3.11B**).

The concentration-dependent decline in the activation of the AKT and ERK pathways was associated with nelfinavir-mediated DNA damage response in both PEO1 and PEO4 cells, evidenced by a concentration-dependent increase of phosphorylated H2AX (γ H2AX) (**Figure 3.11C**). Induction of DNA damage in PEO4 cells is significant as this cell line has a restoration of a DNA-damage repair mechanism [364], which is inherently deficient in its patient-matched pair PEO1, thus conferring the reduced sensitivity to cisplatin observed in PEO4 cells (**Table 3.1**). We further demonstrate that the induction of γ H2AX by nelfinavir is time dependent with high levels detected after 48 and 72 h of exposure to the drug (**Figure 3.11D**).

Previously, in thyroid cancer cells, ROS scavenger N-acetyl cysteine (NAC) reduced nelfinavir-mediated phosphorylation of H2AX, suggesting ROS-dependent DNA damage [223]. We did not observe an improvement in nelfinavir-mediated reduction of the total number of cells and viability, when PEO1 cells were concomitantly treated with NAC (**Figure 3.11 E, F**), which suggests that nelfinavir-mediated cytotoxicity associated with enhanced γ H2AX may not be ROS-dependent.

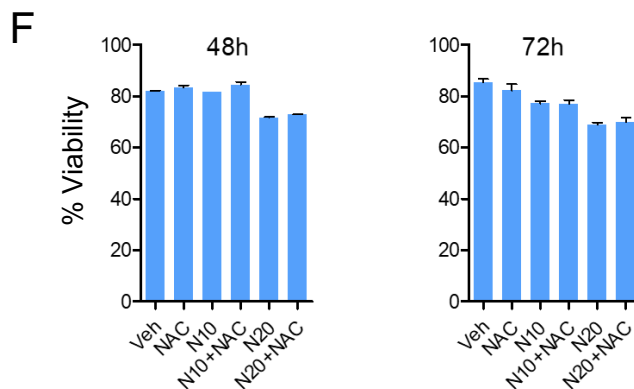
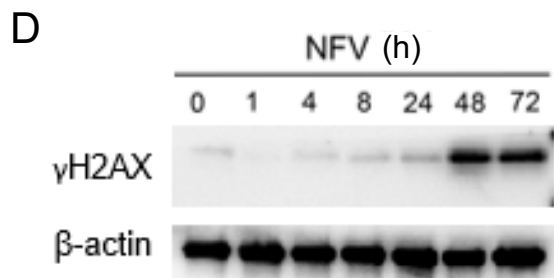
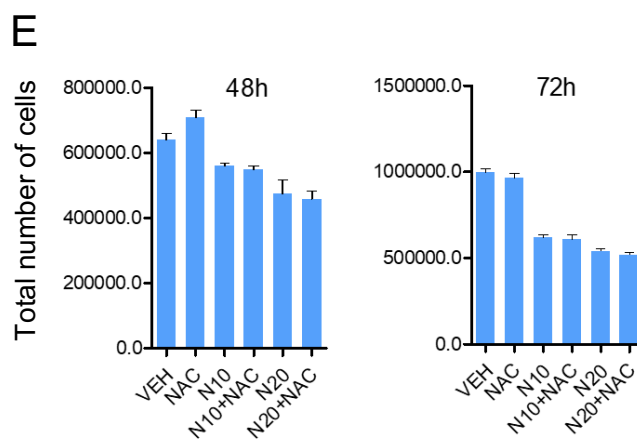
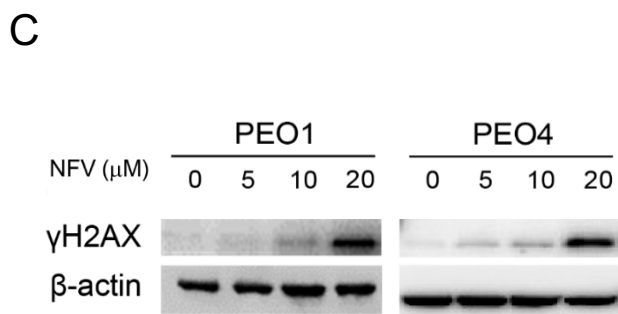
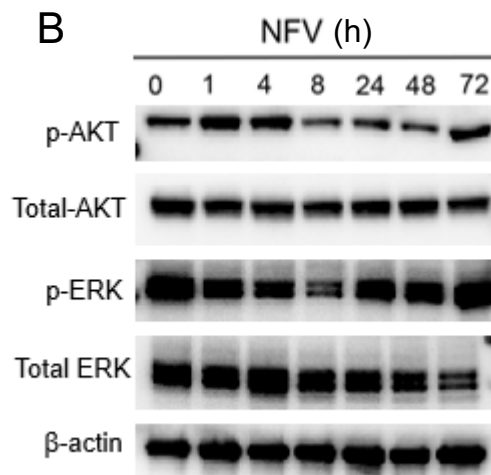
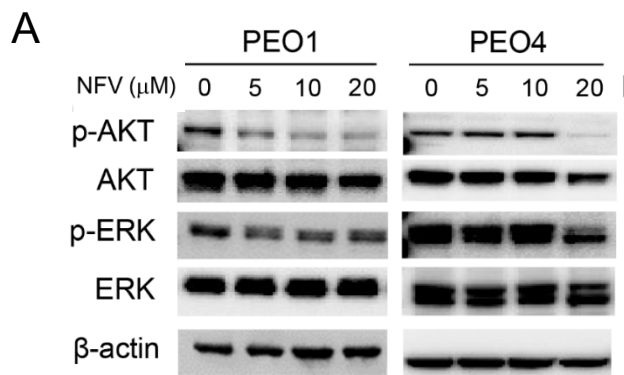


Figure 3.11

(A) PEO1 and PEO4 cells were incubated with the depicted concentrations of nelfinavir (NFV) for 72 h. Protein expression studied by western blot demonstrates concentration-dependent decrease of phosphorylation of AKT and ERK in both sibling cell lines carrying different sensitivities to cisplatin. (B) PEO1 cells were treated with 20 μ M NFV for the indicated time-points. NFV mediated an early decrease (1-4 h) in the phosphorylation of ERK and a late decrease (8-48 h) in the phosphorylation of AKT; (C) Concentration-dependent increase of γ H2AX in both PEO1 and PEO4 cells; (D) PEO1 cells were treated with 20 μ M NFV for the indicated time-points. NFV mediated enhanced phosphorylation of H2AX at 48- and 72-h suggesting DNA damage; (E) PEO1 cells in culture were treated with 5 mM N-acetylcysteine (NAC) for 2 h, prior to the treatment with 10 or 20 μ M NFV, with or without 5 mM NAC for 48 and 72 h. At the end of the experiment, the cells were trypsinized and subjected to microcytometry analysis to attain the total number of viable cells. NAC did not improve NFV mediated reduction of the number of cells and percent viability.

3.9 Nelfinavir induced G1 arrest associated with increased p27^{kip1} and concomitant reduction of cyclin-dependent kinase 2

One of the early steps of mounting DNA damage response is the arrest of the cell cycle at the checkpoints in order to engage the DNA damage repair machinery [365]. Nelfinavir has shown cell type dependent effects on the cell cycle, and, in most instances, the effects manifested as an early event during treatments—preceding the induction of cell death pathways [1]. Notably, nelfinavir-mediated arrest of cancer cells at the G1 phase of the cell cycle has been attributed to reduced cyclin-dependent kinase-2 (CDK2) activity in melanoma cells [210]. Since nelfinavir is a DNA damaging agent against HGSOC, according to our observations, we decided to study if the cells accumulate at any point of the cell cycle. Platinum-sensitive PEO1 and its patient-matched siblings PEO4 and PEO6—showing less sensitivities to cisplatin—were subjected to cell cycle analysis following 72 h of treatment with increasing concentrations of nelfinavir. We observed that the anti-HIV agent arrested PEO1 cells at the G1 phase during treatment with 5 μ M of nelfinavir, and PEO4 and PEO6 at 5 μ M and 10 μ M concentrations (**Fig. 3.12A**).

CDK2 is critical for G1-S transition [366]—which requires a progressive decline of the CDK inhibitor p27^{kip1} [367]. Upregulation of p27^{kip1} has been demonstrated to be essential for G1 arrest following DNA damage [368], and downregulation of p27^{kip1} has been reported to be associated with advanced disease and poor survival [369]. We observed a dose-dependent reduction of the phosphorylated and total form of CDK2 in HGSOC cells (**Figure 3.12B**). The reduction of CDK2 was associated with a concomitant increase of p27^{kip1} (**Figure 3.12B**), suggesting that nelfinavir-mediated G1 arrest might be associated with reduced activity of CDK2 and enhanced levels of CDK inhibitor p27^{kip1}. The time-course experiment done with a single concentration of nelfinavir

(20 μM) revealed a time-dependent increase of p27^{kip1} with a concomitant decrease of both the phosphorylated and total form of CDK2 (**Figure 3.12 C**).

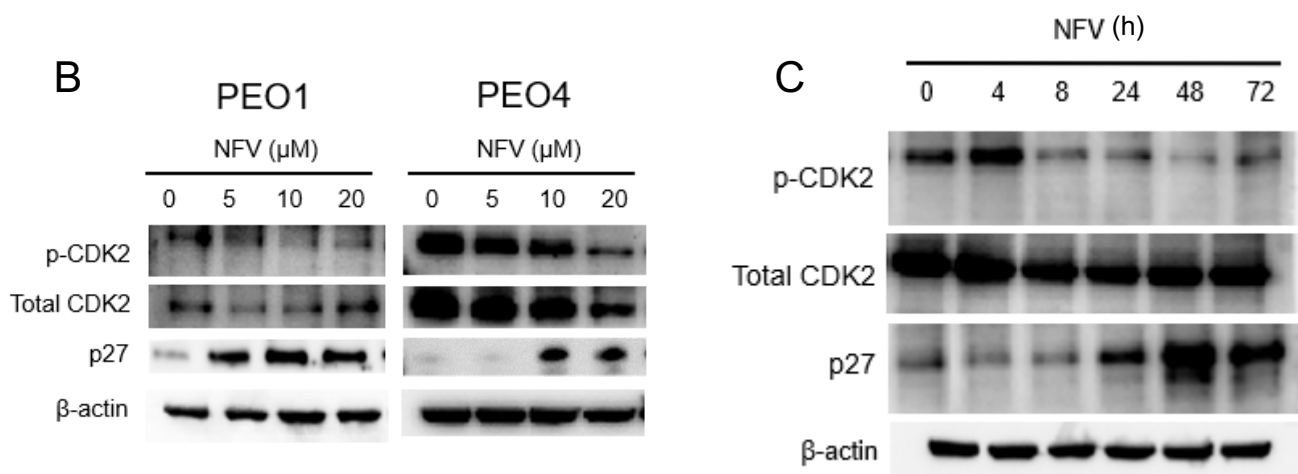
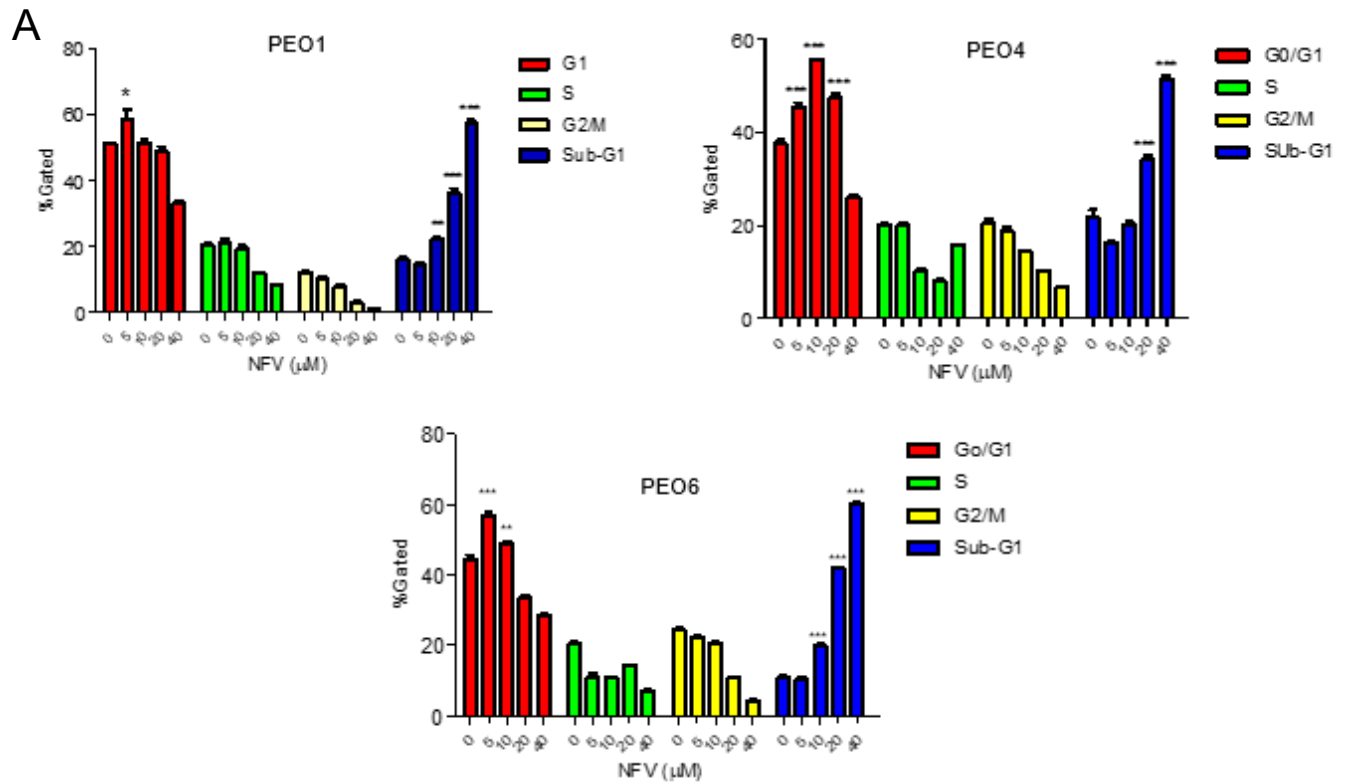


Figure 3.12

(A) PEO1, PEO4, and PEO6 were plated in six-well plates in triplicates and, when exponentially growing, were subjected to treatment with the depicted concentrations of nelfinavir (NFV) for 72 h. At the end of the experiment, the cells were trypsinized, and a fraction of the cellular content was stained with PI and subjected to cell cycle analysis. NFV mediated the accumulation of cells at the G1 phase of the cell cycle at lower concentrations and increased the sub-G1 DNA contents at higher concentrations. (B) Platinum-sensitive PEO1 and less sensitive PEO4 were incubated with the depicted concentrations of NFV for 72 h. At the end of the experiment, whole-cell extracts were obtained, and 20 μ g of protein per sample were electrophoresed. Western blot demonstrates a decrease in the level of p-CDK2 and total CDK2, and an increase in the level of cell cycle inhibitor p27^{kip1} in response to increasing concentrations of NFV in both PEO1 and PEO4 cells. (C) PEO1 cells were treated with 20 μ M NFV for the indicated time points. NFV mediated time-dependent reduction of the level of p-CDK2 and total CDK2 with a concomitant increase of p27^{kip1}. *P<0.05 and ***P<0.001 compared against VEH. All results presented are representative of two experiments that had a similar outcome.

3.10 Bortezomib is cytotoxic against high grade serous ovarian cancer cells of differential platinum sensitivity

Bortezomib (BZ) is the first in generation drug of the proteasome inhibitor group, currently approved to treat hematological malignancies, especially multiple myeloma and mantle cell lymphoma [370]. A dipeptidyl boronic acid by structure, BZ has the propensity for high-affinity binding with the 26S catalytic core of the proteasome and primarily inhibits its $\beta 5$ subunit, resulting in a cascade of mechanistic proteotoxic pathways leading to anti-cancer effects [180,370]. To understand the effect of BZ monotherapy on HGSOc cells, platinum-sensitive PEO1 and its patient-matched sibling less sensitive to platinum, PEO4, were exposed to increasing concentrations of BZ for 72 h. BZ monotherapy resulted in the reduction of the total number of cells and percent viability with increasing concentrations in both PEO1 and PEO4 cells (**Figure 3.13 A and B**). Western blot analysis of BZ monotherapy in PEO1 and PEO4 cells depicted concentration-dependent increase of the poly-ubiquitination, indicating that BZ reached the target in HGSOc cells. BZ increased the level of p27^{kip1} and GRP78 in PEO4 cells but not in PEO1 cells. The cleavage of caspase-3 and its downstream substrate PARP indicated BZ-mediated caspase-related cell death in both PEO1 and PEO4 cells (**Figure 3.13 C**).

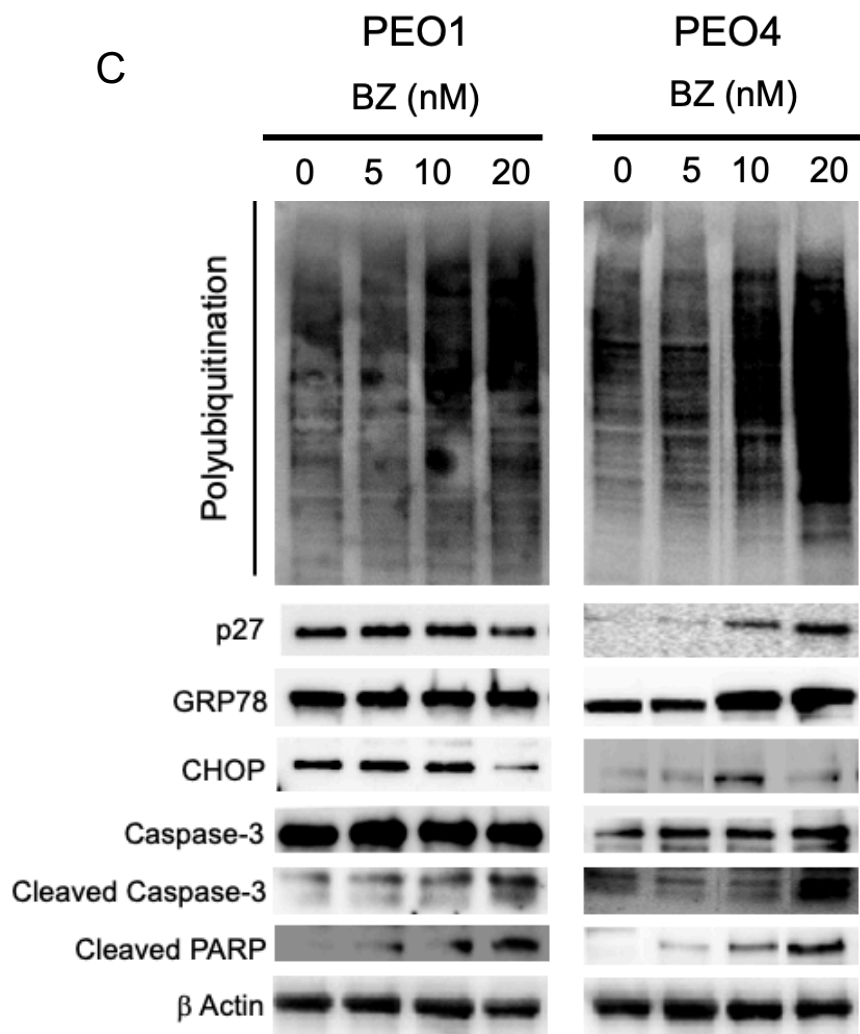
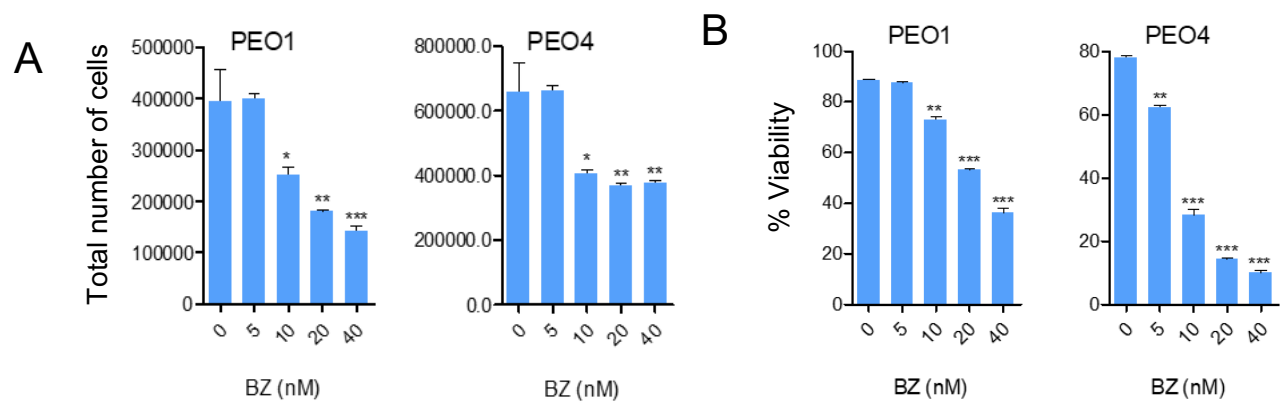


Figure 3.13

PEO1 and PEO4 cells were subjected to the depicted concentrations of bortezomib (BZ) for 72 h. At the end of the experiments, the cells were: (A, B) trypsinized and subjected to microcytometry analysis to attain the total number of cells and percent viability. The number of cells and the percent viability were reduced with increasing concentrations of BZ in both PEO1 and PEO4 cells. (C) Whole cell extracts of BZ-treated PEO1 and PEO4 cells were obtained, and 20 µg of total proteins per sample were electrophoresed. Western blot demonstrates increased ubiquitination in both PEO1 and PEO4 cells in response to the higher concentration of BZ (20 nM), suggesting inhibition of the proteasome. BZ mediated the cleavage of caspase-3 and of its downstream substrate PARP when used at a high concentration (20 nM) in both PEO1 and PEO4 cells. The levels of ER stressor GRP78 and cell cycle inhibitor p27^{kip1} were increased in response to increasing doses of BZ in PEO4 cells but not in PEO1 cells. *p<0.05; ***p<0.001 vs. control (One-way ANOVA followed by Tukey's Multiple Comparison Test)

3.11 Nelfinavir potentiates the toxicity of the proteasome inhibitor bortezomib without modifying its proteasome inhibitory capacity

During the pro-survival phase, the ER stress is relieved by activating ER-associated degradation (ERAD), whereby misfolded proteins are ubiquitinated and translocated to the 26S proteasomes to undergo protein degradation, thus contributing to a reduction in protein overload [333]. Previous studies have shown that the blocking of the 26S proteasomes may further increase the level of misfolded proteins and push the ER stress elicited by ER stressors from a pro-survival phase toward a proapoptotic one [336]. Likewise, we rationalized that nelfinavir, acting as an ER stressor, could potentiate the toxicity of the proteasome inhibitor bortezomib (BZ).

PEO1 and PEO4 cells were exposed to a combination treatment of varying concentrations of BZ and nelfinavir, used at a fixed ratio (1:1000), to assess drug interactions via the combination index of Chou and Talalay by utilizing the total cell count as a readout [343]. Drug synergism was predicted in PEO1 cells at a combination of 10 μ M of nelfinavir and 10 nM of bortezomib (CI = 0.72). Similarly, drug synergism was predicted in PEO4 cells at a combination of 5 μ M of nelfinavir and 5 nM of bortezomib (CI= 0.56), and 10 μ M of nelfinavir and 10 nM of bortezomib (0.55) (**Table 3.3**).

Table 3.3 Analysis of drug interaction between nelfinavir and bortezomib

PEO1		
NFV μ M + BZ nM	Combination index	Interpretation
5 + 5	1.2	Antagonism
10 + 10	0.72	Synergism
20 + 20	0.94	Nearly additive
40 + 40	2.08	Antagonism

PEO4		
NFV μ M + BZ nM	Combination index	Interpretation
5 + 5	0.56	Synergism
10 + 10	0.55	Synergism
20 + 20	0.99	Nearly additive
40 + 40	1	Nearly additive

PEO1 and PEO4 cells were exposed to fixed ratio (1:1000) combination of bortezomib (BZ) and nelfinavir (NFV) for 72 h. The estimate of total cell number was utilized to calculate the combination index (CI) via the Chou-Talalay method of drug interaction in the Calcsyn software. For a specific drug association, $CI < 1$ indicates synergism, $CI > 1$ indicates antagonism, $CI = 1$ indicates additivism, $CI = 0$ indicates no interaction [343].

Cell proliferation assay demonstrated potentiation of toxicity in the predicted combinations of nelfinavir and BZ in PEO1 (**Figure 3.14A**) and PEO4 cells (**Figure 3.14D**). By studying cell cycle distribution, we found that in both cell lines, the combination of nelfinavir and BZ caused the accumulation of cells in the G1 phase of the cell cycle (**Figure 3.14B and E**). When we subjected the cells that remained alive after 72 h of treatment with nelfinavir, BZ, or the combination nelfinavir and BZ —shown in **Figure 3.14 A and B**—to a clonogenic survival assay in the presence of drug-free media, we found that the cells that were still alive at the end of the treatment, were devoid of reproductive capacity as manifested by a reduction in their clonogenic survival, an effect manifested maximally when nelfinavir was combined with BZ, when compared to the results of the drugs studied separately (**Figure 3.14C and F**).

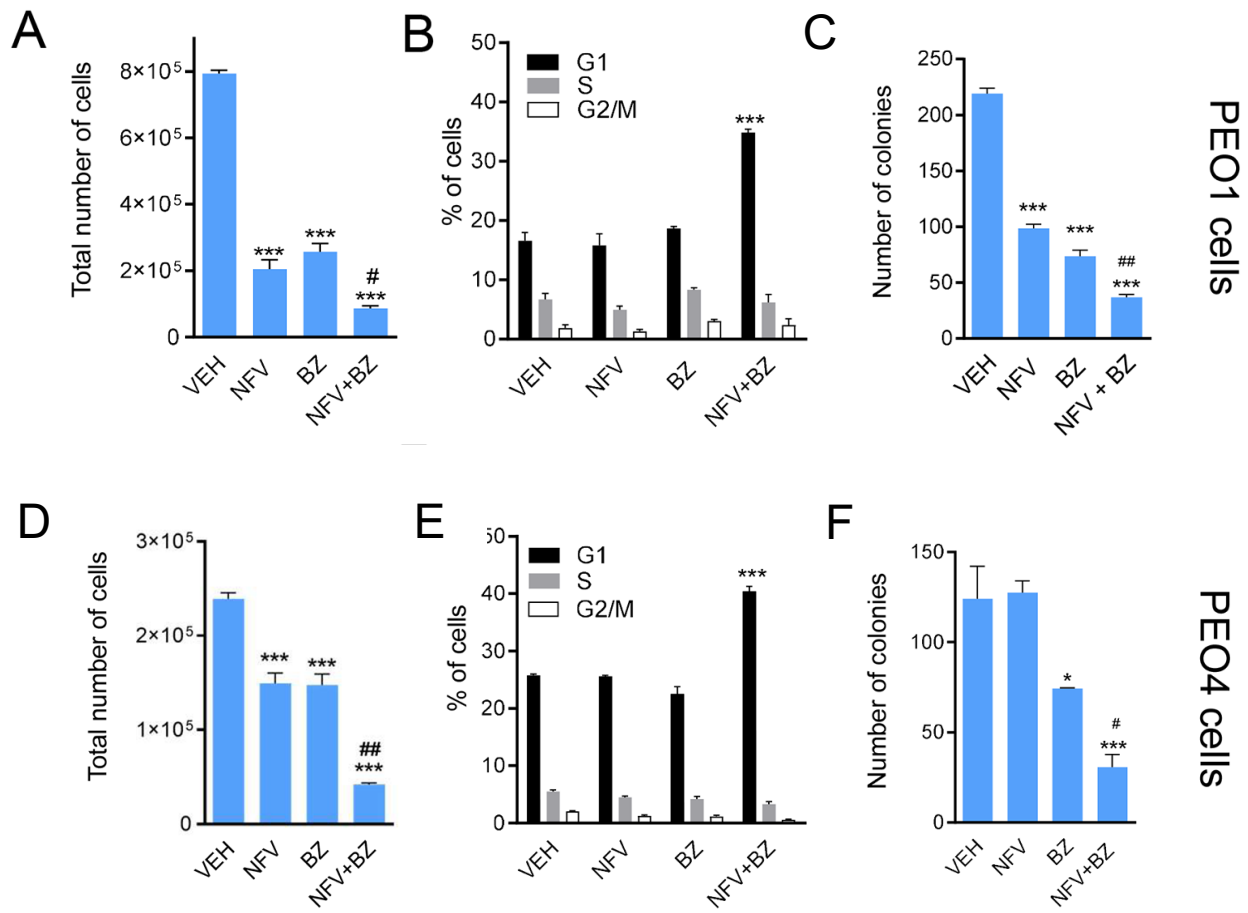


Figure 3.14

PEO1 cells were exposed to 10 μ M nelfinavir (NFV), 10 nM of the proteasome inhibitor bortezomib (BZ), or a combination of 10 μ M NFV and 10 nM BZ for 72 h. PEO4 cells were exposed to 5 μ M NFV, 5 nM of BZ, or a combination of 5 μ M NFV and 5 nM BZ for 72 h. The total number of PEO1 (A) or PEO4 (D) cells were assessed using a viability cell count reagent as described in materials and methods. In the same experiment, a fraction of cells obtained at the end of the experiment was stained with PI and subjected to cell cycle distribution analysis (B, PEO1 cells; E, PEO4 cells). Furthermore, 1000 live cells were collected at the end of the experiment and subjected to a clonogenic survival assay in drug-free media for 21 days (C, PEO1 cells; F, PEO4 cells). In A, C, D and F * $P < 0.05$ and *** $P < 0.001$ compared against VEH, and # $P < 0.05$ when compared NFV+BZ versus NFV or BZ alone. In B and E, *** $P < 0.001$ compared to VEH.

3.12 Nelfinavir and bortezomib combinedly exert cytostatic effects on HGSOC cells by enhancing cell cycle inhibitor p27^{kip1}

To understand the mechanism underlying the synergistic effects of nelfinavir and BZ on HGSOC cells, western blot analysis was performed on PEO1 and PEO4 cells subjected to combined treatment of nelfinavir and BZ. We observed that the G1 arrest demonstrated in the previous experiments (**Figure 3.14 B and E**) was associated with the accumulation of cell cycle inhibitor p27^{kip1} and DNA damage marker γ H2AX (**Figure 3.15 A**). Synergistic combinations between nelfinavir and BZ have been reported before in lung cancer and MM cells, which was associated with the potentiation of ER stress [242]. To determine if the combination of nelfinavir and BZ activate the UPR, we explored the expression of ER associated proteins GRP78, IRE1 α , and CHOP, in PEO1 and PEO4 cells. The combination therapy did not additively increase the level GRP78, IRE1 α , and CHOP, compared to cells receiving monotherapy (**Figure 3.15 A**). Furthermore, combined treatment with nelfinavir and BZ did not cleave executioner caspase-7 (**Figure 3.15 B**). To determine whether the potentiation of the toxicity with the combination nelfinavir/BZ was a consequence of an enhanced inhibition of the proteasome by the drug combination compared with BZ alone, we measured the accumulation of poly-ubiquitinated proteins as a surrogate marker. At the concentrations that cause synergistic effect in terms of growth inhibition, decreased clonogenic survival, and increased levels of p27^{kip1}, we observed that BZ-induced increase in poly-ubiquitinated proteins was not increased further by the presence of nelfinavir (**Figure 3.15 C**). In summary, these results suggest that the potentiated toxicity between BZ and nelfinavir is not the consequence of furthering proteasome inhibition, yet it is associated with a potentiation in cell cycle arrest and reduced long-term clonogenic capacity.

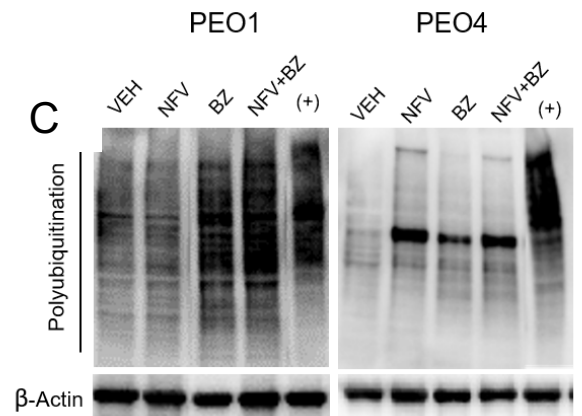
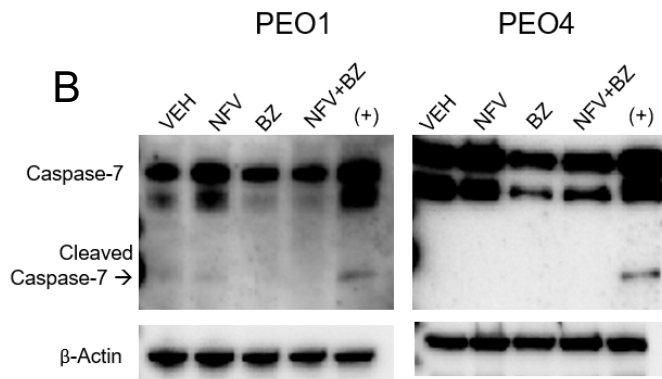
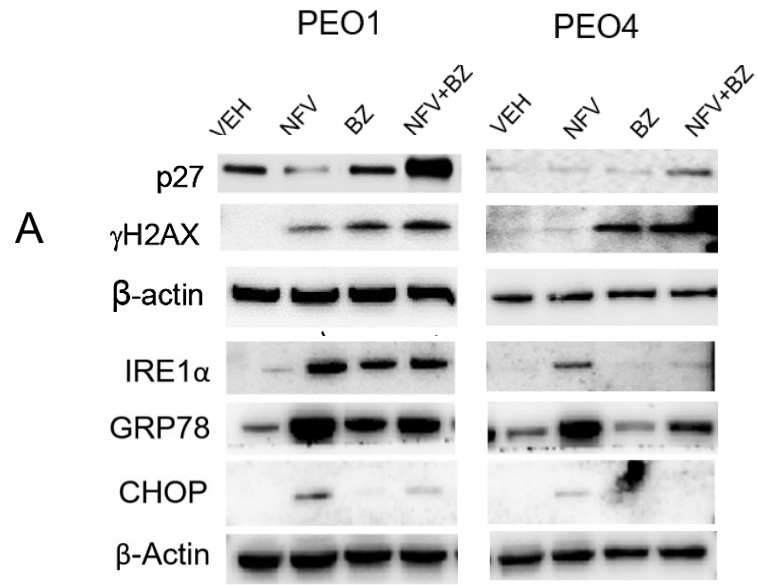


Figure 3.15

Cisplatin-sensitive PEO1 cells were subjected to combined treatment with 10 μ M nelfinavir (NFV) and 10 nM bortezomib (BZ) for 72 h. PEO4—sibling of PEO1 with less sensitivity to cisplatin—were subjected to combined treatment with 5 μ M NFV and 5 nM BZ for 72 h. At the end of the experiments, whole-cell extracts were isolated and electrophoresed. Western blots demonstrated:

(A) Potentiation of expression of cell cycle inhibitor p27^{kip1} during the combination of NFV and BZ in both PEO1 and PEO4 cells. The combination of NFV and BZ did not increase the ER stress, evidenced by the lack of enhanced expression of GRP78, IRE1 α and CHOP along the combination treatment. The combination of NFV and BZ showed enhanced phosphorylation of H2AX in both PEO1 and PEO4 cells; however, it was not higher than the monotherapy with either NFV or BZ.

(B) The combination of NFV and BZ did not promote caspase-7 mediated cell death, evidenced by the lack of cleavage of the executioner caspase-7 in PEO1 and PEO4 cells during the drug combination, compared to the positive control—PEO1 treated with 20 μ M of NFV for 72 h.

(C) NFV does not enhance the proteasome inhibitory function of BZ in PEO1 cells; BZ did not inhibit the proteasome in PEO4 cells at 5 nM dose, evidenced by the lack of poly-ubiquitination. 5 μ M NFV did not promote the inhibition of the proteasome in PEO4 cells treated with 5 nM BZ for 72 h. OV2008 treated with 20 nM BZ for 72 h was used as the positive control (+) to detect poly-ubiquitination in the blot.

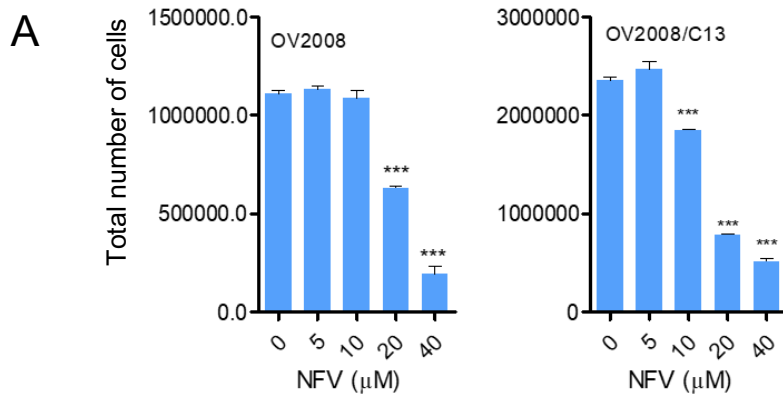
3.13 Nelfinavir targets cells that have acquired resistance to cisplatin upon long-term culture in the presence of the DNA damaging agent

The emergence of cross-resistance to a second drug following chemotherapy with the first line of treatment is common due to the physiological changes conferred by the first drug [371]. So far in our study, we have observed that nelfinavir can effectively target cells which are less sensitive to cisplatin (**Table 3.1**), which were previously described to be selected from pre-existing platinum-resistant sub-clones within the same patient during advanced stages (PEO4, PEO6, PEO23) [155]. These data indicate that cross-resistance to nelfinavir is unlikely in HGSOc clones obtained from patients when clinically resistant to cisplatin. To prove the idea further, we investigated the cytotoxicity of increasing doses of nelfinavir against a cell line made highly insensitive to cisplatin *in vitro*. OV2008/C13 was generated in culture from the parent cell line OV2008 by chronic and intermittent incubation to cisplatin over 13 months until it reached 15-fold less sensitivity to cisplatin compared to OV2008 [338]. OV2008 and its less sensitive to cisplatin pair OV2008/C13 were treated with increasing concentrations of nelfinavir for 72 h. We observed that nelfinavir was cytotoxic to both the cell lines demonstrating a dose-dependent decrease of the total cell number (**Figure 3.16 A**), suggesting nelfinavir is cytotoxic toward mechanistically acquired resistance to cisplatin *in vitro*.

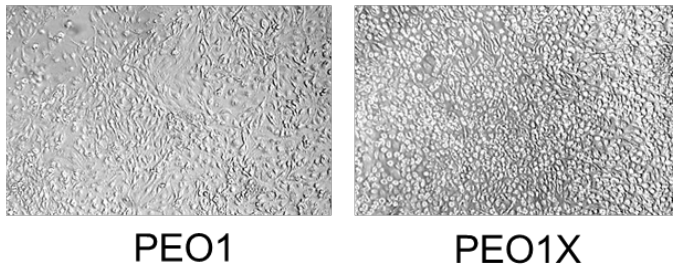
To make the mentioned finding relevant to the research of HGSOc, we decided to test the efficacy of nelfinavir against an HGSOc cell line that has diminished sensitivity to cisplatin *in vitro*. PEO1 cells were exposed to a single dose of cisplatin (10 μ M) for 1 h to mimic the clinical mode of cisplatin administration and the range of initial plasma concentrations in patients [372]. Following the treatment, the damaged cells were washed and replaced with fresh media periodically, and the healthy cells that resisted the cisplatin treatment were allowed to repopulate

the culture to generate the new cell line we termed PEO1X [373]. The platinum sensitivity of PEO1X was tested and was compared with the parent cell line PEO1, which showed significantly lower sensitivity to cisplatin *in vitro*, than that of PEO1 (**Figure 3.16 C**). Light microscopy revealed that PEO1X showed distinct morphological features with homogenous polygonal cells, unlike the heterogenous mesenchymal appearance of PEO1, demonstrating a mixture of spindle-shaped cells and polygonal cells (**Figure 3.16 B**).

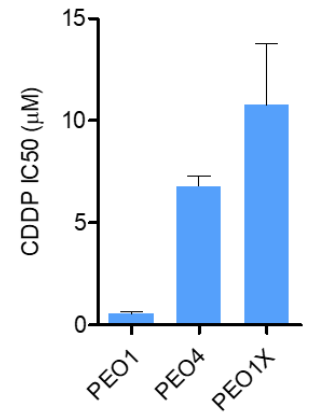
PEO1X cells were exposed to increasing concentrations of nelfinavir for 72 h to obtain the total number of cells, percent viability, and hypodiploid DNA content. We observed a concentration-dependent reduction in the total cell count and the percent viability (**Figure 3.16 D, E**), and a concentration-dependent increase of the hypodiploid DNA content in PEO1X cells during acute treatment with nelfinavir (**Figure 3.16 F**). Clonogenic survival assay of nelfinavir-treated PEO1X cells surviving the acute treatment revealed a concentration-dependent reduction of the number of clones (**Figure 3.16 G**). Taken together, these data provide evidence that nelfinavir can target cells with different sensitivities to cisplatin, either acquired in the patient while becoming clinically resistant to platinum (results from previous sections), or *in vitro* upon sustained exposure to the drug in cell culture (results of this section).



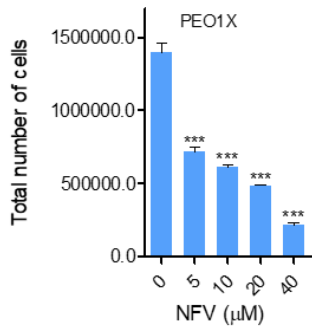
B



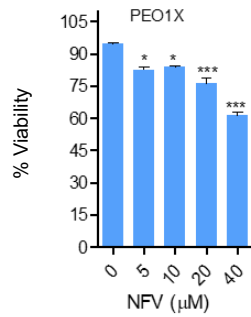
C



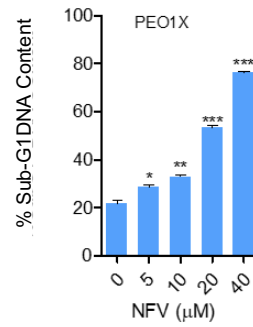
D



E



F



G

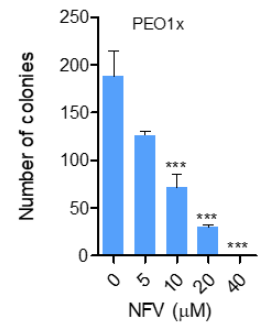


Figure 3.16

(A) Platinum-sensitive OV2008 and its less sensitive to platinum sibling developed *in vitro* OV2008/C13 were exposed to the depicted concentrations of nelfinavir (NFV) for 72 h. At the end of the experiment, the cells were trypsinized and subjected to microcytometry analysis to attain the total number of viable cells. NFV reduces the number of cells in both cell line pairs. (B) PEO1 cells were challenged with 10 μ M cisplatin for 1 h. Thereafter, the toxic agent was removed, the dead cells were eliminated, and the repopulated cells with slightly different morphology were termed PEO1X. (C) PEO1X demonstrates reduced sensitivity to cisplatin than PEO1 and PEO4 cells. (D, E) Following 72 h of treatment with increasing concentrations of NFV, PEO1X cells were trypsinized and subjected to microcytometry analysis to attain the total number of viable cells and percent viability. NFV reduced the total number of cells and viability in PEO1X cells in a concentration-dependent manner. (E) Following 72 h of treatment with increasing concentrations of NFV, PEO1X cells were trypsinized, and a fraction of the cellular content was stained with PI and subjected to cell cycle analysis to determine the hypodiploid DNA content. NFV increased the level of hypodiploid DNA content in a concentration-dependent manner in PEO1X cells. (F) Decreased number of colonies was observed with increased concentrations of NFV in PEO1X cells. * $p < 0.05$; *** $p < 0.001$ vs. control (One-way ANOVA followed by Tukey's Multiple Comparison test).

3.14 Nelfinavir does not re-sensitize cisplatin-resistant cells to short-term cisplatin therapy within physiologically relevant concentrations

To investigate cisplatin re-sensitizing capacity of nelfinavir, we subjected two HGSOc cell lines PEO4 and PEO1X with low platinum sensitivity to drug interaction assays utilizing different combinations of concentrations of nelfinavir and cisplatin, in order to determine the combination index (CI) via the Chou-Talalay method [343].

Determination of doses for drug interaction on each cell line was done based on the IC_{50} s. The IC_{50} of nelfinavir on PEO4 is $12.4 \pm 2.6 \mu\text{M}$, and the IC_{50} of cisplatin on the same cell line was determined to be $6.79 \pm 0.51 \mu\text{M}$. Thus, a dose range between $3.75 \mu\text{M}$ to $15 \mu\text{M}$, with the median dose of $7.5 \mu\text{M}$, was used for a drug interaction assay. Both IC_{50} s of nelfinavir and cisplatin on PEO4 fall within this range. Similarly, the IC_{50} of nelfinavir on PEO1X is $7.56 \pm 0.16 \mu\text{M}$, and the IC_{50} of cisplatin on the same cell line was determined to be $10.75 \pm 3.01 \mu\text{M}$; this means that the IC_{50} s of nelfinavir and cisplatin on PEO1X also falls within the dose range of $3.75 \mu\text{M}$ to $15 \mu\text{M}$. As such, we proceeded to conduct a fixed ratio (1:1) drug-interaction assay with nelfinavir and cisplatin on PEO4 and PEO1X cells, utilizing three concentrations, 3.75, 7.5, and 15 μM .

For a specific drug, a physiologically relevant concentration would be dependent on the peak plasma concentration and the maximum tolerated dose. Nagai and colleagues determined a plasma concentration of $2.56 \mu\text{g/ml}$ ($\sim 8.5 \mu\text{M}$) to be the maximum tolerated dose after a 2 h infusion of 100 mg/m^2 cisplatin [372]. On the other hand, Kattel and colleagues reported the peak plasma concentration of nelfinavir ranging between 4.4 mg/L to 11.3 mg/L ($7.7 \mu\text{M}$ - $20 \mu\text{M}$), obtained from the standard anti-infective dosing of 1250 mg twice daily [329]. As such, the physiologically relevant concentration for cisplatin should be $< 10 \mu\text{M}$, whereas for nelfinavir the physiologically relevant dosing should be $\leq 20 \mu\text{M}$.

Drug interaction analysis revealed that the CI for the three dose-combinations of nelfinavir and cisplatin were higher than 1, in both PEO4 and PEO1X, suggesting that nelfinavir does not synergistically interact with cisplatin in HGSOc cells less sensitive to cisplatin (**Table 3.4**). Furthermore, cell proliferation assay on PEO1X utilizing a single dose nelfinavir (7 μ M) and different concentrations of cisplatin, within the clinically relevant range, show that nelfinavir did not additively reduce the total number of cells during the combination of nelfinavir and cisplatin (**Figure 3.17**), suggesting a lack of interaction between the drugs during short-term exposure within pharmacological relevant concentrations.

Table 8 Analysis of drug interaction between nelfinavir and cisplatin

NFV μM + CDDP μM	Combination index: PEO4	Combination Index: PEO1X
3.75 + 3.75	1.08	1.56
7.5 + 7.5	1.5	1.2
15 + 15	2.5	1.7

PEO1 and PEO4 cells were exposed to fixed ratio (1:1) combination of cisplatin (CDDP) and nelfinavir (NFV). The cells were exposed to different concentrations of cisplatin for 1 h, after which the CDDP was replaced by media or NFV and incubated for 72 h. The estimate of total cell number was utilized to calculate combination index (CI) via Chou-Talalay method of drug interaction in the Calcsyn software. For a specific drug association, CI<1 indicates synergism, CI>1 indicates antagonism, CI=1 indicates additivism, CI=0 indicates no interaction [343]

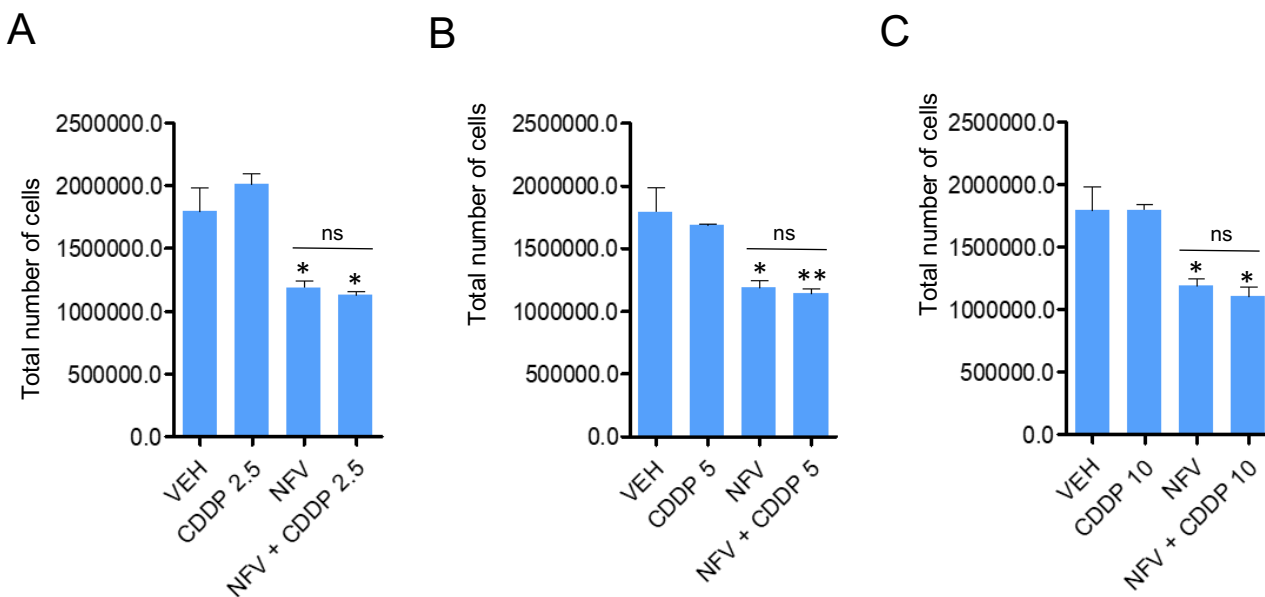


Figure 3.17

PEO1X, low platinum-sensitive sibling of PEO1 selected *in vitro*, were exposed to different concentrations of cisplatin (CDDP) (A) 2.5, (B) 5, or (C) 10 μ M, with or without a fixed concentration of NFV (7 μ M). CDDP treatment was carried out for 1 h before replacement with drug-free media or media carrying NFV (7 μ M). The total length of treatment was 72 h. At the end of the experiment, the cells were trypsinized and subjected to microcytometry analysis to attain the total number of cells. NFV did not synergistically reduce the total number of CDDP-treated cells. * p <0.05; *** p <0.001 vs. control (One-way ANOVA followed by Tukey's Multiple Comparison test).

CHAPTER 4

-

DISCUSSION AND CONCLUSION

HGSOC is the most prevalent subtype of ovarian cancer, demonstrating heterogeneous phenotype and leading to the inevitable emergence of platinum resistance, which warrants the development of novel therapeutic avenues in the treatment protocol of this disease. In this study, we explored the anticancer drug-repurposing potential of the HIV-PI drug nelfinavir, which has been in use to treat AIDS for over 20 years, demonstrating good tolerability as an anti-infective agent. Although nelfinavir was demonstrated to be efficacious against multiple cancers [1], its role against HGSOC has not been explored.

We explored the efficacy of nelfinavir in HGSOC by conducting our study in two parts, in order to reach three objectives. In the first part of the study, nelfinavir was tested as a monotherapy on HGSOC cells to assess its cytotoxicity and investigate the putative mechanistic pathways—especially, endoplasmic reticulum stress—leading to those toxic effects. In the second part, nelfinavir was tested as a combination therapy along with a proteasome inhibitor bortezomib, to assess the possible potentiating effects of nelfinavir.

One of the challenges hindering the preclinical testing of novel treatments against HGSOC has been the lack of genomic similarity with the actual disease in the most-cited HGSOC cell lines [374]. One significant aspect of this study is the usage of patient-derived cell lines established longitudinally at different stages of disease progression and platinum sensitivities. These cell lines demonstrated differential morphological and genetic patterns *in vitro* [155,337], and matched the genomic landscape of HGSOC [375]. We further describe that the cell lines recapitulated *in vitro* the status of the intrinsic cisplatin-sensitivity of the original patients (**Table 3.1**), providing clinical relevance to our study.

We report that nelfinavir elicited effective cytotoxicity in all patient-matched HGSOC cell lines irrespective of their differential cisplatin sensitivity, evidenced by the concentration-

dependent reduction in the total number of cells and percent viability, with the concomitant increase in hypodiploid-DNA content. Following short-term treatment with nelfinavir for 72 h, the cells that remained alive were subjected to clonogenic survival assay in drug-free media to assess whether the cells recovered from the nelfinavir-inflicted cytotoxicity. A concentration-dependent reduction in the number of clones suggested that the cells had sustained irreparable damage caused by nelfinavir. This chronic toxicity may be explained by the induction, by nelfinavir, of concentration- and time-dependent DNA damage as reflected by the increased phosphorylation of the DNA double-strand breaks marker H2AX (a.k.a. γ H2AX) [376].

Since nelfinavir demonstrated cytotoxicity in HGSOc cells originated from different patients, with different disease progression and cisplatin-sensitivity, we hypothesized that similar mechanistic pathways could be responsible for the generalized cytotoxic effects. Indeed, we observed a concentration-dependent increase in the expression of ER stress sensor GRP78, ER-stress related apoptosis mediator CHOP, and cell cycle inhibitor p27^{kip1}, suggesting that ER stress and cell cycle arrest are mechanisms activated in nelfinavir-treated HGSOc cells, which contribute to the generalized cytotoxicity. Previously, Jiang *et al.* reported nelfinavir-mediated upregulation of cell cycle inhibitor p27^{kip1} in melanoma cells, which accompanied reduced cyclin-dependent kinase-2 (Cdk2) activity due to reduced Cdc25A phosphatase [210]. Furthermore, activation of the UPR upon ER stress has been associated with nelfinavir-mediated cytotoxicity against multiple cancers, such as lung cancer, glioblastoma, MM, and breast cancer, to mention some [204,222,225,244].

The UPR represents a series of signaling transduction events that ameliorate the accumulation of unfolded/misfolded proteins in the ER. It can have either a pro-survival or a proapoptotic role in the cells, depending on the intensity or the length of the stress [334,348,377-

381]. Cancer cells have been reported to exploit ER stress for survival within unfavourable conditions, such as nutrient shortage, hypoxia, acidosis, and energy deprivation. As such, two pharmacological approaches can be used to take advantage of the chronically enhanced ER stress in cancer cells, either by shutting down the pro-survival mode of the UPR, or by tilting the cellular environment toward its proapoptotic phase [334,349]. Our study demonstrated a concentration-dependent and temporal proapoptotic shift of the UPR in HGSOc cells in response to nelfinavir treatment, which was evident from the enhanced expression of ER stress-related apoptosis mediators ATF4 and CHOP, accompanied by the increase of the proapoptotic protein Bax and a concomitant cleavage of executioner caspase-7. These results corroborate previous findings in non-small cell lung cancer and MM cells, demonstrating the activation of the ATF4-CHOP pathway, and resulting in a proapoptotic shift of ER stress in response to nelfinavir; the authors additionally reported a reduction of nelfinavir-induced cell death during siRNA-mediated inhibition of CHOP, underpinning a key role of CHOP in the apoptotic process [242]. Pharmacological aggravation of constitutive ER stress by nelfinavir in cancer cells has also been utilized as a chemosensitizing strategy against doxorubicin-resistant breast cancer and castration-resistant prostate cancer [231,246].

A recent study shows high expression of GRP78, PERK, and ATF6 in patients' tumors, which correlated with poor patient survival in HGSOc [335]. Elevated basal expression of ER stress-related proteins in ovarian cancer suggests the existence of a possible therapeutic window whereby further pharmacological aggravation of ER stress may induce apoptosis in ovarian cancer cells without triggering similar outcomes in normal cells. We observed that nelfinavir might achieve such a goal as it activates all three arms of the UPR: IRE1 α -XBP1, PERK-ATF4-CHOP and ATF6 in HGSOc cells, to a comparable level as that caused by the classical ER stressor

tunicamycin. Previously, it was reported an accumulation of non-cleaved ATF6 in prostate cancer cells due to nelfinavir-mediated inhibition of site-2 protease (S2P) enzyme, which interrupted the regulated intramembrane proteolysis (RIP) of ATF6 in the Golgi apparatus for the release of the active soluble form [250]. Our result demonstrating nelfinavir-associated increase in soluble ATF6 in HGSOC cells excludes the Golgi-resided S2P enzyme as a likely target of nelfinavir in the HGSOC cells.

In this study, we reported a concentration- and time-dependent inhibition of protein synthesis by nelfinavir, which was further abrogated by the presence of the protein synthesis inhibitor CHX. These results support the validity of the non-radioactive method for assessing mRNA translation that we used in this study and termed puromycin incorporation assay. Global protein synthesis inhibition was clearly the long-term outcome of nelfinavir treatment in HGSOC cells; such effect, however, did not take place until after 4 h of nelfinavir treatment. This was associated with a transient dephosphorylation of eIF2 α and the cleavage of *XBPI* mRNA, providing proof-of-principle that the initial sustained protein synthesis in the presence of nelfinavir is, at least in part, responsible for triggering the UPR in HGSOC cells. We observed similar results in OV2008 cancer cells treated with the anti-progestin/anti-glucocorticoid agent mifepristone, which killed the cells because of an increase in ER stress that was associated with a short-term spike in protein synthesis that preceded the global abrogation of mRNA translation that concurred with the dying of the cells [336].

Other studies have shown that nelfinavir can increase autophagy [204,264]. In ovarian cancer cells, we have shown previously with the non-canonical ER stressor mifepristone that it caused ER stress-mediated toxicity by increasing autophagic flux and synergized with the lysosome inhibitor chloroquine in killing the cells [336]. In the case of nelfinavir, while we observed an

increase of LC3II in nelfinavir-treated HGSOC cells of differential platinum sensitivities, suggesting an increase of the level of autophagosomes, we did not observe a further enhancement in the level of LC3II during co-treatment with the lysosomal inhibitor bafilomycin A1. This signifies that nelfinavir does not affect autophagic flux, but that the number of autophagosomes actually increases likely because of inhibition of lysosomal function.

We further report the reduction of survival and proliferation signals marked by the decline in p-AKT and p-ERK in HGSOC cells with high or low sensitivity to cisplatin, upon treatment with nelfinavir. Downregulation of AKT is a well-known effect of nelfinavir and has been associated with impaired glucose metabolism, insulin resistance, and lipodystrophy during chronic treatment, which are reversible upon discontinuation of the therapy [186]. This is relevant from a therapeutic standpoint, as an amplified expression of components of the PI3K-AKT pathway has been correlated with reduced overall survival of HGSOC patients [17]. In patients with advanced HGSOC, amplification of the phosphatidylinositol 3-kinase (PI3KCA) and AKT2 has been observed in 12% and 10% of samples, respectively [382], while reduced expression or loss of PTEN has been correlated with advanced staging in HGSOC samples [383,384]. The inhibition of p-AKT by nelfinavir was reported in other cancers, such as breast cancer [215,255], MM [222,257], acute myeloid leukemia [258], pediatric refractory leukemia [229], diffuse B-cell lymphoma [279], prostate cancer [233], and non-small cell lung carcinoma [232]. The reduction in p-AKT by nelfinavir has also been proposed as a radiosensitizing strategy in glioblastoma, bladder, lung, and head and neck cancers [6,283,286,287]. It is interesting to note that the reduction in p-AKT in peripheral blood mononuclear cells (PBMCs) was proposed as a surrogate biomarker to assess the pharmacological efficacy in targeting AKT signaling by nelfinavir [289]. Also, p-AKT was decreased when

nelfinavir was combined with doxorubicin in doxorubicin-resistant chronic myeloid leukemia cells [230], and with the proteasome inhibitor bortezomib in MM cells [257].

In terms of p-ERK inhibition, our data are commensurate with previous reports where reduction of ERK phosphorylation was observed in response to nelfinavir in MM [222,296], HER2-positive and –negative breast cancer cells [272], medullary thyroid cancer [223], and adenoid cystic carcinoma [291].

Another significant finding in this study is the increase, upon nelfinavir treatment, in the phosphorylation of H2AX (γ H2AX)—a marker of DNA double-strand breaks—in PEO1 and PEO4 cells having different sensitivities to cisplatin. HGSOc cells frequently present with TP53 mutations (97%) and a defect in the homologous recombination (HR) DNA repair mechanism (50%) primarily due to germline or somatic mutation of BRCA1/2 [23]. A deficient HR mechanism prevents error-free repair of DNA double-strand breaks induced by platinum adducts, thus confers sensitivity of cancer cells to platinating agents. PEO1 cells carry a germline inactivating mutation to BRCA2 and are sensitive to platinating agents, whereas PEO4 that were obtained when the patient was resistant to platinum showed a functional restoration to the BRCA2 due to a secondary mutation [155,385]. Deficiency in HR forces ovarian cancer cells to be over-reliant on the base-excision repair mechanism by poly (ADP-ribose) polymerase (PARP) classically utilized to repair single-strand DNA breaks. As such, targeting PARP has been a desirable pharmacologic approach to induce synthetic lethality in ovarian cancer cells [125]. It has also been implicated that restoration of BRCA2 confers cross-resistance to PARP inhibitors in parallel to reduced cisplatin sensitivity [152]. Since nelfinavir was able to elicit enhanced γ H2AX in HGSOc cells independent of their BRCA status and sensitivity to cisplatin, a different mechanism of DNA damage may be involved, whereby the cells may not rely on the HR pathway to repair their DNA.

DNA damage response may be elicited to generally elicit two fates for the cells undergoing the stress, 1) cell cycle arrest while the repairing machinery re-establish the DNA integrity and evade abnormal mitosis; 2) initiation of apoptosis when the extent of DNA repair is beyond reparation [140,386]. In this study, we observed the accumulation of HGSOC cells in the G1 phase of the cell cycle at lower concentrations of nelfinavir (5 to 10 μ M), while higher concentrations elicited cell death. We further report the downregulation of protein levels of p-CDK2/CDK2, with concomitant upregulation of p27 in nelfinavir-treated HGSOC having varying sensitivity towards cisplatin. Here, our data corroborate the finding by Jiang *et al.* indicating decreased protein levels of p-CDK2/CDK2 in nelfinavir-treated melanoma cells [210].

In the second part of the study, we explored the combinatorial effects of nelfinavir and proteasome inhibitor bortezomib on HGSOC cells having differential platinum sensitivities. We report that nelfinavir can potentiate the effects of proteasome inhibitor bortezomib by affecting the cell cycle in combination with sustained DNA damage. Inhibition of the proteasomes leads to the accumulation of ubiquitinated proteins, which in turn can increase the protein load in the ER and push the effect of an ER stressor to lethality. Based on this rationale, we demonstrated that the non-canonical ER stressor mifepristone potentiates the effect of bortezomib in OV2008 cancer cells by significantly inhibiting the activity of the proteasome leading to cell death [336]. In the present study using PEO1 and PEO4 HGSOC cells, however, nelfinavir, despite causing ER stress similarly to mifepristone, it did not inhibit the proteasome beyond the inhibition caused by bortezomib alone. This is not surprising as previous reports suggested that the effect of nelfinavir on the proteasome may be cancer and cell-type specific; for instance, nelfinavir did not demonstrate an inhibitory effect on the proteasome in cervical cancer cells [208]. What we found when combining nelfinavir and bortezomib in the current HGSOC cells was an increase in the

expression of the cell cycle inhibitor p27^{kip1}, which was higher than the expression induced by each drug individually; this was associated with a potentiation among the drugs in causing cell cycle arrest at the G1 phase of the cell cycle. In the long-term, likely because of sustained DNA damage, the combination of nelfinavir and bortezomib caused reduced clonogenic survival, suggesting a potentiation among the drugs irreversibly abrogating the reproductive capacity of the cells.

Platinum resistance is one of the primary reasons that has interrupted the improvement of patient survival in advanced stage HGSOC. Hence, a drug targeting the platinum-resistant phenotype is highly desirable in research for newer therapies for this disease. Our data demonstrate that nelfinavir induces toxicity toward HGSOC cells of a wide range of platinum sensitivities, possibly through a DNA-damaging mechanism, which is likely different from that caused by cisplatin as we did not find cross-resistance among the drugs. In PEO1X cells –siblings of highly platinum-sensitive HGSOC cell PEO1 selected via *in vitro* challenge of cisplatin–demonstrated 15-fold less sensitivity to cisplatin compared to that of PEO1; however, they remained highly sensitive to nelfinavir, which suggested an absence of cross-resistance between nelfinavir and cisplatin. One possible reason underlying the lack of synergism observed in HGSOC cells treated with low dose combination of nelfinavir and cisplatin during short-term treatment could be that both drugs act on the same pathway – sparing any additive effect on cytotoxicity. Mechanistically, both nelfinavir and cisplatin have shown induction of ER stress in cancer cell lines contributing to cytotoxicity [1,139]. Mandic *et al.* provided evidence of cisplatin-induced apoptosis coinciding with ER stress in enucleated cancer cells in the absence of DNA damage [139]. It would be worth investigating the possible activation of ER stress in response to short-term low-dose treatment of

cisplatin in HGSOC cells. Furthermore, it is also likely that higher concentrations or prolonged effects of nelfinavir and cisplatin may lead to additive effects.

Several clinical trials have tested the combination of nelfinavir and cisplatin with or without the application of radiotherapy. For instance, Rengan *et al.* reported administration of 1250 mg nelfinavir twice daily, prior to and concurrently with cisplatin, etoposide and 66Gy radiation beam, which resulted in partial response in post-treatment PET-derived metabolic evaluation and improvement in PFS of 11.7 months in locally advanced stage IIIa/IIIb non-small cell lung carcinoma [317,318]. However, in most of the clinical trials, nelfinavir has been utilized as a radiosensitizing agent based on *in vitro* findings [1]; as such, it is not clear whether nelfinavir plays any role in the efficacy of cisplatin in the trials administering cisplatin and radiotherapy concurrently. In the context of our study, it would be important to ask at which time point of the treatment regimen of HGSOC would it be feasible to introduce nelfinavir. Since we did not observe cross-resistance between nelfinavir and cisplatin, in theory, it would be safe to introduce nelfinavir as a maintenance therapy following standard platinum-based therapy in HGSOC with the aim to prolong disease-free survival before the disease relapses. Fortunately, nelfinavir has shown a tolerable toxicity profile in clinical trials against cancers; for instance, Blumenthal *et al.* determined the maximum tolerated dose at 3125 mg with reversible toxicities upon discontinuation, when nelfinavir was given as a monotherapy to adults with advanced solid refractory tumors of varying origins [243].

One challenge in introducing nelfinavir in the clinical practice for treating HGSOC would be maintaining the desired plasma concentration that achieves anticancer effects. The anti-infective dosing of 1250 mg twice daily yielded a wide range of variability in the peak plasma concentration (4.4 -11.3 mg/L), likely due to genomic polymorphism in the metabolizing enzyme

CYP2C19 [329]. Other authors have reported the concentration reached in circulation by nelfinavir of being in the 7.7 to 20 μM range [211], which is within the range of concentrations we used in the current study. Chemical hybridization and combination with other drugs may be used to keep optimal plasma concentrations of nelfinavir to achieve greater anticancer efficacy. For instance, recently, nitric oxide hybridization of HIV-PIs has been promoted as an alternative strategy to improve pharmacokinetics and anticancer efficacy [189].

There are several limitations associated with this study. All the inferences were drawn from *in vitro* studies on HGSOc cell lines, although the origins of the cells were matched with the genotype of the original patients via autosomal short tandem repeat, and multiple approaches were utilized to reach a single inference. Yet, the *in vitro* data needs to be validated through a more complex system, like three-dimensional culture, organoid studies, *in vivo* studies, or on patients. Due to technical and resource limitations, the western blots were performed at least on two biological replicates with similar outcomes. The interpretations of the protein expression data could be improved by increasing the number of replicates and determining statistical significance via densitometry. However, the total protein loading per western blot was visualized on TGX stain-free gels upon ultraviolet activations and on unstained membranes, which was compared with the expression of house-keeping protein β -actin (**Appendix**). This dual assessment of equal protein loading per western blot validated the expression of the investigated proteins on duplicate samples. Furthermore, we observed certain mechanistic avenues related with nelfinavir-induced toxicity in HGSOc; however, overlapping between signaling pathways is common, which leaves room for exploration into other signaling cascades in relation to nelfinavir toxicity. Immunogenic cell death (ICD) has emerged as a novel paradigm to be utilized in cancer therapy whereby pharmacological agents modulate programmed cell death in cancer cells via a tumor-specific adaptive immune

response, leading to long-term benefit [387]. Components of ER stress, especially p-eIF2 α has proven to be a central determinant of ICD; rationalizing a possible role of nelfinavir in eliciting ICD, since we have observed that nelfinavir can act as a potent modulator of eIF2 α phosphorylation [388]. In future, it would be beneficial to investigate the likely ICD modulating role of nelfinavir in HGSOc cells and the outcome of the long-term combinations of nelfinavir and cisplatin on ICD.

Additionally, the primary target of nelfinavir within in the cells is not clear, which elicits the downstream mechanisms we have observed. So far, three putative binding sites have been suggested for nelfinavir via *in silico* and *in vitro* methods: HSP90 [272], S2P [250] and kinases [202]. Since we excluded S2P as a potential target, the observed mechanism may be initiated through HSP90 or binding of nelfinavir with a particular kinase or kinases. Disruption of HSP90 can alter the functionality of its binding partner HSP70, which is required for the correct folding of proteins for intracellular protein homeostasis [389,390]. We have demonstrated a critical role of ER stress in eliciting nelfinavir-mediated cytotoxicity, which may be related to the putative binding of nelfinavir with HSP90 at the upstream level. Furthermore, modulation of AKT and ERK signals by nelfinavir in HGSOc cells may be an outcome of post-translational modification of HSP90 as reported previously [223], or due to the direct yet weak binding of upstream kinases [202]. Precise understanding of the target and its binding partners within the cancer cells may further help in the clinical application of nelfinavir against cancer.

Conclusion

Despite promising advancement in cancer therapeutics, emergence of novel mutations and resistance to chemo-radiotherapy results in low survival rates. Additionally, increased cost and

requirement of highly efficient set-up for chemo-radiotherapy hinders patient access to efficacious treatments within low-income populations and areas with limited resources. Drug-repurposing for cancer therapy can maximize the optimal use of the existing drug repertoire and lower the time and cost of developing new therapies. Nelfinavir has been in use as an anti-infective agent against HIV for more than two decades, demonstrating good safety profile [1]. In this study, we demonstrated multipronged mechanisms whereby nelfinavir targets HGSOc cells independent of their platinum sensitivities. The proposed mechanistic model is depicted in Figure 4, based upon our findings of nelfinavir as a monotherapy and a combinatorial agent with a proteasomal inhibitor bortezomib on HGSOc. As an oral anti-infective drug with a well-documented history of tolerable side effects, the observed anticancer effects of nelfinavir suggest its potential repurposing benefit against HGSOc as an additional adjuvant chemotherapeutic agent.

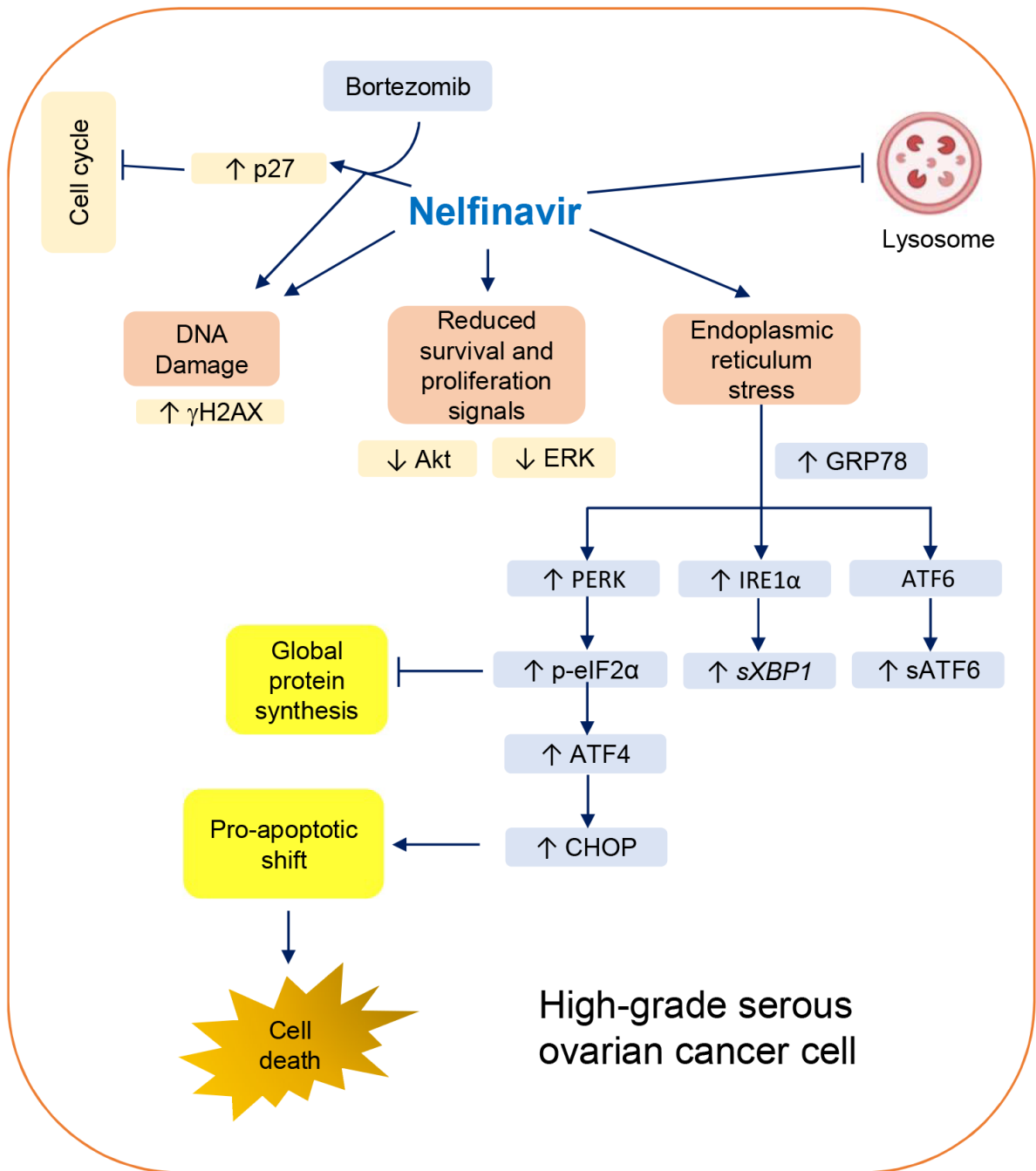


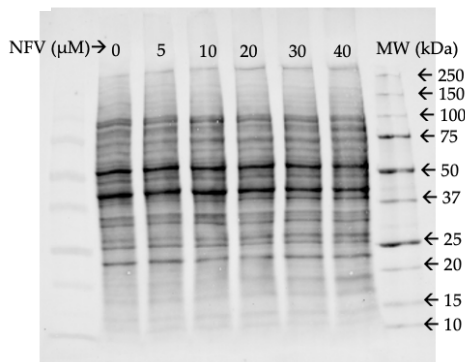
Figure 4

Schematic representation of the proposed mechanism of nelfinavir (NFV)-mediated cytotoxicity in HGSOC cells regardless of platinum sensitivity. NFV triggers DNA damage, reduces survival and proliferation signaled by AKT and ERK, and activates the three arms of the UPR: 1) IRE1 α -XBP1, 2) PERK-eIF2 α -ATF4-CHOP, and 3) ATF6 cleavage. Phospho-eIF2 α leads to inhibition of global protein synthesis, and at the downstream of it, ATF4-CHOP-mediated proapoptotic shift triggers the cleavage of executioner caspase-7 to elicit cell death. Additionally, NFV impairs the autophagic clearance, likely via lysosome inhibition. Finally, NFV potentiates the cytotoxicity of proteasome inhibitor bortezomib (BZ) by increasing the level of cell cycle inhibitor p27^{kip1}, while reducing clonogenic survival (not shown), denoting a long-lasting toxicity likely consequence of sustained DNA damage.

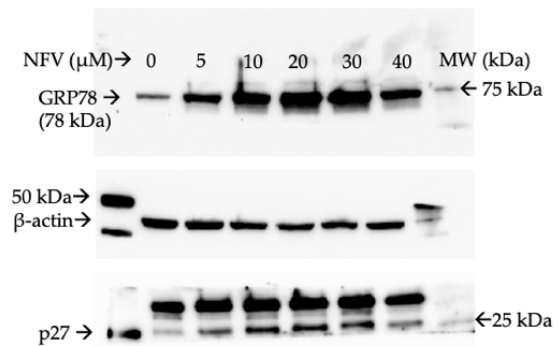
APPENDIX

Raw western blot data corresponding to the figures shown in the results section.

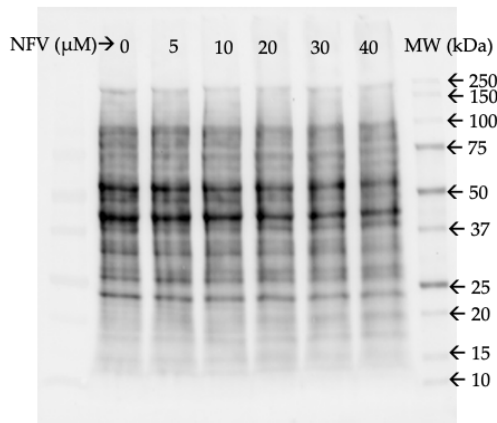
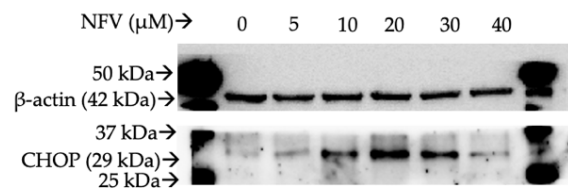
A



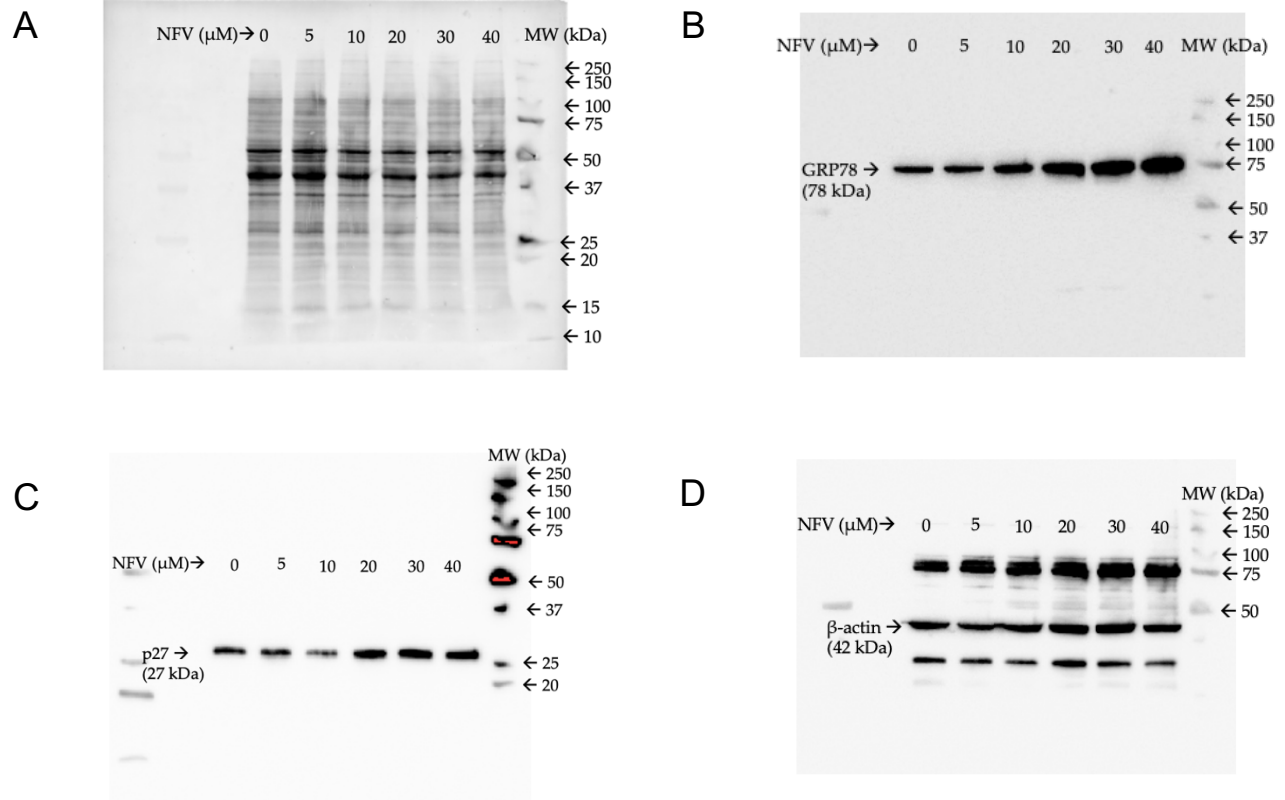
B



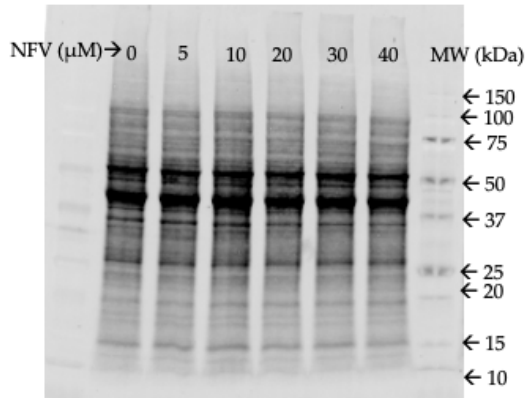
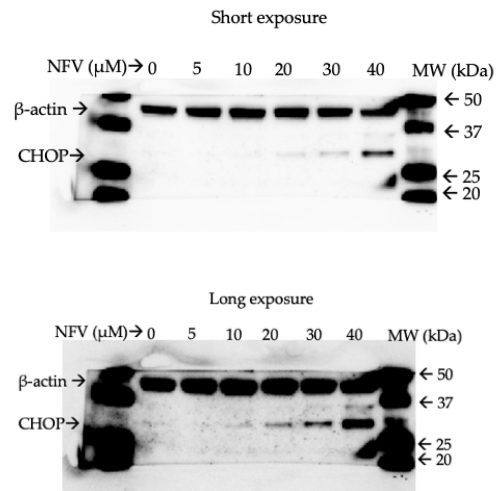
Blot 1. Proteins extracted from PEO1 cells treated with 5-40 μ M NFV were run for 30 min at 200V on TGX stain-free fast cast acrylamide gel (12%). After the run, the gel was activated by UV light. Proteins on the gel were transferred using TransBlot Turbo for 7 min. After transfer, the total protein load was visualized in the unstained membrane using BioRad ChemiDoc imager (A). After 1 h of blocking with 5% non-fat dry milk, blot 1 was cut between 37 and 25 kDa, and between 25 and 20 kDa. The top part above 37 kDa was incubated for GRP78, and the bottom part above 25 kDa for p27^{kip1} (B). After that, the area between 50 kDa and 37 kDa was cut and incubated for β -actin (B). Two stained molecular weights (MW) on each side were used for cutting accuracy. Data from blot 1 were presented in **Figure 3.3A**.

A**B**

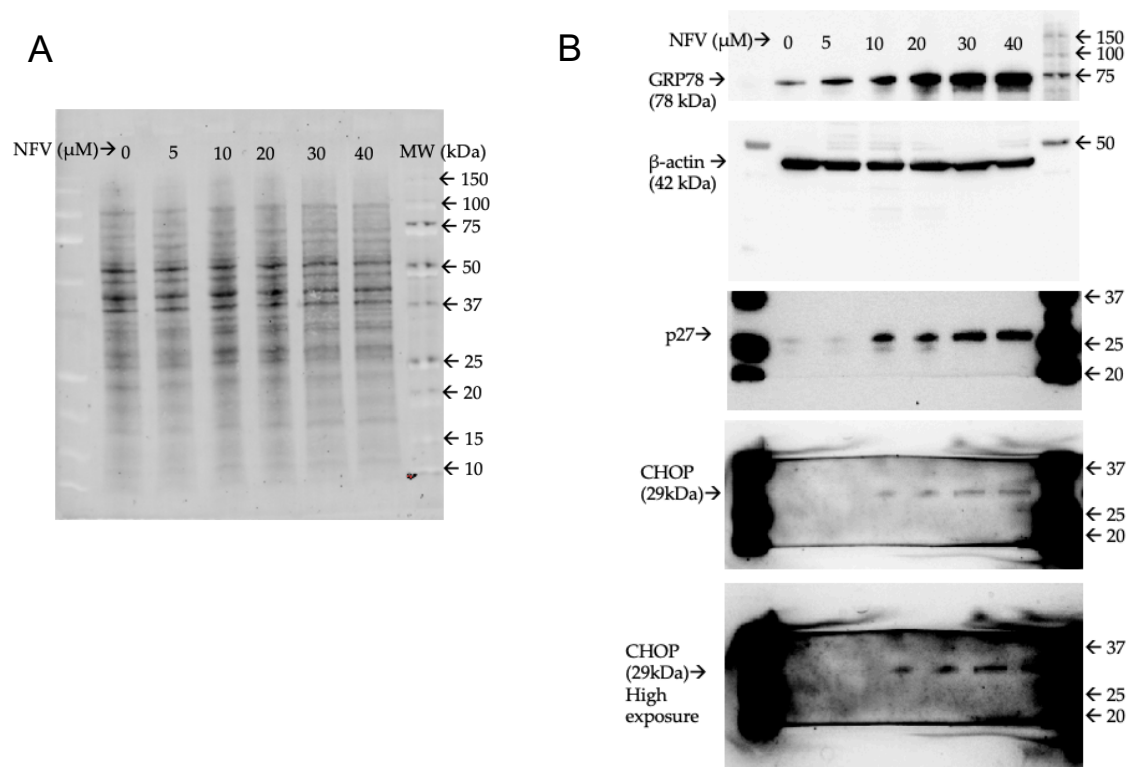
Blot 2. Proteins extracted from PEO1 cells treated with 5-40 μM NFV were run for 30 min at 200V on TGX stain-free fast cast acrylamide gel (12%). After the run, the gel was activated by UV light. Proteins on the gel were transferred using TransBlot Turbo for 7 minutes. After transfer, the total protein load was visualized in the unstained membrane using BioRad ChemiDoc imager (A). After 1 h of blocking with 5% non-fat dry milk, blot 2 was cut below 75 kDa, at 37 kDa and at 25 kDa. The part below 75 kDa and above 37 kDa was incubated for β-actin, the part between 37 kDa to 25 kDa was incubated for CHOP. Two stained molecular weights (MW) on each side were used for cutting accuracy. Data from blot 2 were presented in **Figure 3.3A**.



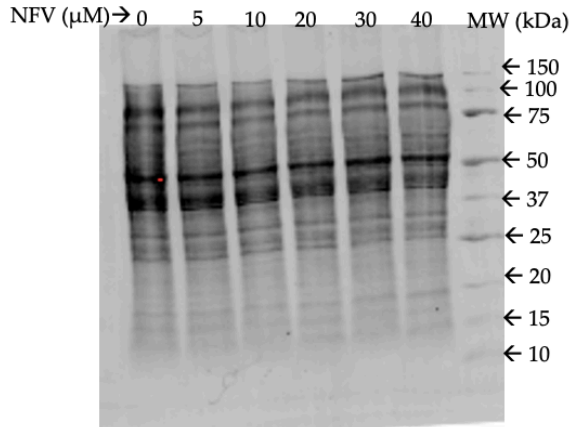
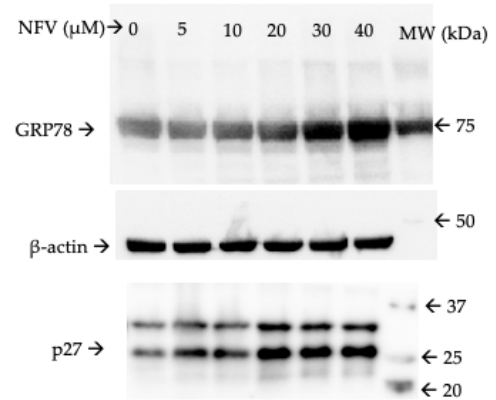
Blot 3. Proteins extracted from PEO14 cells treated with 5-40 μM NFV were run for 30 min at 200V on TGX stain-free fast cast acrylamide gel (12%). After the run, the gel was activated by UV light. Proteins on the gel were transferred using TransBlot Turbo for 7 min. After transfer, the total protein load was visualized in the unstained membrane using BioRad ChemiDoc imager (A). After 1 h of blocking with 5% non-fat dry milk, blot 3 was sequentially incubated for GRP78 (B), p27^{kip1} (C), and β -actin (D). Data from blot 3 were presented in **Figure 3.3A**. MW=molecular weight.

A**B**

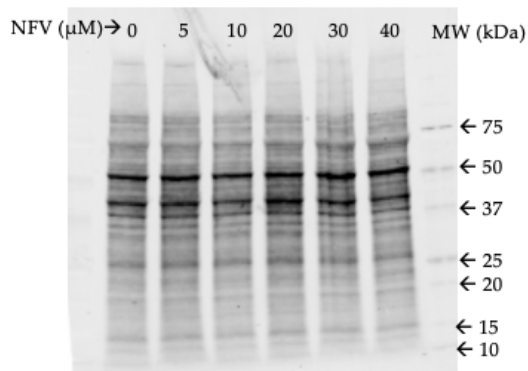
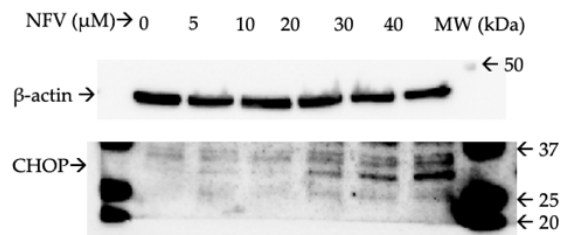
Blot 4. Proteins extracted from PEO14 cells treated with 5-40 μM NFV were run for 30 min at 200V on TGX stain free fast cast acrylamide gel (12%). After the run, the gel was activated by UV light. Proteins on the gel were transferred using TransBlot Turbo for 7 min. After transfer, the total protein load was visualized in the unstained membrane using BioRad ChemiDoc imager (A). After 1 h of blocking with 5% non-fat dry milk, blot 4 was cut below 75kDa and below 20kDa, and the middle part was sequentially incubated for β-actin and CHOP (B). Two stained molecular weights (MW) on each side were used for cutting accuracy. Data from blot 4 were presented in **Figure 3.3A**.



Blot 5. Proteins extracted from PEO4 cells treated with 5-40 μM NFV were run for 30 min at 200V on TGX stain-free fast cast acrylamide gel (12%). After the run, the gel was activated by UV light. Proteins on the gel were transferred using TransBlot Turbo for 7 min. After transfer, the total protein load was visualized in the unstained membrane using BioRad chemiDoc imager (A). After 1 h of blocking with 5% non-fat dry milk, blot 5 was cut below 75 kDa and the top part was incubated for GRP78, and the bottom part was incubated for β -actin (B). After that, the bottom blot was cut at the level of 37 kDa and the bottom part was sequentially incubated for p27^{kip1} and CHOP (B). Two stained molecular weights (MW) on each side were used for cutting accuracy. Data from blot 5 were presented in **Figure 3.3A**.

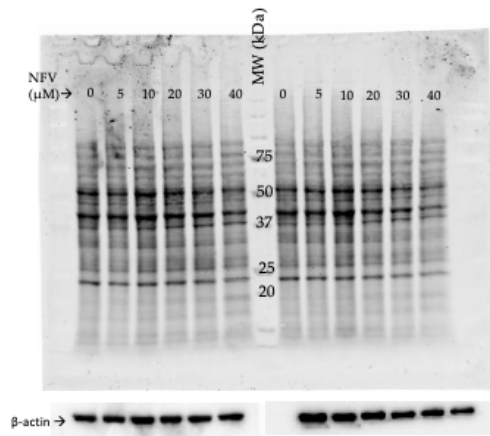
A**B**

Blot 6. Proteins extracted from PEO23 cells treated with 5-40 μM NFV were run for 30 min at 200V on TGX stain-free fast cast acrylamide gel (12%). After the run, the gel was activated by UV light. Proteins on the gel were transferred using TransBlot Turbo for 7 min. After transfer, the total protein load was visualized in the unstained membrane using BioRad ChemiDoc imager (A). After 1 h of blocking with 5% non-fat dry milk blot 6 was cut between 75 and 50 kDa, at 37 kDa and below 20 kDa. The part of the membrane above 75 kDa was incubated for GRP78, the part between 50 and 37 kDa was incubated for β -actin and the part below 37 kDa was incubated for p27^{kip1} (B). Data from blot 6 were presented in **Figure 3.3A**. MW=molecular weight.

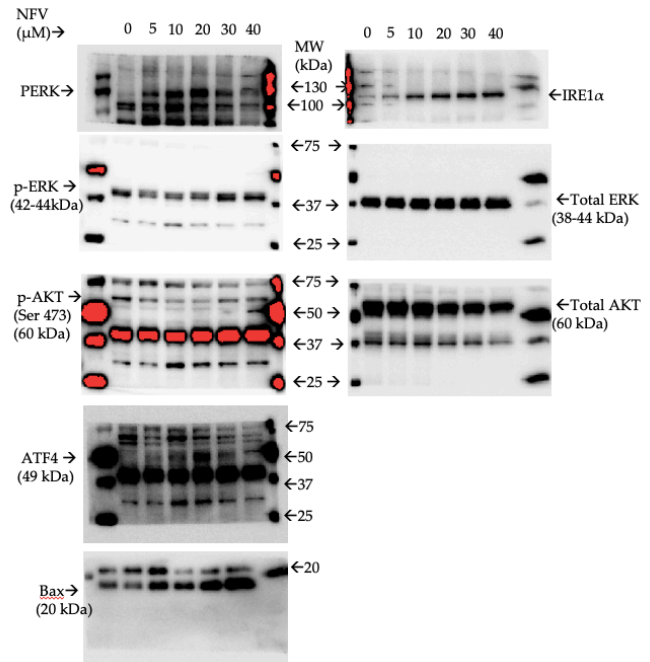
A**B**

Blot 7. Proteins extracted from PEO23 cells treated with 5-40 μM NFV were run for 30 min at 200V on TGX stain-free fast cast acrylamide gel (12%). After the run, the gel was activated by UV light. Proteins on the gel were transferred using TransBlot Turbo for 7 min. After transfer, the total protein load was visualized in the unstained membrane using BioRad ChemiDoc imager (A). After 1 h of blocking with 5% non-fat dry milk, blot 7 was cut at 50 kDa and at 37 kDa and at 20 kDa. Two stained molecular weights (MW) on each side were used for cutting accuracy. The area between 50 and 37 kDa was incubated for β-actin, and the area between 37 kDa to 20 kDa was incubated for CHOP (B). Data from blot 7 were presented in **Figure 3.3A**.

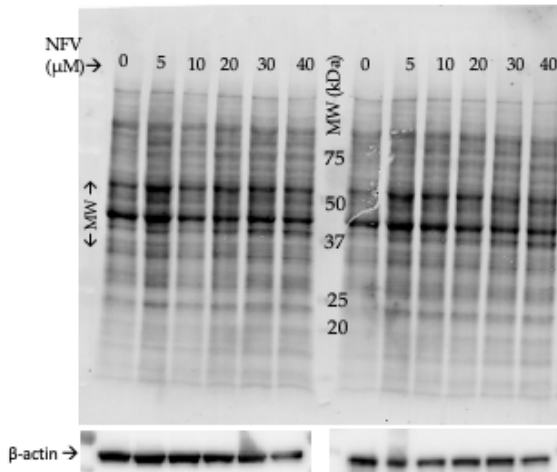
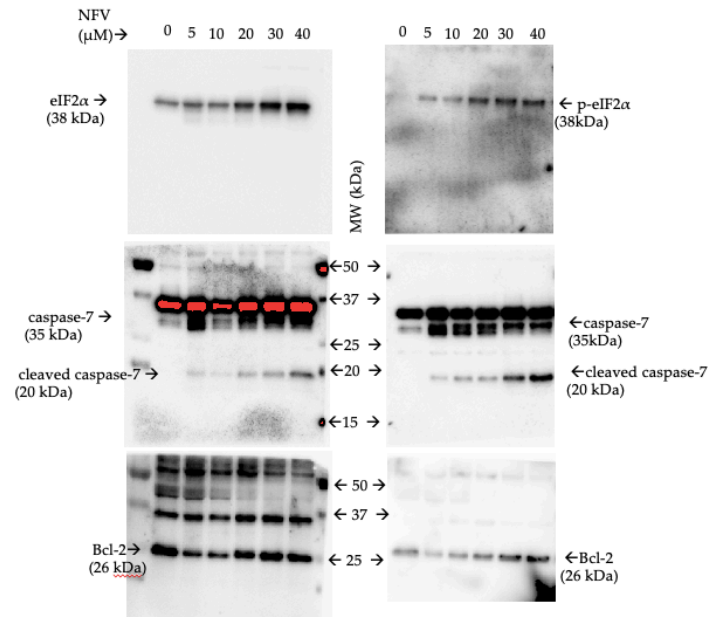
A



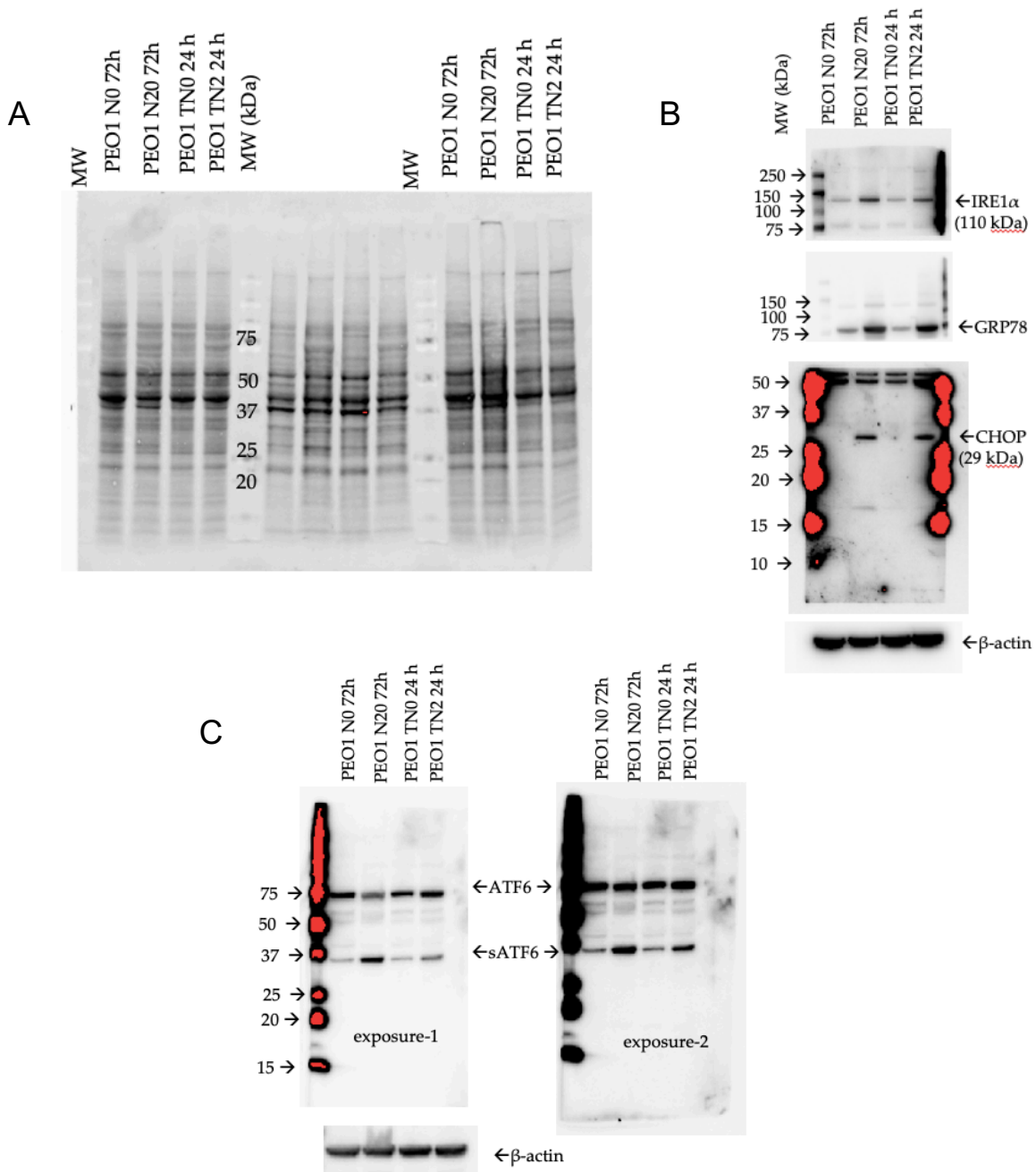
B



Blot 8. Proteins extracted from PEO1 cells treated with 5–40 μM NFV were run for 30 min at 200V on TGX stain-free fast cast acrylamide gel (12%) in two identical sets. After the run, the gel was activated by UV light. Proteins on the gel were transferred using TransBlot Turbo for 7 min. After transfer, total protein load was visualized in the unstained membrane using BioRad ChemiDoc imager (A). After 1 h of blocking with 5% non-fat dry milk, the blot was cut in the middle along the molecular weight ladder to yield two identical sets of blots. The blots were cut at 75 kDa and below 25 kDa. The top part was incubated for IRE1 α and PERK (B). The middle blots were incubated for p-AKT (Ser 473)/AKT, p-ERK/ERK (B) and β -actin (A). The left middle blot was incubated for ATF4 and the bottommost part was incubated for Bax (B). Two stained molecular weights (MW) on each side were used for cutting accuracy. Data from blot 8 were presented in **Figure 3.4A, 3.7B, and 3.11A.**

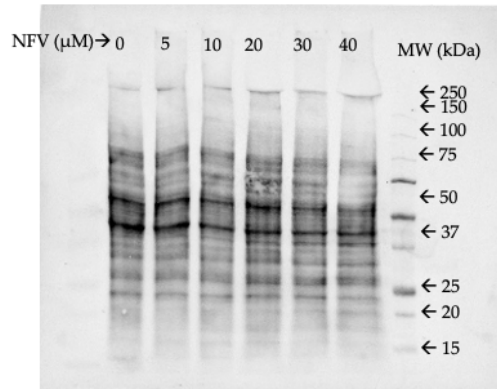
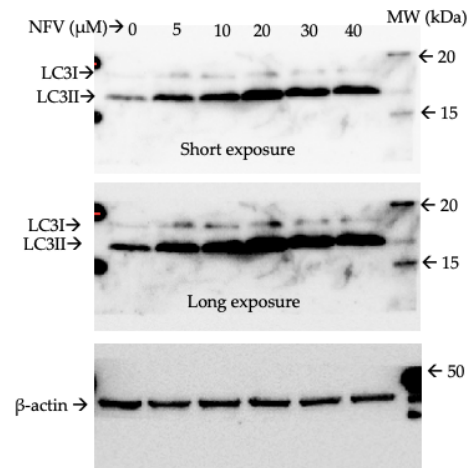
A**B**

Blot 9. Proteins extracted from PEO1 cells treated with 5-40 μ M NFV were run for 30 min at 200V on TGX stain-free fast cast acrylamide gel (12%) in two identical sets. After the run, the gel was activated by UV light. Proteins on the gel were transferred using TransBlot Turbo for 7 min. After transfer, total protein load was visualized in the unstained membrane using BioRad ChemiDoc imager (A). After 1 h blocking with 5% non-fat dry milk, the blot was cut in the middle along the molecular weight ladder to yield two identical sets of blots. The blots were cut below 75 kDa. The bottom part was incubated for p-eIF2 α /eIF2 α (B), caspase-7 (B), Bcl-2 (B) and β -actin (A). Multiple stained molecular weights (MW) were used for cutting accuracy. Data from blot 9 were presented in **Figure 3.4A and 3.7B**.

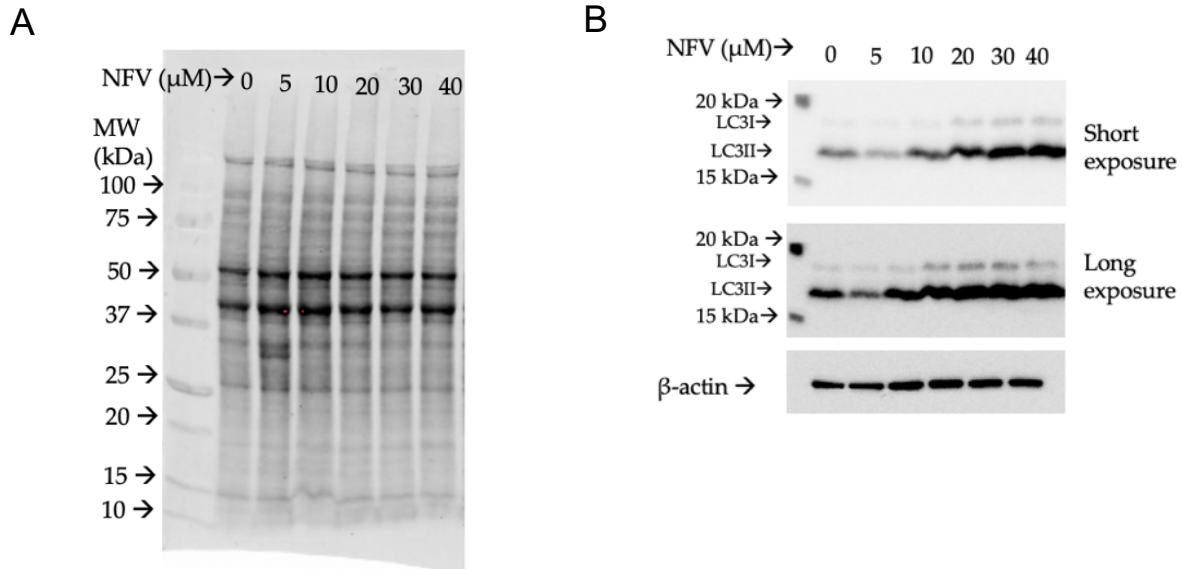


Blot 10. Proteins extracted from PEO1 cells treated with 0 or 20 μ M NFV for 72 hours, and 0 or 2 μ g/ml tunicamycin (TN) for 24 h were run for 30 min at 200V on TGX stain-free fast cast acrylamide

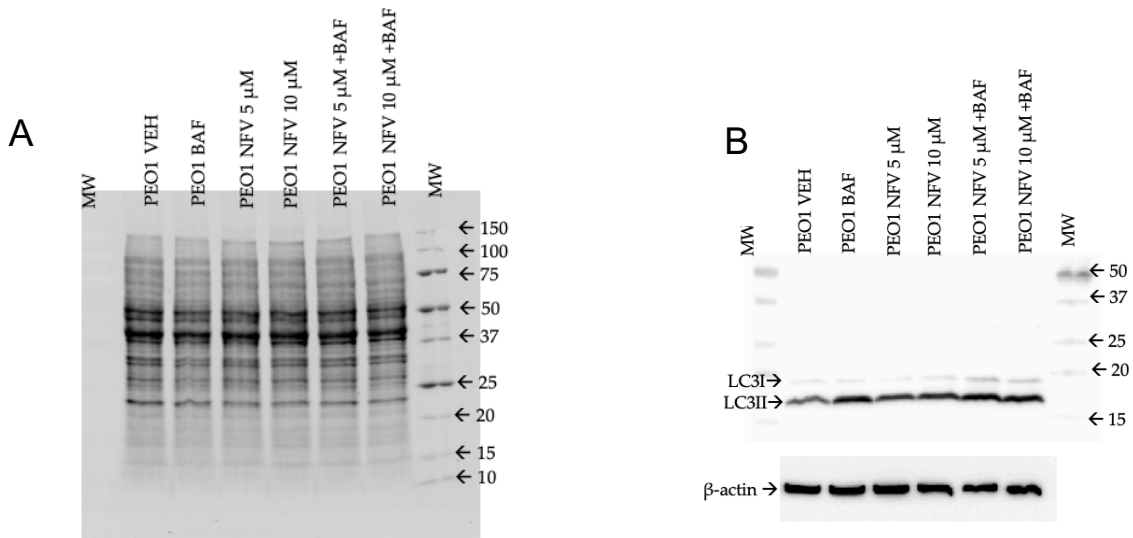
gel (12%) in two identical sets. After the run, the gel was activated by UV light. Proteins on the gel were transferred using TransBlot Turbo for 7 min. After transfer, total protein load was visualized in the unstained membrane using BioRad ChemiDoc imager (A). After 1 h of blocking with 5% non-fat dry milk, blot 11 was cut in the middle along the molecular weight ladder to yield two identical sets of blots. The left blot was again cut below the mark of 75 kDa. The top part was incubated for IRE1 α and GRP78 (B), and the bottom part was incubated for CHOP (B). The right blot was incubated for ATF6 (C). Finally, both blots were incubated for β -actin (B, C). Multiple stained molecular weights (MW) were used for cutting accuracy. Data from blot 10 were presented in **Figure 3.4B**.

A**B**

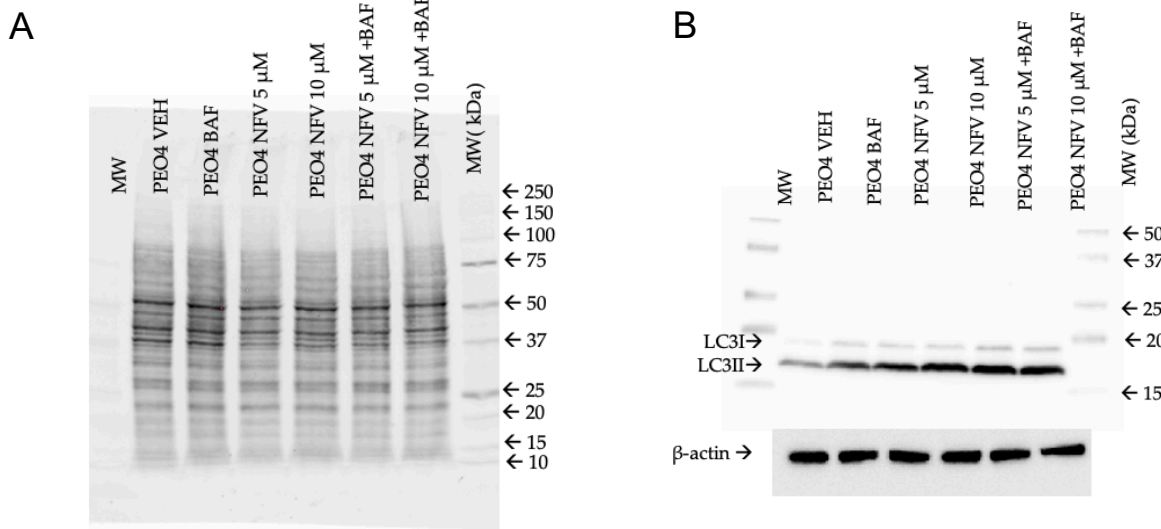
Blot 11. Proteins extracted from PEO1 cells treated with 5-40 μM NFV were run for 30 min at 200V on TGX stain-free fast cast acrylamide gel (12%). After the run, the gel was activated by UV light. Proteins on the gel were transferred using TransBlot Turbo for 7 min. After transfer, total protein load was visualized in the unstained membrane using BioRad ChemiDoc imager (A). After 1 h of blocking with 5% non-fat dry milk, blot 1 was cut below 75 kDa and below 25Kda. The area below 75 to 25 kDa was incubated for β-actin, and the area below 20 kDa was incubated for LC3 (B). Two stained molecular weights on each side were used for cutting accuracy. Data from blot 11 were presented in **Figure 3.5A**.



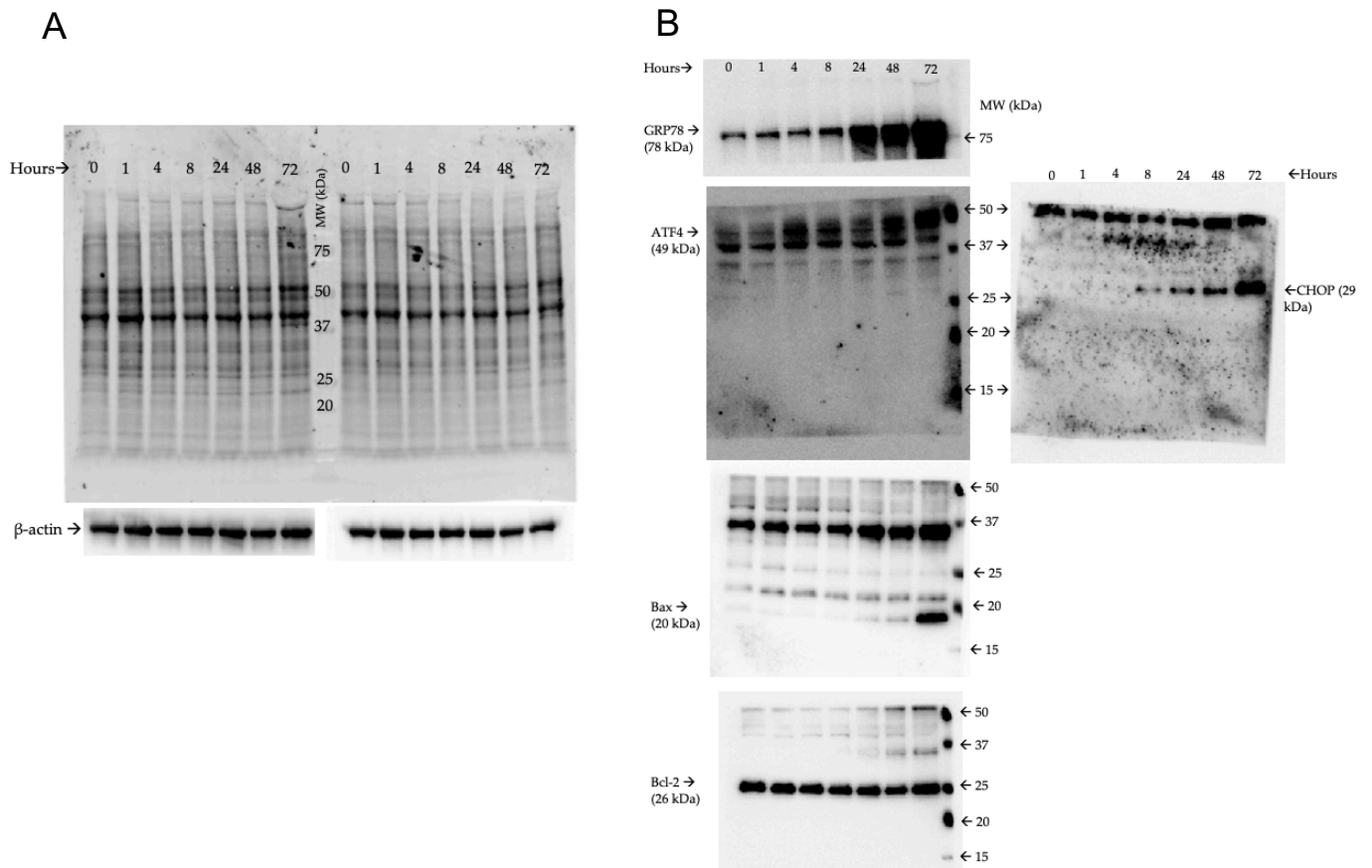
Blot 12. Proteins extracted from PEO4 cells treated with 5-40 μM NFV were run for 30 min at 200V on TGX stain-free fast cast acrylamide gel (12%). After the run, the gel was activated by UV light. Proteins on the gel were transferred using TransBlot Turbo for 7 min. After transfer, total protein load was visualized in the unstained membrane using BioRad ChemiDoc imager (A). After 1 h of blocking with 5% non-fat dry milk, blot 1 was cut below 75 kDa and below 25Kda. The area below 75 to 25 kDa was incubated for β -actin, and the area below 20 kDa was incubated for LC3 (B). Two stained molecular weights on each side were used for cutting accuracy. Data from blot 12 were presented in **Figure 3.5A**.



Blot 13. PEO1 cells were treated with 5 or 10 μ M of NFV for 72 h. One h before terminating the experiment, the cells were incubated with or without 100 nM of bafilomycin A1 (BAF). Extracted proteins from the samples were run for 30 min at 200V on TGX stain-free fast cast acrylamide gel (12%). After the run, the gel was activated by UV light. Proteins on the gel were transferred using TransBlot Turbo for 7 min. After transfer, total protein load was visualized in the unstained membrane using BioRad ChemiDoc imager (A). After 1 h blocking with 5% non-fat dry milk, blot 12 was cut above 50 kDa and the bottom art was incubated for LC3 (B). After that, the area between 50 and 37 kDa was cut and incubated for β -actin (B). Two stained molecular weights (MW) on each side were used for cutting accuracy. Data from blot 13 were presented in **Figure 3.5B**.

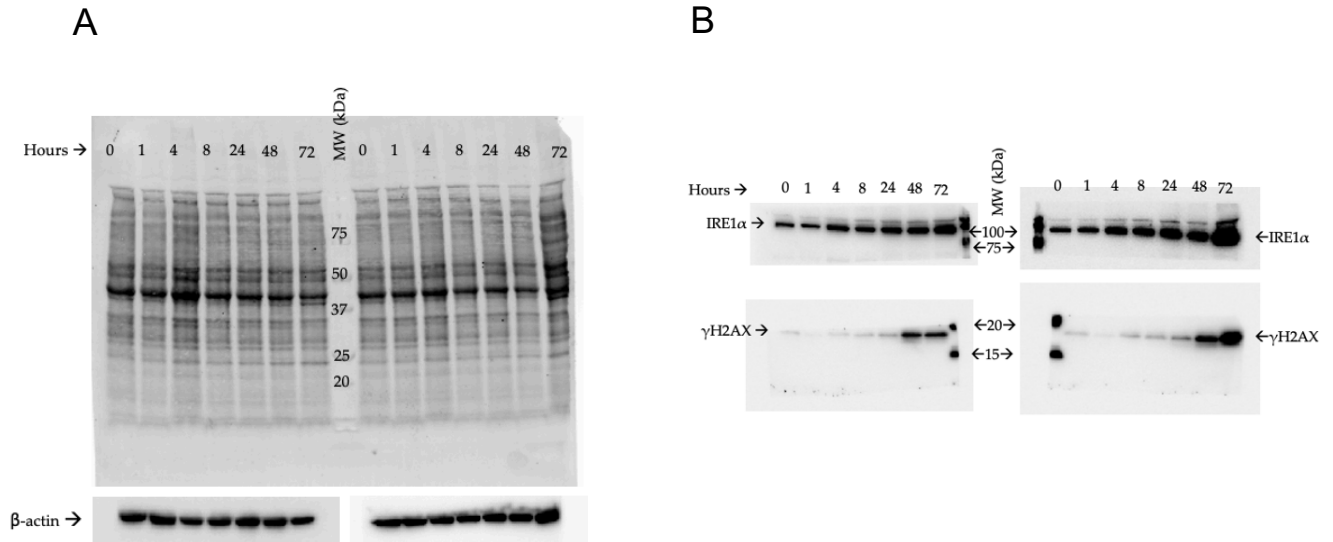


Blot 14. PEO4 cells were treated with 5 or 10 μ M of NFV for 72 h. One h before terminating the experiment, the cells were incubated with or without 100 nM of bafilomycin A1 (BAF). Extracted proteins from the samples were run for 30 min at 200V on TGX stain-free fast cast acrylamide gel (12%). After the run, the gel was activated by UV light. Proteins on the gel were transferred using TransBlot Turbo for 7 min. After transfer, total protein load was visualized in the unstained membrane using BioRad ChemiDoc imager (A). After 1 h blocking with 5% non-fat dry milk, blot 13 was cut above 50 kDa, and the bottom part was incubated for LC3 (B). After that, the area between 50 and 37 kDa was cut and incubated for β -actin (B). Two stained molecular weights (MW) on each side were used for cutting accuracy. Data from blot 14 were presented in **Figure 3.5B**.

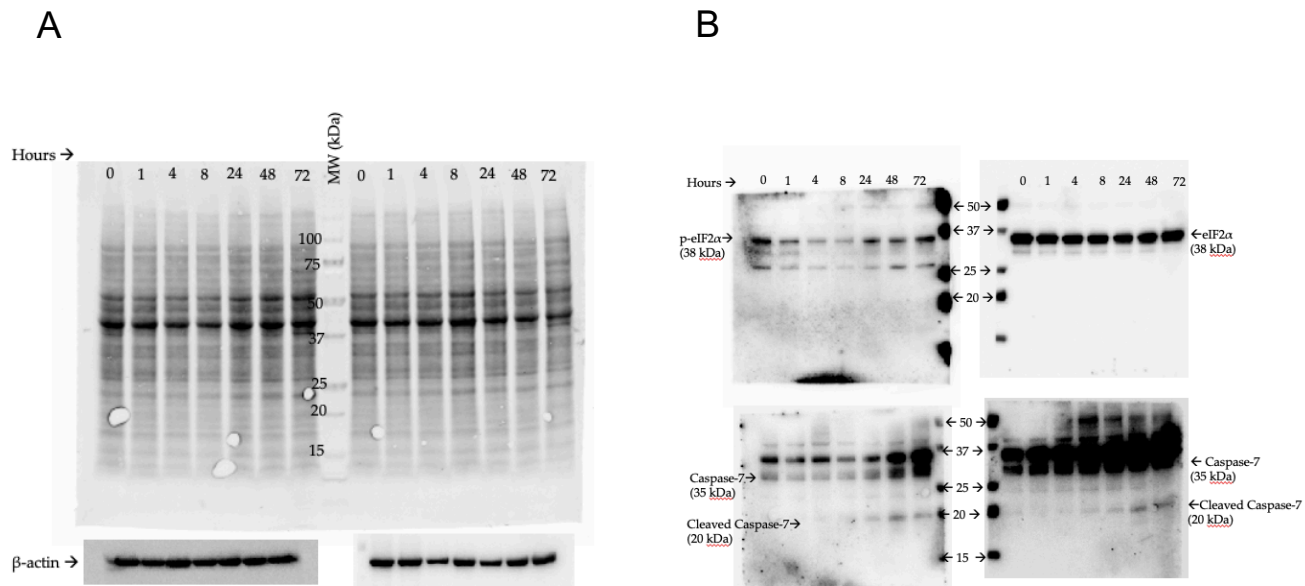


Blot 15. Two identical sets of samples (PEO1 treated with NFV 20 μ M at the demonstrated time points) were run for 30 min at 200V on TGX stain-free fast cast acrylamide gel (12%). After the run, the gel was activated by UV light. Proteins on the gel were transferred using TransBlot Turbo for 7 min. After transfer, total protein load was visualized in the unstained membrane using BioRad ChemiDoc imager (A). After 1 h of blocking with 5% non-fat dry milk, blot 14 was cut in the middle along the molecular weight ladder to yield two identical sets of blots. The blots were further cut at between 75 kDa and 50 kDa. The top left blot was incubated for GRP78 (B). The bottom two blots were incubated for ATF4 and CHOP, respectively (B). Afterwards, the left bottom blot was incubated for Bax and Bcl-2 sequentially. Finally, the blots were incubated for β -actin (A). Multiple

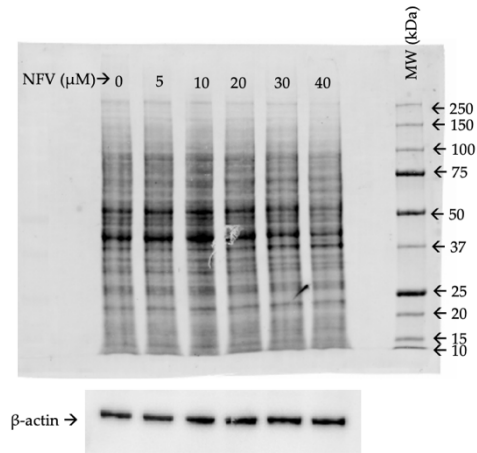
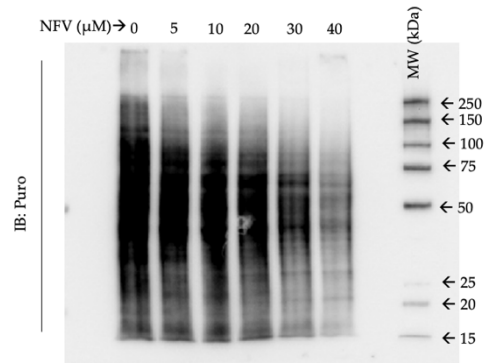
stained molecular weights (MW) were used for cutting accuracy. Data from blot 15 were presented in **Figure 3.7A**.



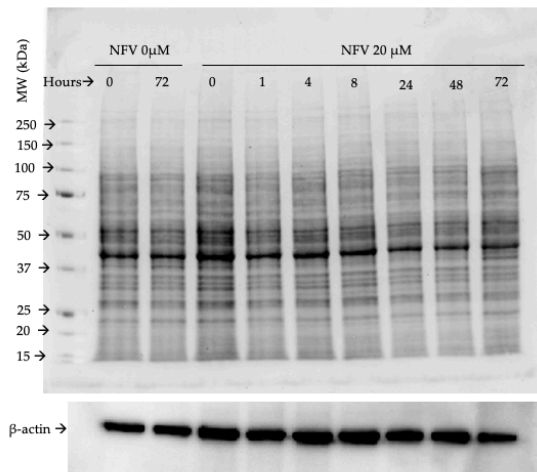
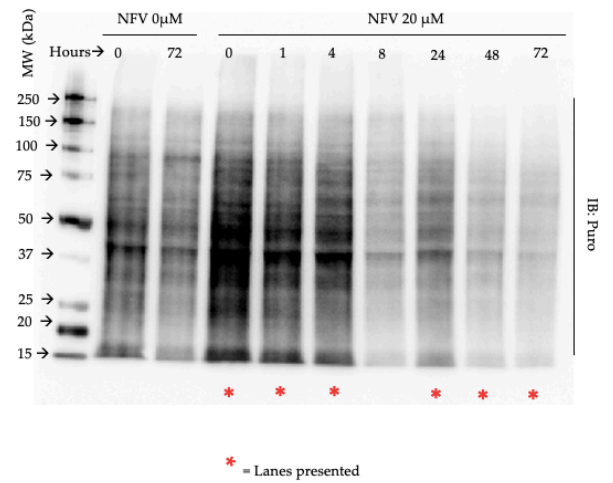
Blot 16. Two identical sets of samples (PEO1 treated with NFV 20 μ M on the demonstrated time points) were run 30 min at 200V on TGX stain-free fast cast acrylamide gel (12%). After the run, the gel was activated by UV light. Proteins on the gel were transferred using TransBlot Turbo for 7 min. After transfer, total protein load was visualized in the unstained membrane using BioRad ChemiDoc imager (A). After 1 h of blocking with 5% non-fat dry milk, blot 15 was cut in the middle along the molecular weight ladder to yield two identical sets of blots. Both blots were again cut below the mark of 75 kDa and above the mark of 20 kDa. The top blots were incubated for IRE1 α , and the bottom blots were incubated for γ H2AX. Finally, the blots were incubated for β -actin. Data from blot 16 were presented in **Figures 3.7A and 3.11D**.



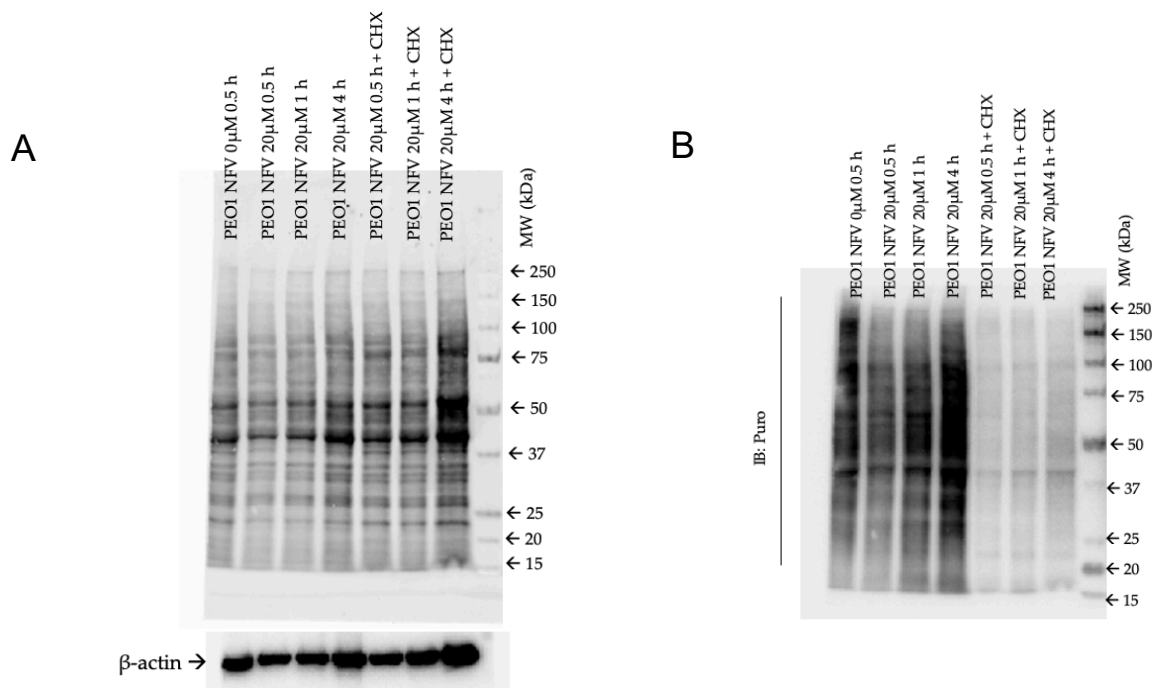
Blot 17. Two identical sets of samples (PEO1 treated with NFV 20 μ M on the demonstrated time points were run 30 min at 200V on TGX stain-free fast cast acrylamide gel (12%). After the run, the gel was activated by UV light. Proteins on the gel were transferred using TransBlot Turbo for 7 min. After transfer, total protein load was visualized in the unstained membrane using BioRad ChemiDoc imager (A). After 1 h of blocking with 5% non-fat dry milk, blot 11 was cut in the middle along the molecular weight ladder to yield two identical sets of blots. Both blots were again cut below the mark of 75 kDa. The bottom blots were incubated for p-eIF2 α (left), eIF2 α (right) and casapase-7. Finally, the blots were incubated for β -actin. Data from blot 17 were presented in **Figures 3.7A and 3.8D.**

A**B**

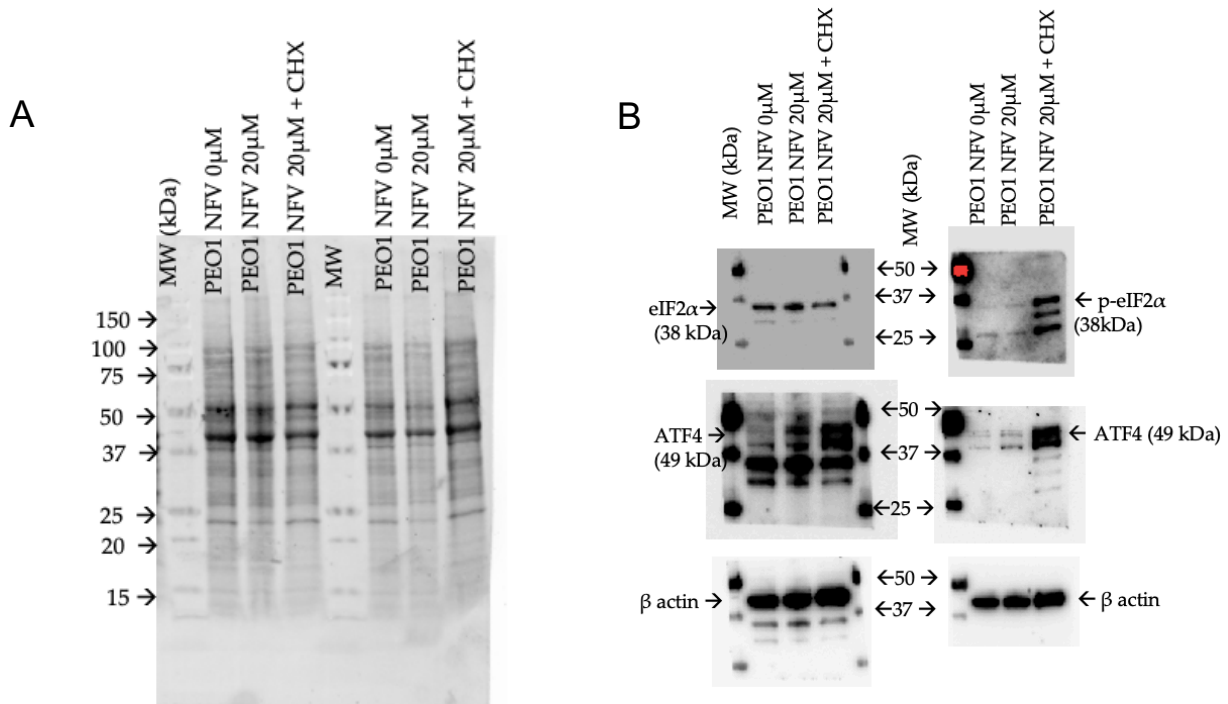
Blot 18. PEO1 cells were treated with 5-40 μM of NFV for 72 h. 30 min before terminating the experiment, the cells were incubated with puromycin at 37°C to a final concentration of 1 μM . Extracted proteins from the samples were run for 30 min at 200V on TGX stain-free fast cast acrylamide gel (10%). After the run, the gel was activated by UV light. Proteins on the gel were transferred using TransBlot Turbo for 7 min. After transfer, total protein load was visualized in the unstained membrane using BioRad ChemiDoc imager (A). After 1 h blocking with 5% non-fat dry milk, the blot was incubated with anti-puromycin antibody (B). Finally, the blot was incubated for β -actin (A). Data from blot 18 were presented in **Figure 3.8A**.

A**B**

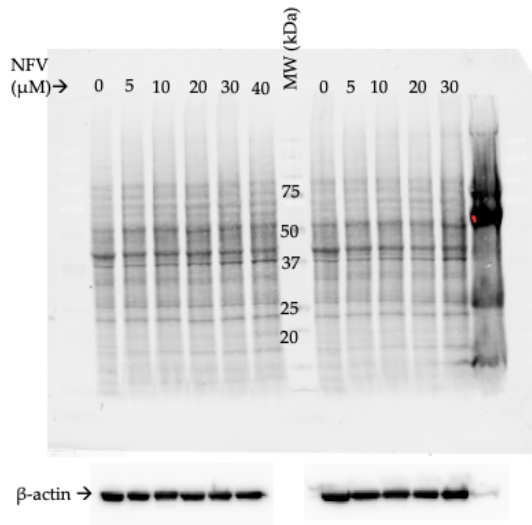
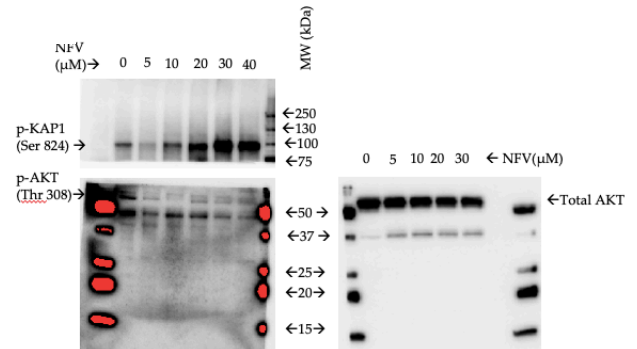
Blot 19. PEO1 cells were treated with or without 20 μM of NFV for the indicated time points in the blot (0-72 h). 30 min before terminating the experiment, the cells were incubated with puromycin at 37°C to a final concentration of 1 μM . Extracted proteins from the samples were run for 30 min at 200V on TGX stain-free fast cast acrylamide gel (10%). After the run, the gel was activated by UV light. Proteins on the gel were transferred using TransBlot Turbo for 7 min. After transfer, total protein load was visualized in the unstained membrane using BioRad ChemiDoc imager (A). After 1 h of blocking with 5% non-fat dry milk, the blot was incubated with anti-puromycin antibody (B). Finally, the blot was incubated for β -actin (A). Data from blot 19 were presented in **Figure 3.8B**.



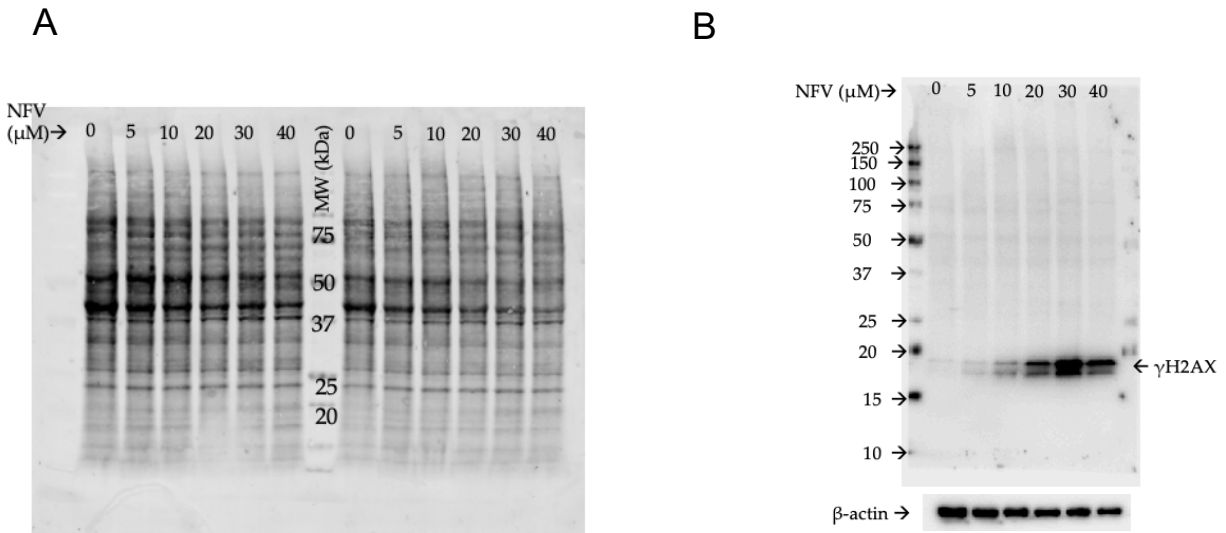
Blot 20. PEO1 cells were treated with 20 μ M NFV with or without 10 μ g/ml cycloheximide (CHX) for 0.5, 1, or 4 h. 30 min before terminating the experiment, the cells were incubated with puromycin at 37°C to a final concentration of 1 μ M. Extracted proteins from the samples were run for 30 min at 200V on TGX stain-free fast cast acrylamide gel (10%). After the run, the gel was activated by UV light. Proteins on the gel were transferred using TransBlot Turbo for 7 min. After transfer, total protein load was visualized in the unstained membrane using BioRad ChemiDoc imager (A). After 1 h of blocking with 5% non-fat dry milk, the blot was incubated with anti-puromycin antibody. Finally, the blot was incubated for β -actin (A). Data from blot 20 were presented in **Figure 3.8C**.



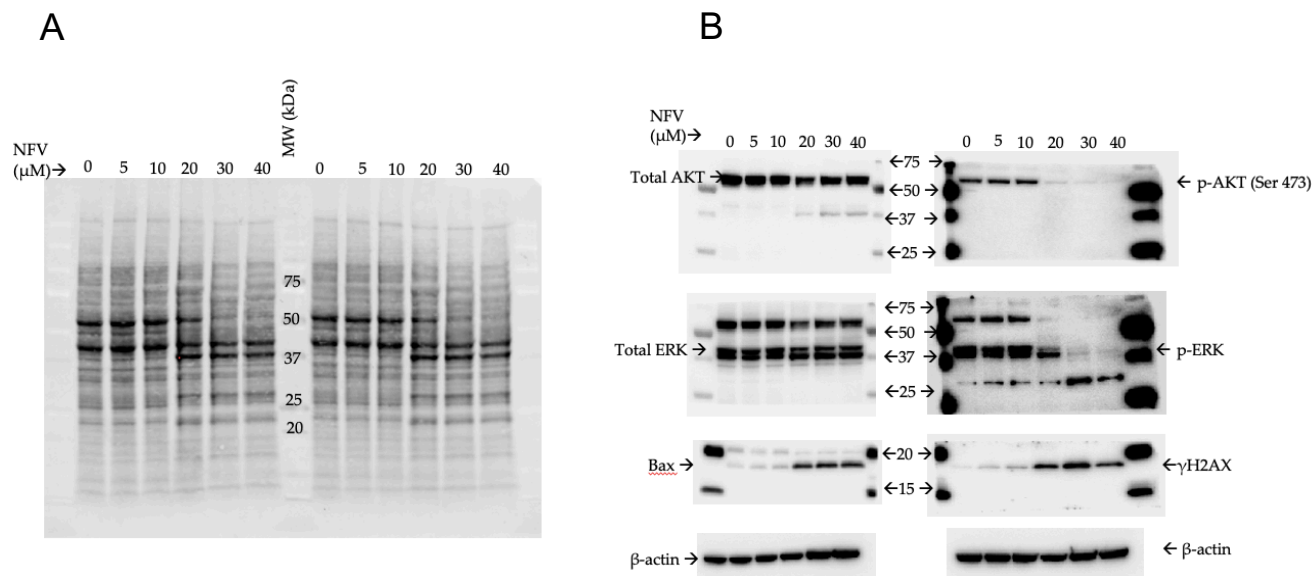
Blot 21. Two identical sets of samples (PEO1 treated with NFV 20 μ M with or without cycloheximide (10 μ g/mL) for 4 h were run 30 min at 200V on TGX stain-free fast cast acrylamide gel (12%). After the run, the gel was activated by UV light. Proteins on the gel were transferred using TransBlot Turbo for 7 min. After transfer, total protein load was visualized in the unstained membrane using BioRad ChemiDoc imager (A). After 1 h of blocking with 5% non-fat dry milk, the blot was cut in the middle along the molecular weight ladder to yield two identical sets of blots. The blots were cut above 50 kDa and below 25 kDa, and the area in between was incubated for p-eIF2 α , eIF2 α , ATF4, and β -actin (B). Data from blot 21 were presented in **Figure 3.8E**.

A**B**

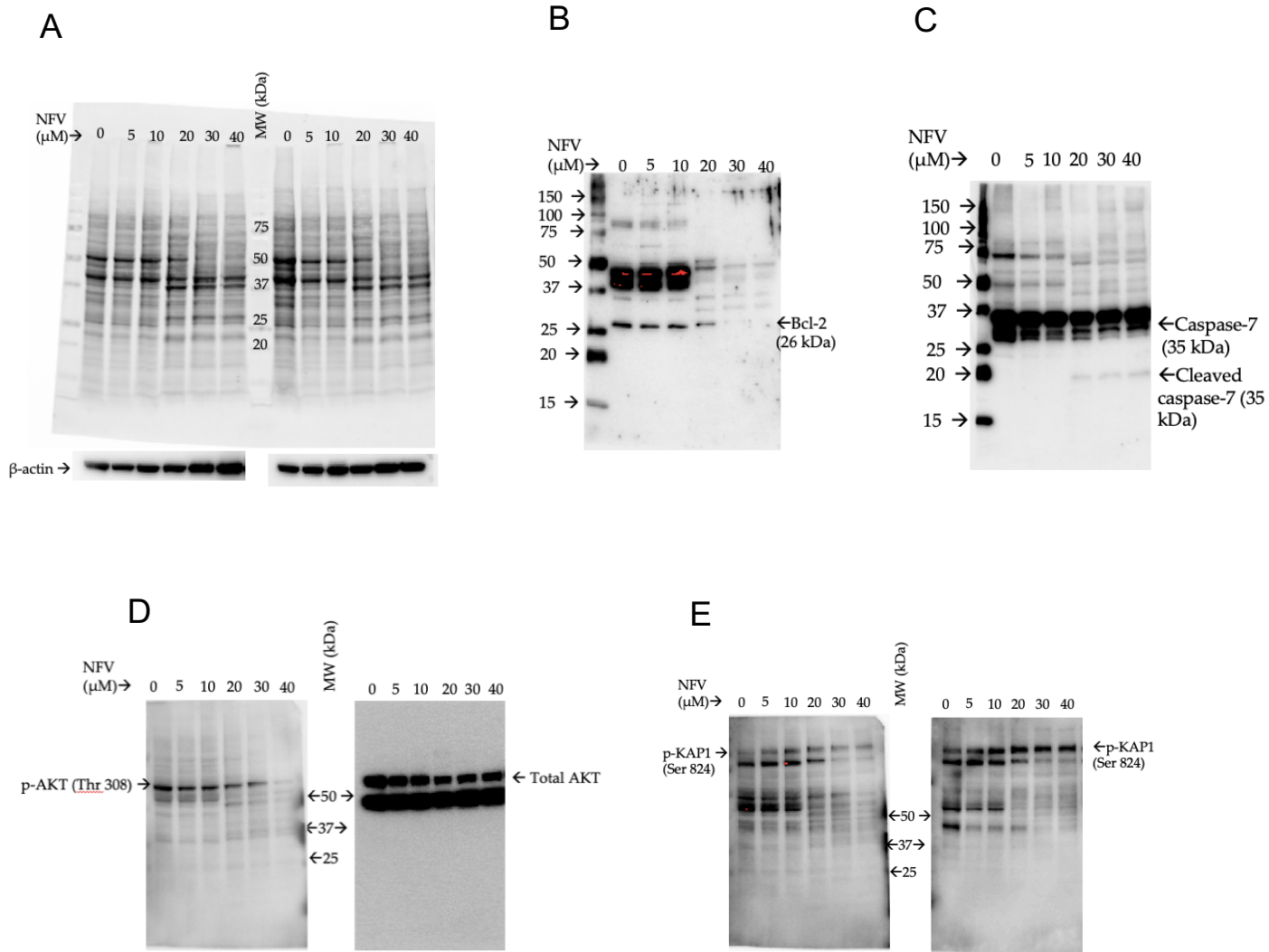
Blot 22. Proteins extracted from PEO1 cells treated with 5–40 μ M NFV were run for 30 min at 200V on TGX stain-free fast cast acrylamide gel (12%) in two identical sets. After the run, the gel was activated by UV light. Proteins on the gel were transferred using TransBlot Turbo for 7 min. After transfer, total protein load was visualized in the unstained membrane using BioRad ChemiDoc imager (A). After 1 h of blocking with 5% non-fat dry milk, the blot was cut in the middle along the molecular weight ladder to yield two identical sets of blots. The blots were cut below 75 kDa and below 25 kDa. The top left part was incubated for p-KAP1 (Ser 824), and the bottom parts were incubated for p-AKT (Thr 308)/ total AKT (B). Finally, the blots were incubated for β -actin (A). Multiple stained molecular weights (MW) were used for cutting accuracy. Data from blot 22 were presented in [391].



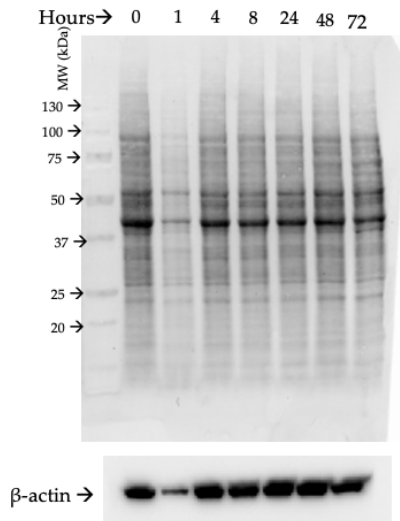
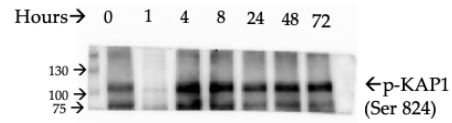
Blot 23. Proteins extracted from PEO1 cells treated with 5-40 μM NFV were run for 30 min at 200V on TGX stain-free fast cast acrylamide gel (12%). After the run, the gel was activated by UV light. Proteins on the gel were transferred using TransBlot Turbo for 7 min. After transfer, total protein load was visualized in the unstained membrane using BioRad ChemiDoc imager (A). After 1 h of blocking with 5% non-fat dry milk, the membrane was cut in the middle along the molecular weight marker to yield two identical sets of blots, and the right blot was incubated for γH2AX and β-actin sequentially (B). Data from blot 23 were presented in **Figure 3.11C**.



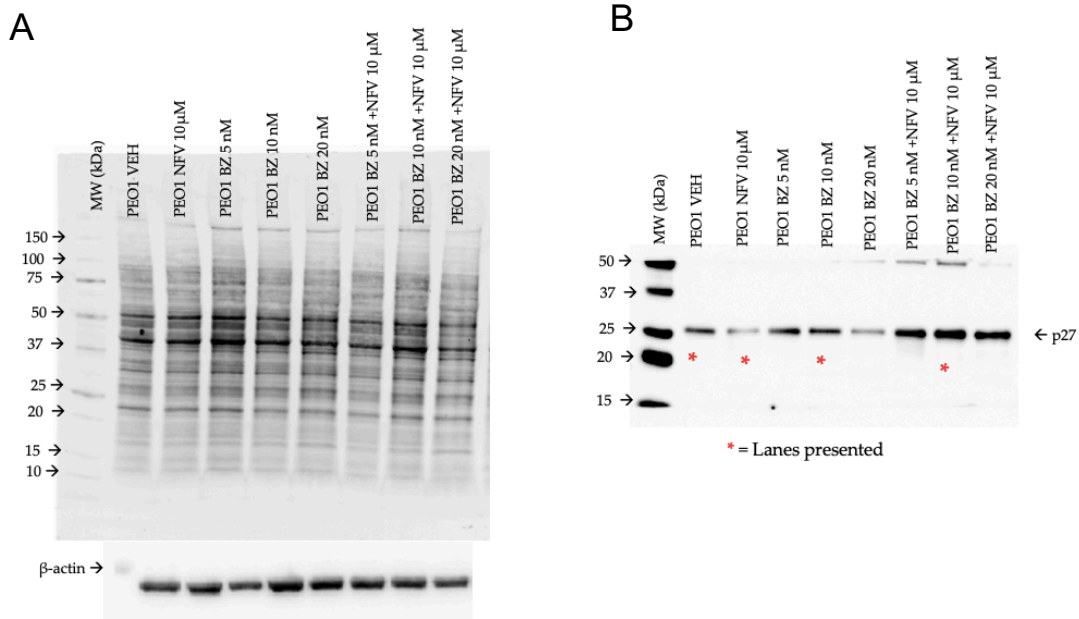
Blot 24. Proteins extracted from PEO4 cells treated with 5-40 μ M NFV were run for 30 min at 200V on TGX stain-free fast cast acrylamide gel (12%) in two identical sets. After the run, the gel was activated by UV light. Proteins on the gel were transferred using TransBlot Turbo for 7 min. After transfer, total protein load was visualized in the unstained membrane using BioRad ChemiDoc imager (A). After 1 h of blocking with 5% non-fat dry milk, the blot was cut in the middle along the molecular weight ladder to yield two identical sets of blots. The blots were cut at 75 kDa and below 25 kDa. The middle parts were incubated for p-AKT (Ser 473)/total AKT, p-ERK/total ERK and β -actin (B). The bottom left blot was incubated for Bax, and the bottom right blot was incubated for γ H2AX (B). Data from blot 24 were presented in **Figures 3.7B and 3.11A**.



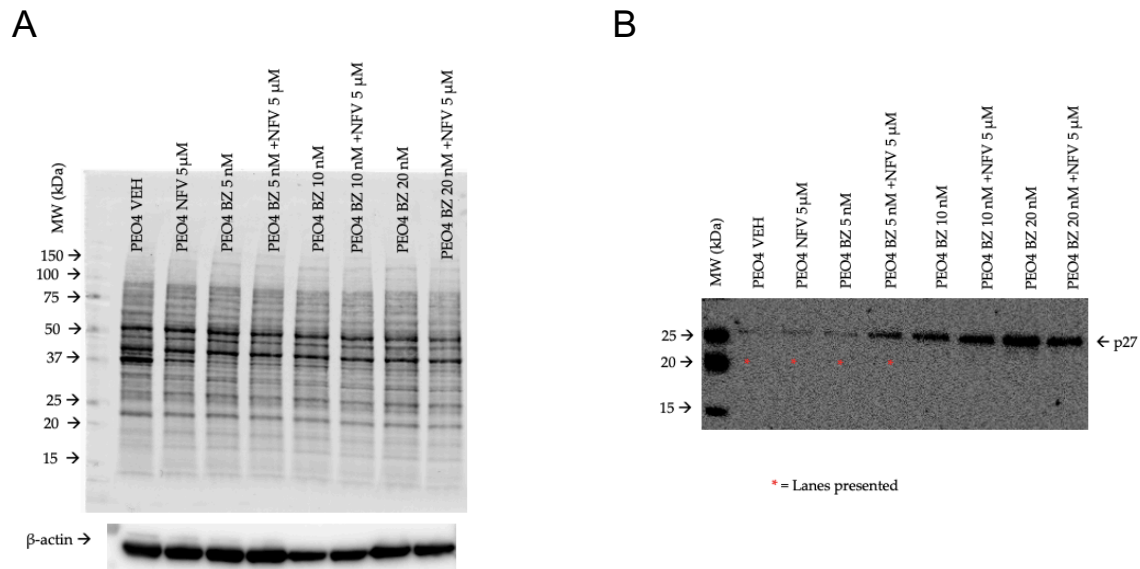
Blot 25. Proteins extracted from PEO4 cells treated with 5-40 μ M NFV were run for 30 min at 200V on TGX stain-free fast cast acrylamide gel (12%) in two identical sets. After the run, the gel was activated by UV light. Proteins on the gel were transferred using TransBlot Turbo for 7 min. After transfer, total protein load was visualized in the unstained membrane using BioRad ChemiDoc imager. After 1 h blocking with 5% non-fat dry milk, the blot was cut in the middle along the molecular weight ladder to yield two identical sets of blots. The left blot was incubated for Bcl-2 (B), p-AKT (Thr 308) (D) and p-KAP1 (Ser 824) (E), and the right blot was incubated for caspase-7 (C), Total AKT (D) and p-KAP1 (Ser 824) (E), sequentially. Finally, both blots were incubated for β -actin (A). Data from blot 25 were presented in **Figures 3.7B and 3.11A.**

A**B**

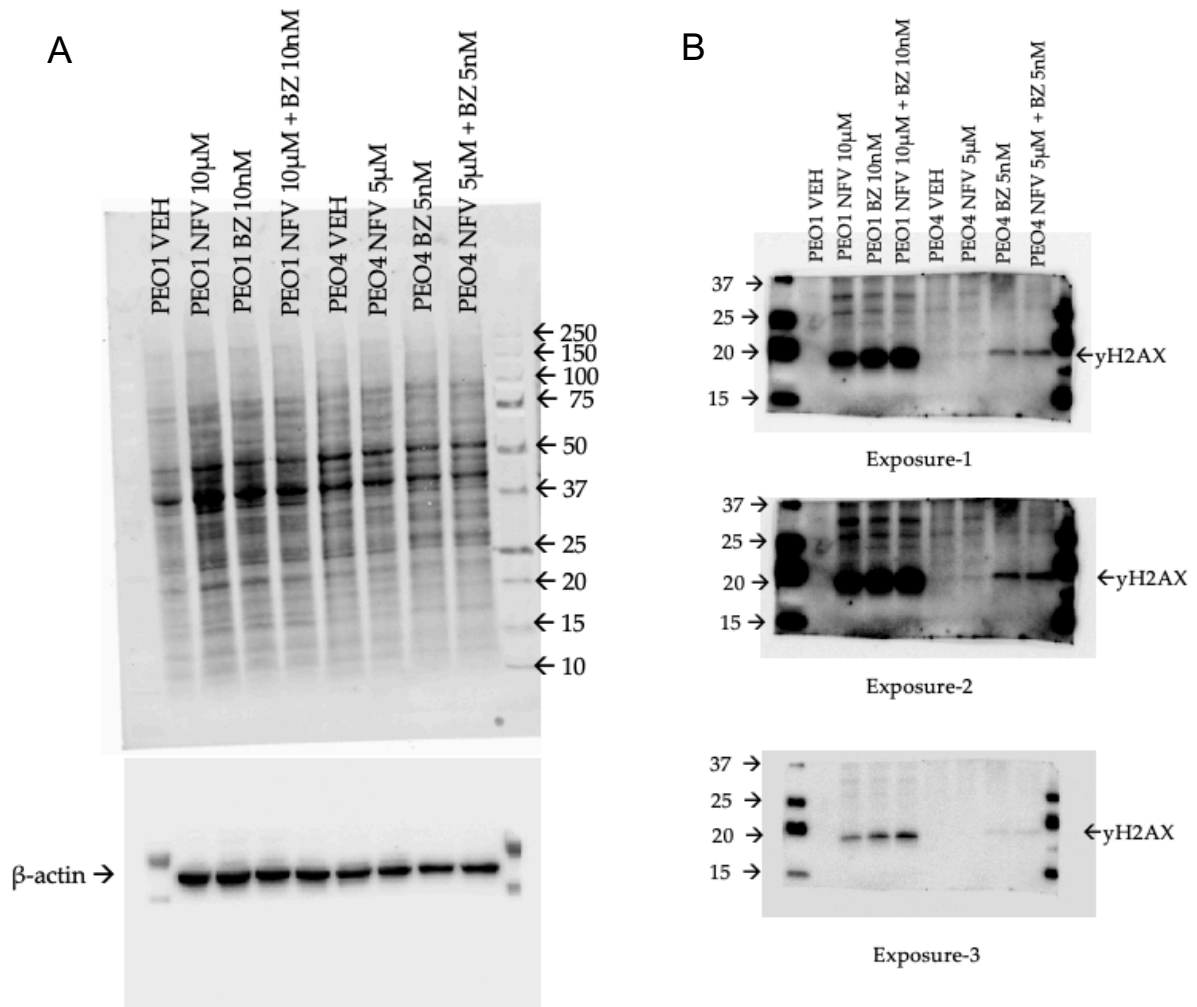
Blot 26. PEO1 treated with NFV 20 μ M at the demonstrated time points were run for 30 min at 200V on TGX stain-free fast cast acrylamide gel (12%). After the run, the gel was activated by UV light. Proteins on the gel were transferred using TransBlot Turbo for 7 min. After transfer, total protein load was visualized in the unstained membrane using BioRad ChemiDoc imager (A). The blot was cut below 75 kDa, and the top part was incubated for p-KAP1 (Ser 824) and the bottom part was incubated for β -actin. Data from blot 26 were presented in [391].



Blot 27. PEO1 cells were treated with 5, 10, or 20 nM bortezomib (BZ) with or without 10 μ M NFV for 72 h. Extracted proteins from the samples were run for 30 min at 200V on TGX stain-free fast cast acrylamide gel (12%). After the run, the gel was activated by UV light. Proteins on the gel were transferred using TransBlot Turbo for 7 min. After transfer, total protein load was visualized in the unstained membrane using BioRad ChemiDoc imager (A). After 1 h of blocking with 5% non-fat dry milk, the blot was cut below 75 kDa, and the bottom part was incubated for p27^{kip1} (B). After that, the area between 50 and 37 kDa was cut and incubated for β -actin (A). Data from blot 27 were presented in **Figure 3.15A**.

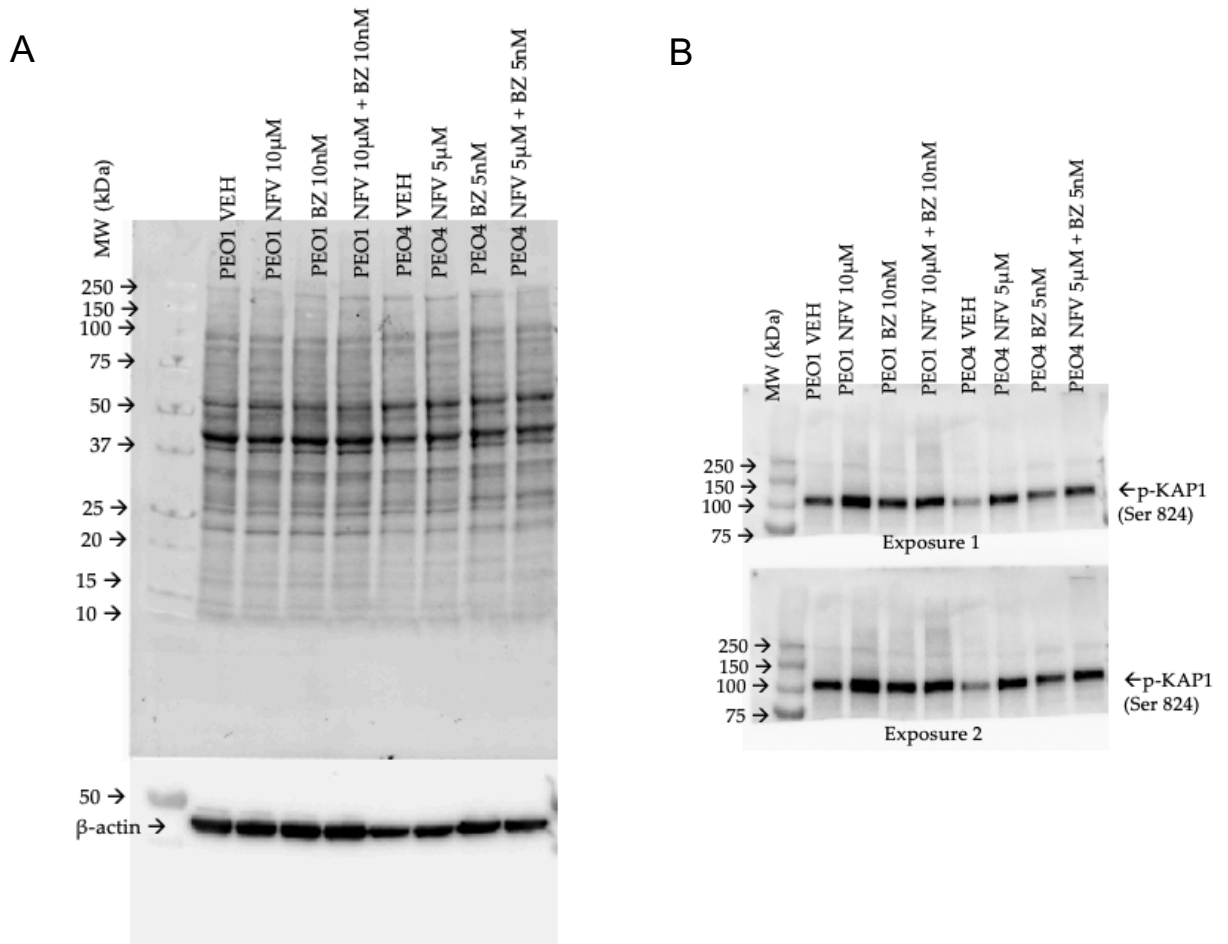


Blot 28. PEO4 cells were treated with 5, 10, or 20 nM bortezomib (BZ) with or without 5 μM NFV for 72 h. Extracted proteins from the samples were run for 30 min at 200V on TGX stain-free fast cast acrylamide gel (12%). After the run, the gel was activated by UV light. Proteins on the gel were transferred using TransBlot Turbo for 7 min. After transfer, total protein load was visualized in the unstained membrane using BioRad ChemiDoc imager (A). After 1 h blocking with 5% non-fat dry milk, the blot was cut below 75 kDa and 37 Kda. The part below 37 kDa was incubated for p27^{kip1} (B), and the part between 50 and 37 kDa was incubated for β-actin (A). Data from blot 28 were presented in **Figure 3.15A**.



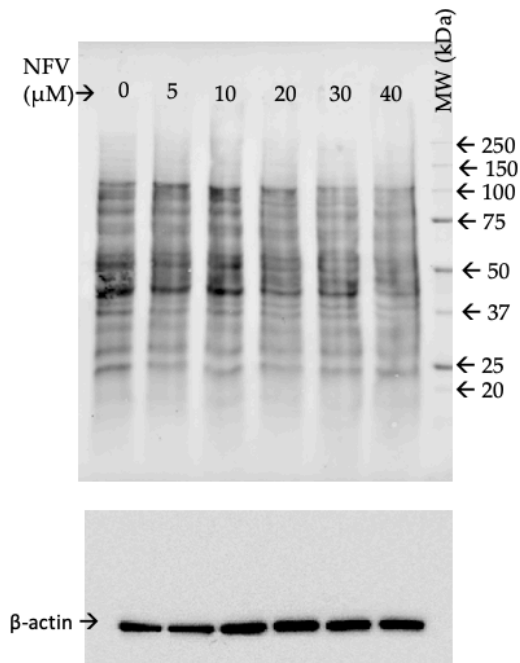
Blot 29. PEO1 cells were treated with 10 nM bortezomib (BZ) with or without 10 μ M NFV, and PEO4 cells were treated with 5 nM bortezomib (BZ) with or without 5 μ M NFV for 72 h. Extracted proteins from the samples were run for 30 min at 200V on TGX stain-free fast cast acrylamide gel

(12%). After the run, the gel was activated by UV light. Proteins on the gel were transferred using TransBlot Turbo for 7 min. After transfer, total protein load was visualized in the unstained membrane using BioRad ChemiDoc imager (A). After 1 h blocking with 5% non-fat dry milk, the blot was cut at 50 kDa and incubated for β -actin (A). Afterwards, the blot was cut at 37 kDa, and was incubated for phosphorylated H2AX (B). Multiple stained molecular weights (MW) were used for cutting accuracy. Data from blot 29 were presented in **Figure 3.15A**.

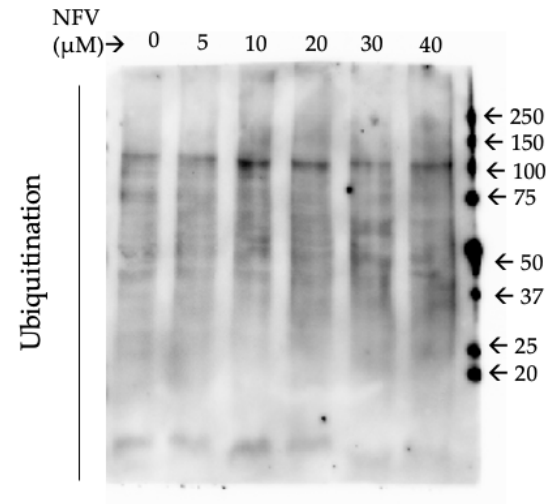


Blot 30. PEO1 cells were treated with 10 nM bortezomib (BZ) with or without 10 μ M NFV, and PEO4 cells were treated with 5 nM bortezomib (BZ) with or without 5 μ M NFV for 72 hours. Extracted proteins from the samples were run for 30 min at 200V on TGX stain-free fast cast acrylamide gel (12%). After the run, the gel was activated by UV light. Proteins on the gel were transferred using TransBlot Turbo for 7 min. After transfer, total protein load was visualized in the unstained membrane using BioRad ChemiDoc imager (A). After 1 h blocking with 5% non-fat dry milk, the blot was cut below 75 kDa, and the top part was incubated for p-KAP1 (Ser 824) (B), and the bottom part was incubated for β -actin (A). Data from blot 30 were presented in [391].

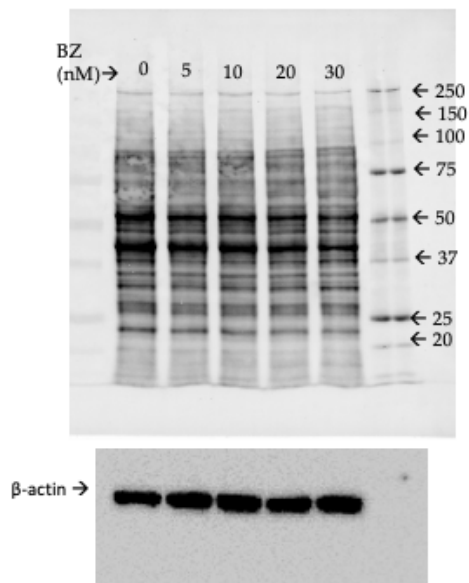
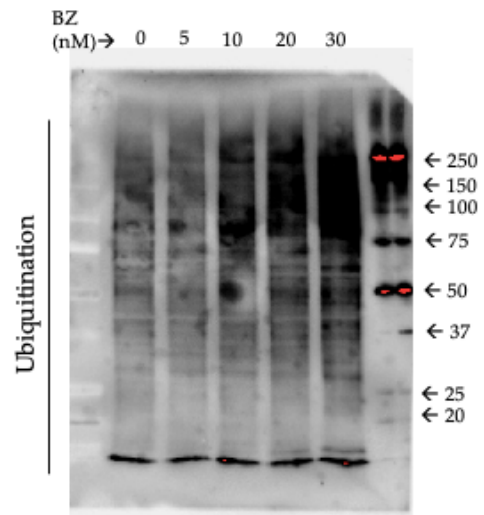
A



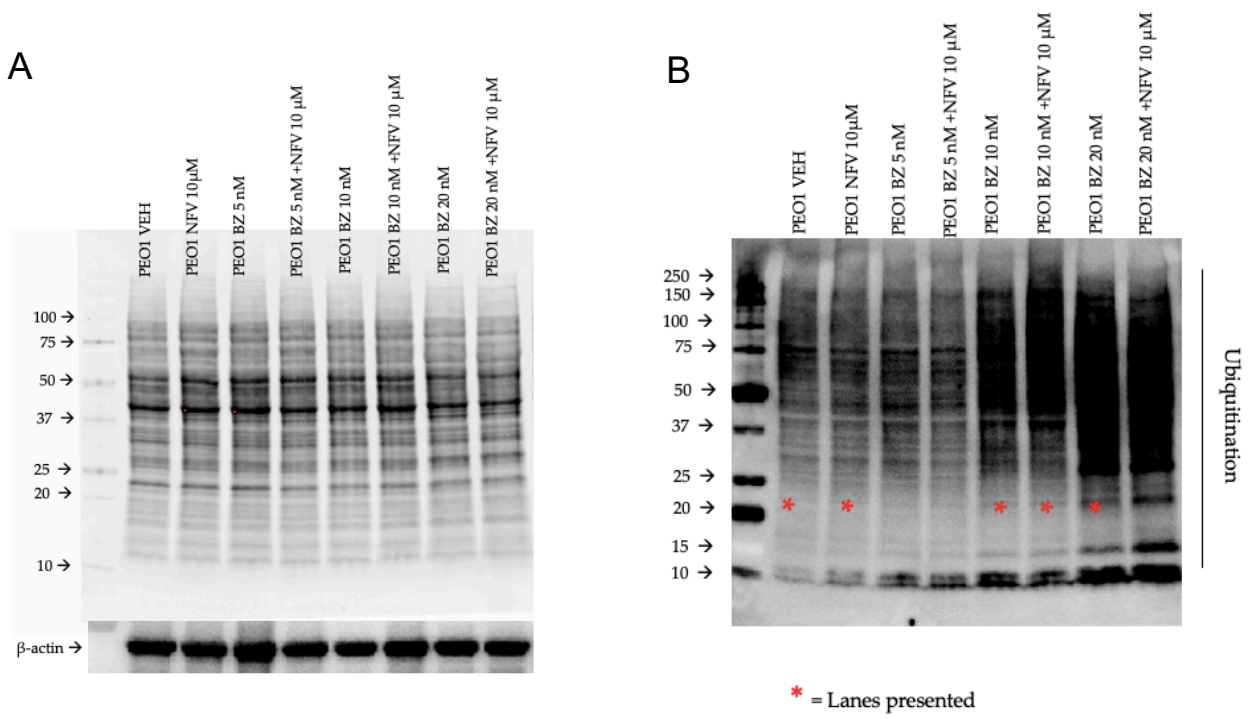
B



Blot 31. Proteins extracted from PEO1 cells treated with 5-40 μM NFV were run for 30 min at 200V on TGX stain-free fast cast acrylamide gel (10%). After the run, the gel was activated by UV light. Proteins on the gel were transferred using TransBlot Turbo for 7 min. After transfer, the total protein load was visualized in the unstained membrane using BioRad ChemiDoc imager (A). After 1 h of blocking with 5% non-fat dry milk, the blot was incubated for ubiquitin (B) and β -actin (A). Data from blot 31 were presented in **Figure 3.6**.

A**B**

Blot 32. Proteins extracted from PEO1 cells treated with 5-40 nM BZ were run for 30 minutes at 200V on TGX stain-free fast cast acrylamide gel (10%). After the run, the gel was activated by UV light. Proteins on the gel were transferred using TransBlot Turbo for 7 min. After transfer, the total protein load was visualized in the unstained membrane using BioRad ChemiDoc imager (A). After 1 h of blocking with 5% non-fat dry milk, the blot was incubated for ubiquitin (B) and β -actin (A). Data from blot 32 were presented in **Figure 3.13C**.



Blot 33. Proteins extracted from PEO1 cells treated with 5, 10, or 20 nM BZ with or without 10 µM NFV for 72 h, were run for 30 min at 200V on TGX stain-free fast cast acrylamide gel (10%). After the run, the gel was activated by UV light. Proteins on the gel were transferred using TransBlot Turbo for 7 min. After transfer, total protein load was visualized in the unstained membrane using BioRad ChemiDoc imager (A). After 1 h of blocking with 5% non-fat dry milk, the blot was incubated for ubiquitin (B) and β-actin (A). Data from blot 33 were presented in **Figure 3.15C**.

REFERENCES

1. Subeha, M.R.; Telleria, C.M. The Anti-Cancer Properties of the HIV Protease Inhibitor Nelfinavir. *Cancers (Basel)* **2020**, *12*, doi:10.3390/cancers12113437.
2. Delaney, J.R.; Patel, C.; McCabe, K.E.; Lu, D.; Davis, M.-A.; Tancioni, I.; von Schalscha, T.; Bartakova, A.; Haft, C.; Schlaepfer, D.D.; et al. A strategy to combine pathway-targeted low toxicity drugs in ovarian cancer. *Oncotarget* **2015**, *6*, 31104-31118, doi:10.18632/oncotarget.5093.
3. Liu, J.; Xu, Y.; Stoleru, D.; Salic, A. Imaging protein synthesis in cells and tissues with an alkyne analog of puromycin. *Proc Natl Acad Sci U S A* **2012**, *109*, 413-418, doi:10.1073/pnas.1111561108.
4. Schmidt, E.K.; Clavarino, G.; Ceppi, M.; Pierre, P. SUnSET, a nonradioactive method to monitor protein synthesis. *Nat Methods* **2009**, *6*, 275-277, doi:10.1038/nmeth.1314.
5. De Gassart, A.; Bujisic, B.; Zaffalon, L.; Decosterd, L.A.; Di Micco, A.; Frera, G.; Tallant, R.; Martinon, F. An inhibitor of HIV-1 protease modulates constitutive eIF2 α dephosphorylation to trigger a specific integrated stress response. *Proc Natl Acad Sci U S A* **2016**, *113*, E117-E126, doi:10.1073/pnas.1514076113.
6. Gupta, A.K.; Cerniglia, G.J.; Mick, R.; McKenna, W.G.; Muschel, R.J. HIV protease inhibitors block Akt signaling and radiosensitize tumor cells both in vitro and in vivo. *Cancer Res* **2005**, *65*, 8256-8265, doi:10.1158/0008-5472.CAN-05-1220.
7. Guan, M.; Fousek, K.; Chow, W.A. Nelfinavir inhibits regulated intramembrane proteolysis of sterol regulatory element binding protein-1 and activating transcription factor 6 in castration-resistant prostate cancer. *FEBS J* **2012**, *279*, 2399-2411, doi:10.1111/j.1742-4658.2012.08619.x.
8. Lisio, M.A.; Fu, L.; Goyeneche, A.; Gao, Z.H.; Telleria, C. High-Grade Serous Ovarian Cancer: Basic Sciences, Clinical and Therapeutic Standpoints. *Int J Mol Sci* **2019**, *20*, doi:10.3390/ijms20040952.
9. Sung, H.; Ferlay, J.; Siegel, R.L.; Laversanne, M.; Soerjomataram, I.; Jemal, A.; Bray, F. Global Cancer Statistics 2020: GLOBOCAN Estimates of Incidence and Mortality Worldwide for 36 Cancers in 185 Countries. *CA Cancer J Clin* **2021**, *71*, 209-249, doi:10.3322/caac.21660.
10. Siegel, R.L.; Miller, K.D.; Jemal, A. Cancer statistics, 2020. *CA Cancer J Clin* **2020**, *70*, 7-30, doi:10.3322/caac.21590.
11. Release notice - Canadian Cancer Statistics 2019. *Health Promot Chronic Dis Prev Can* **2019**, *39*, 255, doi:10.24095/hpcdp.39.8/9.04.
12. Cancer, S.O. Available online: <https://seer.cancer.gov/statfacts/html/ovary.html> (accessed on
13. Matulonis, U.A.; Sood, A.K.; Fallowfield, L.; Howitt, B.E.; Sehouli, J.; Karlan, B.Y. Ovarian cancer. *Nat Rev Dis Primers* **2016**, *2*, 16061, doi:10.1038/nrdp.2016.61.
14. Vaughan, S.; Coward, J.I.; Bast, R.C., Jr.; Berchuck, A.; Berek, J.S.; Brenton, J.D.; Coukos, G.; Crum, C.C.; Drapkin, R.; Etemadmoghadam, D.; et al. Rethinking ovarian cancer: recommendations for improving outcomes. *Nat Rev Cancer* **2011**, *11*, 719-725, doi:10.1038/nrc3144.
15. Berns, E.M.; Bowtell, D.D. The changing view of high-grade serous ovarian cancer. *Cancer Res* **2012**, *72*, 2701-2704, doi:10.1158/0008-5472.CAN-11-3911.

16. Kurman, R.J.; Shih Ie, M. The Dualistic Model of Ovarian Carcinogenesis: Revisited, Revised, and Expanded. *Am J Pathol* **2016**, *186*, 733-747, doi:10.1016/j.ajpath.2015.11.011.
17. Cancer Genome Atlas Research, N. Integrated genomic analyses of ovarian carcinoma. *Nature* **2011**, *474*, 609-615, doi:10.1038/nature10166.
18. Shih, I.M.; Wang, Y.; Wang, T.L. The Origin of Ovarian Cancer Species and Precancerous Landscape. *Am J Pathol* **2021**, *191*, 26-39, doi:10.1016/j.ajpath.2020.09.006.
19. Kurman, R.J. *WHO classification of tumours of female reproductive organs*; International Agency for Research on Cancer: Lyon, 2014.
20. Soslow, R.A.; Han, G.; Park, K.J.; Garg, K.; Olvera, N.; Spriggs, D.R.; Kauff, N.D.; Levine, D.A. Morphologic patterns associated with BRCA1 and BRCA2 genotype in ovarian carcinoma. *Mod Pathol* **2012**, *25*, 625-636, doi:10.1038/modpathol.2011.183.
21. Testa, U.; Petrucci, E.; Pasquini, L.; Castelli, G.; Pelosi, E. Ovarian Cancers: Genetic Abnormalities, Tumor Heterogeneity and Progression, Clonal Evolution and Cancer Stem Cells. *Medicines (Basel)* **2018**, *5*, doi:10.3390/medicines5010016.
22. Zhang, Y.; Cao, L.; Nguyen, D.; Lu, H. TP53 mutations in epithelial ovarian cancer. *Transl Cancer Res* **2016**, *5*, 650-663, doi:10.21037/tcr.2016.08.40.
23. Bowtell, D.D.; Bohm, S.; Ahmed, A.A.; Aspuria, P.J.; Bast, R.C., Jr.; Beral, V.; Berek, J.S.; Birrer, M.J.; Blagden, S.; Bookman, M.A.; et al. Rethinking ovarian cancer II: reducing mortality from high-grade serous ovarian cancer. *Nat Rev Cancer* **2015**, *15*, 668-679, doi:10.1038/nrc4019.
24. Tothill, R.W.; Tinker, A.V.; George, J.; Brown, R.; Fox, S.B.; Lade, S.; Johnson, D.S.; Trivett, M.K.; Etemadmoghadam, D.; Locandro, B.; et al. Novel molecular subtypes of serous and endometrioid ovarian cancer linked to clinical outcome. *Clin Cancer Res* **2008**, *14*, 5198-5208, doi:10.1158/1078-0432.CCR-08-0196.
25. Verhaak, R.G.; Tamayo, P.; Yang, J.Y.; Hubbard, D.; Zhang, H.; Creighton, C.J.; Fereday, S.; Lawrence, M.; Carter, S.L.; Mermel, C.H.; et al. Prognostically relevant gene signatures of high-grade serous ovarian carcinoma. *J Clin Invest* **2013**, *123*, 517-525, doi:10.1172/JCI65833.
26. Klotz, D.M.; Wimberger, P. Cells of origin of ovarian cancer: ovarian surface epithelium or fallopian tube? *Arch Gynecol Obstet* **2017**, *296*, 1055-1062, doi:10.1007/s00404-017-4529-z.
27. Fathalla, M.F. Incessant ovulation--a factor in ovarian neoplasia? *Lancet* **1971**, *2*, 163, doi:10.1016/s0140-6736(71)92335-x.
28. Ahmed, N.; Abubaker, K.; Findlay, J.; Quinn, M. Cancerous ovarian stem cells: obscure targets for therapy but relevant to chemoresistance. *J Cell Biochem* **2013**, *114*, 21-34, doi:10.1002/jcb.24317.
29. Kuhn, E.; Kurman, R.J.; Shih, I.M. Ovarian Cancer Is an Imported Disease: Fact or Fiction? *Curr Obstet Gynecol Rep* **2012**, *1*, 1-9, doi:10.1007/s13669-011-0004-1.
30. Lengyel, E. Ovarian cancer development and metastasis. *Am J Pathol* **2010**, *177*, 1053-1064, doi:10.2353/ajpath.2010.100105.
31. Dubeau, L. The cell of origin of ovarian epithelial tumors and the ovarian surface epithelium dogma: does the emperor have no clothes? *Gynecol Oncol* **1999**, *72*, 437-442, doi:10.1006/gyno.1998.5275.
32. Piek, J.M.; van Diest, P.J.; Zweemer, R.P.; Jansen, J.W.; Poort-Keesom, R.J.; Menko, F.H.; Gille, J.J.; Jongsma, A.P.; Pals, G.; Kenemans, P.; et al. Dysplastic changes in

- prophylactically removed Fallopian tubes of women predisposed to developing ovarian cancer. *J Pathol* **2001**, *195*, 451-456, doi:10.1002/path.1000.
33. Medeiros, F.; Muto, M.G.; Lee, Y.; Elvin, J.A.; Callahan, M.J.; Feltmate, C.; Garber, J.E.; Cramer, D.W.; Crum, C.P. The tubal fimbria is a preferred site for early adenocarcinoma in women with familial ovarian cancer syndrome. *Am J Surg Pathol* **2006**, *30*, 230-236, doi:10.1097/01.pas.0000180854.28831.77.
 34. Kindelberger, D.W.; Lee, Y.; Miron, A.; Hirsch, M.S.; Feltmate, C.; Medeiros, F.; Callahan, M.J.; Garner, E.O.; Gordon, R.W.; Birch, C.; et al. Intraepithelial carcinoma of the fimbria and pelvic serous carcinoma: Evidence for a causal relationship. *Am J Surg Pathol* **2007**, *31*, 161-169, doi:10.1097/01.pas.0000213335.40358.47.
 35. Karnezis, A.N.; Cho, K.R.; Gilks, C.B.; Pearce, C.L.; Huntsman, D.G. The disparate origins of ovarian cancers: pathogenesis and prevention strategies. *Nat Rev Cancer* **2017**, *17*, 65-74, doi:10.1038/nrc.2016.113.
 36. De Leo, A.; Santini, D.; Ceccarelli, C.; Santandrea, G.; Palicelli, A.; Acquaviva, G.; Chiarucci, F.; Rosini, F.; Ravegnini, G.; Pession, A.; et al. What Is New on Ovarian Carcinoma: Integrated Morphologic and Molecular Analysis Following the New 2020 World Health Organization Classification of Female Genital Tumors. *Diagnostics (Basel)* **2021**, *11*, doi:10.3390/diagnostics11040697.
 37. Mittal, N.; Srinivasan, R.; Gupta, N.; Rajwanshi, A.; Nijhawan, R.; Gautam, U.; Sood, S.; Dhaliwal, L. Secretory cell outgrowths, p53 signatures, and serous tubal intraepithelial carcinoma in the fallopian tubes of patients with sporadic pelvic serous carcinoma. *Indian J Pathol Microbiol* **2016**, *59*, 481-488, doi:10.4103/0377-4929.191789.
 38. Lee, Y.; Miron, A.; Drapkin, R.; Nucci, M.R.; Medeiros, F.; Saleemuddin, A.; Garber, J.; Birch, C.; Mou, H.; Gordon, R.W.; et al. A candidate precursor to serous carcinoma that originates in the distal fallopian tube. *J Pathol* **2007**, *211*, 26-35, doi:10.1002/path.2091.
 39. Kurman, R.J.; Shih Ie, M. The origin and pathogenesis of epithelial ovarian cancer: a proposed unifying theory. *Am J Surg Pathol* **2010**, *34*, 433-443, doi:10.1097/PAS.0b013e3181cf3d79.
 40. Zhang, S.; Dolgalev, I.; Zhang, T.; Ran, H.; Levine, D.A.; Neel, B.G. Both fallopian tube and ovarian surface epithelium are cells-of-origin for high-grade serous ovarian carcinoma. *Nat Commun* **2019**, *10*, 5367, doi:10.1038/s41467-019-13116-2.
 41. Lo Riso, P.; Villa, C.E.; Gasparoni, G.; Vingiani, A.; Luongo, R.; Manfredi, A.; Jungmann, A.; Bertolotti, A.; Borgo, F.; Garbi, A.; et al. A cell-of-origin epigenetic tracer reveals clinically distinct subtypes of high-grade serous ovarian cancer. *Genome Med* **2020**, *12*, 94, doi:10.1186/s13073-020-00786-7.
 42. Berek, J.S.; Kehoe, S.T.; Kumar, L.; Friedlander, M. Cancer of the ovary, fallopian tube, and peritoneum. *Int J Gynaecol Obstet* **2018**, *143 Suppl 2*, 59-78, doi:10.1002/ijgo.12614.
 43. Kurman, R.J.; Shih Ie, M. Pathogenesis of ovarian cancer: lessons from morphology and molecular biology and their clinical implications. *Int J Gynecol Pathol* **2008**, *27*, 151-160, doi:10.1097/PGP.0b013e318161e4f5.
 44. Torre, L.A.; Trabert, B.; DeSantis, C.E.; Miller, K.D.; Samimi, G.; Runowicz, C.D.; Gaudet, M.M.; Jemal, A.; Siegel, R.L. Ovarian cancer statistics, 2018. *CA Cancer J Clin* **2018**, *68*, 284-296, doi:10.3322/caac.21456.
 45. Narod, S. Can advanced-stage ovarian cancer be cured? *Nat Rev Clin Oncol* **2016**, *13*, 255-261, doi:10.1038/nrclinonc.2015.224.

46. Bast, R.C., Jr.; Hennessey, B.; Mills, G.B. The biology of ovarian cancer: new opportunities for translation. *Nat Rev Cancer* **2009**, *9*, 415-428, doi:10.1038/nrc2644.
47. Tan, D.S.; Agarwal, R.; Kaye, S.B. Mechanisms of transcoelomic metastasis in ovarian cancer. *Lancet Oncol* **2006**, *7*, 925-934, doi:10.1016/S1470-2045(06)70939-1.
48. Nieman, K.M.; Kenny, H.A.; Penicka, C.V.; Ladanyi, A.; Buell-Gutbrod, R.; Zillhardt, M.R.; Romero, I.L.; Carey, M.S.; Mills, G.B.; Hotamisligil, G.S.; et al. Adipocytes promote ovarian cancer metastasis and provide energy for rapid tumor growth. *Nat Med* **2011**, *17*, 1498-1503, doi:10.1038/nm.2492.
49. Zhao, H.; Li, X.; Chen, D.; Cai, J.; Fu, Y.; Kang, H.; Gao, J.; Gao, K.; Du, N. Intraperitoneal administration of cisplatin plus bevacizumab for the management of malignant ascites in ovarian epithelial cancer: results of a phase III clinical trial. *Med Oncol* **2015**, *32*, 292, doi:10.1007/s12032-014-0292-1.
50. Herr, D.; Sallmann, A.; Bekes, I.; Konrad, R.; Holzheu, I.; Kreienberg, R.; Wulff, C. VEGF induces ascites in ovarian cancer patients via increasing peritoneal permeability by downregulation of Claudin 5. *Gynecol Oncol* **2012**, *127*, 210-216, doi:10.1016/j.ygyno.2012.05.002.
51. Goyeneche, A.; Lisio, M.A.; Fu, L.; Srinivasan, R.; Valdez Capuccino, J.; Gao, Z.H.; Telleria, C. The Capacity of High-Grade Serous Ovarian Cancer Cells to Form Multicellular Structures Spontaneously along Disease Progression Correlates with Their Orthotopic Tumorigenicity in Immunosuppressed Mice. *Cancers (Basel)* **2020**, *12*, doi:10.3390/cancers12030699.
52. Tarin, D.; Price, J.E.; Kettlewell, M.G.; Souter, R.G.; Vass, A.C.; Crossley, B. Mechanisms of human tumor metastasis studied in patients with peritoneovenous shunts. *Cancer Res* **1984**, *44*, 3584-3592.
53. Judson, P.L.; Geller, M.A.; Bliss, R.L.; Boente, M.P.; Downs, L.S., Jr.; Argenta, P.A.; Carson, L.F. Preoperative detection of peripherally circulating cancer cells and its prognostic significance in ovarian cancer. *Gynecol Oncol* **2003**, *91*, 389-394, doi:10.1016/j.ygyno.2003.08.004.
54. Coffman, L.G.; Burgos-Ojeda, D.; Wu, R.; Cho, K.; Bai, S.; Buckanovich, R.J. New models of hematogenous ovarian cancer metastasis demonstrate preferential spread to the ovary and a requirement for the ovary for abdominal dissemination. *Transl Res* **2016**, *175*, 92-102 e102, doi:10.1016/j.trsl.2016.03.016.
55. Menon, U.; Ryan, A.; Kalsi, J.; Gentry-Maharaj, A.; Dawney, A.; Habib, M.; Apostolidou, S.; Singh, N.; Benjamin, E.; Burnell, M.; et al. Risk Algorithm Using Serial Biomarker Measurements Doubles the Number of Screen-Detected Cancers Compared With a Single-Threshold Rule in the United Kingdom Collaborative Trial of Ovarian Cancer Screening. *J Clin Oncol* **2015**, *33*, 2062-2071, doi:10.1200/JCO.2014.59.4945.
56. Bailey, K.; Ryan, A.; Apostolidou, S.; Fourkala, E.; Burnell, M.; Gentry-Maharaj, A.; Kalsi, J.; Parmar, M.; Jacobs, I.; Pikhart, H.; et al. Socioeconomic indicators of health inequalities and female mortality: a nested cohort study within the United Kingdom Collaborative Trial of Ovarian Cancer Screening (UKCTOCS). *BMC Public Health* **2015**, *15*, 253, doi:10.1186/s12889-015-1609-5.
57. Walker, J.L.; Powell, C.B.; Chen, L.M.; Carter, J.; Bae Jump, V.L.; Parker, L.P.; Borowsky, M.E.; Gibb, R.K. Society of Gynecologic Oncology recommendations for the prevention of ovarian cancer. *Cancer* **2015**, *121*, 2108-2120, doi:10.1002/cncr.29321.

58. Yang, G.C.; Wan, L.S. Endometrial biopsy using the Tao Brush method. A study of 50 women in a general gynecologic practice. *J Reprod Med* **2000**, *45*, 109-114.
59. Wang, Y.; Li, L.; Douville, C.; Cohen, J.D.; Yen, T.T.; Kinde, I.; Sundfelt, K.; Kjaer, S.K.; Hruban, R.H.; Shih, I.M.; et al. Evaluation of liquid from the Papanicolaou test and other liquid biopsies for the detection of endometrial and ovarian cancers. *Sci Transl Med* **2018**, *10*, doi:10.1126/scitranslmed.aap8793.
60. Lheureux, S.; Braunstein, M.; Oza, A.M. Epithelial ovarian cancer: Evolution of management in the era of precision medicine. *CA Cancer J Clin* **2019**, *69*, 280-304, doi:10.3322/caac.21559.
61. Harter, P.; Hauke, J.; Heitz, F.; Reuss, A.; Kommoss, S.; Marme, F.; Heimbach, A.; Prieske, K.; Richters, L.; Burges, A.; et al. Prevalence of deleterious germline variants in risk genes including BRCA1/2 in consecutive ovarian cancer patients (AGO-TR-1). *PLoS One* **2017**, *12*, e0186043, doi:10.1371/journal.pone.0186043.
62. du Bois, A.; Reuss, A.; Pujade-Lauraine, E.; Harter, P.; Ray-Coquard, I.; Pfisterer, J. Role of surgical outcome as prognostic factor in advanced epithelial ovarian cancer: a combined exploratory analysis of 3 prospectively randomized phase 3 multicenter trials: by the Arbeitsgemeinschaft Gynaekologische Onkologie Studiengruppe Ovarialkarzinom (AGO-OVAR) and the Groupe d'Investigateurs Nationaux Pour les Etudes des Cancers de l'Ovaire (GINECO). *Cancer* **2009**, *115*, 1234-1244, doi:10.1002/cncr.24149.
63. Chang, S.J.; Bristow, R.E.; Ryu, H.S. Impact of complete cytoreduction leaving no gross residual disease associated with radical cytoreductive surgical procedures on survival in advanced ovarian cancer. *Ann Surg Oncol* **2012**, *19*, 4059-4067, doi:10.1245/s10434-012-2446-8.
64. Chang, S.J.; Hodeib, M.; Chang, J.; Bristow, R.E. Survival impact of complete cytoreduction to no gross residual disease for advanced-stage ovarian cancer: a meta-analysis. *Gynecol Oncol* **2013**, *130*, 493-498, doi:10.1016/j.ygyno.2013.05.040.
65. Horowitz, N.S.; Miller, A.; Rungruang, B.; Richard, S.D.; Rodriguez, N.; Bookman, M.A.; Hamilton, C.A.; Krivak, T.C.; Maxwell, G.L. Does aggressive surgery improve outcomes? Interaction between preoperative disease burden and complex surgery in patients with advanced-stage ovarian cancer: an analysis of GOG 182. *J Clin Oncol* **2015**, *33*, 937-943, doi:10.1200/JCO.2014.56.3106.
66. Kehoe, S.; Hook, J.; Nankivell, M.; Jayson, G.C.; Kitchener, H.; Lopes, T.; Luesley, D.; Perren, T.; Bannoo, S.; Mascarenhas, M.; et al. Primary chemotherapy versus primary surgery for newly diagnosed advanced ovarian cancer (CHORUS): an open-label, randomised, controlled, non-inferiority trial. *Lancet* **2015**, *386*, 249-257, doi:10.1016/S0140-6736(14)62223-6.
67. Vergote, I.; Amant, F.; Leunen, K. Neoadjuvant chemotherapy in advanced ovarian cancer: what kind of evidence is needed to convince US gynaecological oncologists? *Gynecol Oncol* **2010**, *119*, 1-2, doi:10.1016/j.ygyno.2010.08.011.
68. Du Bois, A.; Vergote, I.; Ferron, G.; Reuss, A.; Meier, W.; Greggi, S.; Jensen, P.T.; Selle, F.; Guyon, F.; Pomel, C.; et al. Randomized controlled phase III study evaluating the impact of secondary cytoreductive surgery in recurrent ovarian cancer: AGO DESKTOP III/ENGOT ov20. *Journal of Clinical Oncology* **2017**, *35*, 5501-5501, doi:10.1200/JCO.2017.35.15_suppl.5501.
69. Coleman, R.L.; Enserro, D.; Spirtos, N.; Herzog, T.J.; Sabbatini, P.; Armstrong, D.K.; Kim, B.; Fujiwara, K.; Walker, J.L.; Flynn, P.J.; et al. A phase III randomized controlled

- trial of secondary surgical cytoreduction (SSC) followed by platinum-based combination chemotherapy (PBC), with or without bevacizumab (B) in platinum-sensitive, recurrent ovarian cancer (PSOC): A NRG Oncology/Gynecologic Oncology Group (GOG) study. *Journal of Clinical Oncology* **2018**, *36*, 5501-5501, doi:10.1200/JCO.2018.36.15_suppl.5501.
70. Gomez-Hidalgo, N.R.; Martínez-Cannon, B.A.; Nick, A.M.; Lu, K.H.; Sood, A.K.; Coleman, R.L.; Ramirez, P.T. Predictors of optimal cytoreduction in patients with newly diagnosed advanced-stage epithelial ovarian cancer: Time to incorporate laparoscopic assessment into the standard of care. *Gynecol Oncol* **2015**, *137*, 553-558, doi:10.1016/j.ygyno.2015.03.049.
 71. Fleming, N.D.; Nick, A.M.; Coleman, R.L.; Westin, S.N.; Ramirez, P.T.; Soliman, P.T.; Fellman, B.; Meyer, L.A.; Schmeler, K.M.; Lu, K.H.; et al. Laparoscopic Surgical Algorithm to Triage the Timing of Tumor Reductive Surgery in Advanced Ovarian Cancer. *Obstet Gynecol* **2018**, *132*, 545-554, doi:10.1097/AOG.0000000000002796.
 72. Nicoletto, M.O.; Tumolo, S.; Talamini, R.; Salvagno, L.; Franceschi, S.; Visona, E.; Marin, G.; Angelini, F.; Brigato, G.; Scarabelli, C.; et al. Surgical second look in ovarian cancer: a randomized study in patients with laparoscopic complete remission--a Northeastern Oncology Cooperative Group-Ovarian Cancer Cooperative Group Study. *J Clin Oncol* **1997**, *15*, 994-999, doi:10.1200/JCO.1997.15.3.994.
 73. Markman, M. Antineoplastic agents in the management of ovarian cancer: current status and emerging therapeutic strategies. *Trends Pharmacol Sci* **2008**, *29*, 515-519, doi:10.1016/j.tips.2008.07.007.
 74. Markman, M. Optimizing primary chemotherapy in ovarian cancer. *Hematol Oncol Clin North Am* **2003**, *17*, 957-968, viii, doi:10.1016/s0889-8588(03)00058-3.
 75. Kelland, L. The resurgence of platinum-based cancer chemotherapy. *Nat Rev Cancer* **2007**, *7*, 573-584, doi:10.1038/nrc2167.
 76. Rosenberg, B.; Vancamp, L.; Krigas, T. Inhibition of Cell Division in Escherichia Coli by Electrolysis Products from a Platinum Electrode. *Nature* **1965**, *205*, 698-699, doi:10.1038/205698a0.
 77. Rosenberg, B.; VanCamp, L.; Trosko, J.E.; Mansour, V.H. Platinum compounds: a new class of potent antitumour agents. *Nature* **1969**, *222*, 385-386, doi:10.1038/222385a0.
 78. Wiltshaw, E.; Kroner, T. Phase II study of cis-dichlorodiammineplatinum(II) (NSC-119875) in advanced adenocarcinoma of the ovary. *Cancer Treat Rep* **1976**, *60*, 55-60.
 79. Neijt, J.P.; ten Bokkel Huinink, W.W.; van der Burg, M.E.; van Oosterom, A.T.; Vriesendorp, R.; Kooyman, C.D.; van Lindert, A.C.; Hamerlynck, J.V.; van Lent, M.; van Houwelingen, J.C.; et al. Randomised trial comparing two combination chemotherapy regimens (Hexa-CAF vs CHAP-5) in advanced ovarian carcinoma. *Lancet* **1984**, *2*, 594-600, doi:10.1016/s0140-6736(84)90594-4.
 80. Williams, C.J.; Mead, G.M.; Macbeth, F.R.; Thompson, J.; Whitehouse, J.M.; MacDonald, H.; Harvey, V.J.; Slevin, M.L.; Lister, T.A.; Shepherd, J.H.; et al. Cisplatin combination chemotherapy versus chlorambucil in advanced ovarian carcinoma: mature results of a randomized trial. *J Clin Oncol* **1985**, *3*, 1455-1462, doi:10.1200/JCO.1985.3.11.1455.
 81. Omura, G.; Blessing, J.A.; Ehrlich, C.E.; Miller, A.; Yordan, E.; Creasman, W.T.; Homesley, H.D. A randomized trial of cyclophosphamide and doxorubicin with or without cisplatin in advanced ovarian carcinoma. A Gynecologic Oncology Group Study. *Cancer*

- 1986**, 57, 1725-1730, doi:10.1002/1097-0142(19860501)57:9<1725::aid-cncr2820570903>3.0.co;2-j.
82. Omura, G.A.; Bundy, B.N.; Berek, J.S.; Curry, S.; Delgado, G.; Mortel, R. Randomized trial of cyclophosphamide plus cisplatin with or without doxorubicin in ovarian carcinoma: a Gynecologic Oncology Group Study. *J Clin Oncol* **1989**, 7, 457-465, doi:10.1200/JCO.1989.7.4.457.
 83. Bukowska, B.; Gajek, A.; Marczak, A. Two drugs are better than one. A short history of combined therapy of ovarian cancer. *Contemp Oncol (Pozn)* **2015**, 19, 350-353, doi:10.5114/wo.2014.43975.
 84. Jordan, M.A.; Toso, R.J.; Thrower, D.; Wilson, L. Mechanism of mitotic block and inhibition of cell proliferation by taxol at low concentrations. *Proc Natl Acad Sci U S A* **1993**, 90, 9552-9556, doi:10.1073/pnas.90.20.9552.
 85. De Brabander, M.; Geuens, G.; Nuydens, R.; Willebrords, R.; De Mey, J. Taxol induces the assembly of free microtubules in living cells and blocks the organizing capacity of the centrosomes and kinetochores. *Proc Natl Acad Sci U S A* **1981**, 78, 5608-5612, doi:10.1073/pnas.78.9.5608.
 86. Weaver, B.A. How Taxol/paclitaxel kills cancer cells. *Mol Biol Cell* **2014**, 25, 2677-2681, doi:10.1091/mbc.E14-04-0916.
 87. Einzig, A.I.; Wiernik, P.H.; Sasloff, J.; Runowicz, C.D.; Goldberg, G.L. Phase II study and long-term follow-up of patients treated with taxol for advanced ovarian adenocarcinoma. *J Clin Oncol* **1992**, 10, 1748-1753, doi:10.1200/JCO.1992.10.11.1748.
 88. McGuire, W.P.; Hoskins, W.J.; Brady, M.F.; Kucera, P.R.; Partridge, E.E.; Look, K.Y.; Clarke-Pearson, D.L.; Davidson, M. Cyclophosphamide and cisplatin compared with paclitaxel and cisplatin in patients with stage III and stage IV ovarian cancer. *N Engl J Med* **1996**, 334, 1-6, doi:10.1056/NEJM199601043340101.
 89. Calvert, A.H.; Newell, D.R.; Gumbrell, L.A.; O'Reilly, S.; Burnell, M.; Boxall, F.E.; Siddik, Z.H.; Judson, I.R.; Gore, M.E.; Wiltshaw, E. Carboplatin dosage: prospective evaluation of a simple formula based on renal function. *J Clin Oncol* **1989**, 7, 1748-1756, doi:10.1200/JCO.1989.7.11.1748.
 90. Neijt, J.P.; Engelholm, S.A.; Tuxen, M.K.; Sorensen, P.G.; Hansen, M.; Sessa, C.; de Swart, C.A.; Hirsch, F.R.; Lund, B.; van Houwelingen, H.C. Exploratory phase III study of paclitaxel and cisplatin versus paclitaxel and carboplatin in advanced ovarian cancer. *J Clin Oncol* **2000**, 18, 3084-3092, doi:10.1200/JCO.2000.18.17.3084.
 91. Ozols, R.F.; Bundy, B.N.; Greer, B.E.; Fowler, J.M.; Clarke-Pearson, D.; Burger, R.A.; Mannel, R.S.; DeGeest, K.; Hartenbach, E.M.; Baergen, R.; et al. Phase III trial of carboplatin and paclitaxel compared with cisplatin and paclitaxel in patients with optimally resected stage III ovarian cancer: a Gynecologic Oncology Group study. *J Clin Oncol* **2003**, 21, 3194-3200, doi:10.1200/JCO.2003.02.153.
 92. Bookman, M.A.; Greer, B.E.; Ozols, R.F. Optimal therapy of advanced ovarian cancer: carboplatin and paclitaxel versus cisplatin and paclitaxel (GOG158) and an update on GOG0182-ICON5. *Int J Gynecol Cancer* **2003**, 13 Suppl 2, 149-155, doi:10.1111/j.1525-1438.2003.13362.x.
 93. du Bois, A.; Luck, H.J.; Meier, W.; Adams, H.P.; Mobus, V.; Costa, S.; Bauknecht, T.; Richter, B.; Warm, M.; Schroder, W.; et al. A randomized clinical trial of cisplatin/paclitaxel versus carboplatin/paclitaxel as first-line treatment of ovarian cancer. *J Natl Cancer Inst* **2003**, 95, 1320-1329, doi:10.1093/jnci/djg036.

94. Armstrong, D.K.; Alvarez, R.D.; Bakkum-Gamez, J.N.; Barroilhet, L.; Behbakht, K.; Berchuck, A.; Chen, L.M.; Cristea, M.; DeRosa, M.; Eisenhauer, E.L.; et al. Ovarian Cancer, Version 2.2020, NCCN Clinical Practice Guidelines in Oncology. *J Natl Compr Canc Netw* **2021**, *19*, 191-226, doi:10.6004/jncn.2021.0007.
95. Bookman, M.A. GOG0182-ICON5: 5-arm phase III randomized trial of paclitaxel (P) and carboplatin (C) vs combinations with gemcitabine (G), PEG-liposomal doxorubicin (D), or topotecan (T) in patients (pts) with advanced-stage epithelial ovarian (EOC) or primary peritoneal (PPC) carcinoma. *Journal of Clinical Oncology* **2006**, *24*, 5002-5002, doi:10.1200/jco.2006.24.18_suppl.5002.
96. Katsumata, N.; Yasuda, M.; Takahashi, F.; Isonishi, S.; Jobo, T.; Aoki, D.; Tsuda, H.; Sugiyama, T.; Kodama, S.; Kimura, E.; et al. Dose-dense paclitaxel once a week in combination with carboplatin every 3 weeks for advanced ovarian cancer: a phase 3, open-label, randomised controlled trial. *Lancet* **2009**, *374*, 1331-1338, doi:10.1016/S0140-6736(09)61157-0.
97. Katsumata, N.; Yasuda, M.; Isonishi, S.; Takahashi, F.; Michimae, H.; Kimura, E.; Aoki, D.; Jobo, T.; Kodama, S.; Terauchi, F.; et al. Long-term results of dose-dense paclitaxel and carboplatin versus conventional paclitaxel and carboplatin for treatment of advanced epithelial ovarian, fallopian tube, or primary peritoneal cancer (JGOG 3016): a randomised, controlled, open-label trial. *Lancet Oncol* **2013**, *14*, 1020-1026, doi:10.1016/S1470-2045(13)70363-2.
98. Pignata, S.; Scambia, G.; Katsaros, D.; Gallo, C.; Pujade-Lauraine, E.; De Placido, S.; Bologna, A.; Weber, B.; Raspagliesi, F.; Panici, P.B.; et al. Carboplatin plus paclitaxel once a week versus every 3 weeks in patients with advanced ovarian cancer (MITO-7): a randomised, multicentre, open-label, phase 3 trial. *Lancet Oncol* **2014**, *15*, 396-405, doi:10.1016/S1470-2045(14)70049-X.
99. Clamp, A.R.; McNeish, I.; Dean, A.; Gallardo, D.; Weon-Kim, J.; O'Donnell, D.; Hook, J.; Coyle, C.; Blagden, S.P.; Brenton, J.; et al. 9290_PR - ICON8: A GCIG phase III randomised trial evaluating weekly dose- dense chemotherapy integration in first-line epithelial ovarian/fallopian tube/primary peritoneal carcinoma (EOC) treatment: Results of primary progression- free survival (PFS) analysis. *Annals of Oncology* **2017**, *28*, v627, doi:<https://doi.org/10.1093/annonc/mdx440.039>.
100. Chan, J.K.; Brady, M.F.; Penson, R.T.; Huang, H.; Birrer, M.J.; Walker, J.L.; DiSilvestro, P.A.; Rubin, S.C.; Martin, L.P.; Davidson, S.A.; et al. Weekly vs. Every-3-Week Paclitaxel and Carboplatin for Ovarian Cancer. *N Engl J Med* **2016**, *374*, 738-748, doi:10.1056/NEJMoa1505067.
101. Lopez, J.A.; Krikorian, J.G.; Reich, S.D.; Smyth, R.D.; Lee, F.H.; Issell, B.F. Clinical pharmacology of intraperitoneal cisplatin. *Gynecol Oncol* **1985**, *20*, 1-9, doi:10.1016/0090-8258(85)90118-0.
102. Francis, P.; Rowinsky, E.; Schneider, J.; Hakes, T.; Hoskins, W.; Markman, M. Phase I feasibility and pharmacologic study of weekly intraperitoneal paclitaxel: a Gynecologic Oncology Group pilot Study. *J Clin Oncol* **1995**, *13*, 2961-2967, doi:10.1200/JCO.1995.13.12.2961.
103. Provencher, D.M.; Gallagher, C.J.; Parulekar, W.R.; Ledermann, J.A.; Armstrong, D.K.; Brundage, M.; Gourley, C.; Romero, I.; Gonzalez-Martin, A.; Feeney, M.; et al. OV21/PETROC: a randomized Gynecologic Cancer Intergroup phase II study of intraperitoneal versus intravenous chemotherapy following neoadjuvant chemotherapy and

- optimal debulking surgery in epithelial ovarian cancer. *Ann Oncol* **2018**, *29*, 431-438, doi:10.1093/annonc/mdx754.
104. Armstrong, D.K.; Brady, M.F. Intraperitoneal therapy for ovarian cancer: a treatment ready for prime time. *J Clin Oncol* **2006**, *24*, 4531-4533, doi:10.1200/JCO.2006.06.7140.
 105. Markman, M.; Bundy, B.N.; Alberts, D.S.; Fowler, J.M.; Clark-Pearson, D.L.; Carson, L.F.; Wadler, S.; Sickel, J. Phase III trial of standard-dose intravenous cisplatin plus paclitaxel versus moderately high-dose carboplatin followed by intravenous paclitaxel and intraperitoneal cisplatin in small-volume stage III ovarian carcinoma: an intergroup study of the Gynecologic Oncology Group, Southwestern Oncology Group, and Eastern Cooperative Oncology Group. *J Clin Oncol* **2001**, *19*, 1001-1007, doi:10.1200/JCO.2001.19.4.1001.
 106. Monk, B.J.; Chan, J.K. Is intraperitoneal chemotherapy still an acceptable option in primary adjuvant chemotherapy for advanced ovarian cancer? *Ann Oncol* **2017**, *28*, viii40-viii45, doi:10.1093/annonc/mdx451.
 107. van Driel, W.J.; Koole, S.N.; Sonke, G.S. Hyperthermic Intraperitoneal Chemotherapy in Ovarian Cancer. *N Engl J Med* **2018**, *378*, 1363-1364, doi:10.1056/NEJMc1802033.
 108. Tsang, R.Y.; Al-Fayea, T.; Au, H.-J. Cisplatin Overdose. *Drug Safety* **2009**, *32*, 1109-1122, doi:10.2165/11316640-000000000-00000.
 109. Ghosh, S. Cisplatin: The first metal based anticancer drug. *Bioorg Chem* **2019**, *88*, 102925, doi:10.1016/j.bioorg.2019.102925.
 110. Rybak, L.P.; Whitworth, C.A.; Mukherjea, D.; Ramkumar, V. Mechanisms of cisplatin-induced ototoxicity and prevention. *Hearing Research* **2007**, *226*, 157-167, doi:<https://doi.org/10.1016/j.heares.2006.09.015>.
 111. Liao, Y.; Lu, X.; Lu, C.; Li, G.; Jin, Y.; Tang, H. Selection of agents for prevention of cisplatin-induced hepatotoxicity. *Pharmacological Research* **2008**, *57*, 125-131, doi:<https://doi.org/10.1016/j.phrs.2008.01.001>.
 112. Pace, A.; Giannarelli, D.; Galiè, E.; Savarese, A.; Carpano, S.; Della Giulia, M.; Pozzi, A.; Silvani, A.; Gaviani, P.; Scaioli, V.; et al. Vitamin E neuroprotection for cisplatin neuropathy. *Neurology* **2010**, *74*, 762, doi:10.1212/WNL.0b013e3181d5279e.
 113. platinum. Available online: https://www.accessdata.fda.gov/drugsatfda_docs/label/2011/018057s080lbl.pdf (accessed on
 114. Jayson, G.C.; Kohn, E.C.; Kitchener, H.C.; Ledermann, J.A. Ovarian cancer. *Lancet* **2014**, *384*, 1376-1388, doi:10.1016/S0140-6736(13)62146-7.
 115. Rustin, G.J.; van der Burg, M.E.; Griffin, C.L.; Guthrie, D.; Lamont, A.; Jayson, G.C.; Kristensen, G.; Mediola, C.; Coens, C.; Qian, W.; et al. Early versus delayed treatment of relapsed ovarian cancer (MRC OV05/EORTC 55955): a randomised trial. *Lancet* **2010**, *376*, 1155-1163, doi:10.1016/S0140-6736(10)61268-8.
 116. Marchetti, C.; Muzii, L.; Romito, A.; Benedetti Panici, P. First-line treatment of women with advanced ovarian cancer: focus on bevacizumab. *OncoTargets and therapy* **2019**, *12*, 1095-1103, doi:10.2147/OTT.S155425.
 117. Burger, R.A.; Brady, M.F.; Bookman, M.A.; Fleming, G.F.; Monk, B.J.; Huang, H.; Mannel, R.S.; Homesley, H.D.; Fowler, J.; Greer, B.E.; et al. Incorporation of bevacizumab in the primary treatment of ovarian cancer. *N Engl J Med* **2011**, *365*, 2473-2483, doi:10.1056/NEJMoa1104390.

118. Perren, T.J.; Swart, A.M.; Pfisterer, J.; Ledermann, J.A.; Pujade-Lauraine, E.; Kristensen, G.; Carey, M.S.; Beale, P.; Cervantes, A.; Kurzeder, C.; et al. A phase 3 trial of bevacizumab in ovarian cancer. *N Engl J Med* **2011**, *365*, 2484-2496, doi:10.1056/NEJMoa1103799.
119. Oza, A.M.; Cook, A.D.; Pfisterer, J.; Embleton, A.; Ledermann, J.A.; Pujade-Lauraine, E.; Kristensen, G.; Carey, M.S.; Beale, P.; Cervantes, A.; et al. Standard chemotherapy with or without bevacizumab for women with newly diagnosed ovarian cancer (ICON7): overall survival results of a phase 3 randomised trial. *Lancet Oncol* **2015**, *16*, 928-936, doi:10.1016/S1470-2045(15)00086-8.
120. Pignata, S.; Lorusso, D.; Joly, F.; Gallo, C.; Colombo, N.; Sessa, C.; Bamias, A.; Pisano, C.; Selle, F.; Zaccarelli, E.; et al. Chemotherapy plus or minus bevacizumab for platinum-sensitive ovarian cancer patients recurring after a bevacizumab containing first line treatment: The randomized phase 3 trial MITO16B-MaNGO OV2B-ENGOT OV17. *Journal of Clinical Oncology* **2018**, *36*, 5506-5506, doi:10.1200/JCO.2018.36.15_suppl.5506.
121. Pujade-Lauraine, E.; Hilpert, F.; Weber, B.; Reuss, A.; Poveda, A.; Kristensen, G.; Sorio, R.; Vergote, I.; Witteveen, P.; Bamias, A.; et al. Bevacizumab combined with chemotherapy for platinum-resistant recurrent ovarian cancer: The AURELIA open-label randomized phase III trial. *J Clin Oncol* **2014**, *32*, 1302-1308, doi:10.1200/JCO.2013.51.4489.
122. Hirte, H.; Lheureux, S.; Fleming, G.F.; Sugimoto, A.; Morgan, R.; Biagi, J.; Wang, L.; McGill, S.; Ivy, S.P.; Oza, A.M. A phase 2 study of cediranib in recurrent or persistent ovarian, peritoneal or fallopian tube cancer: a trial of the Princess Margaret, Chicago and California Phase II Consortia. *Gynecol Oncol* **2015**, *138*, 55-61, doi:10.1016/j.ygyno.2015.04.009.
123. Matulonis, U.A.; Berlin, S.; Ivy, P.; Tyburski, K.; Krasner, C.; Zarwan, C.; Berkenblit, A.; Campos, S.; Horowitz, N.; Cannistra, S.A.; et al. Cediranib, an oral inhibitor of vascular endothelial growth factor receptor kinases, is an active drug in recurrent epithelial ovarian, fallopian tube, and peritoneal cancer. *J Clin Oncol* **2009**, *27*, 5601-5606, doi:10.1200/JCO.2009.23.2777.
124. Kaelin, W.G., Jr. The concept of synthetic lethality in the context of anticancer therapy. *Nat Rev Cancer* **2005**, *5*, 689-698, doi:10.1038/nrc1691.
125. Papa, A.; Caruso, D.; Strudel, M.; Tomao, S.; Tomao, F. Update on Poly-ADP-ribose polymerase inhibition for ovarian cancer treatment. *J Transl Med* **2016**, *14*, 267, doi:10.1186/s12967-016-1027-1.
126. Bowtell, D.D. The genesis and evolution of high-grade serous ovarian cancer. *Nat Rev Cancer* **2010**, *10*, 803-808, doi:10.1038/nrc2946.
127. Fong, P.C.; Yap, T.A.; Boss, D.S.; Carden, C.P.; Mergui-Roelvink, M.; Gourley, C.; De Greve, J.; Lubinski, J.; Shanley, S.; Messiou, C.; et al. Poly(ADP)-ribose polymerase inhibition: frequent durable responses in BRCA carrier ovarian cancer correlating with platinum-free interval. *J Clin Oncol* **2010**, *28*, 2512-2519, doi:10.1200/JCO.2009.26.9589.
128. Kaye, S.B.; Lubinski, J.; Matulonis, U.; Ang, J.E.; Gourley, C.; Karlan, B.Y.; Amnon, A.; Bell-McGuinn, K.M.; Chen, L.M.; Friedlander, M.; et al. Phase II, open-label, randomized, multicenter study comparing the efficacy and safety of olaparib, a poly (ADP-ribose) polymerase inhibitor, and pegylated liposomal doxorubicin in patients with BRCA1 or

- BRCA2 mutations and recurrent ovarian cancer. *J Clin Oncol* **2012**, *30*, 372-379, doi:10.1200/JCO.2011.36.9215.
129. Gelmon, K.A.; Tischkowitz, M.; Mackay, H.; Swenerton, K.; Robidoux, A.; Tonkin, K.; Hirte, H.; Huntsman, D.; Clemons, M.; Gilks, B.; et al. Olaparib in patients with recurrent high-grade serous or poorly differentiated ovarian carcinoma or triple-negative breast cancer: a phase 2, multicentre, open-label, non-randomised study. *Lancet Oncol* **2011**, *12*, 852-861, doi:10.1016/S1470-2045(11)70214-5.
 130. Pujade-Lauraine, E.; Ledermann, J.A.; Selle, F.; Gebski, V.; Penson, R.T.; Oza, A.M.; Korach, J.; Huzarski, T.; Poveda, A.; Pignata, S.; et al. Olaparib tablets as maintenance therapy in patients with platinum-sensitive, relapsed ovarian cancer and a BRCA1/2 mutation (SOLO2/ENGOT-Ov21): a double-blind, randomised, placebo-controlled, phase 3 trial. *Lancet Oncol* **2017**, *18*, 1274-1284, doi:10.1016/S1470-2045(17)30469-2.
 131. Mirza, M.R.; Monk, B.J.; Herrstedt, J.; Oza, A.M.; Mahner, S.; Redondo, A.; Fabbro, M.; Ledermann, J.A.; Lorusso, D.; Vergote, I.; et al. Niraparib Maintenance Therapy in Platinum-Sensitive, Recurrent Ovarian Cancer. *N Engl J Med* **2016**, *375*, 2154-2164, doi:10.1056/NEJMoa1611310.
 132. Coleman, R.L.; Oza, A.M.; Lorusso, D.; Aghajanian, C.; Oaknin, A.; Dean, A.; Colombo, N.; Weberpals, J.I.; Clamp, A.; Scambia, G.; et al. Rucaparib maintenance treatment for recurrent ovarian carcinoma after response to platinum therapy (ARIEL3): a randomised, double-blind, placebo-controlled, phase 3 trial. *Lancet* **2017**, *390*, 1949-1961, doi:10.1016/S0140-6736(17)32440-6.
 133. Galluzzi, L.; Senovilla, L.; Vitale, I.; Michels, J.; Martins, I.; Kepp, O.; Castedo, M.; Kroemer, G. Molecular mechanisms of cisplatin resistance. *Oncogene* **2012**, *31*, 1869-1883, doi:10.1038/onc.2011.384.
 134. Ishida, S.; Lee, J.; Thiele, D.J.; Herskowitz, I. Uptake of the anticancer drug cisplatin mediated by the copper transporter Ctr1 in yeast and mammals. *Proc Natl Acad Sci U S A* **2002**, *99*, 14298-14302, doi:10.1073/pnas.162491399.
 135. Dasari, S.; Tchounwou, P.B. Cisplatin in cancer therapy: molecular mechanisms of action. *Eur J Pharmacol* **2014**, *740*, 364-378, doi:10.1016/j.ejphar.2014.07.025.
 136. Baik, M.H.; Friesner, R.A.; Lippard, S.J. Theoretical study of cisplatin binding to purine bases: why does cisplatin prefer guanine over adenine? *J Am Chem Soc* **2003**, *125*, 14082-14092, doi:10.1021/ja036960d.
 137. Kelland, L.R.; Abel, G.; McKeage, M.J.; Jones, M.; Goddard, P.M.; Valenti, M.; Murrer, B.A.; Harrap, K.R. Preclinical antitumor evaluation of bis-acetato-ammine-dichloro-cyclohexylamine platinum(IV): an orally active platinum drug. *Cancer Res* **1993**, *53*, 2581-2586.
 138. Gonzalez, V.M.; Fuertes, M.A.; Alonso, C.; Perez, J.M. Is cisplatin-induced cell death always produced by apoptosis? *Mol Pharmacol* **2001**, *59*, 657-663, doi:10.1124/mol.59.4.657.
 139. Mandic, A.; Hansson, J.; Linder, S.; Shoshan, M.C. Cisplatin induces endoplasmic reticulum stress and nucleus-independent apoptotic signaling. *J Biol Chem* **2003**, *278*, 9100-9106, doi:10.1074/jbc.M210284200.
 140. Vitale, I.; Galluzzi, L.; Castedo, M.; Kroemer, G. Mitotic catastrophe: a mechanism for avoiding genomic instability. *Nat Rev Mol Cell Biol* **2011**, *12*, 385-392, doi:10.1038/nrm3115.

141. Zhao, H.; Piwnicka-Worms, H. ATR-mediated checkpoint pathways regulate phosphorylation and activation of human Chk1. *Mol Cell Biol* **2001**, *21*, 4129-4139, doi:10.1128/MCB.21.13.4129-4139.2001.
142. Galluzzi, L.; Morselli, E.; Kepp, O.; Vitale, I.; Pinti, M.; Kroemer, G. Mitochondrial liaisons of p53. *Antioxid Redox Signal* **2011**, *15*, 1691-1714, doi:10.1089/ars.2010.3504.
143. Brozovic, A.; Ambriovic-Ristov, A.; Osmak, M. The relationship between cisplatin-induced reactive oxygen species, glutathione, and BCL-2 and resistance to cisplatin. *Crit Rev Toxicol* **2010**, *40*, 347-359, doi:10.3109/10408441003601836.
144. Holzer, A.K.; Howell, S.B. The internalization and degradation of human copper transporter 1 following cisplatin exposure. *Cancer Res* **2006**, *66*, 10944-10952, doi:10.1158/0008-5472.CAN-06-1710.
145. Rottenberg, S.; Disler, C.; Perego, P. The rediscovery of platinum-based cancer therapy. *Nat Rev Cancer* **2021**, *21*, 37-50, doi:10.1038/s41568-020-00308-y.
146. Planells-Cases, R.; Lutter, D.; Guyader, C.; Gerhards, N.M.; Ullrich, F.; Elger, D.A.; Kucukosmanoglu, A.; Xu, G.; Voss, F.K.; Reincke, S.M.; et al. Subunit composition of VRAC channels determines substrate specificity and cellular resistance to Pt-based anti-cancer drugs. *EMBO J* **2015**, *34*, 2993-3008, doi:10.15252/embj.201592409.
147. He, Y.J.; Meghani, K.; Caron, M.C.; Yang, C.; Ronato, D.A.; Bian, J.; Sharma, A.; Moore, J.; Niraj, J.; Detappe, A.; et al. DYNLL1 binds to MRE11 to limit DNA end resection in BRCA1-deficient cells. *Nature* **2018**, *563*, 522-526, doi:10.1038/s41586-018-0670-5.
148. Liedert, B.; Materna, V.; Schadendorf, D.; Thomale, J.; Lage, H. Overexpression of cMOAT (MRP2/ABCC2) is associated with decreased formation of platinum-DNA adducts and decreased G2-arrest in melanoma cells resistant to cisplatin. *J Invest Dermatol* **2003**, *121*, 172-176, doi:10.1046/j.1523-1747.2003.12313.x.
149. Ahmad, A.; Robinson, A.R.; Duensing, A.; van Drunen, E.; Beverloo, H.B.; Weisberg, D.B.; Hasty, P.; Hoeijmakers, J.H.; Niedernhofer, L.J. ERCC1-XPF endonuclease facilitates DNA double-strand break repair. *Mol Cell Biol* **2008**, *28*, 5082-5092, doi:10.1128/MCB.00293-08.
150. Wojtaszek, J.L.; Chatterjee, N.; Najeeb, J.; Ramos, A.; Lee, M.; Bian, K.; Xue, J.Y.; Fenton, B.A.; Park, H.; Li, D.; et al. A Small Molecule Targeting Mutagenic Translesion Synthesis Improves Chemotherapy. *Cell* **2019**, *178*, 152-159 e111, doi:10.1016/j.cell.2019.05.028.
151. Farmer, H.; McCabe, N.; Lord, C.J.; Tutt, A.N.; Johnson, D.A.; Richardson, T.B.; Santarosa, M.; Dillon, K.J.; Hickson, I.; Knights, C.; et al. Targeting the DNA repair defect in BRCA mutant cells as a therapeutic strategy. *Nature* **2005**, *434*, 917-921, doi:10.1038/nature03445.
152. Sakai, W.; Swisher, E.M.; Karlan, B.Y.; Agarwal, M.K.; Higgins, J.; Friedman, C.; Villegas, E.; Jacquemont, C.; Farrugia, D.J.; Couch, F.J.; et al. Secondary mutations as a mechanism of cisplatin resistance in BRCA2-mutated cancers. *Nature* **2008**, *451*, 1116-1120, doi:10.1038/nature06633.
153. Rottenberg, S.; Nygren, A.O.; Pajic, M.; van Leeuwen, F.W.; van der Heijden, I.; van de Wetering, K.; Liu, X.; de Visser, K.E.; Gilhuijs, K.G.; van Tellingen, O.; et al. Selective induction of chemotherapy resistance of mammary tumors in a conditional mouse model for hereditary breast cancer. *Proc Natl Acad Sci U S A* **2007**, *104*, 12117-12122, doi:10.1073/pnas.0702955104.

154. Pajic, M.; Blatter, S.; Guyader, C.; Gonggrijp, M.; Kersbergen, A.; Kucukosmanoglu, A.; Sol, W.; Drost, R.; Jonkers, J.; Borst, P.; et al. Selected Alkylating Agents Can Overcome Drug Tolerance of G0-like Tumor Cells and Eradicate BRCA1-Deficient Mammary Tumors in Mice. *Clin Cancer Res* **2017**, *23*, 7020-7033, doi:10.1158/1078-0432.CCR-17-1279.
155. Cooke, S.L.; Ng, C.K.; Melnyk, N.; Garcia, M.J.; Hardcastle, T.; Temple, J.; Langdon, S.; Huntsman, D.; Brenton, J.D. Genomic analysis of genetic heterogeneity and evolution in high-grade serous ovarian carcinoma. *Oncogene* **2010**, *29*, 4905-4913, doi:10.1038/onc.2010.245.
156. Michaud, W.A.; Nichols, A.C.; Mroz, E.A.; Faquin, W.C.; Clark, J.R.; Begum, S.; Westra, W.H.; Wada, H.; Busse, P.M.; Ellisen, L.W.; et al. Bcl-2 blocks cisplatin-induced apoptosis and predicts poor outcome following chemoradiation treatment in advanced oropharyngeal squamous cell carcinoma. *Clin Cancer Res* **2009**, *15*, 1645-1654, doi:10.1158/1078-0432.CCR-08-2581.
157. Han, J.Y.; Hong, E.K.; Choi, B.G.; Park, J.N.; Kim, K.W.; Kang, J.H.; Jin, J.Y.; Park, S.Y.; Hong, Y.S.; Lee, K.S. Death receptor 5 and Bcl-2 protein expression as predictors of tumor response to gemcitabine and cisplatin in patients with advanced non-small-cell lung cancer. *Med Oncol* **2003**, *20*, 355-362, doi:10.1385/MO:20:4:355.
158. Wang, W.; Kryczek, I.; Dostal, L.; Lin, H.; Tan, L.; Zhao, L.; Lu, F.; Wei, S.; Maj, T.; Peng, D.; et al. Effector T Cells Abrogate Stroma-Mediated Chemoresistance in Ovarian Cancer. *Cell* **2016**, *165*, 1092-1105, doi:10.1016/j.cell.2016.04.009.
159. Dijkgraaf, E.M.; Heusinkveld, M.; Tummers, B.; Vogelpoel, L.T.; Goedemans, R.; Jha, V.; Nortier, J.W.; Welters, M.J.; Kroep, J.R.; van der Burg, S.H. Chemotherapy alters monocyte differentiation to favor generation of cancer-supporting M2 macrophages in the tumor microenvironment. *Cancer Res* **2013**, *73*, 2480-2492, doi:10.1158/0008-5472.CAN-12-3542.
160. Sommariva, M.; De Cecco, L.; De Cesare, M.; Sfondrini, L.; Menard, S.; Melani, C.; Delia, D.; Zaffaroni, N.; Pratesi, G.; Uva, V.; et al. TLR9 agonists oppositely modulate DNA repair genes in tumor versus immune cells and enhance chemotherapy effects. *Cancer Res* **2011**, *71*, 6382-6390, doi:10.1158/0008-5472.CAN-11-1285.
161. Gupta, S.C.; Sung, B.; Prasad, S.; Webb, L.J.; Aggarwal, B.B. Cancer drug discovery by repurposing: teaching new tricks to old dogs. *Trends Pharmacol Sci* **2013**, *34*, 508-517, doi:10.1016/j.tips.2013.06.005.
162. Zamboni, W.C.; Torchilin, V.; Patri, A.K.; Hrkach, J.; Stern, S.; Lee, R.; Nel, A.; Panaro, N.J.; Grodzinski, P. Best practices in cancer nanotechnology: perspective from NCI nanotechnology alliance. *Clin Cancer Res* **2012**, *18*, 3229-3241, doi:10.1158/1078-0432.CCR-11-2938.
163. Elliott, R.L. Four lessons from global health drug discovery: medicine for an ailing industry? *ACS Med Chem Lett* **2012**, *3*, 688-690, doi:10.1021/ml3002105.
164. Fojo, T.; Parkinson, D.R. Biologically targeted cancer therapy and marginal benefits: are we making too much of too little or are we achieving too little by giving too much? *Clin Cancer Res* **2010**, *16*, 5972-5980, doi:10.1158/1078-0432.CCR-10-1277.
165. Parvathaneni, V.; Kulkarni, N.S.; Muth, A.; Gupta, V. Drug repurposing: a promising tool to accelerate the drug discovery process. *Drug Discov Today* **2019**, *24*, 2076-2085, doi:10.1016/j.drudis.2019.06.014.

166. Alwael, H.; Connolly, D.; Barron, L.; Paull, B. Development of a rapid and sensitive method for determination of cysteine/cystine ratio in chemically defined media. *J Chromatogr A* **2010**, *1217*, 3863-3870, doi:10.1016/j.chroma.2010.04.036.
167. Hicks, L.K.; Haynes, A.E.; Reece, D.E.; Walker, I.R.; Herst, J.A.; Meyer, R.M.; Imrie, K.; Hematology Disease Site Group of the Cancer Care Ontario Program in Evidence-based, C. A meta-analysis and systematic review of thalidomide for patients with previously untreated multiple myeloma. *Cancer Treat Rev* **2008**, *34*, 442-452, doi:10.1016/j.ctrv.2008.02.003.
168. Knobloch, J.; Ruther, U. Shedding light on an old mystery: thalidomide suppresses survival pathways to induce limb defects. *Cell Cycle* **2008**, *7*, 1121-1127, doi:10.4161/cc.7.9.5793.
169. D'Amato, R.J.; Loughnan, M.S.; Flynn, E.; Folkman, J. Thalidomide is an inhibitor of angiogenesis. *Proc Natl Acad Sci USA* **1994**, *91*, 4082-4085, doi:10.1073/pnas.91.9.4082.
170. Parman, T.; Wiley, M.J.; Wells, P.G. Free radical-mediated oxidative DNA damage in the mechanism of thalidomide teratogenicity. *Nat Med* **1999**, *5*, 582-585, doi:10.1038/8466.
171. Singhal, S.; Mehta, J.; Desikan, R.; Ayers, D.; Roberson, P.; Eddlemon, P.; Munshi, N.; Anaissie, E.; Wilson, C.; Dhodapkar, M.; et al. Antitumor activity of thalidomide in refractory multiple myeloma. *N Engl J Med* **1999**, *341*, 1565-1571, doi:10.1056/NEJM199911183412102.
172. Gagne, D.; Pons, M.; Philibert, D. RU 38486: a potent antiglucocorticoid in vitro and in vivo. *J Steroid Biochem* **1985**, *23*, 247-251, doi:10.1016/0022-4731(85)90401-7.
173. Ulmann, A.; Dubois, C.; Philibert, D. Fertility control with RU 486. *Horm Res* **1987**, *28*, 274-278, doi:10.1159/000180952.
174. Bosc, M.J.; Germain, G.; Nicolle, A.; Mouren, M.; Philibert, D.; Baulieu, E.E. Control of birth in rats by RU 486, an antiprogesterone compound. *J Reprod Fertil* **1987**, *79*, 1-8, doi:10.1530/jrf.0.0790001.
175. Telleria, C.M. Drug Repurposing for Cancer Therapy. *J Cancer Sci Ther* **2012**, *4*, ix-xi, doi:10.4172/1948-5956.1000e108.
176. Noto, H.; Goto, A.; Tsujimoto, T.; Noda, M. Cancer risk in diabetic patients treated with metformin: a systematic review and meta-analysis. *PLoS One* **2012**, *7*, e33411, doi:10.1371/journal.pone.0033411.
177. Del Barco, S.; Vazquez-Martin, A.; Cufi, S.; Oliveras-Ferraros, C.; Bosch-Barrera, J.; Joven, J.; Martin-Castillo, B.; Menendez, J.A. Metformin: multi-faceted protection against cancer. *Oncotarget* **2011**, *2*, 896-917, doi:10.18632/oncotarget.387.
178. Kalender, A.; Selvaraj, A.; Kim, S.Y.; Gulati, P.; Brule, S.; Viollet, B.; Kemp, B.E.; Bardeesy, N.; Dennis, P.; Schlager, J.J.; et al. Metformin, independent of AMPK, inhibits mTORC1 in a rag GTPase-dependent manner. *Cell Metab* **2010**, *11*, 390-401, doi:10.1016/j.cmet.2010.03.014.
179. Lee, M.S.; Hsu, C.C.; Wahlqvist, M.L.; Tsai, H.N.; Chang, Y.H.; Huang, Y.C. Type 2 diabetes increases and metformin reduces total, colorectal, liver and pancreatic cancer incidences in Taiwanese: a representative population prospective cohort study of 800,000 individuals. *BMC Cancer* **2011**, *11*, 20, doi:10.1186/1471-2407-11-20.
180. Robak, P.; Robak, T. Bortezomib for the Treatment of Hematologic Malignancies: 15 Years Later. *Drugs R D* **2019**, *19*, 73-92, doi:10.1007/s40268-019-0269-9.
181. Sanchez-Serrano, I. Success in translational research: lessons from the development of bortezomib. *Nat Rev Drug Discov* **2006**, *5*, 107-114, doi:10.1038/nrd1959.

182. Hatzimouratidis, K. Sildenafil in the treatment of erectile dysfunction: an overview of the clinical evidence. *Clin Interv Aging* **2006**, *1*, 403-414, doi:10.2147/ciaa.2006.1.4.403.
183. Jacquemet, G.; Baghirov, H.; Georgiadou, M.; Sihto, H.; Peuhu, E.; Cettour-Janet, P.; He, T.; Perala, M.; Kronqvist, P.; Joensuu, H.; et al. L-type calcium channels regulate filopodia stability and cancer cell invasion downstream of integrin signalling. *Nat Commun* **2016**, *7*, 13297, doi:10.1038/ncomms13297.
184. Sanders, T.I. The Orphan Drug Act. *Prog Clin Biol Res* **1983**, *127*, 207-215.
185. Pushpakom, S.; Iorio, F.; Eyers, P.A.; Escott, K.J.; Hopper, S.; Wells, A.; Doig, A.; Guilliams, T.; Latimer, J.; McNamee, C.; et al. Drug repurposing: progress, challenges and recommendations. *Nat Rev Drug Discov* **2019**, *18*, 41-58, doi:10.1038/nrd.2018.168.
186. Flexner, C. HIV-protease inhibitors. *N Engl J Med* **1998**, *338*, 1281-1292, doi:10.1056/NEJM199804303381808.
187. Debouck, C. The HIV-1 protease as a therapeutic target for AIDS. *AIDS Res Hum Retroviruses* **1992**, *8*, 153-164, doi:10.1089/aid.1992.8.153.
188. Lv, Z.; Chu, Y.; Wang, Y. HIV protease inhibitors: a review of molecular selectivity and toxicity. *HIV AIDS (Auckl)* **2015**, *7*, 95-104, doi:10.2147/HIV.S79956.
189. Maksimovic-Ivanic, D.; Fagone, P.; McCubrey, J.; Bendtzen, K.; Mijatovic, S.; Nicoletti, F. HIV-protease inhibitors for the treatment of cancer: Repositioning HIV protease inhibitors while developing more potent NO-hybridized derivatives? *Int J Cancer* **2017**, *140*, 1713-1726, doi:10.1002/ijc.30529.
190. Carpenter, C.C.; Fischl, M.A.; Hammer, S.M.; Hirsch, M.S.; Jacobsen, D.M.; Katzenstein, D.A.; Montaner, J.S.; Richman, D.D.; Saag, M.S.; Schooley, R.T.; et al. Antiretroviral therapy for HIV infection in 1998: updated recommendations of the International AIDS Society-USA Panel. *JAMA* **1998**, *280*, 78-86, doi:10.1001/jama.280.1.78.
191. Zhang, K.E.; Wu, E.; Patick, A.K.; Kerr, B.; Zorbas, M.; Lankford, A.; Kobayashi, T.; Maeda, Y.; Shetty, B.; Webber, S. Circulating metabolites of the human immunodeficiency virus protease inhibitor nelfinavir in humans: structural identification, levels in plasma, and antiviral activities. *Antimicrob Agents Chemother* **2001**, *45*, 1086-1093, doi:10.1128/AAC.45.4.1086-1093.2001.
192. Niehues, T.; Horneff, G.; Megahed, M.; Schrotten, H.; Wahn, V. Complete regression of AIDS-related Kaposi's sarcoma in a child treated with highly active antiretroviral therapy. *AIDS* **1999**, *13*, 1148-1149, doi:10.1097/00002030-199906180-00026.
193. Lebbe, C.; Blum, L.; Pellet, C.; Blanchard, G.; Verola, O.; Morel, P.; Danne, O.; Calvo, F. Clinical and biological impact of antiretroviral therapy with protease inhibitors on HIV-related Kaposi's sarcoma. *AIDS* **1998**, *12*, F45-49, doi:10.1097/00002030-199807000-00002.
194. Krischer, J.; Rutschmann, O.; Hirschel, B.; Vollenweider-Roten, S.; Saurat, J.H.; Pechere, M. Regression of Kaposi's sarcoma during therapy with HIV-1 protease inhibitors: a prospective pilot study. *J Am Acad Dermatol* **1998**, *38*, 594-598, doi:10.1016/s0190-9622(98)70124-0.
195. Sgadari, C.; Barillari, G.; Toschi, E.; Carlei, D.; Bacigalupo, I.; Baccarini, S.; Palladino, C.; Leone, P.; Bugarini, R.; Malavasi, L.; et al. HIV protease inhibitors are potent anti-angiogenic molecules and promote regression of Kaposi sarcoma. *Nat Med* **2002**, *8*, 225-232, doi:10.1038/nm0302-225.
196. Sgadari, C.; Monini, P.; Barillari, G.; Ensoli, B. Use of HIV protease inhibitors to block Kaposi's sarcoma and tumour growth. *Lancet Oncol* **2003**, *4*, 537-547.

197. Schmidtke, G.; Holzhutter, H.G.; Bogyo, M.; Kairies, N.; Groll, M.; de Giuli, R.; Emch, S.; Groettrup, M. How an inhibitor of the HIV-I protease modulates proteasome activity. *J Biol Chem* **1999**, *274*, 35734-35740, doi:10.1074/jbc.274.50.35734.
198. Pai, V.B.; Nahata, M.C. Nelfinavir mesylate: a protease inhibitor. *Ann Pharmacother* **1999**, *33*, 325-339, doi:10.1345/aph.18089.
199. Koltai, T. Nelfinavir and other protease inhibitors in cancer: mechanisms involved in anticancer activity. *F1000Res* **2015**, *4*, 9, doi:10.12688/f1000research.5827.2.
200. Gantt, S.; Casper, C.; Ambinder, R.F. Insights into the broad cellular effects of nelfinavir and the HIV protease inhibitors supporting their role in cancer treatment and prevention. *Curr Opin Oncol* **2013**, *25*, 495-502, doi:10.1097/CCO.0b013e328363dfee.
201. Wu, W.; Zhang, R.; Salahub, D.R. Nelfinavir: a magic bullet to annihilate cancer cells? *Cancer Biol Ther* **2009**, *8*, 233-235, doi:10.4161/cbt.8.3.7789.
202. Xie, L.; Evangelidis, T.; Xie, L.; Bourne, P.E. Drug Discovery Using Chemical Systems Biology: Weak Inhibition of Multiple Kinases May Contribute to the Anti-Cancer Effect of Nelfinavir. *PLOS Computational Biology* **2011**, *7*, e1002037, doi:10.1371/journal.pcbi.1002037.
203. Arodola, O.A.; Soliman, M.E. Could the FDA-approved anti-HIV PR inhibitors be promising anticancer agents? An answer from enhanced docking approach and molecular dynamics analyses. *Drug Des Devel Ther* **2015**, *9*, 6055-6065, doi:10.2147/DDDT.S87653.
204. Gills, J.J.; Lopiccolo, J.; Tsurutani, J.; Shoemaker, R.H.; Best, C.J.; Abu-Asab, M.S.; Borojerdi, J.; Warfel, N.A.; Gardner, E.R.; Danish, M.; et al. Nelfinavir, A lead HIV protease inhibitor, is a broad-spectrum, anticancer agent that induces endoplasmic reticulum stress, autophagy, and apoptosis in vitro and in vivo. *Clin Cancer Res* **2007**, *13*, 5183-5194, doi:10.1158/1078-0432.CCR-07-0161.
205. Driessen, C.; Muller, R.; Novak, U.; Cantoni, N.; Betticher, D.; Mach, N.; Rufer, A.; Mey, U.; Samaras, P.; Ribi, K.; et al. Promising activity of nelfinavir-bortezomib-dexamethasone in proteasome inhibitor-refractory multiple myeloma. *Blood* **2018**, *132*, 2097-2100, doi:10.1182/blood-2018-05-851170.
206. Bruning, A.; Burger, P.; Vogel, M.; Rahmeh, M.; Gingelmaiers, A.; Friese, K.; Lenhard, M.; Burges, A. Nelfinavir induces the unfolded protein response in ovarian cancer cells, resulting in ER vacuolization, cell cycle retardation and apoptosis. *Cancer Biol Ther* **2009**, *8*, 226-232, doi:10.4161/cbt.8.3.7339.
207. Bruning, A.; Rahmeh, M.; Gingelmaier, A.; Friese, K. The mitochondria-independent cytotoxic effect of nelfinavir on leukemia cells can be enhanced by sorafenib-mediated mcl-1 downregulation and mitochondrial membrane destabilization. *Mol Cancer* **2010**, *9*, 19, doi:10.1186/1476-4598-9-19.
208. Bruning, A.; Vogel, M.; Mylonas, I.; Friese, K.; Burges, A. Bortezomib targets the caspase-like proteasome activity in cervical cancer cells, triggering apoptosis that can be enhanced by nelfinavir. *Curr Cancer Drug Targets* **2011**, *11*, 799-809.
209. Chow, W.A.; Guo, S.; Valdes-Albini, F. Nelfinavir induces liposarcoma apoptosis and cell cycle arrest by upregulating sterol regulatory element binding protein-1. *Anticancer Drugs* **2006**, *17*, 891-903, doi:10.1097/01.cad.0000224448.08706.76.
210. Jiang, W.; Mikochik, P.J.; Ra, J.H.; Lei, H.; Flaherty, K.T.; Winkler, J.D.; Spitz, F.R. HIV protease inhibitor nelfinavir inhibits growth of human melanoma cells by induction of cell cycle arrest. *Cancer Res* **2007**, *67*, 1221-1227, doi:10.1158/0008-5472.CAN-06-3377.

211. Jensen, K.; Bikas, A.; Patel, A.; Kushchayeva, Y.; Costello, J.; McDaniel, D.; Burman, K.; Vasko, V. Nelfinavir inhibits proliferation and induces DNA damage in thyroid cancer cells. *Endocr Relat Cancer* **2017**, *24*, 147-156, doi:10.1530/ERC-16-0568.
212. Sato, A.; Asano, T.; Okubo, K.; Isono, M.; Asano, T. Nelfinavir and Ritonavir Kill Bladder Cancer Cells Synergistically by Inducing Endoplasmic Reticulum Stress. *Oncol Res* **2018**, *26*, 323-332, doi:10.3727/096504017X14957929842972.
213. Okubo, K.; Sato, A.; Isono, M.; Asano, T.; Asano, T. Nelfinavir Induces Endoplasmic Reticulum Stress and Sensitizes Renal Cancer Cells to TRAIL. *Anticancer Res* **2018**, *38*, 4505-4514, doi:10.21873/anticanres.12754.
214. Okubo, K.; Isono, M.; Asano, T.; Sato, A. Panobinostat and Nelfinavir Inhibit Renal Cancer Growth by Inducing Endoplasmic Reticulum Stress. *Anticancer Res* **2018**, *38*, 5615-5626, doi:10.21873/anticanres.12896.
215. Soprano, M.; Sorriento, D.; Rusciano, M.R.; Maione, A.S.; Limite, G.; Forestieri, P.; D'Angelo, D.; D'Alessio, M.; Campiglia, P.; Formisano, P.; et al. Oxidative Stress Mediates the Antiproliferative Effects of Nelfinavir in Breast Cancer Cells. *PLoS One* **2016**, *11*, e0155970, doi:10.1371/journal.pone.0155970.
216. Sun, L.; Niu, L.; Zhu, X.; Hao, J.; Wang, P.; Wang, H. Antitumour effects of a protease inhibitor, nelfinavir, in hepatocellular carcinoma cancer cells. *J Chemother* **2012**, *24*, 161-166, doi:10.1179/1973947812Y.0000000011.
217. Veschi, S.; De Lellis, L.; Florio, R.; Lanuti, P.; Massucci, A.; Tinari, N.; De Tursi, M.; di Sebastiano, P.; Marchisio, M.; Natoli, C.; et al. Effects of repurposed drug candidates nitroxoline and nelfinavir as single agents or in combination with erlotinib in pancreatic cancer cells. *J Exp Clin Cancer Res* **2018**, *37*, 236, doi:10.1186/s13046-018-0904-2.
218. Xiang, T.; Du, L.; Pham, P.; Zhu, B.; Jiang, S. Nelfinavir, an HIV protease inhibitor, induces apoptosis and cell cycle arrest in human cervical cancer cells via the ROS-dependent mitochondrial pathway. *Cancer Lett* **2015**, *364*, 79-88, doi:10.1016/j.canlet.2015.04.027.
219. Xia, C.; Chen, R.; Chen, J.; Qi, Q.; Pan, Y.; Du, L.; Xiao, G.; Jiang, S. Combining metformin and nelfinavir exhibits synergistic effects against the growth of human cervical cancer cells and xenograft in nude mice. *Sci Rep* **2017**, *7*, 43373, doi:10.1038/srep43373.
220. Bruning, A.; Burger, P.; Vogel, M.; Gingelmaier, A.; Friese, K.; Burges, A. Nelfinavir induces mitochondria protection by ERK1/2-mediated mcl-1 stabilization that can be overcome by sorafenib. *Invest New Drugs* **2010**, *28*, 535-542, doi:10.1007/s10637-009-9281-1.
221. Cande, C.; Cecconi, F.; Dessen, P.; Kroemer, G. Apoptosis-inducing factor (AIF): key to the conserved caspase-independent pathways of cell death? *J Cell Sci* **2002**, *115*, 4727-4734, doi:10.1242/jcs.00210.
222. Bono, C.; Karlin, L.; Harel, S.; Mouly, E.; Labaume, S.; Galicier, L.; Apcher, S.; Sauvageon, H.; Femand, J.P.; Bories, J.C.; et al. The human immunodeficiency virus-1 protease inhibitor nelfinavir impairs proteasome activity and inhibits the proliferation of multiple myeloma cells in vitro and in vivo. *Haematologica* **2012**, *97*, 1101-1109, doi:10.3324/haematol.2011.049981.
223. Kushchayeva, Y.; Jensen, K.; Recupero, A.; Costello, J.; Patel, A.; Klubo-Gwiedzinska, J.; Boyle, L.; Burman, K.; Vasko, V. The HIV protease inhibitor nelfinavir down-regulates RET signaling and induces apoptosis in medullary thyroid cancer cells. *J Clin Endocrinol Metab* **2014**, *99*, E734-745, doi:10.1210/jc.2013-3369.

224. Bruning, A.; Friese, K.; Burges, A.; Mylonas, I. Tamoxifen enhances the cytotoxic effects of nelfinavir in breast cancer cells. *Breast Cancer Res* **2010**, *12*, R45, doi:10.1186/bcr2602.
225. Cho, H.Y.; Thomas, S.; Golden, E.B.; Gaffney, K.J.; Hofman, F.M.; Chen, T.C.; Louie, S.G.; Petasis, N.A.; Schonthal, A.H. Enhanced killing of chemo-resistant breast cancer cells via controlled aggravation of ER stress. *Cancer Lett* **2009**, *282*, 87-97, doi:10.1016/j.canlet.2009.03.007.
226. Thomas, S.; Sharma, N.; Golden, E.B.; Cho, H.; Agarwal, P.; Gaffney, K.J.; Petasis, N.A.; Chen, T.C.; Hofman, F.M.; Louie, S.G.; et al. Preferential killing of triple-negative breast cancer cells in vitro and in vivo when pharmacological aggravators of endoplasmic reticulum stress are combined with autophagy inhibitors. *Cancer Lett* **2012**, *325*, 63-71, doi:10.1016/j.canlet.2012.05.030.
227. Davis, M.A.; Delaney, J.R.; Patel, C.B.; Storgard, R.; Stupack, D.G. Nelfinavir is effective against human cervical cancer cells in vivo: a potential treatment modality in resource-limited settings. *Drug Des Devel Ther* **2016**, *10*, 1837-1846, doi:10.2147/DDDT.S102241.
228. Bruning, A.; Rahmeh, M.; Friese, K. Nelfinavir and bortezomib inhibit mTOR activity via ATF4-mediated sestrin-2 regulation. *Mol Oncol* **2013**, *7*, 1012-1018, doi:10.1016/j.molonc.2013.07.010.
229. Meier-Stephenson, V.; Riemer, J.; Narendran, A. The HIV protease inhibitor, nelfinavir, as a novel therapeutic approach for the treatment of refractory pediatric leukemia. *Onco Targets Ther* **2017**, *10*, 2581-2593, doi:10.2147/OTT.S136484.
230. Liu, W.; Meng, Q.; Sun, Y.; Wang, C.; Huo, X.; Liu, Z.; Sun, P.; Sun, H.; Ma, X.; Liu, K. Targeting P-Glycoprotein: Nelfinavir Reverses Adriamycin Resistance in K562/ADR Cells. *Cell Physiol Biochem* **2018**, *51*, 1616-1631, doi:10.1159/000495650.
231. Mathur, A.; Abd Elmageed, Z.Y.; Liu, X.; Kostochka, M.L.; Zhang, H.; Abdel-Mageed, A.B.; Mondal, D. Subverting ER-stress towards apoptosis by nelfinavir and curcumin coexposure augments docetaxel efficacy in castration resistant prostate cancer cells. *PLoS One* **2014**, *9*, e103109, doi:10.1371/journal.pone.0103109.
232. Yang, Y.; Ikezoe, T.; Nishioka, C.; Bandobashi, K.; Takeuchi, T.; Adachi, Y.; Kobayashi, M.; Takeuchi, S.; Koeffler, H.P.; Taguchi, H. NFV, an HIV-1 protease inhibitor, induces growth arrest, reduced Akt signalling, apoptosis and docetaxel sensitisation in NSCLC cell lines. *Br J Cancer* **2006**, *95*, 1653-1662, doi:10.1038/sj.bjc.6603435.
233. Yang, Y.; Ikezoe, T.; Takeuchi, T.; Adachi, Y.; Ohtsuki, Y.; Takeuchi, S.; Koeffler, H.P.; Taguchi, H. HIV-1 protease inhibitor induces growth arrest and apoptosis of human prostate cancer LNCaP cells in vitro and in vivo in conjunction with blockade of androgen receptor STAT3 and AKT signaling. *Cancer Sci* **2005**, *96*, 425-433, doi:10.1111/j.1349-7006.2005.00063.x.
234. Vandewynckel, Y.P.; Coucke, C.; Laukens, D.; Devisscher, L.; Paridaens, A.; Bogaerts, E.; Vandierendonck, A.; Raevens, S.; Verhelst, X.; Van Steenkiste, C.; et al. Next-generation proteasome inhibitor oprozomib synergizes with modulators of the unfolded protein response to suppress hepatocellular carcinoma. *Oncotarget* **2016**, *7*, 34988-35000, doi:10.18632/oncotarget.9222.
235. Gupta, V.; Samuleson, C.G.; Su, S.; Chen, T.C. Nelfinavir potentiation of imatinib cytotoxicity in meningioma cells via survivin inhibition. *Neurosurg Focus* **2007**, *23*, E9, doi:10.3171/FOC-07/10/E9.
236. Elmore, S. Apoptosis: a review of programmed cell death. *Toxicol Pathol* **2007**, *35*, 495-516, doi:10.1080/01926230701320337.

237. Tian, X.; Ye, J.; Alonso-Basanta, M.; Hahn, S.M.; Koumenis, C.; Dorsey, J.F. Modulation of CCAAT/enhancer binding protein homologous protein (CHOP)-dependent DR5 expression by nelfinavir sensitizes glioblastoma multiforme cells to tumor necrosis factor-related apoptosis-inducing ligand (TRAIL). *J Biol Chem* **2011**, *286*, 29408-29416, doi:10.1074/jbc.M110.197665.
238. Bruning, A.; Vogel, M.; Burger, P.; Rahmeh, M.; Gingelmaier, A.; Friese, K.; Lenhard, M.; Burges, A. Nelfinavir induces TRAIL receptor upregulation in ovarian cancer cells. *Biochem Biophys Res Commun* **2008**, *377*, 1309-1314, doi:10.1016/j.bbrc.2008.10.167.
239. Wang, W.A.; Groenendyk, J.; Michalak, M. Endoplasmic reticulum stress associated responses in cancer. *Biochim Biophys Acta* **2014**, *1843*, 2143-2149, doi:10.1016/j.bbamcr.2014.01.012.
240. Corazzari, M.; Gagliardi, M.; Fimia, G.M.; Piacentini, M. Endoplasmic Reticulum Stress, Unfolded Protein Response, and Cancer Cell Fate. *Front Oncol* **2017**, *7*, 78, doi:10.3389/fonc.2017.00078.
241. Gorman, A.M.; Healy, S.J.; Jager, R.; Samali, A. Stress management at the ER: regulators of ER stress-induced apoptosis. *Pharmacol Ther* **2012**, *134*, 306-316, doi:10.1016/j.pharmthera.2012.02.003.
242. Kawabata, S.; Gills, J.J.; Mercado-Matos, J.R.; Lopiccio, J.; Wilson, W., 3rd; Hollander, M.C.; Dennis, P.A. Synergistic effects of nelfinavir and bortezomib on proteotoxic death of NSCLC and multiple myeloma cells. *Cell Death Dis* **2012**, *3*, e353, doi:10.1038/cddis.2012.87.
243. Blumenthal, G.M.; Gills, J.J.; Ballas, M.S.; Bernstein, W.B.; Komiya, T.; Dechowdhury, R.; Morrow, B.; Root, H.; Chun, G.; Helsabeck, C.; et al. A phase I trial of the HIV protease inhibitor nelfinavir in adults with solid tumors. *Oncotarget* **2014**, *5*, 8161-8172, doi:10.18632/oncotarget.2415.
244. Pyrko, P.; Kardosh, A.; Wang, W.; Xiong, W.; Schonthal, A.H.; Chen, T.C. HIV-1 protease inhibitors nelfinavir and atazanavir induce malignant glioma death by triggering endoplasmic reticulum stress. *Cancer Res* **2007**, *67*, 10920-10928, doi:10.1158/0008-5472.CAN-07-0796.
245. Mahameed, M.; Boukeileh, S.; Obiedat, A.; Darawshi, O.; Dipta, P.; Rimon, A.; McLennan, G.; Fassler, R.; Reichmann, D.; Karni, R.; et al. Pharmacological induction of selective endoplasmic reticulum retention as a strategy for cancer therapy. *Nat Commun* **2020**, *11*, 1304, doi:10.1038/s41467-020-15067-5.
246. Chakravarty, G.; Mathur, A.; Mallade, P.; Gerlach, S.; Willis, J.; Datta, A.; Srivastav, S.; Abdel-Mageed, A.B.; Mondal, D. Nelfinavir targets multiple drug resistance mechanisms to increase the efficacy of doxorubicin in MCF-7/Dox breast cancer cells. *Biochimie* **2016**, *124*, 53-64, doi:10.1016/j.biochi.2016.01.014.
247. Guan, M.; Fousek, K.; Jiang, C.; Guo, S.; Synold, T.; Xi, B.; Shih, C.C.; Chow, W.A. Nelfinavir induces liposarcoma apoptosis through inhibition of regulated intramembrane proteolysis of SREBP-1 and ATF6. *Clin Cancer Res* **2011**, *17*, 1796-1806, doi:10.1158/1078-0432.CCR-10-3216.
248. Sakakura, Y.; Shimano, H.; Sone, H.; Takahashi, A.; Inoue, N.; Toyoshima, H.; Suzuki, S.; Yamada, N. Sterol regulatory element-binding proteins induce an entire pathway of cholesterol synthesis. *Biochem Biophys Res Commun* **2001**, *286*, 176-183, doi:10.1006/bbrc.2001.5375.

249. Brown, M.S.; Ye, J.; Rawson, R.B.; Goldstein, J.L. Regulated intramembrane proteolysis: a control mechanism conserved from bacteria to humans. *Cell* **2000**, *100*, 391-398, doi:10.1016/s0092-8674(00)80675-3.
250. Guan, M.; Su, L.; Yuan, Y.C.; Li, H.; Chow, W.A. Nelfinavir and nelfinavir analogs block site-2 protease cleavage to inhibit castration-resistant prostate cancer. *Sci Rep* **2015**, *5*, 9698, doi:10.1038/srep09698.
251. De Gassart, A.; Martinon, F. Translating the anticancer properties of eEF2K. *Cell Cycle* **2017**, *16*, 299-300, doi:10.1080/15384101.2016.1254974.
252. De Gassart, A.; Demaria, O.; Panes, R.; Zaffalon, L.; Ryazanov, A.G.; Gilliet, M.; Martinon, F. Pharmacological eEF2K activation promotes cell death and inhibits cancer progression. *EMBO Rep* **2016**, *17*, 1471-1484, doi:10.15252/embr.201642194.
253. Johnson, C.E.; Hunt, D.K.; Wiltshire, M.; Herbert, T.P.; Sampson, J.R.; Errington, R.J.; Davies, D.M.; Tee, A.R. Endoplasmic reticulum stress and cell death in mTORC1-overactive cells is induced by nelfinavir and enhanced by chloroquine. *Mol Oncol* **2015**, *9*, 675-688, doi:10.1016/j.molonc.2014.11.005.
254. Johnson, C.E.; Dunlop, E.A.; Seifan, S.; McCann, H.D.; Hay, T.; Parfitt, G.J.; Jones, A.T.; Giles, P.J.; Shen, M.H.; Sampson, J.R.; et al. Loss of tuberous sclerosis complex 2 sensitizes tumors to nelfinavir-bortezomib therapy to intensify endoplasmic reticulum stress-induced cell death. *Oncogene* **2018**, *37*, 5913-5925, doi:10.1038/s41388-018-0381-2.
255. Dunlop, E.A.; Johnson, C.E.; Wiltshire, M.; Errington, R.J.; Tee, A.R. Targeting protein homeostasis with nelfinavir/salinomycin dual therapy effectively induces death of mTORC1 hyperactive cells. *Oncotarget* **2017**, *8*, 48711-48724, doi:10.18632/oncotarget.16232.
256. McCann, H.D.; Johnson, C.E.; Errington, R.J.; Davies, D.M.; Dunlop, E.A.; Tee, A.R. Energy Stress-Mediated Cytotoxicity in Tuberous Sclerosis Complex 2-Deficient Cells with Nelfinavir and Mefloquine Treatment. *Cancers (Basel)* **2018**, *10*, doi:10.3390/cancers10100375.
257. Kraus, M.; Bader, J.; Overkleeft, H.; Driessen, C. Nelfinavir augments proteasome inhibition by bortezomib in myeloma cells and overcomes bortezomib and carfilzomib resistance. *Blood Cancer J* **2013**, *3*, e103, doi:10.1038/bcj.2013.2.
258. Kraus, M.; Muller-Ide, H.; Ruckrich, T.; Bader, J.; Overkleeft, H.; Driessen, C. Ritonavir, nelfinavir, saquinavir and lopinavir induce proteotoxic stress in acute myeloid leukemia cells and sensitize them for proteasome inhibitor treatment at low micromolar drug concentrations. *Leuk Res* **2014**, *38*, 383-392, doi:10.1016/j.leukres.2013.12.017.
259. Driessen, C.; Kraus, M.; Joerger, M.; Rosing, H.; Bader, J.; Hitz, F.; Berset, C.; Xyrafas, A.; Hawle, H.; Berthod, G.; et al. Treatment with the HIV protease inhibitor nelfinavir triggers the unfolded protein response and may overcome proteasome inhibitor resistance of multiple myeloma in combination with bortezomib: a phase I trial (SAKK 65/08). *Haematologica* **2016**, *101*, 346-355, doi:10.3324/haematol.2015.135780.
260. Hitz, F.; Kraus, M.; Pabst, T.; Hess, D.; Besse, L.; Silzle, T.; Novak, U.; Seipel, K.; Rondeau, S.; Studeli, S.; et al. Nelfinavir and lenalidomide/dexamethasone in patients with lenalidomide-refractory multiple myeloma. A phase I/II Trial (SAKK 39/10). *Blood Cancer J* **2019**, *9*, 70, doi:10.1038/s41408-019-0228-2.
261. Mahoney, E.; Maddocks, K.; Flynn, J.; Jones, J.; Cole, S.L.; Zhang, X.; Byrd, J.C.; Johnson, A.J. Identification of endoplasmic reticulum stress-inducing agents by

- antagonizing autophagy: a new potential strategy for identification of anti-cancer therapeutics in B-cell malignancies. *Leuk Lymphoma* **2013**, *54*, 2685-2692, doi:10.3109/10428194.2013.781168.
262. Yoshii, S.R.; Mizushima, N. Monitoring and Measuring Autophagy. *Int J Mol Sci* **2017**, *18*, doi:10.3390/ijms18091865.
263. Mizushima, N.; Yoshimori, T. How to interpret LC3 immunoblotting. *Autophagy* **2007**, *3*, 542-545, doi:10.4161/auto.4600.
264. Gills, J.J.; Lopiccio, J.; Dennis, P.A. Nelfinavir, a new anti-cancer drug with pleiotropic effects and many paths to autophagy. *Autophagy* **2008**, *4*, 107-109, doi:10.4161/auto.5224.
265. Escalante, A.M.; McGrath, R.T.; Karolak, M.R.; Dorr, R.T.; Lynch, R.M.; Landowski, T.H. Preventing the autophagic survival response by inhibition of calpain enhances the cytotoxic activity of bortezomib in vitro and in vivo. *Cancer Chemother Pharmacol* **2013**, *71*, 1567-1576, doi:10.1007/s00280-013-2156-3.
266. Demarchi, F.; Bertoli, C.; Copetti, T.; Tanida, I.; Brancolini, C.; Eskelinen, E.-L.; Schneider, C. Calpain is required for macroautophagy in mammalian cells. *J Cell Biol* **2006**, *175*, 595-605, doi:10.1083/jcb.200601024.
267. Navon, A.; Ciechanover, A. The 26 S proteasome: from basic mechanisms to drug targeting. *J Biol Chem* **2009**, *284*, 33713-33718, doi:10.1074/jbc.R109.018481.
268. Dimopoulos, M.A.; Moreau, P.; Palumbo, A.; Joshua, D.; Pour, L.; Hajek, R.; Facon, T.; Ludwig, H.; Oriol, A.; Goldschmidt, H.; et al. Carfilzomib and dexamethasone versus bortezomib and dexamethasone for patients with relapsed or refractory multiple myeloma (ENDEAVOR): a randomised, phase 3, open-label, multicentre study. *Lancet Oncol* **2016**, *17*, 27-38, doi:10.1016/S1470-2045(15)00464-7.
269. Groll, M.; Berkers, C.R.; Ploegh, H.L.; Ovaas, H. Crystal structure of the boronic acid-based proteasome inhibitor bortezomib in complex with the yeast 20S proteasome. *Structure* **2006**, *14*, 451-456, doi:10.1016/j.str.2005.11.019.
270. Demo, S.D.; Kirk, C.J.; Aujay, M.A.; Buchholz, T.J.; Dajee, M.; Ho, M.N.; Jiang, J.; Laidig, G.J.; Lewis, E.R.; Parlanti, F.; et al. Antitumor activity of PR-171, a novel irreversible inhibitor of the proteasome. *Cancer Res* **2007**, *67*, 6383-6391, doi:10.1158/0008-5472.CAN-06-4086.
271. Besse, A.; Stolze, S.C.; Rasche, L.; Weinhold, N.; Morgan, G.J.; Kraus, M.; Bader, J.; Overkleeft, H.S.; Besse, L.; Driessen, C. Carfilzomib resistance due to ABCB1/MDR1 overexpression is overcome by nelfinavir and lopinavir in multiple myeloma. *Leukemia* **2018**, *32*, 391-401, doi:10.1038/leu.2017.212.
272. Shim, J.S.; Rao, R.; Beebe, K.; Neckers, L.; Han, I.; Nahta, R.; Liu, J.O. Selective inhibition of HER2-positive breast cancer cells by the HIV protease inhibitor nelfinavir. *J Natl Cancer Inst* **2012**, *104*, 1576-1590, doi:10.1093/jnci/djs396.
273. Gupta, A.K.; Li, B.; Cerniglia, G.J.; Ahmed, M.S.; Hahn, S.M.; Maity, A. The HIV protease inhibitor nelfinavir downregulates Akt phosphorylation by inhibiting proteasomal activity and inducing the unfolded protein response. *Neoplasia* **2007**, *9*, 271-278, doi:10.1593/neo.07124.
274. Pajonk, F.; Himmelsbach, J.; Riess, K.; Sommer, A.; McBride, W.H. The human immunodeficiency virus (HIV)-1 protease inhibitor saquinavir inhibits proteasome function and causes apoptosis and radiosensitization in non-HIV-associated human cancer cells. *Cancer Res* **2002**, *62*, 5230-5235.

275. Piccinini, M.; Rinaudo, M.T.; Anselmino, A.; Buccinnà, B.; Ramondetti, C.; Dematteis, A.; Ricotti, E.; Palmisano, L.; Mostert, M.; Tovo, P.A. The HIV protease inhibitors nelfinavir and saquinavir, but not a variety of HIV reverse transcriptase inhibitors, adversely affect human proteasome function. *Antivir Ther* **2005**, *10*, 215-223.
276. Fassmannová, D.; Sedlák, F.; Sedláček, J.; Špička, I.; Grantz Šašková, K. Nelfinavir Inhibits the TCF11/Nrf1-Mediated proteasome recovery pathway in multiple myeloma. *Cancers* **2020**, *12*, 1065.
277. Alfano, L.; Guida, T.; Provitera, L.; Vecchio, G.; Billaud, M.; Santoro, M.; Carlomagno, F. RET is a heat shock protein 90 (HSP90) client protein and is knocked down upon HSP90 pharmacological block. *J Clin Endocrinol Metab* **2010**, *95*, 3552-3557, doi:10.1210/jc.2009-2315.
278. Carlomagno, F.; Guida, T.; Anaganti, S.; Vecchio, G.; Fusco, A.; Ryan, A.J.; Billaud, M.; Santoro, M. Disease associated mutations at valine 804 in the RET receptor tyrosine kinase confer resistance to selective kinase inhibitors. *Oncogene* **2004**, *23*, 6056-6063, doi:10.1038/sj.onc.1207810.
279. Petrich, A.M.; Leshchenko, V.; Kuo, P.Y.; Xia, B.; Thirukonda, V.K.; Ulahannan, N.; Gordon, S.; Fazzari, M.J.; Ye, B.H.; Sparano, J.A.; et al. Akt inhibitors MK-2206 and nelfinavir overcome mTOR inhibitor resistance in diffuse large B-cell lymphoma. *Clin Cancer Res* **2012**, *18*, 2534-2544, doi:10.1158/1078-0432.CCR-11-1407.
280. Goda, J.S.; Pachpor, T.; Basu, T.; Chopra, S.; Gota, V. Targeting the AKT pathway: Repositioning HIV protease inhibitors as radiosensitizers. *Indian J Med Res* **2016**, *143*, 145-159, doi:10.4103/0971-5916.180201.
281. Bernhard, E.J.; Brunner, T.B. Progress towards the use of HIV protease inhibitors in cancer therapy. *Cancer Biol Ther* **2008**, *7*, 636-637, doi:10.4161/cbt.7.5.6087.
282. Gupta, A.K.; Lee, J.H.; Wilke, W.W.; Quon, H.; Smith, G.; Maity, A.; Buatti, J.M.; Spitz, D.R. Radiation response in two HPV-infected head-and-neck cancer cell lines in comparison to a non-HPV-infected cell line and relationship to signaling through AKT. *Int J Radiat Oncol Biol Phys* **2009**, *74*, 928-933, doi:10.1016/j.ijrobp.2009.03.004.
283. Jiang, Z.; Pore, N.; Cerniglia, G.J.; Mick, R.; Georgescu, M.M.; Bernhard, E.J.; Hahn, S.M.; Gupta, A.K.; Maity, A. Phosphatase and tensin homologue deficiency in glioblastoma confers resistance to radiation and temozolomide that is reversed by the protease inhibitor nelfinavir. *Cancer Res* **2007**, *67*, 4467-4473, doi:10.1158/0008-5472.CAN-06-3398.
284. Kimple, R.J.; Vaseva, A.V.; Cox, A.D.; Baerman, K.M.; Calvo, B.F.; Tepper, J.E.; Shields, J.M.; Sartor, C.I. Radiosensitization of epidermal growth factor receptor/HER2-positive pancreatic cancer is mediated by inhibition of Akt independent of ras mutational status. *Clin Cancer Res* **2010**, *16*, 912-923, doi:10.1158/1078-0432.CCR-09-1324.
285. Cuneo, K.C.; Tu, T.; Geng, L.; Fu, A.; Hallahan, D.E.; Willey, C.D. HIV protease inhibitors enhance the efficacy of irradiation. *Cancer Res* **2007**, *67*, 4886-4893, doi:10.1158/0008-5472.CAN-06-3684.
286. Pore, N.; Gupta, A.K.; Cerniglia, G.J.; Jiang, Z.; Bernhard, E.J.; Evans, S.M.; Koch, C.J.; Hahn, S.M.; Maity, A. Nelfinavir down-regulates hypoxia-inducible factor 1alpha and VEGF expression and increases tumor oxygenation: implications for radiotherapy. *Cancer Res* **2006**, *66*, 9252-9259, doi:10.1158/0008-5472.CAN-06-1239.

287. Pore, N.; Gupta, A.K.; Cerniglia, G.J.; Maity, A. HIV protease inhibitors decrease VEGF/HIF-1 α expression and angiogenesis in glioblastoma cells. *Neoplasia* **2006**, *8*, 889-895, doi:10.1593/neo.06535.
288. Zeng, J.; See, A.P.; Aziz, K.; Thiyagarajan, S.; Salih, T.; Gajula, R.P.; Armour, M.; Phallen, J.; Terezakis, S.; Kleinberg, L.; et al. Nelfinavir induces radiation sensitization in pituitary adenoma cells. *Cancer Biol Ther* **2011**, *12*, 657-663, doi:10.4161/cbt.12.7.17172.
289. Plastaras, J.P.; Vapiwala, N.; Ahmed, M.S.; Gudonis, D.; Cerniglia, G.J.; Feldman, M.D.; Frank, I.; Gupta, A.K. Validation and toxicity of PI3K/Akt pathway inhibition by HIV protease inhibitors in humans. *Cancer Biol Ther* **2008**, *7*, 628-635, doi:10.4161/cbt.7.5.5728.
290. Brunner, T.B.; Geiger, M.; Grabenbauer, G.G.; Lang-Welzenbach, M.; Manton, T.S.; Cavallaro, A.; Sauer, R.; Hohenberger, W.; McKenna, W.G. Phase I trial of the human immunodeficiency virus protease inhibitor nelfinavir and chemoradiation for locally advanced pancreatic cancer. *J Clin Oncol* **2008**, *26*, 2699-2706, doi:10.1200/JCO.2007.15.2355.
291. Gupta, A.K.; Wilke, W.W.; Taylor, E.N.; Bodeker, K.L.; Hoffman, H.T.; Milhem, M.M.; Buatti, J.M.; Robinson, R.A. Signaling pathways in adenoid cystic cancers: implications for treatment. *Cancer Biol Ther* **2009**, *8*, 1947-1951, doi:10.4161/cbt.8.20.9596.
292. Hoover, A.C.; Milhem, M.M.; Anderson, C.M.; Sun, W.; Smith, B.J.; Hoffman, H.T.; Buatti, J.M. Efficacy of nelfinavir as monotherapy in refractory adenoid cystic carcinoma: Results of a phase II clinical trial. *Head Neck* **2015**, *37*, 722-726, doi:10.1002/hed.23664.
293. Liebscher, S.; Koi, L.; Lock, S.; Muders, M.H.; Krause, M. The HIV protease and PI3K/Akt inhibitor nelfinavir does not improve the curative effect of fractionated irradiation in PC-3 prostate cancer in vitro and in vivo. *Clin Transl Radiat Oncol* **2017**, *2*, 7-12, doi:10.1016/j.ctro.2016.12.002.
294. Bruning, A. Targeting the off-targets: a computational bioinformatics approach to understanding the polypharmacology of nelfinavir. *Expert Rev Clin Pharmacol* **2011**, *4*, 571-573, doi:10.1586/ecp.11.37.
295. Xie, L.; Evangelidis, T.; Xie, L.; Bourne, P.E. Drug discovery using chemical systems biology: weak inhibition of multiple kinases may contribute to the anti-cancer effect of nelfinavir. *PLoS Comput Biol* **2011**, *7*, e1002037, doi:10.1371/journal.pcbi.1002037.
296. Ikezoe, T.; Saito, T.; Bandobashi, K.; Yang, Y.; Koeffler, H.P.; Taguchi, H. HIV-1 protease inhibitor induces growth arrest and apoptosis of human multiple myeloma cells via inactivation of signal transducer and activator of transcription 3 and extracellular signal-regulated kinase 1/2. *Mol Cancer Ther* **2004**, *3*, 473-479.
297. Smith, M.P.; Brunton, H.; Rowling, E.J.; Ferguson, J.; Arozarena, I.; Miskolczi, Z.; Lee, J.L.; Girotti, M.R.; Marais, R.; Levesque, M.P.; et al. Inhibiting Drivers of Non-mutational Drug Tolerance Is a Salvage Strategy for Targeted Melanoma Therapy. *Cancer Cell* **2016**, *29*, 270-284, doi:10.1016/j.ccell.2016.02.003.
298. Bali, P.; Pranpat, M.; Bradner, J.; Balasis, M.; Fiskus, W.; Guo, F.; Rocha, K.; Kumaraswamy, S.; Boyapalle, S.; Atadja, P.; et al. Inhibition of histone deacetylase 6 acetylates and disrupts the chaperone function of heat shock protein 90: a novel basis for antileukemia activity of histone deacetylase inhibitors. *J Biol Chem* **2005**, *280*, 26729-26734, doi:10.1074/jbc.C500186200.
299. Liu, J.; Wang, Z. Increased Oxidative Stress as a Selective Anticancer Therapy. *Oxid Med Cell Longev* **2015**, *2015*, 294303, doi:10.1155/2015/294303.

300. Kushchayeva, Y.; Jensen, K.; Burman, K.D.; Vasko, V. Repositioning therapy for thyroid cancer: new insights on established medications. *Endocr Relat Cancer* **2014**, *21*, R183-194, doi:10.1530/ERC-13-0473.
301. Xia, C.; He, Z.; Liang, S.; Chen, R.; Xu, W.; Yang, J.; Xiao, G.; Jiang, S. Metformin combined with nelfinavir induces SIRT3/mROS-dependent autophagy in human cervical cancer cells and xenograft in nude mice. *Eur J Pharmacol* **2019**, *848*, 62-69, doi:10.1016/j.ejphar.2019.01.045.
302. Chen, Y.; Fu, L.L.; Wen, X.; Wang, X.Y.; Liu, J.; Cheng, Y.; Huang, J. Sirtuin-3 (SIRT3), a therapeutic target with oncogenic and tumor-suppressive function in cancer. *Cell Death Dis* **2014**, *5*, e1047, doi:10.1038/cddis.2014.14.
303. Rockwell, S.; Dobrucki, I.T.; Kim, E.Y.; Marrison, S.T.; Vu, V.T. Hypoxia and radiation therapy: past history, ongoing research, and future promise. *Curr Mol Med* **2009**, *9*, 442-458, doi:10.2174/156652409788167087.
304. Qayum, N.; Im, J.; Stratford, M.R.; Bernhard, E.J.; McKenna, W.G.; Muschel, R.J. Modulation of the tumor microvasculature by phosphoinositide-3 kinase inhibition increases doxorubicin delivery in vivo. *Clin Cancer Res* **2012**, *18*, 161-169, doi:10.1158/1078-0432.CCR-11-1413.
305. Bourlier, V.; Zakaroff-Girard, A.; De Barros, S.; Pizzacalla, C.; de Saint Front, V.D.; Lafontan, M.; Bouloumie, A.; Galitzky, J. Protease inhibitor treatments reveal specific involvement of matrix metalloproteinase-9 in human adipocyte differentiation. *J Pharmacol Exp Ther* **2005**, *312*, 1272-1279, doi:10.1124/jpet.104.077263.
306. Kast, R.E.; Halatsch, M.E. Matrix metalloproteinase-2 and -9 in glioblastoma: a trio of old drugs-captopril, disulfiram and nelfinavir-are inhibitors with potential as adjunctive treatments in glioblastoma. *Arch Med Res* **2012**, *43*, 243-247, doi:10.1016/j.arcmed.2012.04.005.
307. Al-Assar, O.; Bittner, M.I.; Lunardi, S.; Stratford, M.R.; McKenna, W.G.; Brunner, T.B. The radiosensitizing effects of Nelfinavir on pancreatic cancer with and without pancreatic stellate cells. *Radiother Oncol* **2016**, *119*, 300-305, doi:10.1016/j.radonc.2016.03.024.
308. Darini, C.Y.; Martin, P.; Azoulay, S.; Drici, M.D.; Hofman, P.; Obba, S.; Dani, C.; Ladoux, A. Targeting cancer stem cells expressing an embryonic signature with anti-proteases to decrease their tumor potential. *Cell Death Dis* **2013**, *4*, e706, doi:10.1038/cddis.2013.206.
309. Giardino Torchia, M.L.; Ciaglia, E.; Masci, A.M.; Vitiello, L.; Fogli, M.; la Sala, A.; Mavilio, D.; Racioppi, L. Dendritic cells/natural killer cross-talk: a novel target for human immunodeficiency virus type-1 protease inhibitors. *PLoS One* **2010**, *5*, e11052, doi:10.1371/journal.pone.0011052.
310. Rees, D.C.; Johnson, E.; Lewinson, O. ABC transporters: the power to change. *Nat Rev Mol Cell Biol* **2009**, *10*, 218-227, doi:10.1038/nrm2646.
311. Misra, S.; Ghatak, S.; Toole, B.P. Regulation of MDR1 expression and drug resistance by a positive feedback loop involving hyaluronan, phosphoinositide 3-kinase, and ErbB2. *J Biol Chem* **2005**, *280*, 20310-20315, doi:10.1074/jbc.M500737200.
312. Kim, J.Y.; Park, Y.J.; Lee, B.M.; Yoon, S. Co-treatment With HIV Protease Inhibitor Nelfinavir Greatly Increases Late-phase Apoptosis of Drug-resistant KBV20C Cancer Cells Independently of P-Glycoprotein Inhibition. *Anticancer Res* **2019**, *39*, 3757-3765, doi:10.21873/anticancer.13524.
313. Lucia, M.B.; Anu, R.; Handley, M.; Gillet, J.P.; Wu, C.P.; De Donatis, G.M.; Cauda, R.; Gottesman, M.M. Exposure to HIV-protease inhibitors selects for increased expression of

- P-glycoprotein (ABCB1) in Kaposi's sarcoma cells. *Br J Cancer* **2011**, *105*, 513-522, doi:10.1038/bjc.2011.275.
314. Perloff, M.D.; von Moltke, L.L.; Fahey, J.M.; Daily, J.P.; Greenblatt, D.J. Induction of P-glycoprotein expression by HIV protease inhibitors in cell culture. *AIDS* **2000**, *14*, 1287-1289, doi:10.1097/00002030-200006160-00034.
315. Gupta, A.; Zhang, Y.; Unadkat, J.D.; Mao, Q. HIV protease inhibitors are inhibitors but not substrates of the human breast cancer resistance protein (BCRP/ABCG2). *J Pharmacol Exp Ther* **2004**, *310*, 334-341, doi:10.1124/jpet.104.065342.
316. Fukuda, Y.; Takenaka, K.; Sparreboom, A.; Cheepala, S.B.; Wu, C.P.; Ekins, S.; Ambudkar, S.V.; Schuetz, J.D. Human immunodeficiency virus protease inhibitors interact with ATP binding cassette transporter 4/multidrug resistance protein 4: a basis for unanticipated enhanced cytotoxicity. *Mol Pharmacol* **2013**, *84*, 361-371, doi:10.1124/mol.113.086967.
317. Rengan, R.; Mick, R.; Pryma, D.; Rosen, M.A.; Lin, L.L.; Maity, A.M.; Evans, T.L.; Stevenson, J.P.; Langer, C.J.; Kucharczuk, J.; et al. A phase I trial of the HIV protease inhibitor nelfinavir with concurrent chemoradiotherapy for unresectable stage IIIA/IIIB non-small cell lung cancer: a report of toxicities and clinical response. *J Thorac Oncol* **2012**, *7*, 709-715, doi:10.1097/JTO.0b013e3182435aa6.
318. Rengan, R.; Mick, R.; Pryma, D.A.; Lin, L.L.; Christodouleas, J.; Plastaras, J.P.; Simone, C.B., 2nd; Gupta, A.K.; Evans, T.L.; Stevenson, J.P.; et al. Clinical Outcomes of the HIV Protease Inhibitor Nelfinavir With Concurrent Chemoradiotherapy for Unresectable Stage IIIA/IIIB Non-Small Cell Lung Cancer: A Phase 1/2 Trial. *JAMA Oncol* **2019**, doi:10.1001/jamaoncol.2019.2095.
319. Wilson, J.M.; Fokas, E.; Dutton, S.J.; Patel, N.; Hawkins, M.A.; Eccles, C.; Chu, K.Y.; Durrant, L.; Abraham, A.G.; Partridge, M.; et al. ARCII: A phase II trial of the HIV protease inhibitor Nelfinavir in combination with chemoradiation for locally advanced inoperable pancreatic cancer. *Radiother Oncol* **2016**, *119*, 306-311, doi:10.1016/j.radonc.2016.03.021.
320. Strauss, V.Y.; Shaw, R.; Virdee, P.S.; Hurt, C.N.; Ward, E.; Tranter, B.; Patel, N.; Bridgewater, J.; Parsons, P.; Radhakrishna, G.; et al. Study protocol: a multi-centre randomised study of induction chemotherapy followed by capecitabine +/- nelfinavir with high- or standard-dose radiotherapy for locally advanced pancreatic cancer (SCALOP-2). *BMC Cancer* **2019**, *19*, 121, doi:10.1186/s12885-019-5307-z.
321. Lin, C.; Verma, V.; Ly, Q.P.; Lazenby, A.; Sasson, A.; Schwarz, J.K.; Meza, J.L.; Are, C.; Li, S.; Wang, S.; et al. Phase I trial of concurrent stereotactic body radiotherapy and nelfinavir for locally advanced borderline or unresectable pancreatic adenocarcinoma. *Radiother Oncol* **2019**, *132*, 55-62, doi:10.1016/j.radonc.2018.11.002.
322. Lin, C.; Verma, V.; Lazenby, A.; Ly, Q.P.; Berim, L.D.; Schwarz, J.K.; Madiyalakan, M.; Nicodemus, C.F.; Hollingsworth, M.A.; Meza, J.L.; et al. Phase I/II Trial of Neoadjuvant Oregovomab-based Chemoimmunotherapy Followed by Stereotactic Body Radiotherapy and Nelfinavir For Locally Advanced Pancreatic Adenocarcinoma. *Am J Clin Oncol* **2019**, *42*, 755-760, doi:10.1097/COC.0000000000000599.
323. Pan, J.; Mott, M.; Xi, B.; Hepner, E.; Guan, M.; Fousek, K.; Magnusson, R.; Tinsley, R.; Valdes, F.; Frankel, P.; et al. Phase I study of nelfinavir in liposarcoma. *Cancer Chemother Pharmacol* **2012**, *70*, 791-799, doi:10.1007/s00280-012-1961-4.

324. Leung-Hagesteijn, C.; Erdmann, N.; Cheung, G.; Keats, J.J.; Stewart, A.K.; Reece, D.E.; Chung, K.C.; Tiedemann, R.E. Xbpl1-negative tumor B cells and pre-plasmablasts mediate therapeutic proteasome inhibitor resistance in multiple myeloma. *Cancer Cell* **2013**, *24*, 289-304, doi:10.1016/j.ccr.2013.08.009.
325. Hill, E.J.; Roberts, C.; Franklin, J.M.; Enescu, M.; West, N.; MacGregor, T.P.; Chu, K.Y.; Boyle, L.; Blesing, C.; Wang, L.M.; et al. Clinical Trial of Oral Nelfinavir before and during Radiation Therapy for Advanced Rectal Cancer. *Clin Cancer Res* **2016**, *22*, 1922-1931, doi:10.1158/1078-0432.CCR-15-1489.
326. Buijsen, J.; Lammering, G.; Jansen, R.L.; Beets, G.L.; Wals, J.; Sosef, M.; Den Boer, M.O.; Leijtens, J.; Riedl, R.G.; Theys, J.; et al. Phase I trial of the combination of the Akt inhibitor nelfinavir and chemoradiation for locally advanced rectal cancer. *Radiother Oncol* **2013**, *107*, 184-188, doi:10.1016/j.radonc.2013.03.023.
327. Bernstein, W.B.; Dennis, P.A. Repositioning HIV protease inhibitors as cancer therapeutics. *Curr Opin HIV AIDS* **2008**, *3*, 666-675, doi:10.1097/COH.0b013e328313915d.
328. Alonso-Basanta, M.; Fang, P.; Maity, A.; Hahn, S.M.; Lustig, R.A.; Dorsey, J.F. A phase I study of nelfinavir concurrent with temozolomide and radiotherapy in patients with glioblastoma multiforme. *J Neurooncol* **2014**, *116*, 365-372, doi:10.1007/s11060-013-1303-3.
329. Kattel, K.; Evande, R.; Tan, C.; Mondal, G.; Grem, J.L.; Mahato, R.I. Impact of CYP2C19 polymorphism on the pharmacokinetics of nelfinavir in patients with pancreatic cancer. *Br J Clin Pharmacol* **2015**, *80*, 267-275, doi:10.1111/bcp.12620.
330. Evans, T.; Matulonis, U. Next-Generation Sequencing: Role in Gynecologic Cancers. *J Natl Compr Canc Netw* **2016**, *14*, 1165-1173, doi:10.6004/jncn.2016.0123.
331. Ota, S.; Ushijima, K.; Fujiyoshi, N.; Fujimoto, T.; Hayashi, R.; Murakami, F.; Komai, K.; Fujiyoshi, K.; Hori, D.; Kamura, T. Desmoplastic small round cell tumor in the ovary: Report of two cases and literature review. *J Obstet Gynaecol Res* **2010**, *36*, 430-434, doi:10.1111/j.1447-0756.2009.01126.x.
332. Ushijima, K. Treatment for recurrent ovarian cancer-at first relapse. *J Oncol* **2010**, *2010*, 497429, doi:10.1155/2010/497429.
333. Avril, T.; Vauleon, E.; Chevet, E. Endoplasmic reticulum stress signaling and chemotherapy resistance in solid cancers. *Oncogenesis* **2017**, *6*, e373, doi:10.1038/oncsis.2017.72.
334. Schonthal, A.H. Pharmacological targeting of endoplasmic reticulum stress signaling in cancer. *Biochem Pharmacol* **2013**, *85*, 653-666, doi:10.1016/j.bcp.2012.09.012.
335. Samanta, S.; Tamura, S.; Dubeau, L.; Mhaweche-Fauceglia, P.; Miyagi, Y.; Kato, H.; Lieberman, R.; Buckanovich, R.J.; Lin, Y.G.; Neamati, N. Clinicopathological significance of endoplasmic reticulum stress proteins in ovarian carcinoma. *Sci Rep* **2020**, *10*, 2160, doi:10.1038/s41598-020-59116-x.
336. Zhang, L.; Hapon, M.B.; Goyeneche, A.A.; Srinivasan, R.; Gamarra-Luques, C.D.; Callegari, E.A.; Drapeau, D.D.; Terpstra, E.J.; Pan, B.; Knapp, J.R.; et al. Mifepristone increases mRNA translation rate, triggers the unfolded protein response, increases autophagic flux, and kills ovarian cancer cells in combination with proteasome or lysosome inhibitors. *Mol Oncol* **2016**, *10*, 1099-1117, doi:10.1016/j.molonc.2016.05.001.

337. Langdon, S.P.; Lawrie, S.S.; Hay, F.G.; Hawkes, M.M.; McDonald, A.; Hayward, I.P.; Schol, D.J.; Hilgers, J.; Leonard, R.C.; Smyth, J.F. Characterization and properties of nine human ovarian adenocarcinoma cell lines. *Cancer Res* **1988**, *48*, 6166-6172.
338. Andrews, P.A.; Albright, K.D. Mitochondrial defects in cis-diamminedichloroplatinum(II)-resistant human ovarian carcinoma cells. *Cancer Res* **1992**, *52*, 1895-1901.
339. Korch, C.; Spillman, M.A.; Jackson, T.A.; Jacobsen, B.M.; Murphy, S.K.; Lessey, B.A.; Jordan, V.C.; Bradford, A.P. DNA profiling analysis of endometrial and ovarian cell lines reveals misidentification, redundancy and contamination. *Gynecol Oncol* **2012**, *127*, 241-248, doi:10.1016/j.ygyno.2012.06.017.
340. Freeburg, E.M.; Goyeneche, A.A.; Seidel, E.E.; Telleria, C.M. Resistance to cisplatin does not affect sensitivity of human ovarian cancer cell lines to mifepristone cytotoxicity. *Cancer Cell Int* **2009**, *9*, 4, doi:10.1186/1475-2867-9-4.
341. Freeburg, E.M.; Goyeneche, A.A.; Telleria, C.M. Mifepristone abrogates repopulation of ovarian cancer cells in between courses of cisplatin treatment. *Int J Oncol* **2009**, *34*, 743-755, doi:10.3892/ijo_00000200.
342. Taylor, S.C.; Berkelman, T.; Yadav, G.; Hammond, M. A defined methodology for reliable quantification of Western blot data. *Mol Biotechnol* **2013**, *55*, 217-226, doi:10.1007/s12033-013-9672-6.
343. Chou, T.C.; Motzer, R.J.; Tong, Y.; Bosl, G.J. Computerized quantitation of synergism and antagonism of taxol, topotecan, and cisplatin against human teratocarcinoma cell growth: a rational approach to clinical protocol design. *J Natl Cancer Inst* **1994**, *86*, 1517-1524.
344. Gamarra-Luques, C.D.; Goyeneche, A.A.; Hapon, M.B.; Telleria, C.M. Mifepristone prevents repopulation of ovarian cancer cells escaping cisplatin-paclitaxel therapy. *BMC Cancer* **2012**, *12*, 200, doi:10.1186/1471-2407-12-200.
345. Lee, A.S. Glucose-regulated proteins in cancer: molecular mechanisms and therapeutic potential. *Nat Rev Cancer* **2014**, *14*, 263-276, doi:10.1038/nrc3701.
346. Oyadomari, S.; Mori, M. Roles of CHOP/GADD153 in endoplasmic reticulum stress. *Cell Death Differ* **2004**, *11*, 381-389, doi:10.1038/sj.cdd.4401373.
347. Clarke, H.J.; Chambers, J.E.; Liniker, E.; Marciniak, S.J. Endoplasmic reticulum stress in malignancy. *Cancer Cell* **2014**, *25*, 563-573, doi:10.1016/j.ccr.2014.03.015.
348. Gardner, B.M.; Pincus, D.; Gotthardt, K.; Gallagher, C.M.; Walter, P. Endoplasmic reticulum stress sensing in the unfolded protein response. *Cold Spring Harb Perspect Biol* **2013**, *5*, a013169, doi:10.1101/cshperspect.a013169.
349. Nagelkerke, A.; Bussink, J.; Sweep, F.C.; Span, P.N. The unfolded protein response as a target for cancer therapy. *Biochim Biophys Acta* **2014**, *1846*, 277-284, doi:10.1016/j.bbcan.2014.07.006.
350. Ojha, R.; Amaravadi, R.K. Targeting the unfolded protein response in cancer. *Pharmacol Res* **2017**, *120*, 258-266, doi:10.1016/j.phrs.2017.04.003.
351. Miyake, H.; Hara, I.; Arakawa, S.; Kamidono, S. Stress protein GRP78 prevents apoptosis induced by calcium ionophore, ionomycin, but not by glycosylation inhibitor, tunicamycin, in human prostate cancer cells. *J Cell Biochem* **2000**, *77*, 396-408, doi:10.1002/(sici)1097-4644(20000601)77:3<396::aid-jcb5>3.0.co;2-5.
352. Noda, I.; Fujieda, S.; Seki, M.; Tanaka, N.; Sunaga, H.; Ohtsubo, T.; Tsuzuki, H.; Fan, G.K.; Saito, H. Inhibition of N-linked glycosylation by tunicamycin enhances sensitivity

- to cisplatin in human head-and-neck carcinoma cells. *Int J Cancer* **1999**, *80*, 279-284, doi:10.1002/(sici)1097-0215(19990118)80:2<279::aid-ijc18>3.0.co;2-n.
353. Al-Bari, M.A.A.; Ito, Y.; Ahmed, S.; Radwan, N.; Ahmed, H.S.; Eid, N. Targeting Autophagy with Natural Products as a Potential Therapeutic Approach for Cancer. *Int J Mol Sci* **2021**, *22*, doi:10.3390/ijms22189807.
354. Rubinsztein, D.C.; Codogno, P.; Levine, B. Autophagy modulation as a potential therapeutic target for diverse diseases. *Nat Rev Drug Discov* **2012**, *11*, 709-730, doi:10.1038/nrd3802.
355. Yang, K.C.; Sathiyaseelan, P.; Ho, C.; Gorski, S.M. Evolution of tools and methods for monitoring autophagic flux in mammalian cells. *Biochem Soc Trans* **2018**, *46*, 97-110, doi:10.1042/BST20170102.
356. Lemus, L.; Goder, V. Regulation of Endoplasmic Reticulum-Associated Protein Degradation (ERAD) by Ubiquitin. *Cells* **2014**, *3*, 824-847, doi:10.3390/cells3030824.
357. Bao, M.; Qian, Y.; Su, H.; Wu, B.; Qiu, L.; Hu, W.; Xu, X. Gold(I)-Catalyzed and H₂O-Mediated Carbene Cascade Reaction of Propargyl Diazoacetates: Furan Synthesis and Mechanistic Insights. *Org Lett* **2018**, *20*, 5332-5335, doi:10.1021/acs.orglett.8b02251.
358. Ri, M. Endoplasmic-reticulum stress pathway-associated mechanisms of action of proteasome inhibitors in multiple myeloma. *Int J Hematol* **2016**, *104*, 273-280, doi:10.1007/s12185-016-2016-0.
359. Koromilas, A.E. Roles of the translation initiation factor eIF2alpha serine 51 phosphorylation in cancer formation and treatment. *Biochim Biophys Acta* **2015**, *1849*, 871-880, doi:10.1016/j.bbagr.2014.12.007.
360. Bhat, M.; Robichaud, N.; Hulea, L.; Sonenberg, N.; Pelletier, J.; Topisirovic, I. Targeting the translation machinery in cancer. *Nat Rev Drug Discov* **2015**, *14*, 261-278, doi:10.1038/nrd4505.
361. Boyce, M.; Bryant, K.F.; Jousse, C.; Long, K.; Harding, H.P.; Scheuner, D.; Kaufman, R.J.; Ma, D.; Coen, D.M.; Ron, D.; et al. A selective inhibitor of eIF2alpha dephosphorylation protects cells from ER stress. *Science* **2005**, *307*, 935-939, doi:10.1126/science.1101902.
362. Gao, B.; Zhang, X.Y.; Han, R.; Zhang, T.T.; Chen, C.; Qin, Z.H.; Sheng, R. The endoplasmic reticulum stress inhibitor salubrinal inhibits the activation of autophagy and neuroprotection induced by brain ischemic preconditioning. *Acta Pharmacol Sin* **2013**, *34*, 657-666, doi:10.1038/aps.2013.34.
363. Gong, T.; Wang, Q.; Lin, Z.; Chen, M.L.; Sun, G.Z. Endoplasmic reticulum (ER) stress inhibitor salubrinal protects against ceramide-induced SH-SY5Y cell death. *Biochem Biophys Res Commun* **2012**, *427*, 461-465, doi:10.1016/j.bbrc.2012.08.068.
364. Wang, Q.E.; Milum, K.; Han, C.; Huang, Y.W.; Wani, G.; Thomale, J.; Wani, A.A. Differential contributory roles of nucleotide excision and homologous recombination repair for enhancing cisplatin sensitivity in human ovarian cancer cells. *Mol Cancer* **2011**, *10*, 24, doi:10.1186/1476-4598-10-24.
365. Visconti, R.; Della Monica, R.; Grieco, D. Cell cycle checkpoint in cancer: a therapeutically targetable double-edged sword. *J Exp Clin Cancer Res* **2016**, *35*, 153, doi:10.1186/s13046-016-0433-9.
366. Matthews, H.K.; Bertoli, C.; de Bruin, R.A.M. Cell cycle control in cancer. *Nat Rev Mol Cell Biol* **2021**, doi:10.1038/s41580-021-00404-3.

367. Chu, I.M.; Hengst, L.; Slingerland, J.M. The Cdk inhibitor p27 in human cancer: prognostic potential and relevance to anticancer therapy. *Nat Rev Cancer* **2008**, *8*, 253-267, doi:10.1038/nrc2347.
368. Cassimere, E.K.; Mauvais, C.; Denicourt, C. p27Kip1 Is Required to Mediate a G1 Cell Cycle Arrest Downstream of ATM following Genotoxic Stress. *PLoS One* **2016**, *11*, e0162806, doi:10.1371/journal.pone.0162806.
369. D'Andrilli, G.; Giordano, A.; Bovicelli, A. Epithelial ovarian cancer: the role of cell cycle genes in the different histotypes. *Open Clin Cancer J* **2008**, *2*, 7-12, doi:10.2174/1874189400802010007.
370. Roeten, M.S.F.; Cloos, J.; Jansen, G. Positioning of proteasome inhibitors in therapy of solid malignancies. *Cancer Chemother Pharmacol* **2018**, *81*, 227-243, doi:10.1007/s00280-017-3489-0.
371. Giai, M.; Biglia, N.; Sismondi, P. Chemoresistance in breast tumors. *Eur J Gynaecol Oncol* **1991**, *12*, 359-373.
372. Nagai, N.; Ogata, H.; Wada, Y.; Tsujino, D.; Someya, K.; Ohno, T.; Masuhara, K.; Tanaka, Y.; Takahashi, H.; Nagai, H.; et al. Population pharmacokinetics and pharmacodynamics of cisplatin in patients with cancer: analysis with the NONMEM program. *J Clin Pharmacol* **1998**, *38*, 1025-1034, doi:10.1177/009127009803801107.
373. Michael lisisio. Thesis. Available online: <https://escholarship.mcgill.ca/concern/theses/d791sj55t> (accessed on
374. Domcke, S.; Sinha, R.; Levine, D.A.; Sander, C.; Schultz, N. Evaluating cell lines as tumour models by comparison of genomic profiles. *Nat Commun* **2013**, *4*, 2126, doi:10.1038/ncomms3126.
375. Beaufort, C.M.; Helmijr, J.C.; Piskorz, A.M.; Hoogstraat, M.; Ruigrok-Ritstier, K.; Besselink, N.; Murtaza, M.; van, I.W.F.; Heine, A.A.; Smid, M.; et al. Ovarian cancer cell line panel (OCCP): clinical importance of in vitro morphological subtypes. *PLoS One* **2014**, *9*, e103988, doi:10.1371/journal.pone.0103988.
376. Bao, Y. Chromatin response to DNA double-strand break damage. *Epigenomics* **2011**, *3*, 307-321, doi:10.2217/epi.11.14.
377. Hetz, C. The unfolded protein response: controlling cell fate decisions under ER stress and beyond. *Nat Rev Mol Cell Biol* **2012**, *13*, 89-102, doi:10.1038/nrm3270.
378. Luo, B.; Lee, A.S. The critical roles of endoplasmic reticulum chaperones and unfolded protein response in tumorigenesis and anticancer therapies. *Oncogene* **2013**, *32*, 805-818, doi:10.1038/onc.2012.130.
379. Rutkowski, D.T.; Kaufman, R.J. That which does not kill me makes me stronger: adapting to chronic ER stress. *Trends Biochem Sci* **2007**, *32*, 469-476, doi:10.1016/j.tibs.2007.09.003.
380. Sano, R.; Reed, J.C. ER stress-induced cell death mechanisms. *Biochim Biophys Acta* **2013**, *1833*, 3460-3470, doi:10.1016/j.bbamcr.2013.06.028.
381. Verfaillie, T.; Garg, A.D.; Agostinis, P. Targeting ER stress induced apoptosis and inflammation in cancer. *Cancer letters* **2013**, *332*, 249-264, doi:10.1016/j.canlet.2010.07.016.
382. Huang, J.; Zhang, L.; Greshock, J.; Colligon, T.A.; Wang, Y.; Ward, R.; Katsaros, D.; Lassus, H.; Butzow, R.; Godwin, A.K.; et al. Frequent genetic abnormalities of the PI3K/AKT pathway in primary ovarian cancer predict patient outcome. *Genes Chromosomes Cancer* **2011**, *50*, 606-618, doi:10.1002/gcc.20883.

383. Martins, F.C.; Santiago, I.; Trinh, A.; Xian, J.; Guo, A.; Sayal, K.; Jimenez-Linan, M.; Deen, S.; Driver, K.; Mack, M.; et al. Combined image and genomic analysis of high-grade serous ovarian cancer reveals PTEN loss as a common driver event and prognostic classifier. *Genome Biol* **2014**, *15*, 526, doi:10.1186/s13059-014-0526-8.
384. Dunn, G.P.; Cheung, H.W.; Agarwalla, P.K.; Thomas, S.; Zektser, Y.; Karst, A.M.; Boehm, J.S.; Weir, B.A.; Berlin, A.M.; Zou, L.; et al. In vivo multiplexed interrogation of amplified genes identifies GAB2 as an ovarian cancer oncogene. *Proc Natl Acad Sci U S A* **2014**, *111*, 1102-1107, doi:10.1073/pnas.1311909111.
385. Sakai, W.; Swisher, E.M.; Jacquemont, C.; Chandramohan, K.V.; Couch, F.J.; Langdon, S.P.; Wurz, K.; Higgins, J.; Villegas, E.; Taniguchi, T. Functional restoration of BRCA2 protein by secondary BRCA2 mutations in BRCA2-mutated ovarian carcinoma. *Cancer Res* **2009**, *69*, 6381-6386, doi:10.1158/0008-5472.CAN-09-1178.
386. Chatterjee, N.; Walker, G.C. Mechanisms of DNA damage, repair, and mutagenesis. *Environ Mol Mutagen* **2017**, *58*, 235-263, doi:10.1002/em.22087.
387. Zhou, J.; Wang, G.; Chen, Y.; Wang, H.; Hua, Y.; Cai, Z. Immunogenic cell death in cancer therapy: Present and emerging inducers. *J Cell Mol Med* **2019**, *23*, 4854-4865, doi:10.1111/jcmm.14356.
388. Kepp, O.; Semeraro, M.; Bravo-San Pedro, J.M.; Bloy, N.; Buque, A.; Huang, X.; Zhou, H.; Senovilla, L.; Kroemer, G.; Galluzzi, L. eIF2alpha phosphorylation as a biomarker of immunogenic cell death. *Semin Cancer Biol* **2015**, *33*, 86-92, doi:10.1016/j.semcancer.2015.02.004.
389. Schopf, F.H.; Biebl, M.M.; Buchner, J. The HSP90 chaperone machinery. *Nat Rev Mol Cell Biol* **2017**, *18*, 345-360, doi:10.1038/nrm.2017.20.
390. Lackie, R.E.; Maciejewski, A.; Ostapchenko, V.G.; Marques-Lopes, J.; Choy, W.Y.; Duennwald, M.L.; Prado, V.F.; Prado, M.A.M. The Hsp70/Hsp90 Chaperone Machinery in Neurodegenerative Diseases. *Front Neurosci* **2017**, *11*, 254, doi:10.3389/fnins.2017.00254.
391. Subeha, M.R.; Goyeneche, A.A.; Bustamante, P.; Lisio, M.A.; Burnier, J.V.; Telleria, C.M. Nelfinavir Induces Cytotoxicity towards High-Grade Serous Ovarian Cancer Cells, Involving Induction of the Unfolded Protein Response, Modulation of Protein Synthesis, DNA Damage, Lysosomal Impairment, and Potentiation of Toxicity Caused by Proteasome Inhibition. *Cancers* **2022**, *14*, 99.